1871
ИнБЮМ – IBSS

ISSN 2499-9768 print

МОРСКОЙ БИОЛОГИЧЕСКИЙ ЖУРНАЛ

MARINE BIOLOGICAL JOURNAL

Vol. 10 No. 4

2025

МОРСКОЙ БИОЛОГИЧЕСКИЙ ЖУРНАЛ
MARINE BIOLOGICAL JOURNAL

Журнал включён в перечень рецензируемых научных изданий, рекомендованных ВАК Российской Федерации, а также в базу данных Russian Science Citation Index (RSCI).
Журнал реферируется международной библиографической и реферативной базой данных Scopus (Elsevier), международной информационной системой по водным наукам и рыболовству ASFA (ProQuest), Всероссийским институтом научно-технической информации (ВИНИТИ), а также Российским индексом научного цитирования (РИНЦ) на базе Научной электронной библиотеки elibrary.ru.
Все материалы проходят независимое двойное слепое рецензирование.

Редакционная коллегия

Главный редактор
Егоров В. Н., акад. РАН, д. б. н., проф., ФИЦ ИнБЮМ
Заместитель главного редактора
Солдатов А. А., д. б. н., проф., ФИЦ ИнБЮМ
Ответственный секретарь
Корнийчук Ю. М., к. б. н., ФИЦ ИнБЮМ

Адрианов А. В., акад. РАН, д. б. н., проф., ННЦМБ ДВО РАН
Азовский А. И., д. б. н., проф., МГУ
Васильева Е. Д., д. б. н., МГУ
Генкал С. И., д. б. н., проф., ИБВВ РАН
Денисенко С. Г., д. б. н., ЗИН РАН
Довгаль И. В., д. б. н., проф., ФИЦ ИнБЮМ
Зуев Г. В., д. б. н., проф., ФИЦ ИнБЮМ
Картавцев Ю. Ф., д. б. н., проф., ННЦМБ ДВО РАН
Коновалов С. К., чл.-корр. РАН, д. г. н., ФИЦ МГИ
Мильчакова Н. А., к. б. н., ФИЦ ИнБЮМ
Неврова Е. Л., д. б. н., ФИЦ ИнБЮМ
Празукин А. В., д. б. н., ФИЦ ИнБЮМ
Рябушко В. И., д. б. н., ФИЦ ИнБЮМ
Самышев Э. З., д. б. н., проф., ФИЦ ИнБЮМ
Санжарова Н. И., чл.-корр. РАН, д. б. н., ВНИИРАЭ
Совга Е. Е., д. г. н., проф., ФИЦ МГИ
Стельмах Л. В., д. б. н., ФИЦ ИнБЮМ
Фесенко С. В., д. б. н., проф., ВНИИРАЭ
Arvanitidis Chr., D. Sc., HCMR, Greece
Bat L., D. Sc., Prof., Sinop University, Turkey
Ben Souissi J., D. Sc., Prof., INAT, Tunis
Kociolek J. P., D. Sc., Prof., CU, USA
Magni P., PhD, CNR-IAS, Italy
Moncheva S., D. Sc., Prof., IO BAS, Bulgaria
Pešić V., D. Sc., Prof., University of Montenegro, Montenegro
Zaharia T., D. Sc., NIMRD, Romania

Editorial Board

Editor-in-Chief
Egorov V. N., Acad. of RAS, D. Sc., Prof., IBSS, Russia
Assistant Editor
Soldatov A. A., D. Sc., Prof., IBSS, Russia
Managing Editor
Kornyychuk Yu. M., PhD, IBSS, Russia

Adrianov A. V., Acad. of RAS, D. Sc., Prof., NSCMB FEB RAS, Russia
Arvanitidis Chr., D. Sc., HCMR, Greece
Azovsky A. I., D. Sc., Prof., MSU, Russia
Bat L., D. Sc., Prof., Sinop University, Turkey
Ben Souissi J., D. Sc., Prof., INAT, Tunis
Denisenko S. G., D. Sc., ZIN, Russia
Dovgal I. V., D. Sc., Prof., IBSS, Russia
Fesenko S. V., D. Sc., Prof., RIRAE, Russia
Genkal S. I., D. Sc., Prof., IBIW RAS, Russia
Kartavtsev Yu. Ph., D. Sc., Prof., NSCMB FEB RAS, Russia
Kociolek J. P., D. Sc., Prof., CU, USA
Konovalov S. K., Corr. Member of RAS, D. Sc., Prof., MHI RAS, Russia
Magni P., PhD, CNR-IAS, Italy
Milchakova N. A., PhD, IBSS, Russia
Moncheva S., D. Sc., Prof., IO BAS, Bulgaria
Nevrova E. L., D. Sc., IBSS, Russia
Pešić V., D. Sc., Prof., University of Montenegro, Montenegro
Prazukin A. V., D. Sc., IBSS, Russia
Ryabushko V. I., D. Sc., IBSS, Russia
Samyshev E. Z., D. Sc., Prof., IBSS, Russia
Sanzharova N. I., Corr. Member of RAS, D. Sc., RIRAE, Russia
Sovga E. E., D. Sc., Prof., MHI RAS, Russia
Stelmakh L. V., D. Sc., IBSS, Russia
Vasil'eva E. D., D. Sc., MSU, Russia
Zaharia T., D. Sc., NIMRD, Romania
Zuyev G. V., D. Sc., Prof., IBSS, Russia

Адрес учредителя, издателя и редакции:
ФИЦ «Институт биологии южных морей имени А. О. Ковалевского РАН».
Пр-т Нахимова, 2, Севастополь, 299011, РФ.
Тел.: +7 8692 54-41-10. E-mail: *mbj@imbr-ras.ru*.
Сайт журнала: https://marine-biology.ru.
Адрес соиздателя:
Зоологический институт РАН.
Университетская наб., 1, Санкт-Петербург, 199034, РФ.

Founder, Publisher, and Editorial Office address:
A. O. Kovalevsky Institute of Biology of the Southern Seas of Russian Academy of Sciences.
2 Nakhimov ave., Sevastopol, 299011, Russia.
Tel.: +7 8692 54-41-10. E-mail: *mbj@imbr-ras.ru*.
Journal website: https://marine-biology.ru.
Co-publisher address:
Zoological Institute Russian Academy of Sciences.
1 Universitetskaya emb., Saint Petersburg, 199034, Russia.

© Зоологический институт РАН, 2025
© ФИЦ «Институт биологии южных морей имени А. О. Ковалевского РАН», 2025

ZOOLOGICAL INSTITUTE OF RAS
A. O. KOVALEVSKY INSTITUTE OF BIOLOGY OF THE SOUTHERN SEAS OF RAS

МОРСКОЙ БИОЛОГИЧЕСКИЙ ЖУРНАЛ

MARINE BIOLOGICAL JOURNAL

2025 Vol. 10 No. 4

Established in February 2016 SCIENTIFIC JOURNAL *4 issues per year*

CONTENTS

Scientific communications

Dantsyuk N., Krivenko O., Mansurova I., and Degtyar I.
A new strain of a carotenogenic green microalga *Coelastrella rubescens*, promising for cultivation in the climatic conditions of southern Russia 3–20

Dmitrieva E., Diakité S., Koïvogui P., Pronkina N., Uppe V., Konate L., Sow M., Balde A., Camara M., Polevoy D., Machkevsky R., Vodiasova E., Keita I., and Diallo A.
Schistosoma mansoni (Trematoda: Schistosomatidae) occurrence in *Biomphalaria pfeifferi* (Gastropoda: Planorbidae) in water bodies of Kindia Prefecture (Republic of Guinea) 21–36

Dogan N. and Tunc Dede O.
Assessment of radioactivity status in coastal waters of Türkiye 37–50

Zolotova A., Grintsov V., Ryabushko V., and Kartavtsev Yu.
Variability of nucleotide sequences in two gene markers (*COI* and *H3*) of *Litorogammarus karadagiensis* (Grintsov, 2009) (Amphipoda, Gammaridae) and the systematics of the genus *Litorogammarus* 51–59

Kirienko E. and Davidovich N.
The effect of nitrogen and phosphorus on the accumulation of extracellular marennine-like pigment in the culture of *Haslea karadagensis* (Bacillariophyta) 60–69

Ryumina A., Mazur M., Tishchenko P., and Shkirnikova E.
Preliminary results of the comprehensive assessment of contamination and toxic effects of bottom sediments in shallow bights of Amur Bay (Sea of Japan) 70–87

Sudakova E.
The role of quorum sensing and infochemicals in the interaction between pro- and microeukaryotes in aquatic ecosystems 88–101

Tiralongo F., Torre G., and De Maddalena A.
Trophic interactions between the giant devil ray *Mobula mobular* and sharks in Sicilian waters (Mediterranean Sea) 102–105

Khlopkova M., Barkhalov R., and Lobachev E.
Expansion of the range of a new invasive species, *Mytilus galloprovincialis* (Bivalvia: Mytilidae), in the Caspian Sea 106–112

Shiroyan A., Bondarenko A., and Ryabushko L.
Annotated list of epiphytic diatoms from macrophytes of the aquatic-rock complex Kazantip Cape (the Crimea, Sea of Azov) 113–122

Chronicle and information

On the anniversary of Sergey Fesenko 123–124

1871
ИнБЮМ – IBSS

Морской биологический журнал
Marine Biological Journal
2025, vol. 10, no. 4, pp. 3–20
https://marine-biology.ru/mbj/article/view/508

SCIENTIFIC COMMUNICATIONS

UDC [582.263.1:57.083.1]:582.29

A NEW STRAIN OF A CAROTENOGENIC GREEN MICROALGA *COELASTRELLA RUBESCENS*, SUITABLE FOR CULTIVATION IN THE CLIMATIC CONDITIONS OF SOUTHERN RUSSIA

© 2025 **N. Dantsyuk[1], O. Krivenko[1], I. Mansurova[1], and I. Degtyar[2]**

[1]A. O. Kovalevsky Institute of Biology of the Southern Seas of RAS, Sevastopol, Russian Federation
[2]Sevastopol State University, Sevastopol, Russian Federation
E-mail: *krivenko@ibss-ras.ru*

Received 10.12.2024; revised 24.01.2025;
accepted 12.08.2025.

A new carotenogenic strain of a green microalga *Coelastrella* Chodat (Scenedesmaceae, Sphaeropleales) was isolated in unialgal culture from the thallus of a Crimean epilithic lichen sampled in Sevastopol in March 2024. The strain is characterized by a pronounced ability to accumulate secondary carotenoids under acute abiotic stress conditions. We describe the methods we used to isolate phycobionts from small lichen samples, purify algae, establish axenic culture, adapt cells to laboratory conditions, and maintain strains in long-term culture collection. Species identification was performed using a combination of morphological (light and scanning electron microscopy) and molecular genetic approaches (analysis of the ITS1–5.8S–ITS2 fragment of the 18S rRNA gene cluster). The novel strain was identified as *Coelastrella rubescens* (Vinatzer) Kaufnerová & Eliás, 2013 and deposited into the collection of living cultures of carotenogenic microalgae at IBSS (https://algae.ibss-ras.ru), designated as IBSS-156. The growth characteristics of the IBSS-156 strain were evaluated under two-stage batch culture conditions. The data indicate high specific growth rates of the alga at the vegetative stage: up to (0.62 ± 0.11) day^{-1}. The dynamics of the algal pigment composition that we received reflects the massive accumulation of secondary carotenoids under stressful conditions. We found that measuring the absorption spectra of living microalgal cultures in the visible region allows for a rapid assessment of their physiological state and the rate of ketocarotenoid accumulation in biomass during two-stage cultivation. The obtained results highlight the potential of Crimean lichens as a source of promising astaxanthin-producing strains suitable for mass cultivation in arid and hot climates, such as those found in the Crimea and adjacent regions of southern Russia.

Keywords: carotenogenic microalgae, phycobionts, *Coelastrella*, two-stage cultivation

The term “carotenogenic microalgae” refers to a taxonomically and ecologically heterogeneous group of unicellular algae with a pronounced capacity for secondary carotenogenesis. This trait constitutes a key adaptation mechanism in extremophiles enabling survival during abrupt environmental deterioration through the massive accumulation of ketocarotenoids in cytoplasmic lipid inclusions (oleosomes) [Cheng, Shah, 2023; Debnath et al., 2024; Patel et al., 2022; Solovchenko, Minyuk, 2021].

The main biological features of carotenogenic microalgae include ephemerality of vegetation, the presence of a resting stage in their life cycle, the induction of secondary carotenoid and neutral lipid biosynthesis during the transition to the resting stage, and the ability to rapidly shift between rest and active growth.

The rising research interest in this algal group is rooted in both fundamental and applied aspects. On the one hand, it aims to advance our understanding of the general patterns and specific features of adaptation mechanisms in diverse ketocarotenoid producers. On the other hand, it seeks to reveal new commercially promising sources of C_{40} ketocarotenoids of the astaxanthin group and neutral lipids suitable for the production of high-quality biodiesel [Islam et al., 2013; Karpagam et al., 2015; Patel et al., 2022].

The most extensively studied and still the only astaxanthin producer successfully introduced into mass cultivation is a freshwater microalga *Haematococcus lacustris* (Girod-Chantrans) Rostafinski, 1875 (Chlorophyceae, Chlamydomonadales, Haematococcaceae). With a two-stage cultivation protocol, astaxanthin in its biomass can reach 5 % of dry weight [Han et al., 2013; Mota et al., 2022]. However, the low ecological plasticity of this species restricts its large-scale cultivation to areas with a subtropical maritime climate, where temperature does not exceed +28 °C during the hottest part of the day [Mohanasundaram et al., 2023]. Within the Russian Federation, such areas are localized zones on the Crimean and Caucasian coasts, which are of significant recreational value. Consequently, Russian companies interested in astaxanthin are completely dependent on import. Solving this problem requires searching for and introducing into cultivation new, high-yielding strains of astaxanthin producers that are easily adaptable to local conditions, resistant to contamination, and tolerant to extreme environmental factors [Patel et al., 2022; Solovchenko, Minyuk, 2021]. In literature, over 130 such species are reported [Minyuk, 2020]. Many of them occur in the algal flora of both the Crimean subtropics and the steppe and foothill zones of the peninsula. These are chiefly representatives of two orders of green microalgae: Chlamydomonadales and Sphaeropleales [Dantsyuk et al., 2021]. Their growth characteristics in culture and the specific mechanisms regulating astaxanthin biosynthesis remain poorly understood. Nevertheless, several studies conducted at IBSS suggest that some of these species may be undemanding and highly productive sources of astaxanthin [Chelebieva et al., 2018; Dantsyuk et al., 2021]. These considerations underscore the need for a comprehensive analysis of the Crimean carotenogenic microalgal flora, an assessment of its bioresource potential, and a search for novel strains with high potential for industrial cultivation across diverse natural and climatic zones of the peninsula and adjacent areas of southern Russia.

A poorly characterized group of carotenogenic microalgae includes phycobionts of Crimean crustose and foliose epilithic lichens adapted to extreme conditions: high daytime temperatures, low humidity, and intense solar radiation. These lichens form dense, bright orange-red crusts on rock surfaces [Czeczuga, Osorio, 1989; Voitsekhovich, 2013; Voytsekhovich, Beck, 2016]. Those are promising candidates for open-air mass cultivation in Crimean regions unsuitable for conventional agriculture.

The aim of this work was to isolate astaxanthin-producing microalgae from Crimean lichens, with a focus on strains adapted to local conditions. The following tasks were solved:

1) to isolate and obtain algologically pure cultures of phycobionts from Crimean lichens;
2) to reveal a strain with high ketocarotenoid accumulation potential and identify it taxonomically using an integrative approach;
3) to assess the biotechnological potential of the selected strain by evaluating its growth performance during the vegetative stage and pigment dynamics under combined abiotic stress conditions.

MATERIAL AND METHODS

Crustose lichens – bright orange, tightly attached crusts on rock surfaces, tree bark, and limestone boulders – were sampled in foothills of the Western Crimea (Sevastopol area) in spring and summer (Fig. 1). Sampling sites were as follows:

- A, the Victory Park (Sevastopol, 44°36′10″N, 33°27′23″E, isolated by I. Drobetskaya in March 2024);
- B, the Chelebi Yaurn Beli mount (Baydar Gate mountain pass, Orlinoye settlement, Sevastopol, 44°24′18″N, 33°46′49″E, isolated by N. Dantsyuk in April 2024);
- C, the Saint George monastery (Cape Fiolent, Sevastopol, 44°30′29″N, 33°30′29″E, isolated by N. Dantsyuk in April 2024);
- D, the Toropova Dacha forest park (Balaklava municipal district, Sevastopol, 44°30′34″N, 33°41′2″E, isolated by I. Mansurova in May 2024).

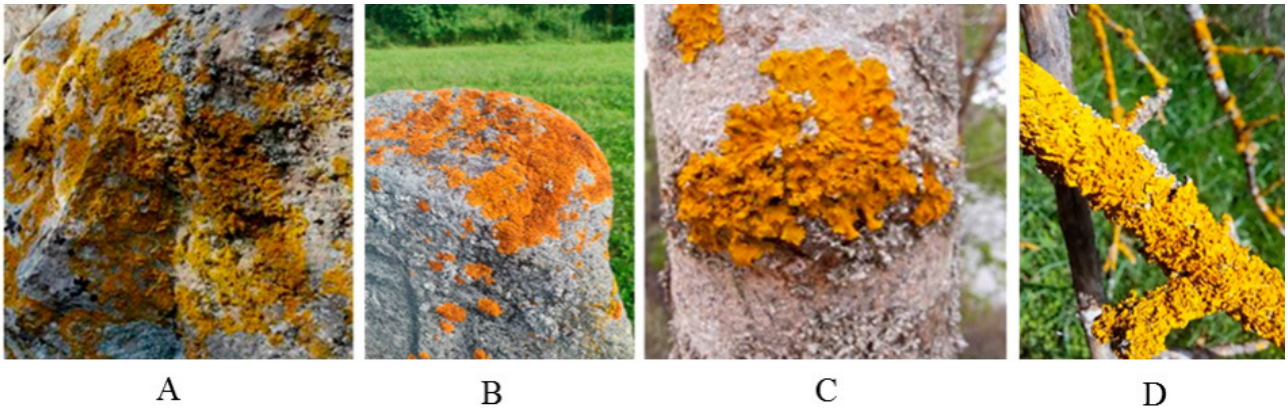


Fig. 1. Crustose epilithic (A, B) and foliose epiphytic (C, D) lichens

Material was separated from a substrate with a sharp spatula and placed in labeled polyethylene bags, each marked with sample number, sampling date, GPS coordinates, and sampler's surname. In a laboratory, samples were air-dried at room temperature for 24 h and then stored at +20 °C in labeled paper envelopes in a dark and dry place until analysis.

Isolation of algologically pure phycobiont cultures. To isolate microalgal cells into unialgal culture, we used a modified method of density gradient centrifugation proposed by [Fontaniella et al., 2000]. The technique involves step-by-step centrifugation of macerated lichen thalli in a density gradient of solutions: 0.25 M sucrose – 80% potassium iodide solution – 10 mM phosphate buffer. The core of our modification was the optimization of sample-to-solution ratios for biomass inputs of 0.1–0.3 g.

A sample of a dry lichen thallus was washed with distilled water to remove debris and ground in a mortar with 5 mL of distilled H_2O. A homogenate was filtered through six layers of gauze into a polypropylene Falcon tube and centrifuged at 200 g for 10 min. The supernatant was discarded, and the pellet was resuspended in 4 mL of 0.25 M sucrose. Into a centrifuge tube, 3 mL of 80% KI solution were placed. Along the inner wall of the tube, 2 mL of the resulting cell suspension in sucrose was carefully layered on top of the solution. The tube was centrifuged at 50 g for 1 min. Large fragments of lichen thalli precipitated and concentrated in the lower KI layer, while microalgal cells remained suspended in the upper sucrose layer. This layer was carefully transferred with a micropipette into a new tube containing 3 mL of 80% KI solution. Then, 2 mL of 10 mM phosphate buffer was added, and the samples were centrifuged

at 130 g for 2 min. Microalgal cells formed an intermediate layer (an interphase) between the phosphate buffer and KI solution, while fungal hyphae fragments passed into the KI layer as a dense pellet. The interphase containing algal cells was carefully sampled with a micropipette and transferred into 3 mL of 80% KI solution. Along the inner wall of the tube, 3 mL of the phosphate buffer was carefully layered on top of the KI solution and centrifuged at 200 g for 3 min. If necessary, this step was repeated. Subsequently, 1 mL of distilled H_2O was added to the microalgal cell suspension sampled from the interphase layer, and the sample was centrifuged at 290 g for 5 min. The resulting cell pellet was resuspended in 0.5–1.0 mL of twice diluted BBM (Bold's Basal Medium) [Bischoff, Bold, 1963]. The resulting "primary inoculum" was transferred into a glass tube with a cotton plug and stored at room temperature under illumination with a photosynthetically active radiation (hereinafter PAR) flux density not exceeding 35 μmol photons·m^{-2}·s^{-1} until antiseptic treatment.

Antiseptic treatment. To combat microbial contamination, antibiotics with a broad spectrum of antimicrobial activity were used: cefotaxime ("Biokhimik") and ampicillin ("Belmedpreparaty"). A mixture was prepared by combining 500 μg·mL^{-1} of ampicillin and 100 μg·mL^{-1} of cefotaxime [Kan, Pan, 2010]. As a fungicide, "Fundazol" was used ("Zelenaya Apteka Sadovoda"): when penetrating plant tissue, it blocks the reproductive function of fungi. Its solution (40 μg·mL^{-1}) was added to suppress micromycete contamination [Mokrosnop, Zolotareva, 2012].

Isolation of unialgal cultures. After antiseptic treatment, an alga was acclimated to laboratory conditions by maintaining the cell culture on liquid BBM under optimal temperature for lichen phycobionts, +18…+20 °C, and PAR flux density of < 35 μmol·m^{-2}·s^{-1} [Voitsekhovich, 2013]. To obtain unialgal cultures, we applied the standard streak plate method [Gaisina et al., 2008; Temraleeva et al., 2014]. Microalgae were inoculated on agar-enriched (1.5–2%) BBM in Petri dishes. The dishes with microalgae were incubated in a refrigerated cabinet at +14…+16 °C and a PAR flux density of 20–26 μmol photons·m^{-2}·s^{-1} in a 15 h light : 9 h dark mode. Germinated colonies were transferred with an inoculation loop into separate test tubes containing approximately 0.3 mL of liquid BBM to obtain an actively growing cell culture. Within one week, the alga was examined under a microscope to assess algological purity. If necessary, the procedure was repeated until obtaining a monoclonal culture of phycobiont cells. Once a unialgal culture was obtained, it was inoculated into agar slants for long-term storage in the collection of living cultures of carotenogenic microalgae at IBSS.

Conditions for two-stage culturing of phycobiont cells. Phycobiont cell were cultured in a two-stage batch culture mode [Minyuk et al., 2016]. *Prior* to cultivation, a synchronized cell culture in an actively growing state was obtained: an algal inoculum was prepared and grown on BBM for 7 days under unilateral side illumination (JazzWay DL 8W 6500K LED lamps, China) with continuous air bubbling. PAR photon flux density incident on the culture surface was 120 μmol·m^{-2}·s^{-1}. The photoperiod was 15 h light : 9 h dark (close to natural mode and recommended for carotenogenic microalgae cultivation). Temperature was maintained at the level of (+23 ± 1) °C.

During the I stage (the "green" one), which lasted 11 days, the alga was cultivated in 0.5-L glass conical flasks. Cultivation conditions did not differ from those of the preliminary phase. The cultures were continuously aerated with air at a rate of 1 L·min^{-1} using an air compressor Hailea ACO-9620 (China). During the light period, the medium pH was maintained at 7 by pulsed addition of carbon dioxide (CO_2 volume fraction of 99.8% according to [GOST 8050-85, 2006]) with a solenoid valve Camozzi A7E (Italy) and a digital pH controller Aqua Medic pH 2001 C (Germany). The initial cell abundance in flasks was $1.5 \cdot 10^6$ cells·mL^{-1}, and the culture volume was 0.45 L.

To proceed to the II stage (the "red" one), the culture was concentrated by centrifugation at 290 g for 5 min. The supernatant was discarded, and the cell pellet was resuspended in BBM with a 10-fold reduction in nitrogen and phosphorus content. The initial cell abundance at the "red" stage was approximately $1.5 \cdot 10^6$ cells·mL^{-1}, with a culture volume of 0.45 L in each flask. The mode of lighting was switched to continuous bilateral (140 μmol photons photons·m^{-2}·s^{-1} from each side). This configuration, combined with the 10-fold reduction in cell abundance, resulted in a 20-fold positive gradient of cell irradiation [Minyuk et al., 2017]. The supply of CO_2 was adjusted to a level that maintained the medium pH close to 7 around the clock.

Monitoring of culture growth and cell sizes. Cell abundance (n) was analyzed using a MACSQuant Analyzer flow cytometer ("Miltenyi Biotec," Germany), equipped with three lasers (405, 488, and 635 nm), at "Spectrometry and Chromatography" core facility at IBSS. Data were processed applying FCS Express 7 Research Edition software.

The average specific growth rate (μ) of cultures at the "green" stage was calculated from the daily increase in n [Wood et al., 2005]:

$$\mu_n = \frac{\ln \frac{n_i}{n_0}}{(t_i - t_0)},$$

where μ_n is specific growth rate for Δn, day^{-1};

n_0 is initial cell abundance, cells·mL^{-1};

n_i is cell abundance on day i, cells·mL^{-1};

$t_i - t_0$ is duration of the cultivation period, days.

Light microscopy and scanning electron microscopy. For light microscopy, we used an inverted microscope Nikon Eclipse Ts2R. Cell sizes were determined from micrographs taken with an Infinity 3 Lumenera camera applying ImageJ software (NIH, the USA).

For scanning electron microscopy (hereinafter SEM), 2.5 mL of culture of vegetative microalgal cells was sampled during the exponential growth phase (day 4 of the experiment) and fixed by adding 25% glutaraldehyde solution to a final concentration of 0.5%. Fixation requires a neutral, slightly alkaline environment [Chubchikova et al., 2022], and to ensure this, pH in the medium was adjusted to 7.3 right before fixation by regulating the supply of CO_2. Fixed samples were immediately mixed with a microvortex (Microspin FV-2400, "Biosan," Latvia), placed in a refrigerator at +3 °C, and mixed every 10–15 min for 1 h. If necessary, samples fixed according to this protocol can be stored refrigerated for two weeks [Rylkova et al., 2024]. At the next stage, microalgal suspension was concentrated on polycarbonate track-etched membranes with a pore size of 2 μm (manufacture by Joint Institute for Nuclear Research, Russia) placed on moist filter paper supports [Rylkova et al., 2024]. Filtration was carried out under a vacuum of no more than 0.2 atm. Fixative was washed off from the suspension on the filters treating them twice with 1 mL of Na/K phosphate buffer (chloride-free), the use of which is preferred for Scenedesmales [Chubchikova et al., 2022], and then rinsed once with 1 mL of deionized H_2O. Then, the filters with the alga were placed together with the supports into a 16-well plate and dehydrated in increasing concentrations of ethanol: 20, 30, and 50%, for 5 min; 57 and 96%, for 10 min; and 100%, twice for 10 min. Solutions were changed using a dispenser. Critical point drying was performed in a Leica EM CPD300 (Germany) in a soft mode for 2.5 h. Sputter coating (Au/Pd, 0.5–1.0 min) was carried out with a Leica EM ACE200 system. SEM images of cells were obtained under a Hitachi SU3500 scanning electron microscope (Japan) in the Microscopy Laboratory at IBSS.

Molecular genetic analysis. Genomic DNA was extracted from concentrated algal cultures with a "DNA-Extran-3" kit ("Syntol," Russia) following the manufacturer's protocol. DNA quality was assessed by electrophoresis in a 1.5% agarose gel stained with ethidium bromide (0.2 μg·mL^{-1}). Amplification of a DNA fragment encoding the 5.8S region and the adjacent ITS1 and ITS2 regions of the nuclear ribosomal gene cluster was performed by polymerase chain reaction (PCR) using the ready-to-use ScreenMix kit ("Evrogen," Russia) and ITS1 (TCCGTAGGTGAACCTGCGG) and ITS4 (TCCTCCGCTTATTGATATGC) primers [White et al., 1990]. The protocol was as follows: initial denaturation at +94 °C for 3 min; 34 amplification cycles (+94 °C for 30 s; +60 °C for 30 s; and +72 °C for 60 s); and a final extension at +72 °C for 10 min. PCR product was purified with Cleanup Standard reagents ("Evrogen") according to the manufacturer's protocol and sequenced with GenSeq reagents ("Syntol") on a genetic analyzer Nanophore 5 (Institute of Analytical Instrumentation of RAS, Russia).

The search for similarity between the obtained sequence and that available in the GenBank database (National Center for Biotechnology Information, NCBI) was carried out applying the BLASTN algorithm [Morgulis et al., 2008; Zhang et al., 2000]. Alignment was performed using MAFFT v. 7.48 [Katoh, Toh, 2010] with L-INS-I option; ambiguously aligned 5' and 3' ends were trimmed. Genetic distances between nucleotide sequences were calculated using the Kimura's two parameter model (K2P model) with MEGA 11 software [Kimura, 1980; Tamura et al., 2021]. Phylogenetic analysis and tree construction involving the maximum likelihood (ML) algorithms were performed in IQ-TREE 1.6.12 [Trifinopoulos et al., 2016] with the SYM + G4 nucleotide substitution model automatically selected by ModelFinder based on the Bayesian information criterion (BIC). Branch support was assessed using an SH-aLRT test and ultrafast bootstrap with 10,000 replicates, and also an approximate Bayes test with search stopping after 1,000 iterations and perturbation strength set to 0.1. Tree topology accuracy was evaluated by bootstrap analysis with 1,000 replicates. Trees were visualized and edited using the service https://phylo.io/index.html.

Spectrophotometry. Absorption spectra of cell suspensions of living microalgal cultures at the "green" and "red" stages were recorded on a Shimadzu UV-2600i spectrophotometer ("Spectrometry and Chromatography" core facility at IBSS) over the wavelength range of 380–800 nm in a 1-cm quartz cuvette. Right before measurement, each sample was thoroughly mixed to minimize sedimentation effects; the measurement time *per* sample was within 30 s. As the reference, BBM was used.

Graphs were plotted in Golden Software Grapher 17.3.454. Measurements were performed in three biological replicates and three analytical replicates. Data in figures and text are presented as mean values and standard error of the mean.

RESULTS AND DISCUSSION

Cells of green algae, lichen photobionts, were isolated from specimens of epilithic and epiphytic lichens sampled in foothills of the Western Crimea. Isolation involved a method of density gradient centrifugation adapted for small samples. Microscopic analysis revealed the absence of thallus debris and foreign impurities in resulting cell suspensions (Fig. 2A). During one week of acclimation to laboratory conditions, isolated cells acquired characteristics typical of free-living populations: more uniform cell sizes, shape, and intracellular content (Fig. 2B).

During the isolation of algologically pure cultures on agar-enriched nutrient media in Petri dishes, the first colonies appeared within 2–4 weeks. Similar germination times for photobionts on agar media have been reported by other researchers [Bačkor et al., 1998; Gasulla et al., 2010].

The colonies varied in morphology and consistency, appearing as powdery, smooth, or granular, with various shades of green (Fig. 2C–E). Such features of cell colonies may serve as secondary taxonomic criteria.

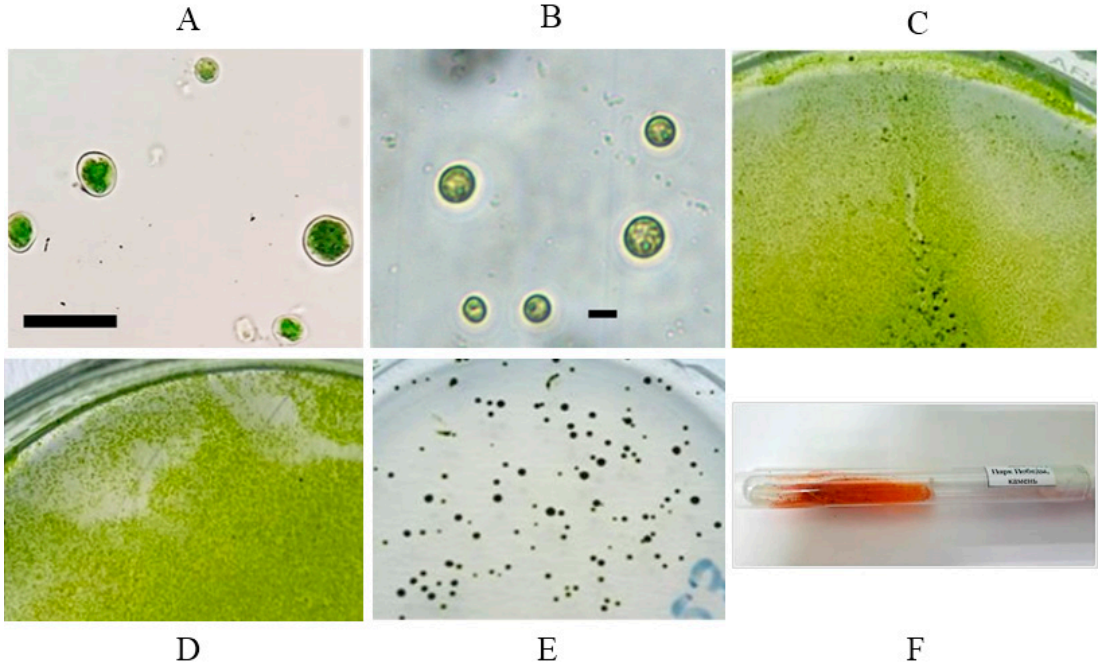


Fig. 2. The stages of isolating phycobionts into a pure culture: cells under a light microscope immediately after the isolation (A) and after one week of culturing (B); solid media cultures of phycobionts isolated from epilithic (C, D) and epiphytic (E) lichens; aging culture of the IBSS-156 strain on agar (F). Scale bars are 10 μm

Repeated subculturing allowed obtaining axenic cultures suitable for long-term preservation. After a month of incubation on agar slants in a refrigerated cabinet, the aging culture of a strain isolated from a thallus of a crustose epilithic lichen sampled in the Victory Park in Sevastopol (see Fig. 1A) changed its color from green to red-orange (Fig. 2F). This color change indicates the accumulation of secondary carotenoids in the microalga: a characteristic trait of extremophiles under abiotic stress.

Taxonomic identification of a strain using morphological and molecular approaches. Cell morphology and the life cycle of the isolated strain were examined *via* light microscopy and SEM. In actively growing cultures, light microscopy revealed single vegetative cells of oval or lemon shape (Fig. 3A). Mean cell length was 5–7 μm, and width was 3.5–6 μm. The chloroplast was parietal, with one pyrenoid. Asexual reproduction occurred *via* autospore formation. Those are enclosed in a spherical sporangium (typically 2 or 4 *per* sporangium) and released after rupture of a sporangial wall (Fig. 3D). Sexual reproduction with gamete formation was not observed. Mature cells at the stage of secondary carotenogenesis turned orange while retaining an oval shape. Mean cell length was 8 μm, and width was 6.5 μm (Fig. 3B).

SEM images of vegetative cells at magnification ×7000 (Fig. 3C) reveal 8 meridional ribs converging at the cell poles and forming a thickening. The cell wall architecture, in conjunction with distinctive cell sizes and other morphological traits, enables unambiguous classification of the isolated strain within the genus *Coelastrella* Chodat (Scenedesmaceae, Sphaeropleales) [Krivina et al., 2024;

Wang et al., 2019]. Algae of this genus are widely distributed, and many species are cosmopolitan ones, exhibiting tolerance to a broad temperature range. *Coelastrella* representatives are typically soil-associated species inhabiting various types of soils and water bodies: from wetlands to hot springs. Many species are aerophytes; those colonize natural and artificial solid substrates and contribute to biofilm formation [Kawasaki et al., 2020; Mikhailyuk et al., 2019; Wang et al., 2019]. To date, documented report of *Coelastrella* sp. as a lichen photobiont is restricted to one publication [Loureiro et al., 2024]. It describes the morphological and molecular genetic traits of three *Coelastrella* sp. strains isolated from lichens in northern Portugal.

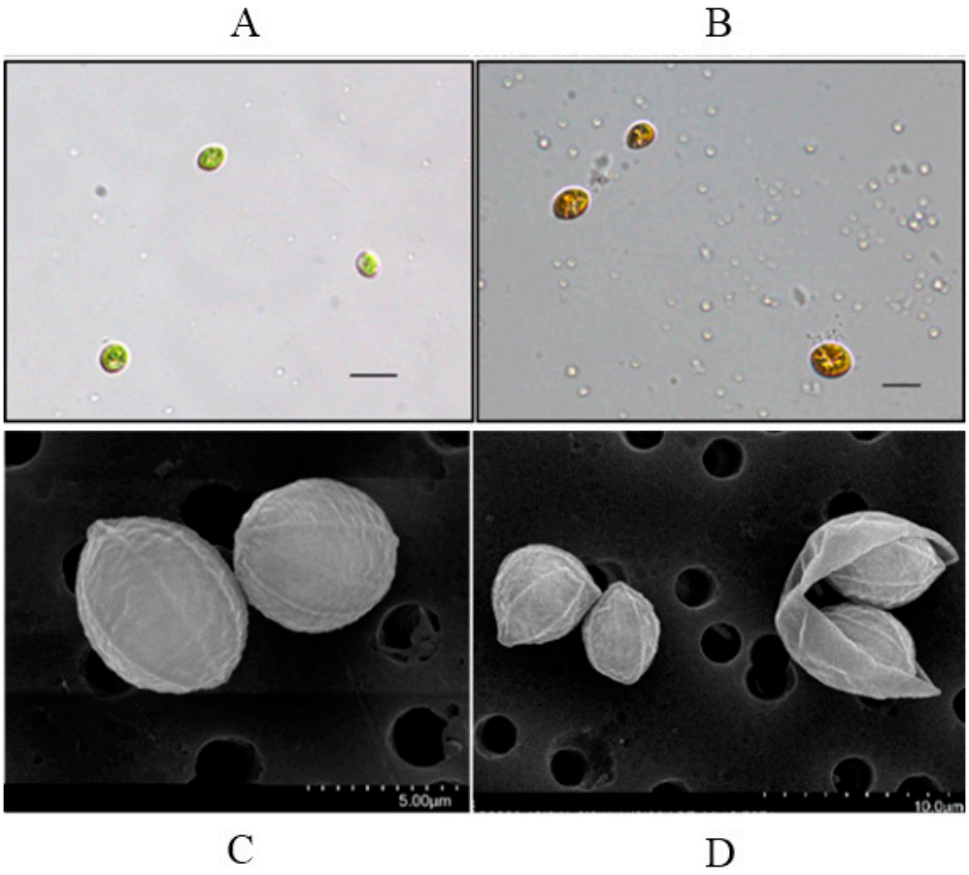


Fig. 3. Cells of the IBSS-156 strain under a light (A, B) and electron (C, D) microscope. Scale bars are 10 µm (A, B, D) and 5 µm (C)

As known, analysis of even ultrastructural cell features does not allow unambiguous identification of certain *Coelastrella* species [Krivina et al., 2024]. Therefore, conducting parallel molecular genetic studies is a standard practice when investigating representatives of this genus, as well as other green microalgae with similar phenotypes [Kawasaki et al., 2020; Mikhailyuk et al., 2019; Wang et al., 2019]. The issue of the most suitable genomic regions for studying this genus remains unresolved. However, an increasing number of researchers use the ITS1–5.8S–ITS2 region of 18S rRNA gene cluster when describing new strains [Kawasaki et al., 2020; Krivina et al., 2024; Maltsev et al., 2021]. For the IBSS-156 strain isolated from a Crimean epilithic lichen, a nucleotide sequence of 411 base pairs was obtained from this DNA region (GenBank NCBI accession number is PV022508).

Phylogenetic analysis of this region allowed constructing a phylogenetic tree (Fig. 4). It unequivocally supports the classification of the studied strain within the genus *Coelastrella*.

With robust support, the strain is placed within the *Coelastrella rubescens* (Vinatzer) Kaufnerová & Eliás, 2013 clade, which constitutes a well-supported lineage in the genus phylogeny. The obtained sequence shows full identity with the corresponding fragment of an authentic strain *C. rubescens* CCALA 475. These two sequences form a subgroup sister to *C. rubescens* var. *oocystiformis* Qinghua Wang, Huiyin Song, Xudong Liu, Guoxiang Liu & Zhengyu Hu, 2019 FACHB-2297a, with a K2P genetic distance of 0.017. This value is close to the minimum interspecific threshold for the ITS1–5.8S–ITS2 region based on pairwise comparisons of authentic strains *Coelastrella corcontica* (Kalina & Puncochárová) Hegewald & N. Hanagata, 2002 CCALA 308 and *Coelastrella multistriata* (Trenkwalder) Kalina & Puncochárová, 1987 CCALA 309.

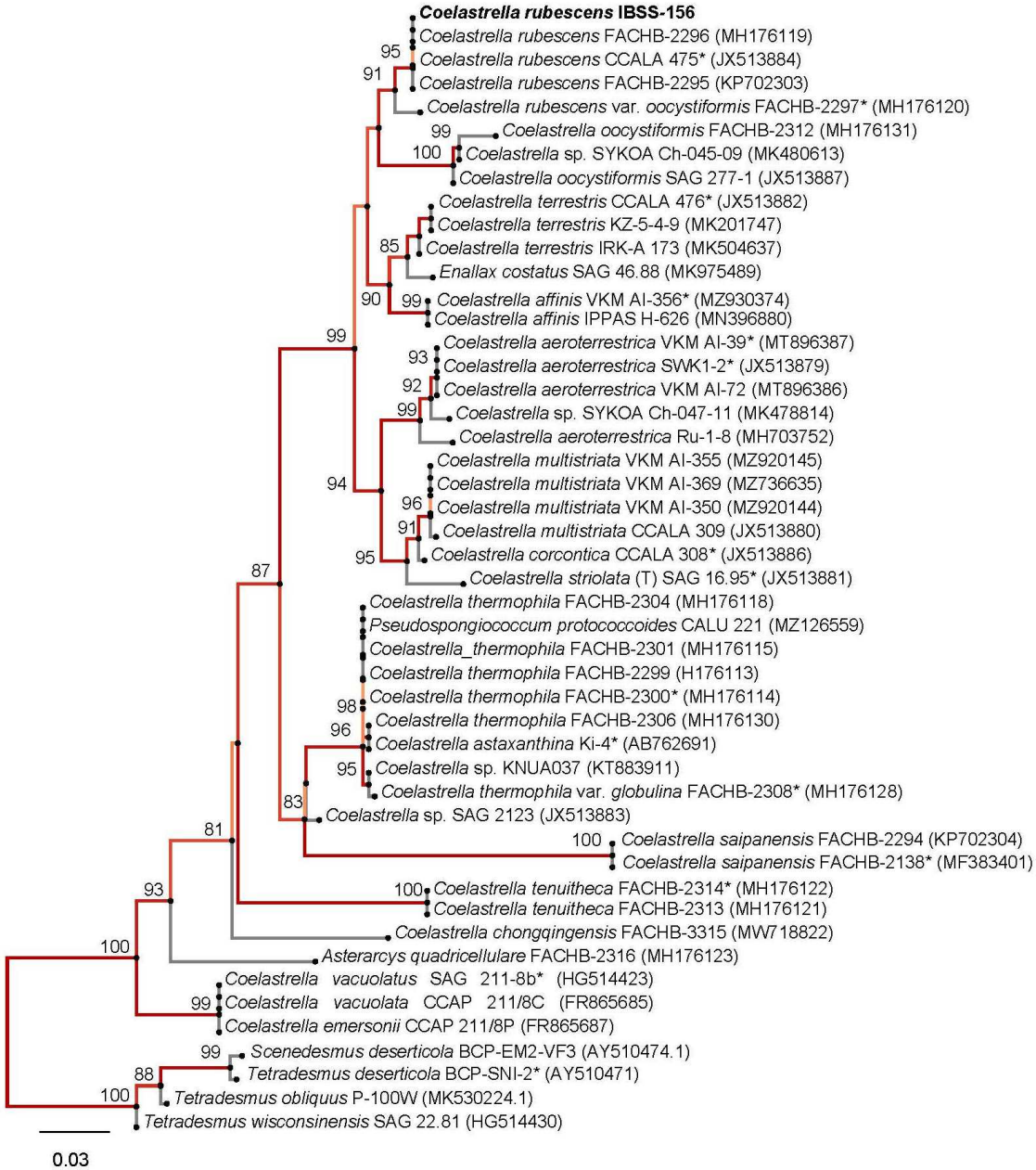


Fig. 4. The phylogenetic position of the IBSS-156 *Coelastrella* strain (Scenedesmaceae, Sphaeropleales) based on the maximum likelihood (ML) inference from partial ITS1–5.8S–ITS2 region of the 18S rRNA gene cluster. Bootstrap support values (> 80) are shown at the nodes. Authentic strains are marked with *; the type species is marked with T

The obtained topology of the tree constructed from a relatively small ribosomal DNA fragment agrees well with phylogenies based on complete 18S rRNA gene sequences [Krivina et al., 2024; Maltsev et al., 2021; Wang et al., 2019]. Specifically, the *C. rubescens* lineage belongs to a subgroup with species usually assigned to a so-called core subclade. The latter one is strongly supported as a sister one to a clade comprising *Coelastrella thermophila* Qinghua Wang, Huiyin Song, Xudong Liu, Guoxiang Liu & Zhengyu Hu, 2019 and *Coelastrella saipanensis* N. Hanagata, 2001; this is fully consistent with phylogenies presented in [Krivina et al., 2024; Maltsev et al., 2021]. Thus, the strain isolated from a Crimean lichen can be assigned with high confidence to *C. rubescens*. This conclusion is corroborated by morphological data: in terms of maximum linear sizes, number and position of cell wall ribs, and number of autospores *per* sporangium, our strain matches *C. rubescens* var. *rubescens*, with its key taxonomic traits summarized in [Andreyeva, 1998; Kaufnerová, Eliáš, 2013; Krivina et al., 2024]. Accordingly, this isolate was registered in the general catalogue of the collection of living cultures of carotenogenic microalgae at IBSS (https://algae.ibss-ras.ru) as the IBSS-156 strain *Coelastrella rubescens* (Vinatzer) Kaufnerová & Eliás, 2013 (Scenedesmaceae, Sphaeropleales).

Study of the growth characteristics of the IBSS-156 strain in batch culture and under stress conditions. A two-stage cultivation scheme is the main approach for growing microalgae to obtain valuable products of secondary carotenogenesis: ketocarotenoids of the astaxanthin group and neutral lipids [Solovchenko, Minyuk, 2021]. At the I, vegetative ("green") stage, the alga is maintained under optimal growth conditions to maximize accumulation of vegetative cell biomass. Upon reaching the stationary growth phase and the onset of nutrient depletion, cultures are transferred to the II ("red") stage by inducing multifactorial stress that triggers the biosynthesis of astaxanthin and neutral lipids. The most commonly applied stress factor is acute nitrogen and phosphorus deprivation, along with a significant increase in light intensity and temperature. To study the growth performance of the IBSS-156 strain, an optimized two-stage cultivation scheme was chosen [Minyuk et al., 2016]. This approach enables investigation of the morphophysiological traits of the alga during the "green" stage and assessment of its capacity to accumulate valuable target products under stress conditions.

The growth dynamics of the IBSS-156 strain in batch culture at the vegetative stage is shown in Fig. 5A. The exponential growth phase lasted from day 1 to day 5, with an average specific growth rate of (0.52 ± 0.11) day^{-1} and a maximum of (0.62 ± 0.11) day^{-1} on day 3. From day 7, the culture remained at the stationary phase. Cell abundance increased 8-fold over 11 days of vegetative growth. High growth rates and the ability to rapidly accumulate biomass are characteristic of *Coelastrella* species [Corato et al., 2022; Goecke et al., 2020; Maltsev et al., 2021; Nayana et al., 2022]. For a reference strain (a free-living one) Vinatzer/Innsbruck V 195 (IPPAS H-350 = CCALA 475) *Coelastrella rubescens* (Vinatzer) Kaufnerová & Eliás, 2013, the maximum specific growth rate at the "green" stage was 0.95 day^{-1} under cultivation conditions comparable to those in our study [Minyuk et al., 2017].

After transfer to abiotic stress conditions, by the day 3 of the "red" stage (Fig. 5B), cell abundance rose 1.6-fold relative to the initial concentration. No further growth occurred. A similar response of *C. rubescens* culture at the onset of the "red" stage under the same stress protocol was reported previously [Minyuk et al., 2017]. This increase may be attributed to the algae utilizing nutrients introduced when the concentrated cell suspension was diluted with a medium, despite the medium being depleted in nitrogen and phosphorus. The first signs of secondary carotenogenesis were observed on day 3 after stress. Visually, the culture in flasks changed its color from green to brown-orange; light microscopy revealed a rise in cell size and altered coloration (see Fig. 3B).

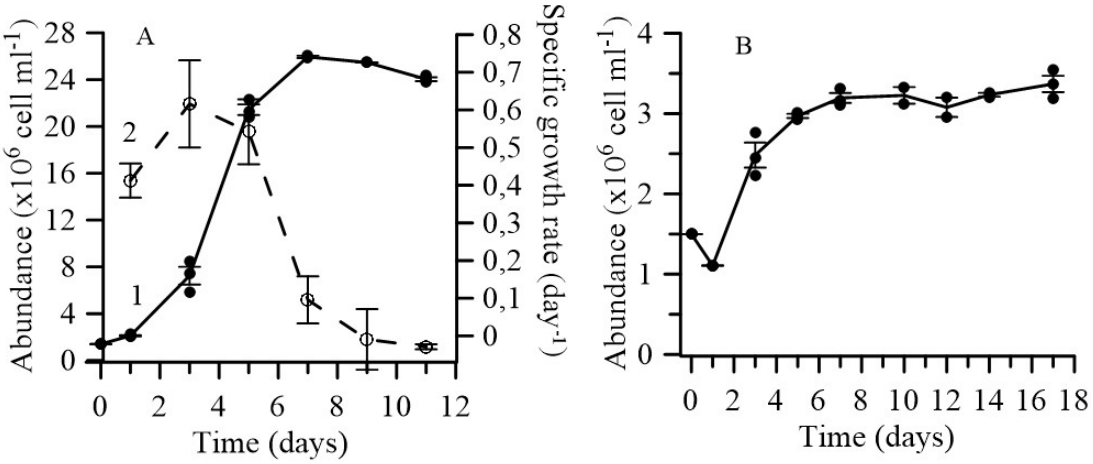


Fig. 5. Dynamics of the cell abundance (1) and the average daily specific growth rate (2) for the IBSS-156 *Coelastrella rubescens* strain during the vegetative stage (A) and secondary carotenogenesis stage (B)

Changes in pigment composition definitely indicate the development of secondary carotenogenesis in cells in response to abiotic stress. This phenomenon is manifested in a decrease in the specific content of chlorophyll and associated primary carotenoids in cells relative to secondary carotenoids [Lemoine, Schoefs, 2010; Shah et al., 2016]. To quantitatively evaluate the dynamics of these processes, researchers use the ratio of absorption peaks of pigment extracts at wavelengths corresponding to the absorption maximums of chlorophyll and secondary carotenoids [Solovchenko, Minyuk, 2021]. To carry out a rapid assessment, we analyzed the absorption spectra of living microalgal cultures at the "green" stage (Fig. 6A) and the "red" one (Fig. 6B). It is evident that spectral profiles of a cell suspension of a living *C. rubescens* culture differ significantly under different cultivation conditions.

At the "green" stage, distinct absorption maximums attributable to chlorophyll *a* were observed in its blue (425 nm) and red (680 nm) regions. An additional shoulder noted at 650 nm in the red region (at 650 nm) is related to chlorophyll *b* absorption: an accessory photosynthetic pigment of green algae. In the blue region, this pigment contributes to a peak at 470–480 nm together with primary carotenoids. Absorption intensities at blue-region maximums exhibited a continuous increase throughout the experiment reaching their highest levels on day 11. Absorption intensities at red-region maximums remained unchanged after day 5 (Fig. 6A).

During the "red" stage, a progressive smoothing of the absorption spectrum was noted in chlorophyll absorption bands, culminating in a unimodal profile with a broad peak shifted towards the blue-green region by day 12 of the experiment. At 480–490 nm, a progressive increase in peak intensity was recorded reflecting accumulation of secondary carotenoids. By day 17, the values dropped sharply without spectral change. Concurrently, initial indicators of the alga's transition to a resting state were observed: complete cessation of cell division and thickening of the outer cell membrane. The observed spectral dynamics aligns with the established concept of gradual degradation of the photosynthetic apparatus in microalgae during their transition to a resting state, and also with the accumulation of ketocarotenoids in cells. The absorption maximums of these pigments are shifted to longer wavelengths compared to those of primary carotenoids [Lemoine, Schoefs, 2010]. Thus, changes in the absorption spectra of living cultures of carotenogenic microalgae during cultivation can be used for rapid assessment of the physiological state of cells and for monitoring the accumulation of ketocarotenoids in a culture.

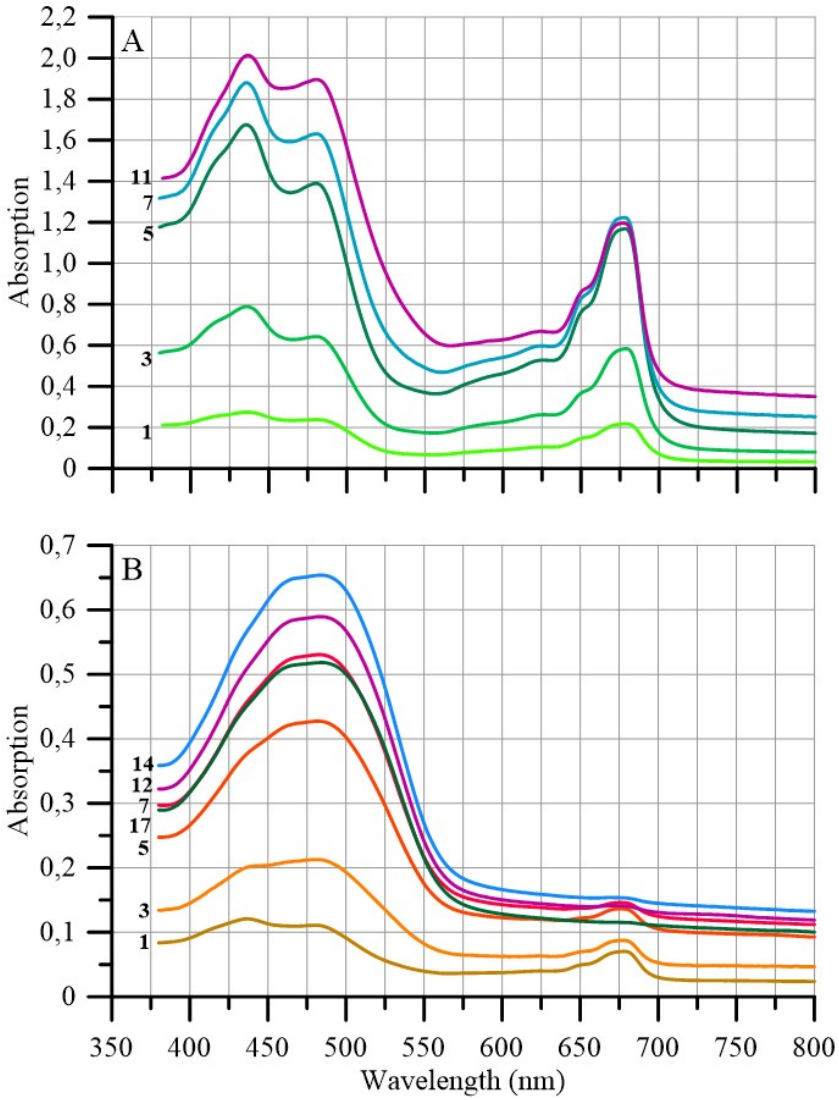


Fig. 6. Changes in the shape of optical absorption spectra of a cell suspension of a living culture of the IBSS-156 *Coelastrella rubescens* strain during the "green" (A) and "red" (B) stages of cultivation (digits on curves indicate the experiment duration in days)

Conclusions:

1. This study reports the first successful isolation of *Coelastrella* cells (Scenedesmaceae, Sphaeropleales) from a thallus of a Crimean epilithic lichen into a unialgal culture. The demonstrated simplicity and reproducibility of the isolation protocol substantiate the utility of the modified method of density gradient centrifugation described in the paper for routine isolation of lichen photobiont cells into a culture.
2. The taxonomic position of the isolated strain within Chlorophyta was confirmed by molecular genetic identification and scanning electron microscopy. Based on a comprehensive combination of morphological and molecular traits, the strain is assigned to the genus *Coelastrella* of the family Scenedesmaceae within the order Sphaeropleales. Phylogenetic analysis of the ITS1–5.8S–ITS2 fragment of the ribosomal DNA cluster with high statistical support assigns the strain to the species *C. rubescens*. The isolate has been deposited in the collection of living cultures of carotenogenic microalgae at IBSS (https://algae.ibss-ras.ru) as IBSS-156 *Coelastrella rubescens*.

3. The strain demonstrated high specific growth rate, up to (0.62 ± 0.11) day^{-1}, and the capacity to accumulate both green biomass and secondary carotenoids under two-stage cultivation conditions. Absorption spectra of cell suspensions at the "red" stage clearly reflect the degradation of green photosynthetic pigments and biosynthesis of secondary carotenoids. Spectral monitoring of living microalgal cultures is a method for rapid assessment of their physiological state and for analysis of ketocarotenoid accumulation during cultivation.

These findings indicate the possibility of isolating promising astaxanthin producers adapted to local conditions from Crimean lichens. Further research is required on the biological properties and commercial potential of the new strain IBSS-156 *Coelastrella rubescens* as a candidate biotechnological object for mass cultivation under the climatic conditions of Crimea and southern Russia, with the aim of producing ketocarotenoids of the astaxanthin group, which are of high medical and nutritional value.

This work was supported by the Russian Science Foundation, grant No. 24-26-20121 "Creation of a bioresource collection of carotenogenic algae of the Crimean region" (state registration No. 124102900026-9).

Acknowledgements. The authors express their sincere gratitude to PhD G. Minyuk for her valuable comments and advice during the preparation of the manuscript; to PhD E. Bocharova, for obtaining light microscopy images of algal cells and measuring their linear sizes; to V. Lishaev, head of the Microscopy Laboratory, for obtaining SEM images of microalgae; to PhD O. Rylkova, PhD I. Drobetskaya, and I. Chubchikova, for their consultations on sample preparation for SEM; and to PhD N. Shoman and PhD E. Solomonova, for their consultations on the operation of the spectrophotometer and flow cytometer.

REFERENCES

1. Andreyeva V. M. *Terrestrial and Aerophilic Green Algae (Chlorophyta: Tetrasporales, Chlorococcales, Chlorosarcinales).* Saint Petersburg : Nauka, 1998, 351 p. (in Russ.)
2. Voitsekhovich A. *Fotobionty lishainikov: raznoobrazie, ekologiya i vzaimootnosheniya s mikobiontami.* Saarbrücken, Germany : LAP LAMBERT Academic Publishing, 2013, 102 p. (in Russ.)
3. Gaisina L. A., Fazlutdinova A. I., Kabirov R. R. *Sovremennye metody vydeleniya i kul'tivirovaniya vodoroslei* : uchebnoe posobie. Ufa : Izd-vo BGPU, 2008, 152 p. (in Russ.). https://elibrary.ru/qktkil
4. GOST 8050-85. *Dvuokis' ugleroda gazoobraznaya i zhidkaya. Tekhnicheskie usloviya = Gaseous and liquid carbon dioxide. Specifications* : mezhgosudarstvennyi standart : izdanie ofitsial'noe : utverzhden i vveden v deistvie postanovleniem Gosudarstvennogo komiteta SSSR po standartam ot 29.07.85 no. 2423 : vzamen GOST 8050-76 : data vvedeniya 1987-01-01 / podgotovlen Gosudarstvennoi assotsiatsiei "Agrokhim". Moscow : Standartinform, 2006, 25 p. (in Russ.)
5. Dantsyuk N. V., Chelebieva E. S., Minyuk G. S. Working collection of carotenogenic microalgae living cultures of A. O. Kovalevsky Institute of Biology of the Southern Seas. *Marine Biological Journal*, 2021, vol. 6, no. 4, pp. 3–18. (in Russ.). https://doi.org/10.21072/mbj.2021.06.4.01
6. Minyuk G. S. *Karotinogennye mikrovodorosli. Baza dannykh.* A. s. no. 2020621092. Zayavka no. 2020620921. 10.06.2020, opubl. 30.06.2020. Byul. no. 7. (in Russ.)
7. Minyuk G. S., Chelebieva E. S., Chubchikova I. N., Dantsyuk N. V., Drobetskaya I. V., Sakhon E. G., Chivkunova O. B., Chekanov K. A., Lobakova E. S., Sidorov R. A., Solovchenko A. E. pH and CO_2 effects on *Coelastrella (Scotiellopsis) rubescens*

growth and metabolism. *Fiziologiya rastenii*, 2016, vol. 63, iss. 4, pp. 601–610. (in Russ.). http://doi.org/10.7868/S0015330316040102

8. Mokrosnop V. M., Zolotareva E. K. The effect of selected fungicides on growth of *Euglena gracilis* Klebs (Euglenophyta) culture. *Al'gologiya*, 2012, vol. 22, no. 4, pp. 337–344. (in Russ.). https://doi.org/10.1615/InterJAlgae.v15.i2.60
9. Rylkova O. A., Borovkov A. B., Khanaychenko A. N., Kharchuk I. A., Gudvilovich I. N., Lishaev V. N. Peculiarities of sample preparation of samples of monadic forms of microalgae for scanning electron microscopy. *Bioraznoobrazie i ustoichivoe razvitie*, 2024, vol. 8, no. 4, pp. 62–74. (in Russ.). https://elibrary.ru/afkodh
10. Temraleeva A. D., Mincheva E. V., Bukin Yu. S., Andreeva A. M. *Modern Methods of Isolation, Cultivation and Identification of Green Algae (Chlorophyta)*. Kostroma : Kostromskoi pechatnyi dom, 2014, 215 p. (in Russ.). https://elibrary.ru/uyyvqt
11. Chubchikova I. N., Drobetskaya I. V., Dantsyuk N. V., Chelebieva E. S. Optimization of freshwater microalgae (Scenedesmaceae, Chlorophyta) fixation method for primary taxonomic identification by scanning electron microscopy. *Voprosy sovremennoi al'gologii*, 2022, no. 1 (28), pp. 102–109. (in Russ.). https://doi.org/10.33624/2311-0147-2022-1(28)-102-109
12. Bačkor M., Hudák J., Ziegler W., Bačkorová M. Methods for isolation and cultivation of the eukaryotic lichen photobionts – looking for a universal method. A review. *Thaiszia – Journal of Botany*, 1998, vol. 8, pp. 1–6.
13. Bischoff H. W., Bold H. C. *Phycological Studies.* IV. *Some Soil Algae from Enchanted Rock and Related Algal Species.* Austin, TX : University of Texas, 1963, vol. 6318, 95 p.
14. Chelebieva E. S., Dantsyuk N. V., Chekanov K. A., Chubchikova I. N., Drobetskaya I. V., Minyuk G. S., Lobakova E. S., Solovchenko A. E. Identification and morphological-physiological characterization of astaxanthin producer strains of *Haematococcus pluvialis* from the Black Sea region. *Applied Biochemistry and Microbiology*, 2018, vol. 54, no. 6, pp. 639–648. https://doi.org/10.1134/S0003683818060078
15. Cheng X., Shah M. Astaxanthin from *Haematococcus*: Production, applications, and advances. In: *Handbook of Food and Feed from Microalgae. Production, Application, Regulation, and Sustainability*. London, UK ; San Diego, CA ; Cambridge, MA ; Oxford, UK : Academic Press, 2023, chap. 19, pp. 221–236. https://doi.org/10.1016/B978-0-323-99196-4.00033-4
16. Corato A., Le T. T., Baurain D., Jacques P., Remacle C., Franck F. A fast-growing oleaginous strain of *Coelastrella* capable of astaxanthin and canthaxanthin accumulation in phototrophy and heterotrophy. *Life*, 2022, vol. 12, iss. 3, art. no. 334 (21 p.). https://doi.org/10.3390/life12030334
17. Czeczuga B., Osorio H. S. Investigations on carotenoids in lichens. XXI. Astaxanthin, the dominant carotenoid in some lichens from Uruguay. *Israel Journal of Plant Sciences*, 1989, vol. 38, iss. 2–3, pp. 115–120.
18. Debnath T., Bandyopadhyay T. K., Vanitha K., Bobby Md. N., Tiwari O. N., Bhunia B., Muthuraj M. Astaxanthin from microalgae: A review on structure, biosynthesis, production strategies and application. *Food Research International*, 2024, vol. 176, art. no. 113841 (18 p.). https://doi.org/10.1016/j.foodres.2023.113841
19. Fontaniella B., Molina M. C., Vicente C. An improved method for the separation of lichen symbionts. *Phyton (Horn, Austria)*, 2000, vol. 40, fasc. 2, pp. 323–328.

20. Gasulla F., Guéra A., Barreno E. "A simple and rapid method for isolating lichen photobionts". *Symbiosis*, 2010, vol. 51, iss. 2, pp. 175–179. https://doi.org/10.1007/s13199-010-0064-4
21. Goecke F., Noda J., Paliocha M., Gislerød H. R. Revision of *Coelastrella* (Scenedesmaceae, Chlorophyta) and first register of this green coccoid microalga for continental Norway. *World Journal of Microbiology and Biotechnology*, 2020, vol. 36, iss. 10, art. no. 149 (17 p.). https://doi.org/10.1007/s11274-020-02897-0
22. Han D., Li Y., Hu Q. Astaxanthin in microalgae: Pathways, functions and biotechnological implications. *Algae*, 2013, vol. 28, no. 2, pp. 131–147. https://doi.org/10.4490/algae.2013.28.2.131
23. Islam M. A., Magnusson M., Brown R. J., Ayoko G. A., Nabi M. N., Heimann K. Microalgal species selection for biodiesel production based on fuel properties derived from fatty acid profiles. *Energies*, 2013, vol. 6, iss. 11, pp. 5676–5702. https://doi.org/10.3390/en6115676
24. Kan Y., Pan J. A one-shot solution to bacterial and fungal contamination in the green alga *Chlamydomonas reinhardtii* culture by using an antibiotic cocktail. *Journal of Phycology*, 2010, vol. 46, iss. 6, pp. 1356–1358. https://doi.org/10.1111/j.1529-8817.2010.00904.x
25. Karpagam R., Preeti R., Ashokkumar B., Varalakshmi P. Enhancement of lipid production and fatty acid profiling in *Chlamydomonas reinhardtii*, CC1010 for biodiesel production. *Ecotoxicology and Environmental Safety*, 2015, vol. 121, pp. 253–257. https://doi.org/10.1016/j.ecoenv.2015.03.015
26. Katoh K., Toh H. Parallelization of the MAFFT multiple sequence alignment program. *Bioinformatics*, 2010, vol. 26, iss. 15, pp. 1899–1900. https://doi.org/10.1093/bioinformatics/btq224
27. Kaufnerová V., Eliáš M. The demise of the genus *Scotiellopsis* Vinatzer (Chlorophyta). *Nova Hedwigia*, 2013, Bd 97, Heft 3–4, S. 415–428. https://doi.org/10.1127/0029-5035/2013/0116
28. Kawasaki S., Yoshida R., Ohkoshi K., Toyoshima H. *Coelastrella astaxanthina* sp. nov. (Sphaeropleales, Chlorophyceae), a novel microalga isolated from an asphalt surface in midsummer in Japan. *Phycological Research*, 2020, vol. 68, iss. 2, pp. 107–114. https://doi.org/10.1111/pre.12412
29. Kimura M. A simple method for estimating evolutionary rate of base substitutions through comparative studies of nucleotide sequences. *Journal of Molecular Evolution*, 1980, vol. 16, iss. 2, pp. 111–120. https://doi.org/10.1007/bf01731581
30. Krivina E., Sinetova M., Zadneprovskaya E., Ivanova M., Starikov A., Shibzukhova K., Lobakova E., Bukin Yu., Portnov A., Temraleeva A. The genus *Coelastrella* (Chlorophyceae, Chlorophyta): Molecular species delimitation, biotechnological potential, and description of a new species *Coelastrella affinis* sp. nov., based on an integrative taxonomic approach. *Antonie van Leeuwenhoek*, 2024, vol. 117, iss. 1, art. no. 113 (33 p.). https://doi.org/10.1007/s10482-024-02008-1
31. Lemoine Y., Schoefs B. Secondary ketocarotenoid astaxanthin biosynthesis in algae: A multifunctional response to stress. *Photosynthesis Research*, 2010, vol. 106, iss. 1–2, pp. 155–177. https://doi.org/10.1007/s11120-010-9583-3
32. Loureiro L., Morais J., Silva R., Martins J. T., Geada P., Vasconcelos V., Vicente A. A. Isolation and identification of lichen photobionts collected from different environments in north of Portugal and evaluation

of bioactivities of their extracts. *Foods*, 2024, vol. 13, iss. 11, art. no. 1759 (18 p.). https://doi.org/10.3390/foods13111759

33. Maltsev Y., Krivova Z., Maltseva S., Maltseva K., Gorshkova E., Kulikovskiy M. Lipid accumulation by *Coelastrella multistriata* (Scenedesmaceae, Sphaeropleales) during nitrogen and phosphorus starvation. *Scientific Reports*, 2021, vol. 11, art. no. 19818 (13 p.). https://doi.org/10.1038/s41598-021-99376-9
34. Mikhailyuk T., Glaser K., Tsarenko P., Demchenko E., Karsten U. Composition of biological soil crusts from sand dunes of the Baltic Sea coast in the context of an integrative approach to the taxonomy of microalgae and cyanobacteria. *European Journal of Phycology*, 2019, vol. 54, iss. 3, pp. 263–290. https://doi.org/10.1080/09670262.2018.1557257
35. Minyuk G., Chelebieva E., Chubchikova I., Dantsyuk N., Drobetskaya I., Sakhon E., Chekanov K., Solovchenko A. Stress-induced secondary carotenogenesis in *Coelastrella rubescens* (Scenedesmaceae, Chlorophyta), a producer of value-added keto-carotenoids. *Algae*, 2017, vol. 32, iss. 3, pp. 245–259. https://doi.org/10.4490/algae.2017.32.8.6
36. Mohanasundaram Y., Arumugam N., Sarangam B., Alagarsamy A., Raja R. An introduction to *Haematococcus*. In: *Haematococcus. Biochemistry, Biotechnology and Biomedical Applications* / R. Raja, S. Hemaiswarya, M. Narayanan, S. Kandasamy, K. Jayappriyan (Eds). Singapore : Springer, 2023, pp. 1–10. https://doi.org/10.1007/978-981-99-2901-6_1
37. Morgulis A., Coulouris G., Raytselis Y., Madden T. L., Agarwala R., Schäffer A. A. Database indexing for production MegaBLAST searches. *Bioinformatics*, 2008, vol. 24, iss. 16, pp. 1757–1764. https://doi.org/10.1093/bioinformatics/btn322
38. Mota G. C. P., Moraes L. B. S. D., Oliveira C. Y. B., Oliveira D. W. S., Abreu J. L. D., Dantas D. M. M., Gálvez A. O. Astaxanthin from *Haematococcus pluvialis*: Processes, applications, and market. *Preparative Biochemistry & Biotechnology*, 2022, vol. 52, iss. 5, pp. 598–609. https://doi.org/10.1080/10826068.2021.1966802
39. Nayana K., Sudhakar M. P., Arunkumar K. Biorefinery potential of *Coelastrella* biomass for fuel and bioproducts – a review. *Biomass Conversion and Biorefinery*, 2022, 14 p. https://doi.org/10.1007/s13399-022-02519-9
40. Patel A. K., Tambat V. S., Chen C. W., Chauhan A. S., Kumar P., Vadrale A. P., Huang C.-Y., Dong C., Singhania R. R. Recent advancements in astaxanthin production from microalgae: A review. *Bioresource Technology*, 2022, vol. 364, art. no. 128030 (12 p.). https://doi.org/10.1016/j.biortech.2022.128030
41. Shah M. R., Liang Y., Cheng J. J., Daroch M. Astaxanthin-producing green microalga *Haematococcus pluvialis*: From single cell to high value commercial products. *Frontiers in Plant Science*, 2016, vol. 7, art. no. 531 (28 p.). https://doi.org/10.3389/fpls.2016.00531
42. Solovchenko A., Minyuk G. The physiology of astaxanthin production by carotenogenic microalgae. In: *Global Perspectives on Astaxanthin. From Industrial Production to Food, Health, and Pharmaceutical Applications* / G. A. Ravishankar, A. Ranga Rao (Eds). London, UK ; San Diego, CA ; Cambridge, MA ; Oxford, UK : Academic Press, 2021, chap. 2, pp. 19–35. https://doi.org/10.1016/B978-0-12-823304-7.00026-X
43. Tamura K., Stecher G., Kumar S. MEGA11: Molecular Evolutionary Genetics Analysis version 11. *Molecular Biology and Evolution*, 2021, vol. 38, iss. 7, pp. 3022–3027. https://doi.org/10.1093/molbev/msab120

44. Trifinopoulos J., Nguyen L.-T., von Haeseler A., Minh B. Q. W-IQ-TREE: A fast online phylogenetic tool for maximum likelihood analysis. *Nucleic Acids Research*, 2016, vol. 44, iss. W1, pp. W232–W235. https://doi.org/10.1093/nar/gkw256
45. Voytsekhovich A., Beck A. Lichen photobionts of the rocky outcrops of Karadag massif (Crimean Peninsula). *Symbiosis*, 2016, vol. 68, iss. 1–3, pp. 9–24. https://doi.org/10.1007/s13199-015-0346-y
46. Wang Q., Song H., Liu X., Liu B., Hu Z., Liu G. Morphology and molecular phylogeny of coccoid green algae *Coelastrella* sensu lato (Scenedesmaceae, Sphaeropeales), including the description of three new species and two new varieties. *Journal of Phycology*, 2019, vol. 55, iss. 6, pp. 1290–1305. https://doi.org/10.1111/jpy.12915
47. White T. J., Bruns T., Lee S., Taylor J. Amplification and direct sequencing of fungal ribosomal RNA genes for phylogenetics. In: *PCR Protocols. A Guide to Methods and Applications* / M. A. Innis, D. H. Gelfand, J. J. Sninsky, T. White (Eds). San Diego, CA ; New York : Academic Press, 1990, pp. 315–322.
48. Wood A. M., Everroad R. C., Wingard L. M. Measuring growth rates in microalgal cultures. In: *Algal Culturing Techniques* / R. A. Andersen (Ed.). New York : Elsevier Academic Press, 2005, chap. 18, pp. 269–286.
49. Zhang Z., Schwartz S., Wagner L., Miller W. A greedy algorithm for aligning DNA sequences. *Journal of Computational Biology*, 2000, vol. 7, no. 1–2, pp. 203–214. https://doi.org/10.1089/10665270050081478

НОВЫЙ ШТАММ ЗЕЛЁНОЙ КАРОТИНОГЕННОЙ МИКРОВОДОРОСЛИ *COELASTRELLA RUBESCENS*, ПЕРСПЕКТИВНЫЙ ДЛЯ КУЛЬТИВИРОВАНИЯ В КЛИМАТИЧЕСКИХ УСЛОВИЯХ ЮГА РОССИИ

Н. В. Данцюк[1], О. В. Кривенко[1], И. М. Мансурова[1], И. В. Дегтяр[2]

[1]ФГБУН ФИЦ «Институт биологии южных морей имени А. О. Ковалевского РАН», Севастополь, Российская Федерация
[2]ФГАОУ ВО «Севастопольский государственный университет», Севастополь, Российская Федерация
E-mail: *krivenko@ibss-ras.ru*

Впервые из таллома эпилитного крымского лишайника выделена альгологически чистая культура зелёной каротиногенной микроводоросли рода *Coelastrella* Chodat (Scenedesmaceae, Sphaeropleales), которая характеризуется выраженной способностью к накоплению вторичных каротиноидов в условиях острого абиотического стресса. Детально описаны методы выделения фикобионта из малых навесок образца лишайника, получения альгологически чистой и аксеничной культур, адаптации клеток к условиям лабораторного культивирования и длительного хранения в коллекционном фонде. Выполнена таксономическая идентификация фикобионта с использованием морфологических подходов (световой и сканирующей электронной микроскопии) и молекулярно-генетических методов (анализа фрагмента последовательности региона ITS1 — 5.8S — ITS2 гена 18S rRNA). Полученный штамм внесён в каталог коллекции живых культур каротиногенных микроводорослей ФИЦ ИнБЮМ (https://algae.ibss-ras.ru) как IBSS-156 *Coelastrella rubescens* (Vinatzer) Kaufnerová & Eliás, 2013. Проведена оценка ростовых характеристик штамма IBSS-156 в условиях двухстадийной накопительной культуры. Получены данные, свидетельствующие о высоких, до (0,62 ± 0,11) сут$^{-1}$, удельных скоростях роста культуры

на вегетативной стадии. Динамика пигментного состава водорослей при действии комплексного стресса свидетельствует о накоплении вторичных каротиноидов. Показано, что регистрация спектров поглощения живых культур микроводорослей в видимой области может быть эффективным способом экспресс-оценки их состояния и скорости накопления кетокаротиноидов в биомассе в процессе двухстадийного культивирования. Результаты работы указывают на возможность выделения из крымских лишайников перспективных продуцентов астаксантина, которые могут быть предложены для массового культивирования в зонах с засушливым и жарким климатом, в том числе в Крыму и прилегающих районах юга России.

Ключевые слова: каротиногенные микроводоросли, фикобионты, *Coelastrella*, двухстадийное культивирование

1871
ИнБЮМ – IBSS

Морской биологический журнал
Marine Biological Journal
2025, vol. 10, no. 4, pp. 21–36
https://marine-biology.ru/mbj/article/view/498

UDC 591.69-438-512.222(665.2)

SCHISTOSOMA MANSONI (TREMATODA: SCHISTOSOMATIDAE) OCCURRENCE IN *BIOMPHALARIA PFEIFFERI* (GASTROPODA: PLANORBIDAE) IN WATER BODIES OF KINDIA PREFECTURE (REPUBLIC OF GUINEA)

© 2025 **E. Dmitrieva[1], S. Diakité[2], P. Koïvogui[2], N. Pronkina[1], V. Uppe[1], L. Konate[2], M. Sow[2], A. Balde[2], M. Camara[3], D. Polevoy[1], R. Machkevsky[1], E. Vodiasova[1], I. Keita[2], and A. Diallo[2]**

[1]A. O. Kovalevsky Institute of Biology of the Southern Seas of RAS, Sevastopol, Russian Federation
[2]Guinea Centre for Marine and Coastal Research, Conakry, Republic of Guinea
[3]Institute of Applied Biology, Kindia, Republic of Guinea
E-mail: *evdmitrieva@ibss-ras.ru*

Received 23.02.2025; revised 23.03.2025;
accepted 12.08.2025.

Molluscs of the genera *Biomphalaria* and *Bulinus*, intermediate hosts of human-pathogenic *Schistosoma* trematodes, were found in 8 freshwater bodies in the western region of Kindia Prefecture of Guinea. While *Bulinus* snails were free from schistosome infection, *Biomphalaria* specimens were parasitized, with infection foci revealed in 4 water bodies. Morphological analysis of shells of infected snails confirmed that they belong to the species *Biomphalaria pfeifferi*. The movement behavior, body shape, internal anatomy, and morphometric characteristics of the cercariae shed from the snails matched those of *Schistosoma mansoni*. The obtained ITS1 rDNA gene sequences showed 100% identity with homologous loci of *S. mansoni* parasitizing on humans and rats in Africa and Brazil. In contrast, they differed by 6 nucleotide substitutions from those of the closest relative, *S. rodhaini*, and by 2–6 substitutions from those of *S. rodhaini* × *S. mansoni* hybrids. Phylogenetic analysis strongly supported (100% bootstrap) the clustering of the sampled sequences with that of *S. mansoni*, distinct from those of *S. rodhaini* and hybrid lineages, confirming species identification. This study reports the first documented evidence of *S. mansoni* infection in *B. pfeifferi* and its molecular characterization in the Republic of Guinea. Infected snails (n = 32) were significantly larger on average than uninfected ones (n = 1,110) in samples where trematodes were found. Analysis of environmental factors revealed no effect of pH, dissolved oxygen, or water temperature within their observed ranges during the study period (October and November) on occurrence of *B. pfeifferi* and prevalence of infection with *S. mansoni*. Notably, *B. pfeifferi* exhibited tolerance to slightly hypoxic conditions, likely explaining their persistence in excrement-contaminated waters and facilitating schistosome larvae transmission. The presence of schistosomes was associated with specific biocenosis features, including slack or slow-flowing water and abundant submerged vegetation. All infected water bodies were located within urban areas. Obtained data are significant for developing schistosomiasis control strategies in the region.

Keywords: *Schistosoma*, schistosomiasis, natural focus of infection, intermediate hosts, *Biomphalaria*, ITS1 rDNA, Republic of Guinea

Human schistosomiasis is a tropical disease caused by six trematode species of the genus *Schistosoma* Weinland, 1858. Out of them, two species, *S. haematobium* (Bilharz, 1852) and *S. mansoni* Sambon, 1907, are responsible for 99% of schistosomiasis infections worldwide. The World Health Organization considers schistosomiasis to be one of the most serious tropical diseases, with approximately 90% of cases occurring in Africa [Onasanya et al., 2021]. Furthermore, the prevalence of schistosomiasis has increased among the African population over the past two decades [Salari et al., 2020]. Because of human migration from Africa to the Eurasian continent, climate warming, and the associated risk of introducing the trematode intermediate hosts, molluscs, to new areas, studying various aspects of schistosome ecology is relevant not only in African countries, but also in other ones, including Russia. Thus, publications have reported the recent spread of schistosomiasis in Corsica and Portugal, even among residents who have not visited endemic areas [Gabrielli, Garba Djirmay, 2023].

The spread of schistosomiasis is associated with two key factors: water contamination by human excrement containing parasite eggs and the presence of infected molluscs in natural water bodies. Current control programs focus on analyzing the infection rate in the population. However, human infection originates from free-swimming larvae: cercariae produced by schistosome sporocysts that parasitize snails. Even if parasite eggs are prevented from entering water, infected snails will continue to produce new cercariae for some time. Moreover, "human" *Schistosoma* species can parasitize other mammals [Aula et al., 2021] meaning that animal reservoirs allow the infection to circulate independently of humans. Therefore, preventing and treating infection in humans alone is insufficient to control the spread of schistosomiasis. It is also necessary to monitor the presence of the parasite in molluscs in water bodies.

A large number of various kinds of research, from morphology, biology, and ecology to genomic surveys, transcriptomic works, and development of PCR diagnostics, is focused on trematodes that cause human schistosomiasis, and also on other representatives of the family Schistosomatidae Stiles & Hassall, 1898 which they belong to (*e. g.*, [Alzaylaee et al., 2020; Gandasegui et al., 2016; Sato et al., 2018]). However, given the diversity of climatic conditions in regions where these helminths are revealed, the spread and variability of their mollusc hosts, the possible inclusion of "human" schistosomes in parasite systems of various reservoir and random hosts (both definitive and intermediate ones) [Aula et al., 2021], and the occurrence of interspecific hybrids [De Elías-Escribano et al., 2025; Savassi et al., 2020; Webster et al., 2013], data on their morphological, ecological, and molecular genetic characteristics in different habitats are still insufficient. For example, in literature, there is no information on the occurrence of *Schistosoma* species in molluscs in the Republic of Guinea. Notably, in the monograph [Brown, 2005], the presence of *S. mansoni* and *S. haematobium* in two molluscs, *Biomphalaria pfeifferi* (Krauss, 1848) and *Bulinus globosus* (Morelet, 1866), within Guinea is stated by registration of trematodes in humans and the occurrence in this region of both mollusc species, which are the main hosts of these parasites in Africa. In the genetic database GenBank NCBI (National Center for Biotechnological Information), among 556,222 records for various schistosome DNA fragments, there are no deposited nucleotide sequences of representatives of this genus from the Republic of Guinea [Nucleotide database, 2024].

Currently, two *Schistosoma* species pathogenic to humans, *S. mansoni* and *S. haematobium*, are known to be common among the population of Guinea. Both species are native for the territory of the republic [Aula et al., 2021]. According to the analysis of human surveys conducted in 1989–2019, the prevalence of the parasites varies 1 to 15% in different areas [Guilavogui et al., 2023]. However, some publications provide significantly higher values. Thus, in Forested Guinea, the occurrence of *S. mansoni*

in schoolchildren reached 86.1%, and that of *S. haematobium*, 75% [Hodges et al., 2011]. Besides, in the region neighboring Guinea (Guinea-Bissau, Cameroon, Equatorial Guinea, Gabon, and Nigeria), another species parasitizing humans occurs: *S. guineensis* [Kane et al., 2003; Webster et al., 2006]; interspecific hybrids were revealed as well [Savassi et al., 2020]. In the Republic of Guinea, it has not been registered so far. Given that species identification based on egg morphology (the most common method applied for schistosomiasis pathogens) may be inaccurate, especially for hybrids [De Elías-Escribano et al., 2025], it is necessary to confirm the data using molecular genetic markers. At the same time, accurate species identification is crucial for diagnosing and treating, assessing epidemiological consequences, and developing control strategies for natural foci of infection.

In connection with the above, the aims of the paper are to characterize the occurrence of human pathogenic schistosomes in molluscs in Kindia Prefecture (the Republic of Guinea), to identify *Schistosoma* species based on the morphology of cercariae and DNA sequences, and to analyze the relationship between the indicators of mollusc infection with schistosomes and environmental parameters.

MATERIAL AND METHODS

Sampling. In October and November 2024, on the territory of the Koya and Kindia prefectures (Kindia Region, the Republic of Guinea), 27 sites in the coastal zone of 21 water bodies were surveyed (see the map: https://www.google.com/maps/d/edit?mid=1JeRUjZ5VpumfQxLM7R-GmriHB73BXss&usp=sharing).

The following parameters were recorded at the sampling sites: water temperature and pH, dissolved O_2, and characteristics of the biocenosis – the presence of vegetation, the bottom type (rocky, sandy, or silty), and the relative flow velocity (slack water, weak flow, and strong flow). Physical and chemical parameters were measured with a multifunctional water quality tester DO-100 (China) calibrated and used in accordance with the manufacturer's protocol; the measurement error was ±1.5%. The list of the surveyed water bodies, the coordinates of the sampling sites, the hydrochemical characteristics, and the number of sampled molluscs are provided in the table (see Supplement 1: https://marine-biology.ru/mbj/article/view/498).

Mollusc species were identified based on the shell morphometric features in accordance with guides [Brown, 2005; Mandahl-Barth, 1957]. To analyze the normality of the distribution of mollusc sizes, the Shapiro–Wilk test, W, was used. To check the reliability of differences between their samples, the Mann–Whitney U test was applied. For both tests, $p \leq 0.05$.

Examination for the presence of parasites. The sampled molluscs were delivered to a laboratory and maintained in clean bottled water for 2 weeks. *Prior* to examination, those were kept in the shade for 48 h; then, the specimens were placed individually into containers with a small amount of clean water and exposed to natural light at 7:00. Emissions of cercariae were detected by examining the containers with molluscs under a Micromed MC-4-ZOOM LED stereomicroscope (China) at ×20 to ×30 magnification every 2 h until 16:00. Each sample was examined for 2–3 days. If schistosome cercariae were not found, a mollusc was dissected and examined for sporocyst infection. The detected cercariae, which by external features and movement pattern corresponded to those of the genus *Schistosoma*, and the infected molluscs were fixed in 70% and 96% ethanol, respectively, for subsequent morphological and molecular genetic studies.

The cercariae fixed in 70% ethanol were stained with alum carmine and differentiated in acidified 70% ethanol. After subsequent dehydration *via* an ethanol series (80–100%) and clearing in clove

oil, the specimens were mounted on a microscope slide in Canada balsam [Bykhovskaya-Pavlovskaya, 1985]. Measurements and description of the cercarial morphology were performed based on total mounts ($n = 17$), as well as on micrographs of live cercariae using an Olympus CX41 microscope (Japan) at ×200 to ×400 magnification, an Olympus SC50 digital camera, and CellSens Standard v. 1.18 software. Measurements of cercariae are given in mm (ranges and a mean value with the standard error in parentheses). The infection rate was characterized by the prevalence: the proportion of infected molluscs in a sample, %.

Molecular genetic investigation. Genomic DNA was isolated from a whole cercariae using a commercial PureLink Genomic DNA Mini Kit (Invitrogen, the USA) according to the manufacturer's protocol, with elution in the minimum recommended volume. The concentration and quality of the extracted DNA were determined with a Nano-500 spectrophotometer (Allsheng, China) and a Qubix fluorimeter (Syntol, Russia). Amplification of the ITS1 region of rDNA was performed with the primers BD1 (5'-GTCGTAACAAGGTTTCCGTA-3') and 4S (5'-TCTAGATGCGTTCGAARTGTCGATG-3') [Bowles, McManus, 1993]. The PCR reaction solution contained 5X ScreenMix (Evrogen, Russia), 5 pmol of each primer, and 5 ng·μL^{-1} of total genomic DNA. The amplification protocol was as follows: initial denaturation at +95 °C for 3 min; 35 cycles (+95 °C, 30 s; +55 °C, 30 s; +72 °C, 30 s); and a final extension at +72 °C for 7 min. The amplification products were detected by electrophoresis in a 1% agarose gel stained with ethidium bromide and visualized under ultraviolet light. The PCR products were sequenced in both directions with a BrilliantDye Terminator v3.1 kit (NimaGen, the Netherlands) on a Nanophor-5 genetic analyzer (Institute for Analytical Instrumentation of RAS, Russia).

The ITS1 sequence obtained was aligned with similar sequences available in GenBank NCBI for *S. mansoni* (PP658717, FJ750523, and JQ289742), *S. bovis* (PP312969, PP313016, and PP312959), *S. haematobium* (LC726151, PP963804, and PP963802), *S. rodhaini* (AF531312), and a *S. mansoni* × *S. rodhaini* hybrid (EU599364–EU599378) using MUSCLE algorithm implemented in MEGA 11 [Tamura et al., 2021]. *Schistosoma turkestanicum* sequence (MF145062) was used as the outgroup. A phylogenetic tree was constructed by the maximum likelihood and the GTR + G model (generalized time reversible with gamma distribution) [Rossi, 2018]. Bootstrap analysis with 1,000 repetitions was used to assess the reliability of the clusters.

RESULTS

Occurrence of *Schistosoma* trematodes. These trematodes were found in molluscs of the genus *Biomphalaria* Preston, 1910 in 4 out of the 27 water bodies surveyed in Kindia Prefecture (Table 1). Out of the 1,376 *Biomphalaria* snails examined, cercariae and sporocysts of schistosomes were registered in 32 ind. The percentage of infected snails in samples ranged within 1.2–5.6.

Notably, in addition to schistosomes, other trematodes were revealed in *Biomphalaria* molluscs: sporocysts and cercariae of the families Plagiorchidae and Echinostomatidae, as well as apharyngeal brevifurcocercariae and metacercariae, which could not be identified. Two *Biomphalaria* specimens infected with schistosomes were also co-infected with plagiorchiid sporocysts.

Identification of a mollusc species. Our samples covered specimens of three morphotypes corresponding to the genera *Biomphalaria*, *Radix* Montfort, 1810, and *Bulinus* O. F. Müller, 1781. No schistosome infection was revealed in representatives of the latter two genera.

Table 1. Characterization of *Biomphalaria* sp. samples and prevalence of *Schistosoma* sp.

Date	Sampling site	*Biomphalaria* sp.				PI, %
		Number, ind.	Shell length, mm	Number of infected molluscs, ind.	Shell length of infected molluscs, mm	
27.10.2024	Molokhoure 1	56	4.0–7.0	0	–	0
28.10.2024	Molokhoure 1	90	5.5–8.0	5	6.0–8.0	5.56
	Molokhoure 2	82	5.0–8.5	2	7.0	2.44
29.10.2024	Lac Bamba	106	5.0–8.0	0	–	0
	Foulayah 1	14	4.5–6.5	0	–	0
	Foulayah 2	24	5.0–6.5	0	–	0
31.10.2024	Yabara 1	34	4.5–6.0	0	–	0
	Yabara 2	327	5.0–10.0	6	6.0–7.5	1.83
	Sinanya fontaine	163	5.5–9.5	2	7.0; 8.0	1.23
01.11.2024	Molokhoure 1	172	6.0–9.5	7	6.5–9.0	4.07
	Molokhoure 2	154	6.5–9.0	7	7.0–9.0	4.55
	Sinanya fontaine	73	5.5–7.0	1	6.0	1.37
08.11.2024	Molokhoure 1	20	4.5–7.0	1	7.0	5.0
	Sinanya fontaine	61	5.0–8.0	1	7.0	1.64
In total, 8 sites		1,376	4.0–10.0	32	5.5–9.0	2.33

Note: PI is prevalence of infection. For coordinates of sampling sites, see Supplement 1: https://marine-biology.ru/mbj/article/view/498.

Biomphalaria representatives (Fig. 1) had an oval and flattened shell coiled in a single plane, making 3–4 whorls, with a smooth upper surface and a slightly obtuse-angled underside, featuring a deep umbilicus. The shell length (SL) was 4.0–10.0 mm (1,110 ind.), and the shell width (SW) was 3.5–7.0 mm (50 ind.). The aperture length (AL), its width (AW), and the umbilicus length (UL) were 3.0–5.0 mm (50 ind.), 2.0–3.0 mm (50 ind.), and 1.5–3.0 mm (50 ind.), respectively. Thus, the umbilicus occupied about ⅓ of the shell length. The height of the last whorl (SH) was 2.0–3.5 mm (50 ind.); it was approximately equal to the aperture width. Based on morphometric and morphological characteristics of shell, these molluscs were identified as *B. pfeifferi* [Brown, 2005; Mandahl-Barth, 1957].

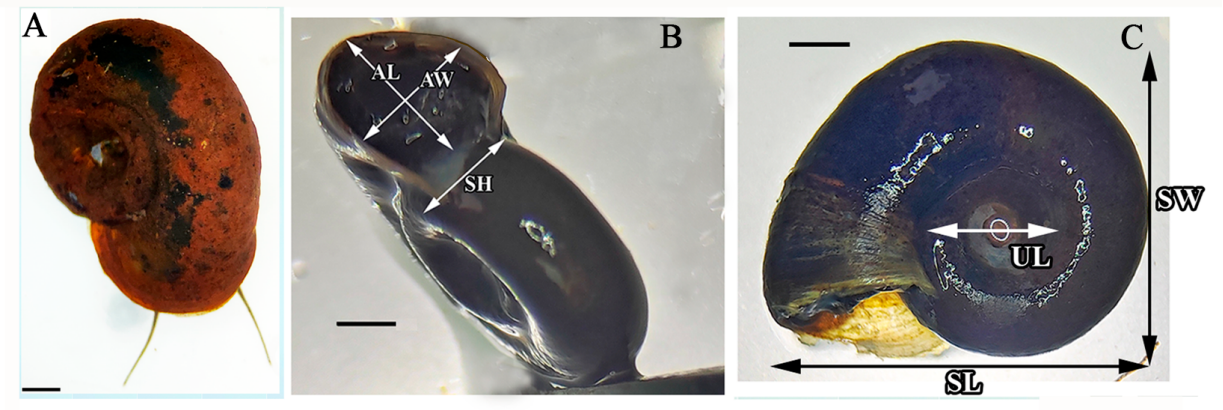


Fig. 1. *Biomphalaria pfeifferi* from water bodies in Kindia Prefecture (Guinea) (A) and scheme of the mollusc shell measurements (B, C). AL, aperture length; AW, aperture width; SH, the height of the last whorl (shell height); SL, shell length; SW, shell width; UL, umbilicus length. Scale bars are 1 mm

Identification of *Schistosoma* species based on morphological data. Daughter sporocysts and cercariae were found in *B. pfeifferi*; those were identified as trematodes of the genus *Schistosoma* based on their morphological characters and movement patterns (see Supplements 2 and 3: https://marine-biology.ru/mbj/article/view/498). Two daughter sporocysts, 0.365 and 0.488 mm long and 0.122 mm wide, were elongated sacs filled with cercariae of varying degree of maturity (Fig. 2A) which is consistent with the description of sporocysts of this genus [Ataev et al., 2016; Meuleman et al., 1980].

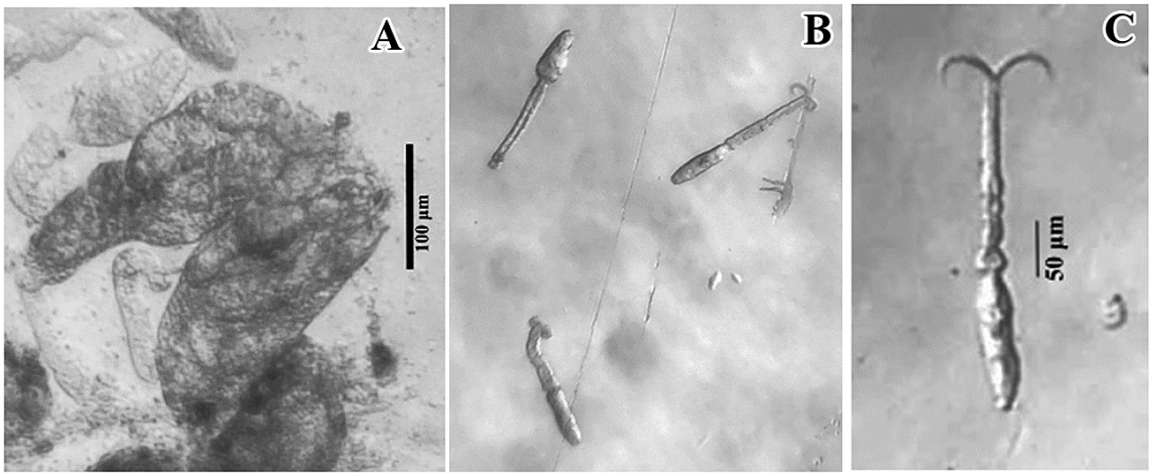


Fig. 2. *Schistosoma mansoni* sporocysts (A) and cercariae (B, C) from a mollusc *Biomphalaria pfeifferi* sampled in Kindia Prefecture (Guinea)

Cercariae are apharyngeal brevifurcocercariae without eye spots, with a typical forked tail (Fig. 2B, C, Fig. 3). Body oval, 0.122–0.139 mm long [(0.123 ± 0.003) mm], 0.044–0.058 mm maximum wide [(0.048 ± 0.009) mm], and 0.042–0.058 mm wide at the level of the ventral sucker [(0.046 ± 0.002) mm]. Tail stem cylindrical, slightly tapering distally; 0.144–0.180 mm long [(0.162 ± 0.008) mm] and 0.042–0.058 mm wide at the anterior end [(0.046 ± 0.002) mm]. Furcae 0.055–0.067 mm long [(0.062 ± 0.002) mm] and 0.006–0.012 mm wide [(0.009 ± 0.0006) mm]. Body and tail covered with minute spines. Oral sucker muscular, oval, 0.042–0.058 mm long [(0.046 ± 0.002) mm] and 0.027–0.033 mm wide [(0.03 ± 0.0005) mm], occupying about ⅓ of the body. Large pre- and postacetabular penetration gland cells in five pairs, fill nearly ⅔ of the body. Two pairs of preacetabular glands located anterior to the ventral sucker, with one pair, elongated and cylindrical, dorsally to the second pair, spheroidal. Three pairs of postacetabular glands, smaller and spheroidal ones, positioned posterior to the ventral sucker, slightly overlapping. Penetration gland ducts extend anteriorly and open at the anterior end of the body. Ventral sucker well-developed, 0.013–0.016 mm long [(0.015 ± 0.0005) mm] and 0.016–0.02 mm wide [(0.017 ± 0.0006) mm], placed in the posterior third of the body, 0.088–0.101 mm from the anterior end [(0.095 ± 0.002) mm]. Digestive system represented by esophagus: thin-walled tube with a spherical terminal dilation reaching the middle of the body. Mouth opening ventral. Nervous system consists of nerve cells forming clusters connected by thin fibers (neuropil) at the esophagus level. In the examined specimens, ciliated flame cells (cyrtocytes) and fine excretory capillaries arising from them not observed. Two larger excretory canals run anteriorly on either side of the body; two short canals located on either side of the anterior part of the tail stem; and a single excretory canal placed along the middle of the tail stem, opening at the tips of the furcae. Reproductive system undifferentiated and represented by some spherical cells posteriorly to the ventral sucker.

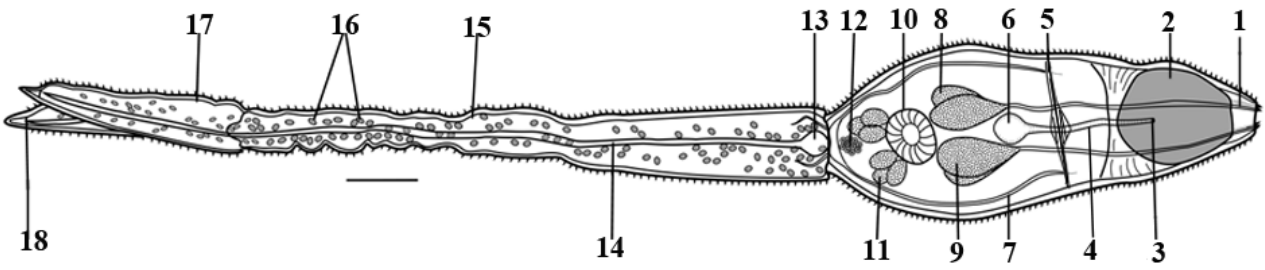


Fig. 3. Body shape and scheme of the internal morphology of *Schistosoma mansoni* cercariae from *Biomphalaria pfeifferi* molluscs sampled in Kindia Prefecture (Guinea): 1, penetration gland ducts; 2, oral sucker; 3, mouth; 4, esophagus; 5, neuropile; 6, caecum; 7, excretory ducts; 8, dorsal preacetabular gland; 9, ventral preacetabular gland; 10, ventral sucker (acetabulum); 11, postacetabular glands; 12, primordia of the reproductive system; 13, excretory bladder; 14, excretory canal; 15, tail; 16, sensilla on the tail surface; 17, tail furcae; 18, excretory pore. Scale bar is 0.02 mm

In general, the described cercariae are morphologically and morphometrically consistent with those of *S. mansoni* and *S. rodhaini* [Dorsey et al., 2002; Faust, 1919; Fripp, 1967; Skryabin, 1951; Stirewalt, 1974]. These species have nearly identical cercariae and both use *Biomphalaria* molluscs as intermediate hosts, but the second species has not been recorded in West Africa [Steinauer et al., 2008]. Taking this into account, the cercariae found were identified as *S. mansoni*.

Identification of *Schistosoma* species based on molecular genetic data. The ITS1 region (518 base pairs) was sequenced based on DNA extracted from *Schistosoma* cercariae from a mollusc *B. pfeifferi* sampled in Kindia Prefecture (the Republic of Guinea). Its sequence is available in GenBank NCBI under the accession number PV771189.

The obtained ITS1 fragment showed 100% identity with three similar DNA sequences of *S. mansoni* from Africa and Brazil (PP658717, FJ750523, and JQ289742). Comparison with a sequence of the closely related species, *S. rodhaini* (AF531312), revealed 6 nucleotide substitutions (98.96% identity). Comparison with sequences of *S. haematobium* (LC726151, PP963804, and PP963802) showed 95–96% identity (22–28 substitutions), and with *S. bovis*, 95% identity (28 substitutions). At the same time, this DNA locus differed by 2–6 substitutions (98.96–99.66% identity) from those of *S. mansoni* × *S. rodhaini* hybrid (EU599364–EU599378). However, phylogenetic analysis revealed that the sequenced sample and *S. mansoni* sequences formed a strongly supported clade, distinct from *S. rodhaini* and its hybrid with *S. mansoni* (Fig. 4). This result confirms that the found parasite belongs to *S. mansoni*.

Effect of mollusc size on *Schistosoma mansoni* occurrence. Sizes of the studied *B. pfeifferi* specimens were relatively small: the length of the molluscs did not exceed 1 cm (Table 1), while it can reach 1.5 cm. The material was sampled at the onset of the cold dry season (October and November), when *Biomphalaria* abundance was just starting to increase due to juveniles. Obviously, this affected the size composition: the predominance of small individuals caused a deviation from the normal distribution among uninfected snails (Table 2). At the same time, infected individuals, which were encountered much less frequently, showed a normal size distribution in most samples.

The mean length of *B. pfeifferi* infected with schistosomes was greater than that of uninfected individuals, but the differences between the samples were significant only for one sample (that with the number of infected snails exceeding 10) and when comparing all infected and uninfected molluscs (Table 2).

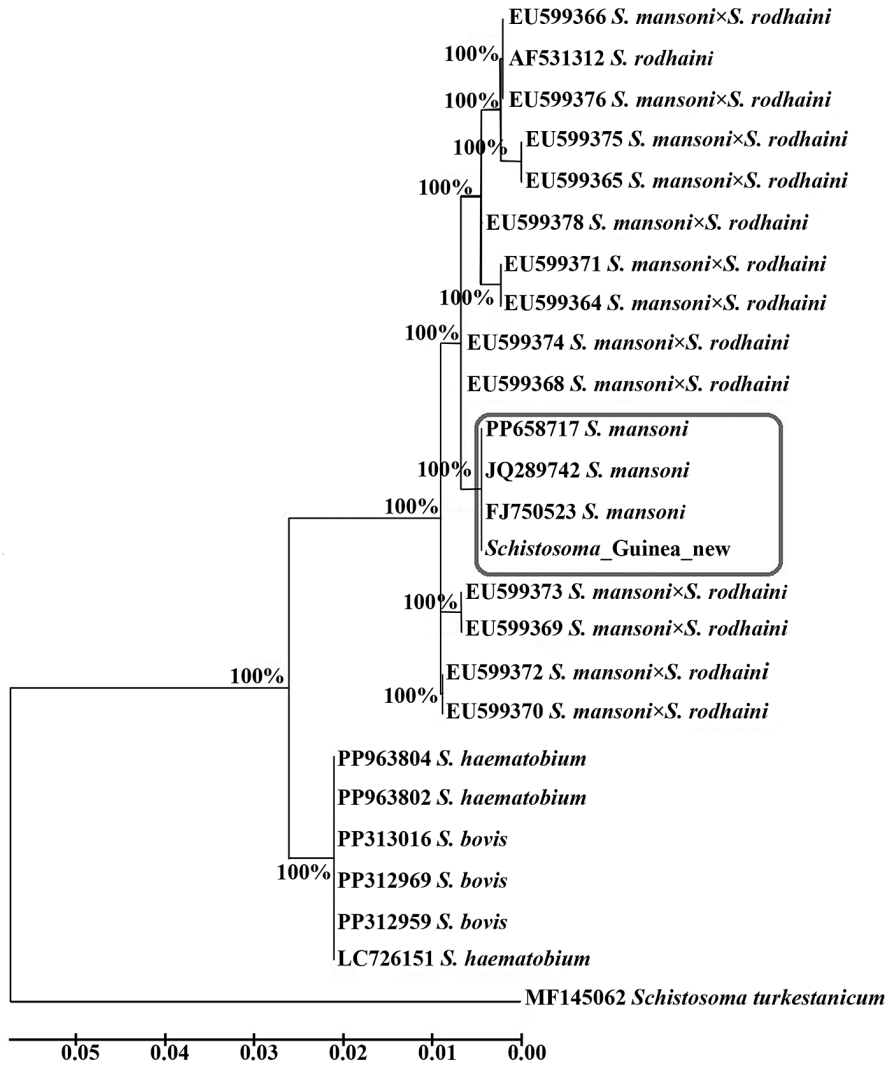


Fig. 4. Maximum likelihood phylogenetic tree based on ITS1 sequence showing the relationships between the *Schistosoma mansoni* sample from Guinea and related schistosome species available in GenBank NCBI. Nodal numbers are bootstrap support. Alignment length is 518 base pairs

Table 2. Characteristics of the distribution normality (Shapiro–Wilk test, *W*) of mollusc shell length and the significance of differences (Mann–Whitney *U* test) between samples of infected and uninfected specimens

Sampling site	Uninfected molluscs				Infected molluscs				Uninfected *vs.* infected molluscs	
	Number, ind.	Median length, mm	*W*	*p*	Number, ind.	Median length, mm	*W*	*p*	*U*	*p*
Molokhoure 1	269	7.0	0.94	< 0.01	13	7.5	0.94	**0.48**	1,177	**0.046**
Molokhoure 2	227	7.0	0.96	< 0.01	9	7.5	0.78	0.01	633	0.054
Yabara 2	321	7.0	0.94	< 0.01	6	6.8	0.96	**0.80**	914	0.833
Sinanya fontaine	293	6.5	0.92	< 0.01	4	7.0	–	–	–	–
All samples	1,110	7.0	0.95	< 0.01	32	7.3	0.94	**0.06**	12,192	**< 0.01**

Note: *p*-values indicating normal distribution and significance of differences between medians are highlighted in bold.

Effect of environmental parameters on *Schistosoma mansoni* occurrence. All water bodies where *Biomphalaria* molluscs, potential hosts of schistosomes, were recorded, were located within the city of Kindia (see Supplement 1: https://marine-biology.ru/mbj/article/view/498). Four sampling sites where schistosome invasion was revealed covered water bodies near private houses, schools, and public toilets with no wastewater treatment system (Figs 1, 2 in Supplement 1: https://marine-biology.ru/mbj/article/view/498); those are used by the local population for household needs and agricultural work.

Moreover, all water bodies in which molluscs of the genus *Biomphalaria* were registered were shallow, with slack or slow-flowing water, and abundantly overgrown with sedge and/or rice. However, among water bodies where *Biomphalaria* snails were not detected, half have the same biocenosis characteristics, and the ranges of physical and chemical parameters of water (pH, temperature, and dissolved oxygen) overlap (Table 3). A comparison of water bodies with molluscs as hosts but without cases of schistosome invasion and water bodies with reported invasion also revealed an overlap of the values of the analyzed abiotic factors.

The reduced dissolved O_2 content is obviously not a limiting factor for either *Biomphalaria* representatives or schistosomes. Thus, several water bodies where these molluscs and trematodes were revealed had the values < 5 mg·L^{-1} (see Table 3). In the biocenoses, the environmental acidity ranged from slightly acidic to slightly alkaline. No relationship between these factors and the occurrence of molluscs in water bodies was determined. Notably, the highest density of *Biomphalaria* populations was recorded at the Yabara 2 station where the environment was slightly acidic (see Supplement 1: https://marine-biology.ru/mbj/article/view/498).

Table 3. Comparative characteristics of surveyed water bodies with *Biomphalaria pfeifferi* and *Schistosoma mansoni* and without these species

Occurrence of *Biomphalaria* and *Schistosoma* in samples	Number of sampling sites	Physical and chemical parameters			Biocenosis characteristics			
		pH	T, °C	O_2, mg·L^{-1}	Current	Bottom type	Depth, m	Vegetation
No molluscs	19	4.5–6.8	+27…+34	3.3–10.3	S, 50%, W, 50%	R, 13%, Sn, 37%, Sl, 50%	0.5–1.5	In, 50%, Ab, 50%
Uninfected molluscs	4	6.3–6.8	+28…+34	4.3–5.0	W, 100%	Sl, 100%	0.02–0.5	Ab, 100%
Infected molluscs	4	5.8–7.8	+29…+32	4.5–6.1	W, 100%	Sl, 100%	0.02–0.4	Ab, 100%

Note: in the biocenosis characteristics, the proportions of sites with the corresponding parameters from the total number of sampling sites are indicated. Current (flow velocity): S, strong flow; W, weak flow or slack water. Bottom type: R, rocky; Sn, sandy; Sl, silty. Vegetation: In, an insignificant amount of semi-submerged and submerged vegetation; Ab, abundant semi-submerged and submerged vegetation.

DISCUSSION

Despite the fact that *S. mansoni* natural range covers the Republic of Guinea [Aula et al., 2021], with an infection rate up to 86% in the population in some regions [Hodges et al., 2011], data on the prevalence of infection in an intermediate host, *B. pfeifferi*, were obtained there for the first time.

Morphology-based identification of schistosome cercariae is challenging due to a small set of characters used and the existence of similar species and hybrids [Steinauer et al., 2008]. Thus, schistosome cercariae from *Biomphalaria* snails sampled in freshwater bodies of Kindia Prefecture (the Republic of Guinea) are morphologically similar to both *S. mansoni* and *S. rodhaini* which parasitizes the same mollusc. Moreover, in nature, these species can form hybrids [Morgan et al., 2003]. So far, *S. rodhaini* has been registered only in East Africa [Steinauer et al., 2008], although we cannot exclude that this species may be recorded in other regions where its hosts occur. To distinguish *S. mansoni* and *S. rodhaini*, it was proposed to use the ITS1 region of the ribosomal DNA cluster which showed stable differences between these species in three base pairs [Steinauer et al., 2008]. The ITS1 sequence obtained in this study differed from that of *S. rodhaini* in these base pairs and three more ones. This allows us to confidently identify the cercariae we found as *S. mansoni*. Thus, *B. pfeifferi* infection with these trematodes in Guinean water bodies has been proven for the first time.

The prevalence of infection (see Table 1) was generally consistent with the infection level of *Biomphalaria* snails with *S. mansoni* trematodes in Africa: 5.6% on average [Hailegebriel et al., 2020]. However, a recent study in Côte d'Ivoire, a neighboring country to Guinea, reported significantly higher *S. mansoni* occurrence: up to 100% of infected molluscs in a sample (56% on average) [Sokouri et al., 2024]. Noticeable (differing by orders of magnitude) seasonal variations in the infection with schistosomes in *Biomphalaria* molluscs have previously been established, as well as regional variations in the revealed dynamics. Thus, in Senegal and Uganda, *S. mansoni* occurrence in *B. pfeifferi* varied 0.08 to 3.7% and 8.7 to 13.3%, respectively, and was higher during the rainy seasons [Andrus et al., 2023; Bakhoum et al., 2021], while in Ethiopia, the values ranged 1.5 to 10.6% and were higher during the dry season [Hailegebriel et al., 2022]. So, to assess levels of *S. mansoni* infection for *Biomphalaria* molluscs in Guinean water bodies and to reveal seasonal peaks, similar studies should be carried out during the wet season.

Furthermore, molluscs infected with schistosomes were found only in water bodies within the city of Kindia. According to surveys of 2010–2016, the infection level of the city population with this trematode ranged 4.5 to 34% [Guilavogui et al., 2023]. Importantly, in 2010, for the age group of 1–17 years, the value was 5%, and in 2016, it was 34%. It is obvious that the infection levels of molluscs and final hosts, humans, are interconnected. It is necessary to continue studying *S. mansoni* occurrence in water bodies of the region in order to determine the reasons for the increase in the infection level among people.

It has been previously shown as follows: abiotic and biotic environmental conditions can noticeably affect both the occurrence of molluscs, potential hosts of *Schistosoma* trematodes, and the spread of cercariae [Brown, 2005]. First of all, the growth rate and population size of *Biomphalaria* snails depend on abiotic factors: depth, flow velocity, bottom type, and physical and chemical parameters of water [McCreesh, Booth, 2014]. Thus, the highest population density of molluscs was recorded for a depth of < 30 cm, silty bottom, and weak flow [Brown, 2005; Magero et al., 2025; McCreesh, Booth, 2014]. This is consistent with the results of our studies: *Biomphalaria* snails were found only in shallow bodies (< 60 cm), with a weak flow or slack water and with a silty bottom (Table 3).

However, we did not reveal a dependence of *Biomphalaria* occurrence and its infection with schistosomes on temperature, pH, and dissolved O_2 content in water; this is likely to result from the small range of values of the parameters analyzed (Table 2) within one month of the study. As shown

for neighboring Senegal, the abundance of molluscs and *S. mansoni* occurrence in them are positively correlated with the values of temperature and oxygen and negatively with pH (parameters which vary across the seasons) [Bakhoum et al., 2019].

Notably, most surveyed water bodies *Biomphalaria* snails were found in were characterized by relatively low levels of dissolved O_2: 4.3–5.0 mg·L^{-1}. Moderate eutrophication accompanied by a drop in the oxygen content in water has previously been shown to facilitate the development of *Biomphalaria* representatives [Hoover et al., 2020]. Such a tolerance of these snails to O_2 deficiency in water contributes to their occurrence in excrement-contaminated water and forms conditions for mollusc infection with schistosome larvae.

Temperature is an important factor that not only limits the geographic distribution of *B. pfeifferi* to tropical and subtropical regions but also regulates its fecundity and mortality [Bakhoum et al., 2021]. Experiments have shown that *Biomphalaria* molluscs are active at +18…+32 °C, while the optimal range for their reproduction and survival is +20…+26 °C [Sturrock, 1965]. In Senegal, for example, the highest density of *Biomphalaria* snails was recorded at +20…+32.5 °C [Bakhoum et al., 2021], and in East African water bodies, those were not found at sites where the temperature exceeded +30 °C [Magero et al., 2025]. Within this study, *Biomphalaria* representatives were sampled from water bodies with the water temperature reaching +34 °C. The temperature conditions the molluscs are adapted to seem to vary by region; in the Republic of Guinea, a range of +30…+34 °C does not limit *B. pfeifferi* occurrence.

Water temperature affects not only mollusc population, but also the development of sporocysts and the production of schistosome cercariae. According to the results of experiments, an increase in temperature from +23 to +33 °C reduces the development period of *S. mansoni* sporocysts in molluscs [Stirewalt, 1974]. The emission of cercariae is limited to a range of +16…+35 °C, decreasing by approximately three times at temperatures below +18 °C or above +33 °C [Pflüger, 1980]. After analyzing a large set of empirical data on the effect of temperature on both molluscs and schistosomes, I. H. Aslan *et al.* [2024] established a theoretical temperature optimum for the spread of *S. mansoni* in sub-Saharan African waters: +23…+27 °C. These values are lower than the temperatures at which schistosome-infected molluscs were found in Guinean waters (Table 3); this may evidence for the fact that infection level in the region may be higher (under different temperature conditions) than the level established in the present study.

Another characteristic of the biocenosis, which is considered a key factor affecting the spread of schistosomes, is the presence of semi-submerged and submerged vegetation. The high abundance of aquatic plants is positively related with the abundance of mollusc hosts of *S. mansoni* [Brown, 2005]; also, it may be positively correlated with the number of schistosome cercariae produced by infected snails [Haggerty et al., 2020]. In the present study, *B. pfeifferi*, both infected with *S. mansoni* and uninfected, were found only in water bodies abundantly covered with semi-submerged plants: sedge and rice (Table 3).

It was also shown that the level of schistosome infection depends on the mollusc size. Thus, as established experimentally, the size of *Biomphalaria* snails was negatively correlated with susceptibility to *S. mansoni* infection, and this seems to be due to their increased immunity with age. The smallest molluscs (1.5–2.9 mm) had the highest infection level and produced the largest number of cercariae [Spaan et al., 2023]. However, the relationship between the size and age of molluscs and their infection with schistosomes under natural conditions is more complex, is mediated by many factors (the number of snail generations *per* year, their population density, and the survival of infected individuals), and can vary

depending on the season [Woolhouse, 1989]. In our samples, infected *B. pfeifferi* were on average larger (see Table 2), but the largest and smallest snails were uninfected. This is probably governed by the study period: October and November are the onset of the dry season marking the development of a new generation of molluscs, and they have not yet been infected with schistosomes.

The obtained results are limited to one season and region of the Republic of Guinea. Those demonstrate the need to continue research on mollusc infection with schistosomes in various regions of the country to understand the conditions of the parasite transmission to humans. It is important for developing measures to control schistosomiasis at the local level.

The work was carried out with the financial support of the project of the Russian Federation represented by the Ministry of Science and Higher Education of the Russian Federation: a grant in the form of subsidies in accordance with paragraph 4 of article 78.1 of the Budget Code of the RF (agreement No. 075-15-2024-655 on the project No. 13.2251.21.0260).

REFERENCES

1. Ataev G. L., Bazhenova D. R., Tokmakova A. S. Reproduction of *Schistosoma mansoni* mother sporocyst. *Parazitologiya*, 2016, vol. 50, no. 2, pp. 114–120. (in Russ.). https://elibrary.ru/vrnyhr
2. Bykhovskaya-Pavlovskaya I. E. *Parazity ryb. Rukovodstvo po izucheniyu* / AN SSSR, Zoologicheskii institut. Leningrad : Nauka, Leningr. otd-nie, 1985, 121 p. (in Russ.). https://doi.org/10.21072/bykhovskaya-pavlovskaya-1985
3. Skryabin K. I. *Trematody zhivotnykh i cheloveka. Osnovy trematodologii.* Vol. 5 / AN SSSR, Gel'mintologicheskaya laboratoriya. Moscow : Izd-vo AN SSSR, 1951, 624 p. (in Russ.)
4. Alzaylaee H., Collins R. A., Shechonge A., Ngatunga B. P., Morgan E. R., Genner M. J. Environmental DNA-based xenomonitoring for determining *Schistosoma* presence in tropical freshwaters. *Parasites & Vectors*, 2020, vol. 13, art. no. 63 (11 p.). https://doi.org/10.1186/s13071-020-3941-6
5. Andrus P. S., Stothard J. R., Wade C. M. Seasonal patterns of *Schistosoma mansoni* infection within *Biomphalaria* snails at the Ugandan shorelines of Lake Albert and Lake Victoria. *PLoS Neglected Tropical Diseases*, 2023, vol. 17, iss. 8, art. no. e0011506 (18 p.). https://doi.org/10.1371/journal.pntd.0011506
6. Aslan I. H., Pourtois J. D., Chamberlin A. J., Mitchell K. R., Mari L., Lwiza K. M., Wood C. L., Mordecai E. A., Yu A., Tuan R., Palasio R. G. S., Monteiro A. M. V., Kirk D., Athni T. S., Sokolow S. H., N'Goran E. K., Diakite N. R., Ouattara M., Gatto M., Casagrandi R., Little D. C., Ozretich R. W., Norman R., Allan F., Brierley A. S., Liu P., Pereira T. A., de Leo G. A. Re-assessing thermal response of schistosomiasis transmission risk: Evidence for a higher thermal optimum than previously predicted. *PLoS Neglected Tropical Diseases*, 2024, vol. 18, iss. 6, art. no. e0011836 (23 p.). https://doi.org/10.1371/journal.pntd.0011836
7. Aula O. P., McManus D. P., Jones M. K., Gordon C. A. Schistosomiasis with a focus on Africa. *Tropical Medicine and Infectious Disease*, 2021, vol. 6, iss. 3, art. no. 109 (40 p.). https://doi.org/10.3390/tropicalmed6030109
8. Bakhoum S., Ba C. T., Haggerty C. J. E., Jouanard N., Riveau G., Rohr J. R. Risk of human exposure to the intestinal schistosome, *Schistosoma mansoni*, across seasons along the Senegal River. *Journal of Gastroenterology & Hepatology Research*, 2021, vol. 6, iss. 2, art. no. 038 (9 p.). https://doi.org/10.24966/ghr-2566/100038
9. Bakhoum S., Ndione R. A., Haggerty C. J. E., Wolfe C., Sow S., Ba C. T., Riveau G., Rohr J. R. Influence des paramètres physico-chimiques sur la répartition spatiale des mollusques hôtes intermédiaires des schistosomes humains dans le delta du fleuve Sénégal. *Médecine et Santé*

Tropicales, 2019, vol. 29, no. 1, pp. 61–67.

10. Bowles J., McManus D. P. Rapid discrimination of *Echinococcus* species and strains using a polymerase chain reaction-based RFLP method. *Molecular and Biochemical Parasitology*, 1993, vol. 57, iss. 2, pp. 231–239. https://doi.org/10.1016/0166-6851(93)90199-8
11. Brown D. S. *Freshwater Snails of Africa and Their Medical Importance.* 2nd edition. London : Taylor & Francis, 2005, 642 p.
12. De Elías-Escribano A., Artigas P., Salas-Coronas J., Luzon-Garcia M. P., Reguera-Gomez M., Cabeza-Barrera M. I., Vázquez-Villegas J., Boissier J., Mas-Coma S., Bargues M. D. *Schistosoma mansoni* × *S. haematobium* hybrids frequently infecting sub-Saharan migrants in southeastern Europe: Egg DNA genotyping assessed by RD-PCR, sequencing and cloning. *PLoS Neglected Tropical Diseases*, 2025, vol. 19, iss. 3, art. no. e0012942 (27 p.). https://doi.org/10.1371/journal.pntd.0012942
13. Dorsey C. H., Cousin C. E., Lewis F. A., Stirewalt M. A. Ultrastructure of the *Schistosoma mansoni* cercaria. *Micron*, 2002, vol. 33, iss. 3, pp. 279–323. https://doi.org/10.1016/s0968-4328(01)00019-1
14. Faust E. C. Notes on South African cercariae. *The Journal of Parasitology*, 1919, vol. 5, no. 4, pp. 164–175. https://doi.org/10.2307/3271082
15. Fripp P. J. On the morphology of *Schistosoma rodhaini* (Trematoda, Digenea, Schistosomatidae). *Journal of Zoology*, 1967, vol. 151, iss. 4, pp. 433–452. https://doi.org/10.1111/j.1469-7998.1967.tb02124.x
16. Gabrielli A. F., Garba Djirmay A. Schistosomiasis in Europe. *Current Tropical Medicine Reports*, 2023, vol. 10, iss. 3, pp. 79–87. https://doi.org/10.1007/s40475-023-00286-9
17. Gandasegui J., Fernández-Soto P., Hernández-Goenaga J., López-Abán J., Vicente B., Muro A. Biompha-LAMP: A new rapid loop-mediated isothermal amplification assay for detecting *Schistosoma mansoni* in *Biomphalaria glabrata* snail host. *PLoS Neglected Tropical Diseases*, 2016, vol. 10, iss. 12, art. no. e0005225 (14 p.). https://doi.org/10.1371/journal.pntd.0005225
18. Guilavogui T., Verdun S., Koïvogui A., Viscogliosi E., Certad G. Prevalence of intestinal parasitosis in Guinea: Systematic review of the literature and meta-analysis. *Pathogens*, 2023, vol. 12, iss. 2, art. no. 336 (30 p.). https://doi.org/10.3390/pathogens12020336
19. Haggerty C. J. E., Bakhoum S., Civitello D. J., de Leo G. A., Jouanard N., Ndione R. A., Remais J. V., Riveau G., Senghor S., Sokolow S. H., Sow S., Wolfe C., Wood C. L., Jones I., Chamberlin A. J., Rohr J. R. Aquatic macrophytes and macroinvertebrate predators affect densities of snail hosts and local production of schistosome cercariae that cause human schistosomiasis. *PLoS Neglected Tropical Diseases*, 2020, vol. 14, iss. 7, art. no. e0008417 (25 p.). https://doi.org/10.1371/journal.pntd.0008417
20. Hailegebriel T., Nibret E., Munshea A. Distribution and seasonal abundance of *Biomphalaria* snails and their infection status with *Schistosoma mansoni* in and around Lake Tana, northwest Ethiopia. *Scientific Reports*, 2022, vol. 12, art. no. 17055 (12 p.). https://doi.org/10.1038/s41598-022-21306-0
21. Hailegebriel T., Nibret E., Munshea A. Prevalence of *Schistosoma mansoni* and *S. haematobium* in snail intermediate hosts in Africa: A systematic review and meta-analysis. *Journal of Tropical Medicine*, 2020, vol. 2020, art. no. 8850840 (18 p.). https://doi.org/10.1155/2020/8850840
22. Hodges M., Koroma M. M., Baldé M. S., Turay H., Fofanah I., Divall M. J., Winkler M. S., Zhang Y. Current status of schistosomiasis and soil-transmitted helminthiasis in Beyla and Macenta Prefectures, Forest Guinea. *Transactions of the Royal Society of Tropical Medicine and Hygiene*, 2011, vol. 105, iss. 11, pp. 672–674. https://doi.org/10.1016/j.trstmh.2011.07.008
23. Hoover C. M., Rumschlag S. L., Strgar L., Arakala A., Gambhir M., de Leo G. A., Sokolow S. H., Rohr J. R., Remais J. V. Effects of agrochemical pollution on schistosomiasis transmission: A systematic review and modelling analysis. *The Lancet Planetary Health*, 2020, vol. 4, iss. 7, pp. e280–e291.

24. Kane R. A., Southgate V. R., Rollinson D., Littlewood D. T. J., Lockyer A. E., Pagès J. R., Tchuem Tchuenté L.-A., Jourdane J. A phylogeny based on three mitochondrial genes supports the division of *Schistosoma intercalatum* into two separate species. *Parasitology*, 2003, vol. 127, pt 2, pp. 131–137. https://doi.org/10.1017/s0031182003003421
25. Magero V. O., Kisara S., Suleman M. A., Wade C. M. Distribution of the schistosome intermediate snail host *Biomphalaria pfeifferi* in East Africa's river systems and the prevalence of *Schistosoma mansoni* infection. *Transactions of the Royal Society of Tropical Medicine and Hygiene*, 2025, vol. 119, iss. 3, pp. 253–265. https://doi.org/10.1093/trstmh/trae115
26. Mandahl-Barth G. Intermediate hosts of *Schistosoma*. African *Biomphalaria* and *Bulinus*: I. *Bulletin of the World Health Organization*, 1957, vol. 16, no. 6, pp. 1103–1163.
27. Meuleman E. A., Holzmann P. J., Peet R. C. The development of daughter sporocysts inside the mother sporocyst of *Schistosoma mansoni* with special reference to the ultrastructure of the body wall. *Zeitschrift für Parasitenkunde*, 1980, vol. 61, iss. 3, pp. 201–212. https://doi.org/10.1007/bf00925512
28. McCreesh N., Booth M. The effect of increasing water temperatures on *Schistosoma mansoni* transmission and *Biomphalaria pfeifferi* population dynamics: An agent-based modelling study. *PLoS One*, 2014, vol. 9, iss. 7, art. no. e101462 (7 p.). https://doi.org/10.1371/journal.pone.0101462
29. Morgan J. A. T., DeJong R. J., Lwambo N. J. S., Mungai B. N., Mkoji G. M., Loker E. S. First report of a natural hybrid between *Schistosoma mansoni* and *S. rodhaini*. *Journal of Parasitology*, 2003, vol. 89, iss. 2, pp. 416–418. https://doi.org/10.1645/0022-3395(2003)089[0416:froanh]2.0.CO;2
30. Nucleotide database. In: *National Library of Medicine. National Center for Biotechnology Information* : official site. 2024. URL: https://www.ncbi.nlm.nih.gov/nucleotide/ [accessed: 27.11.2024].
31. Onasanya A., Bengtson M., Oladepo O., Van Engelen J., Diehl J. C. Rethinking the top-down approach to schistosomiasis control and elimination in sub-Saharan Africa. *Frontiers in Public Health*, 2021, vol. 9, art. no. 622809 (6 p.). https://doi.org/10.3389/fpubh.2021.622809
32. Pflüger W. Experimental epidemiology of schistosomiasis. *Zeitschrift für Parasitenkunde*, 1980, vol. 63, iss. 2, pp. 159–169. https://doi.org/10.1007/bf00927532
33. Rossi R. J. *Mathematical Statistics: An Introduction to Likelihood Based Inference.* New York : John Wiley & Sons, 2018, 448 p.
34. Salari P., Fürst T., Knopp S., Utzinger J., Tediosi F. Cost of interventions to control schistosomiasis: A systematic review of the literature. *PLoS Neglected Tropical Diseases*, 2020, vol. 14, iss. 3, art. no. e0008098 (23 p.). https://doi.org/10.1371/journal.pntd.0008098
35. Savassi B. A. E. S., Mouahid G., Lasica C., Mahaman S.-D. K., Garcia A., Courtin D., Allienne J.-F., Ibikounlé M., Moné H. Cattle as natural host for *Schistosoma haematobium* (Bilharz, 1852) Weinland, 1858 × *Schistosoma bovis* Sonsino, 1876 interactions, with new cercarial emergence and genetic patterns. *Parasitology Research*, 2020, vol. 119, iss. 7, pp. 2189–2205. https://doi.org/10.1007/s00436-020-06709-0
36. Sato M. O., Rafalimanantsoa A., Ramarokoto C., Rahetilahy A. M., Ravoniarimbinina P., Kawai S., Minamoto T., Sato M., Kirinoki M., Rasolofo V., De Calan M., Chigusa Y. Usefulness of environmental DNA for detecting *Schistosoma mansoni* occurrence sites in Madagascar. *International Journal of Infectious Diseases*, 2018, vol. 76, pp. 130–136. https://doi.org/10.1016/j.ijid.2018.08.018
37. Sokouri E. A., Ahouty Ahouty B., N'Djetchi M., Abé I. A., Yao B. G. F. D., Konan T. K., MacLeod A., Noyes H., Nyangiri O., Enock Matovu E., Koffi M. Impact of environmental factors on *Biomphalaria pfeifferi* vector capacity leading to human infection by *Schistosoma mansoni* in two regions of western Côte d'Ivoire. *Parasites & Vectors*, 2024, vol. 17, art. no. 179 (12 p.). https://doi.org/10.1186/s13071-024-06163-2

38. Spaan J. M., Pennance T., Laidemitt M. R., Sims N., Roth J., Lam Y., Rawago F., Ogara G., Loker E. S., Odiere M. R., Steinauer M. L. Multi-strain compatibility polymorphism between a parasite and its snail host, a neglected vector of schistosomiasis in Africa. *Current Research in Parasitology & Vector-Borne Diseases*, 2023, vol. 3, art. no. 100120 (10 p.). https://doi.org/10.1016/j.crpvbd.2023.100120
39. Steinauer M. L., Hanelt B., Mwangi I. N., Maina G. M., Agola L. E., Kinuthia J. M., Mutuku M. W., Mungai B. N., Wilson W. D., Mkoji G. M., Loker E. S. Introgressive hybridization of human and rodent schistosome parasites in western Kenya. *Molecular Ecology*, 2008, vol. 17, iss. 23, pp. 5062–5074. https://doi.org/10.1111/j.1365-294x.2008.03957.x
40. Stirewalt M. A. *Schistosoma mansoni*: Cercaria to schistosomule. In: *Advances in Parasitology* / B. Dawes (Ed.). London ; New York : Academic Press, 1974, vol. 12, pp. 115–182. https://doi.org/10.1016/S0065-308X(08)60388-7
41. Sturrock R. F. The development of irrigation and its influence on the transmission of bilharziasis in Tanganyika. *Bulletin of the World Health Organization*, 1965, vol. 32, no. 2, pp. 225–236.
42. Tamura K., Stecher G., Kumar S. MEGA11: Molecular Evolutionary Genetics Analysis version 11. *Molecular Biology and Evolution*, 2021, vol. 38, iss. 7, pp. 3022–3027. https://doi.org/10.1093/molbev/msab120
43. Webster B. L., Southgate V. R., Littlewood D. T. J. A revision of the interrelationships of *Schistosoma* including the recently described *Schistosoma guineensis*. *International Journal for Parasitology*, 2006, vol. 36, iss. 8, pp. 947–955. https://doi.org/10.1016/j.ijpara.2006.03.005
44. Webster B. L., Diaw O. T., Seye M. M., Webster J. P., Rollinson D. Introgressive hybridization of *Schistosoma haematobium* group species in Senegal: Species barrier break down between ruminant and human schistosomes. *PLoS Neglected Tropical Diseases*, 2013, vol. 7, iss. 4, art. no. e2110 (9 p.). https://doi.org/10.1371/journal.pntd.0002110
45. Woolhouse M. E. On the interpretation of age-prevalence curves for schistosome infections of host snails. *Parasitology*, 1989, vol. 99, pt 1, pp. 47–56. https://doi.org/10.1017/s0031182000061011

ВСТРЕЧАЕМОСТЬ *SCHISTOSOMA MANSONI* (TREMATODA: SCHISTOSOMATIDAE) У *BIOMPHALARIA PFEIFFERI* (GASTROPODA: PLANORBIDAE) В ВОДОЁМАХ ПРЕФЕКТУРЫ КИНДИЯ (ГВИНЕЙСКАЯ РЕСПУБЛИКА)

Е. В. Дмитриева[1], С. Диаките[2], П. Койвоги[2], Н. В. Пронькина[1], В. А. Уппе[1], Л. Конате[2], М. Д. Соу[2], А. М. Балде[2], М. Камара[3], Д. М. Полевой[1], Р. В. Мачкевский[1], Е. А. Водясова[1], И. Кейта[2], А. И. П. Диалло[2]

[1]ФГБУН ФИЦ «Институт биологии южных морей имени А. О. Ковалевского РАН», Севастополь, Российская Федерация
[2]Центр морских и прибрежных исследований Гвинеи, Конакри, Гвинейская Республика
[3]Институт прикладной биологии, Киндия, Гвинейская Республика
E-mail: *evdmitrieva@ibss-ras.ru*

На территории Гвинейской Республики, в западной области префектуры Киндия, в 8 пресноводных водоёмах найдены моллюски родов *Biomphalaria* и *Bulinus* — промежуточные хозяева трематод рода *Schistosoma*, патогенных для человека. Моллюски *Bulinus* были свободны от шистосом, в то время как биомфалярии были ими заражены. В 4 водоёмах выявлены очаги заражённости моллюсков этим паразитом. На основе морфологического анализа раковин заражённых моллюсков установлена их принадлежность к виду *Biomphalaria pfeifferi*. Особенности движения,

форма тела, внутренняя анатомия и морфометрические характеристики церкарий, выходящих из моллюсков, соответствовали таковым *S. mansoni*. Полученные последовательности участка ITS1 рДНК показали 100%-ную идентичность с аналогичными локусами *S. mansoni*, паразитирующих у людей и крыс из Африки и Бразилии. В то же время они отличались от таковых ближайшего вида, *S. rodhaini*, на 6 нуклеотидных замен, а от таковых его гибридов с *S. mansoni* — на 2–6 замен. Филогенетический анализ показал достоверное (100 %) включение секвенированной пробы в кластер с другими последовательностями *S. mansoni* и дистанцирование от линий *S. rodhaini* и гибридов *S. rodhaini* × *S. mansoni*. Этот результат подтверждает идентификацию вида как *S. mansoni*. Данные о встречаемости этого паразита у моллюсков, а также последовательности его ДНК получены для территории Гвинеи впервые. В целом заражённые моллюски (32 экз.) имели достоверно бóльшие средние размеры раковин, чем незаражённые (1110 экз.). Анализ влияния ряда факторов среды на встречаемость моллюсков *B. pfeifferi* и их заражённость трематодами *S. mansoni* не выявил их зависимости от pH, насыщенности кислородом и температуры воды в пределах изменчивости этих показателей в период исследования (октябрь — ноябрь). Отмечена относительная толерантность биомфалярий к дефициту кислорода в воде, что способствует, очевидно, их встречаемости в загрязнённых экскрементами водах и создаёт условия для заражения моллюсков мирацидиями шистосом. Показана связь присутствия шистосом в биоценозе с определёнными характеристиками среды, а именно со стоячей или медленно текущей водой и с наличием обильной прибрежной растительности. Кроме того, все водоёмы, в которых найден паразит, находились в черте города. Полученные результаты важны для разработки мер борьбы с шистосомозом в регионе.

Ключевые слова: *Schistosoma*, шистосомоз, природный очаг заражения, промежуточный хозяин, *Biomphalaria*, ITS1 рДНК, Гвинейская Республика

1871
ИнБЮМ – IBSS

Морской биологический журнал
Marine Biological Journal
2025, vol. 10, no. 4, pp. 37–50
https://marine-biology.ru/mbj/article/view/501

UDC [502.175:614.73](262.5:560)

ASSESSMENT OF RADIOACTIVITY STATUS IN COASTAL WATERS OF TÜRKIYE

© 2025 **N. Dogan[1] and O. Tunc Dede[2]**

[1]State Hydraulic Works, Department of Technical Research and Quality Control, Ankara, Türkiye
[2]Giresun University, Environmental Engineering Department, Giresun, Türkiye
E-mail: *ozlem@tuncdede.com*

Received 03.03.2025; revised 07.05.2025;
accepted 12.08.2025.

Anatolia has a geopolitical location between Europe and Asia, surrounded by sea on three sides. The Black Sea washes the northern coast of Türkiye, stretching 1,700 km from the suburbs of Istanbul to the town of Hopa. Following the Chernobyl Nuclear Power Plant accident, the dust cloud containing radioactive elements (first of all, an artificial radionuclide ^{137}Cs) reached western Türkiye in May 1986 and affected Thrace, Istanbul, and the western Black Sea. Upon the increase in radioactive fallout in these regions, a nationwide radiation monitoring program was initiated by the Turkish Atomic Energy Agency to determine the nuclear and radiological hazard status and geographical distribution of radionuclides. Many studies were focused on environmental radioactivity measurements in air, water, soil, rocks, and sediments in order to reveal the possible health effects of their radioactive pollution on the population of Türkiye after the Chernobyl NPP accident.

Keywords: Türkiye, the Black Sea water, the Chernobyl NPP accident, natural and artificial radionuclides

Radioactivity is the spontaneous disintegration of atomic nuclei, and occurs naturally or artificially [Bayrak, 2018; TAEK, 1988]. Until the beginning of the 20th century, living beings were only under the effect of natural radiation sources, such as ionizing radiations from natural radioactive materials and cosmic rays emanating from the Sun and space. However, with the discovery of radioactivity, radioactive sources began to be used in medicine, industry, agriculture, and research. The nuclear technology applications, atmospheric, aquatic, and underground nuclear weapon tests, as well as nuclear reactor explosions, are factors that initiate radioactive pollution and can cause releasing of artificial radionuclides – iodine-131 (^{131}I), iodine-129 (^{129}I), strontium-90 (^{90}Sr), cesium-137 (^{137}Cs), cesium-134 (^{134}Cs), and plutonium-239 (^{239}Pu) – into the environment [IAEA, 2011; TAEK, 2013]. By-products and waste of nuclear sources can be another source of artificial radioisotopes. Environmental toxicity risk may occur due to leakages that may arise from underground or undersea warehouses which are used for storing nuclear wastes for a long period. All these reasons have led researchers to focus on environmental radioactivity measurements in air, water, soil, rocks, and sediments to reveal possible effects of radioactive pollution on human health and environmental quality. World Health Organization (hereinafter WHO) determined the gross alpha and gross beta radioactivity limits in drinking water as 0.5 and 1.0 Bq·L^{-1}, respectively, and the annual effective dose limit as 0.1 mSv·year^{-1} [WHO, 2004]. Also, in the Republic of Türkiye, within the scope of the “Regulation on Water Intended for Human Consumption” published

by the Ministry of Health, the annual effective dose limit has been determined as 0.1 mSv·year^{-1} [Ministry of Health, 2005]. In cases where gross alpha and gross beta in drinking water are above the limit values, the total dose calculation, which is a detailed radionuclide analysis, is performed.

The main radioactive substances frequently encountered in groundwater are potassium-40 (^{40}K), thorium-232 (^{232}Th), and uranium-238 (^{238}U). In addition, radon-222 (^{222}Rn) and radium-226 (^{226}Ra), which are formed as a result of ^{238}U decay, can be found in groundwater. It is known that ^{238}U, ^{232}Th, ^{40}K and their decay products, which are the key sources of radioactivity, are most enriched in granitic rocks [Abdel Hady et al., 1994]. For this reason, water taken from granitic aquifers is always approached with close attention.

The main source of environmental radioactivity is radioactive fallout after a nuclear or radiological accident. It is extremely important to know the dimensions of the radioactive fallout to accurately determine the possible effects of radiation and radioactive contamination on human health and the environment [TAEK, 2013]. As several European countries, Türkiye began raising these issues after the Chernobyl disaster in 1986. Shortly after the Chernobyl Nuclear Power Plant (NPP) accident, the dust cloud containing radioactive elements reached western Türkiye and affected especially Thrace, Istanbul, and the western Black Sea region through rain. Another important area affected by this accident was the eastern Black Sea region, where the dust cloud left its radioactive content along the coast after heavy rain. Conducted studies showed that artificial radionuclide ^{137}Cs originating from Chernobyl was detected in the Black Sea region [Environmental Radioactivity, 2020; Gokmen et al., 1995; Kapdan et al., 2012a].

Anatolia has a geopolitical location between Europe and Asia, and is surrounded by seas on three sides. The Black Sea is situated in the north of Türkiye, between Asia and Europe, and covers an area of approximately 497.000 km^2 together with the Sea of Azov. The Black Sea is connected to the Mediterranean Sea in the south after the Bosphorus Strait and the Sea of Marmara and next after the Dardanelles Strait and the Aegean Sea [Akengin et al., 2016]. Although Türkiye is surrounded by seas on three sides, it has limited water resources, and the protection of water quality in the country is very important. Following the Chernobyl NPP accident, a major radioactive fallout (^{137}Cs, a common fission product with its high water solubility) was released from the atmosphere. It affected the Eastern Europe, the Black Sea, and northern coasts of Türkiye [Kulahci, Doğru, 2006; Özmen, Güven, 2021]. After radioactive fallout resulting from the Chernobyl NPP accident, the increase of the specific activity of artificial radionuclides in natural environments in Türkiye was recorded.

Upon seeing the rising values, a nationwide radiation monitoring program was started by the Turkish Atomic Energy Agency [1988]. Recently, a comprehensive study was conducted by the Agency to determine the nuclear and radiological hazard status and geographical distribution of radionuclides present in surface soils and in drinking and utility waters in 81 provinces in Türkiye between 2002 and 2011 [TAEK, 2013].

The aim of the research is to assess the current quality of coastal ecosystems of the Black Sea along the coast of Türkiye in relation to natural and artificial radionuclides based on a generalized analysis of our own and literature data.

MATERIAL AND METHODS

This study was carried out to assess the quality of Turkish coastal ecosystems in terms of natural and artificial radionuclides. In the research, the analysis results of Turkish coastal waters, sediment, and soil samples given in the literature between 2000 and 2021 were evaluated. The most commonly

used methods in the literature for determining the activities of natural and artificial radionuclides are alpha/beta counters, gamma spectroscopy, alpha spectroscopy, liquid scintillation spectroscopy, and nuclear track detectors.

The data evaluated also include the results of gross alpha and gross beta analysis, conducted by N. Dogan, one of the authors of this article, on water samples taken from various parts of Türkiye in 2017. The collected water samples are prepared for measurements as described in EPA method 900.0 [2025]. The water sample is evaporated on a heater until approximately 10–15 mL remains, providing sufficient residue for counting (5 mg·cm^{-2} for alpha and 10 mg·cm^{-2} for beta). The remaining water is transferred to ~5-cm (2-inch) diameter steel planchets under an infrared lamp, dried in an oven at +105 °C until a constant weight is obtained, and then counted. Total alpha and total beta activity values from the residual water sample are measured with a 10-channel multi-detector system (Berthold LB 770) with low natural background counting and calculated using equation 1:

$$A_{\alpha,\beta}(Bq/L) = \frac{N}{(60 \times Eff \times V)}, \quad (1)$$

where $A_{\alpha,\beta}$ is total alpha/beta activity of the sample (Bq·L^{-1});

N in net count rate of the sample (counts *per* minute, cpm);

Eff is counting efficiency of the system (cpm·dpm^{-1});

V is volume of the sample (L);

60 is conversion factor (min·s^{-1}).

The Berthold LB 770 system is a proportional gas counter operating on the principle that both alphas and betas are counted independently of each other simultaneously [Dogan, 2017; EPA Method 900.0, 2025].

RESULTS AND DISCUSSION

Radioactivity status of coastal waters in Türkiye. The first effects of the Chernobyl NPP accident occurred on 30 April, 1986, in the North-Western (Thrace) region and the Black Sea coast of Türkiye with increases in environmental natural gamma radiation levels. In the meantime, radioactive substances in the air descended to the earth with heavy rains, which caused significant contamination in the region. According to the measurements made, the gross beta activity accumulated in the soil in Istanbul and its surroundings in the first two weeks of May was 3,000 Bq·m^{-2}. The gross beta activity concentration of the rainwater collected in Kapıkule (Edirne) on 4 May was found to be around 9,000 Bq·L^{-1}, and the gross beta activity of rainwater collected in Istanbul on 10 May was around 3,500 Bq·L^{-1}. These activity increases in rain water did not affect the groundwater in Edirne region, but caused minor activity increases in surface waters around Istanbul. As a matter of fact, in the gross beta activity measurements made on 5–22 May in Istanbul drinking and tap water, the highest activity concentration was found to be around 9 Bq·L^{-1} on 5 May. In the following days, it gradually decreased to its normal level [TAEK, 1988].

The data of studies conducted in order to determine gross alpha and gross beta radioactivity levels in water (Bq·L^{-1}) at different locations in Türkiye are given in Table 1. High gross alpha activity values were observed in Izmir Golcuk Lake [Akyil et al., 2009] and the Mediterranean Sea water near Adana (Karatas and Incirli regions) [Degerlier, Karahan, 2010].

Table 1. Gross alpha and gross beta radioactivity levels ($Bq \cdot L^{-1}$) in water of the seas along the Turkish coast and inland waters at different locations of Türkiye

Area	Gross alpha	Gross beta	References
Canakkale Strait	0.05–0.06	10.53–14.33	Kam et al., 2017
Seawater near Istanbul	0.4	4.9	Karahan et al., 2000
Kucuk Cekmece Lake	0.06	3	
Buyuk Cekmece Lake	0.05	0.3	
Terkos Lake	0.02	0.2	
Omerli Dam Lake	0.034	0.04	
The Marmara Sea water	0.5	5.0	
The Black Sea water	0.4	5.6	
The Black Sea and the Boshporus Strait water	0.3	5.3	
The Marmara Sea	0.01–0.09	6.51–19.09	Otansev et al., 2016
Izmit Bay seawater	0.03	9.74	Bayrak, 2018
Surface waters in Kastamonu near the Black Sea	0.001–0.026	0.016–2.241	Kam, Bozkurt, 2007
Surface waters in Samsun near the Black Sea	0.024–0.116	0.041–0.191	Görür et al., 2011
The Yesilırmak River	0.128	0.170	
The Kızılırmak River	0.156	0.191	
The Fırtına River	0.012–0.066	0.028–0.133	Küçükömeroğlu et al., 2008
Surface waters in Hatay near the Mediterranean Sea	0.010–0.086	0.014–0.949	Turgay et al., 2016
Surface waters in Giresun near the Black Sea	0.003–0.011	0.040–0.264	Damla et al., 2006
Surface waters in Trabzon near the Black Sea	0.004–0.039	0.022–0.191	Damla et al., 2006; Küçükömeroğlu et al., 2021
Surface waters in Rize near the Black Sea	0.0002–0.042	0.025–0.238	Damla et al., 2006; Islam, 2016
Surface waters in Adana near the Mediterranean Sea	0.0003–0.023	0.019–0.291	Degerlier, Karahan, 2010
The Mediterranean Sea water near Adana (Karatas)	0.8463	3.7395	
The Mediterranean Sea water near Adana (İncirli)	0.703	6.81	
Seyhan Lake (Adana)	0.012	0.0426	
The Seyhan River (Adana)	0.005	0.2453	
Karagol Lake (Izmir)	0.03	2.62	Akyil et al., 2009
Golcuk Lake (Izmir)	0.75	2.35	
Cakalbogaz Lake (Izmir)	0.03	1.77	
Surface waters in Zonguldak near the Black Sea	0.0029–0.1705	0.0154–0.2443	Aytekin, Bayraktaroğlu, 2017
SHW Bursa Regional Directorate	0.022–0.302	0.06–0.32	Dogan, 2017
SHW Izmir Regional Directorate	0.098–0.193	0.15–0.46	
SHW Adana Regional Directorate	0.031–0.096	0.04–0.18	
SHW Samsun Regional Directorate	0.027–0.070	0.05–0.12	
SHW Edirne Regional Directorate	0.040–0.100	0.01–0.24	
SHW Antalya Regional Directorate	0.008–0.083	0.02–0.18	
SHW Istanbul Regional Directorate	0.035–0.178	0.06–0.43	
SHW Aydın Regional Directorate	0.025–0.054	0.05–0.15	
SHW Trabzon Regional Directorate	0.011–0.086	0.03–0.17	
SHW Kastamonu Regional Directorate	0.030–0.131	0.01–0.11	
SHW Balıkesir Regional Directorate	0.047–0.233	0.06–0.31	

Note: SHW, State Hydraulic Works.

High gross beta activity values were observed in the Canakkale Strait [Kam et al., 2017], seawater near Istanbul, Kucuk Cekmece Lake [Karahan et al., 2000], the Marmara Sea water [Karahan et al., 2000; Otansev et al., 2016], the Black Sea and the Boshporus Strait water [Karahan et al., 2000], Izmit Bay seawater [Bayrak, 2018], Izmir Karagol Lake, Izmir Golcuk Lake, Izmir Cakalbogaz Lake [Akyil et al., 2009], and the Mediterranean Sea water near Adana, Karatas, and Incirli regions [Degerlier, Karahan, 2010]. Spatial concentrations of gross alpha and beta activity values in surface waters of Turkish coastal area are shown in Figs 1 and 2, respectively.



Fig. 1. Spatial concentration of gross alpha activity in surface waters along the Turkish coast

Рис. 1. Пространственное распределение суммарной альфа-активности в поверхностных водах вдоль турецкого побережья



Fig. 2. Spatial concentration of gross beta activity in surface waters along the Turkish coast

The concentrations of environmental radioactivity were investigated in sediment cores sampled at different depths (5–5.5, 10–10.5, and 15–15.5 m at the same point) from Kulakcayırı Lake situated in Istanbul. While ^{40}K concentrations increased with depth, the maximum value was found

as 367 Bq·kg^{-1} d. w. (dry weight). Maximum ^{232}Th concentration was registered as 43 Bq·kg^{-1} d. w. at the middle depth, while maximum ^{226}Ra was found as 29 Bq·kg^{-1} d. w. at the first depth. It was reported that the activity of ^{137}Cs was below the minimum detectable activity value [Kam et al., 2018].

The specific activity of natural and artificial radionuclides was determined in bottom sediments of the Golden Horn Bay located in the center of Istanbul. The specific activity values of these radionuclides were the following: 7.18–20.16 Bq·kg^{-1} d. w. for ^{238}U; 6.41–27.25 Bq·kg^{-1} d. w. for ^{232}Th; 281.9–683 Bq·kg^{-1} d. w. for ^{40}K; and 1.12–67.92 Bq·kg^{-1} d. w. for ^{137}Cs [Kılıç, Çotuk, 2011].

The radioactivity concentrations in sediment and seawater samples of the Marmara Sea were determined. Seawater samples were collected from various depths: surface samples, from 5 m below the water line, and bottom samples, from depths of 47–89 m. As revealed, the gross alpha and beta activity levels rose with increasing water depth. The mean gross alpha and beta activity concentrations in seawater samples from the Marmara Sea were 0.042 and 13.402 Bq·L^{-1}, respectively. The radionuclide activity was also determined in sediment samples. The maximum values were found for ^{226}Ra (34.2 Bq·kg^{-1} d. w.), ^{238}U (25.9 Bq·kg^{-1} d. w.), ^{232}Th (31.1 Bq·kg^{-1} d. w.), ^{40}K (693.6 Bq·kg^{-1} d. w.), and ^{137}Cs (16.3 Bq·kg^{-1} d. w.). The obtained results revealed that the mean amounts of ^{226}Ra, ^{238}U, and ^{232}Th were below the limit value; however, the mean amount of ^{40}K was higher than the world mean level [Otansev et al., 2016].

The natural and artificial radionuclide levels in the Marmara Sea region were studied both in Izmit Bay Yalova and Kocaeli. Surface sediment samples were analyzed in Izmit Bay, which is located in industrialized zone of the Marmara Sea. The mean activity concentration of ^{137}Cs was detected as 21 Bq·kg^{-1} d. w., while that of natural radioisotopes, ^{40}K and ^{226}Ra, as 568 and 18 Bq·kg^{-1} d. w., respectively. The highest value for natural radionuclide activities was recorded near petrochemical, phosphate, and fertilizer processing facilities. The mean ^{137}Cs activities were 10 times higher than those in marine sediments in the Middle East and lower than in sediments in Northern Europe [Ergül et al., 2013]. Marine sediments in the Yalova region were sampled from 6 different points ranging 7 to 38 m; mean activities of ^{40}K, ^{232}Th, ^{226}Ra, and ^{137}Cs of sediment samples were found as 589.2, 32.7, 19.7, and 4.17 Bq·kg^{-1} d. w., respectively. Mean activities of gross alpha and beta of three seawater samples were 0.028 and 9.739 Bq·L^{-1}, respectively [Bayrak, 2018].

Soil samples from 27 points in Kocaeli Basin were analyzed in terms of radionuclides. The concentrations determined were as follows: 2–25 Bq·kg^{-1} d. w. for ^{137}Cs; 11–49 Bq·kg^{-1} d. w. for ^{238}U; 161–964 Bq·kg^{-1} d. w. for ^{40}K; 10–58 Bq·kg^{-1} d. w. for ^{226}Ra; and 11–65 Bq·kg^{-1} d. w. for ^{232}Th [Karakelle et al., 2002]. The Canakkale Strait has a strategic position between the Gallipoli and Biga peninsulas and is connected with the Sea of Marmara and the Aegean Sea. Within the study conducted in the Canakkale Strait, the levels of gross alpha and beta radioactivity in seawater were of 0.046–0.064 and 10.53–14.325 Bq·L^{-1}, respectively. The gross alpha values in the study area were lower compared to gross beta values in the same area [Kam et al., 2017].

The effect of radioactive pollution on the habitat of benthic Foraminifera was analyzed in another study conducted in the Canakkale Strait [Yümün, Kam, 2017]. The radionuclide concentrations were measured on 7 core samples and 1 drilling sample from the shallow marine environment. The values for different radionuclides were in the following ranges: 17.5 to 58.3 Bq·kg^{-1} d. w. for ^{232}Th; 16.9 to 48.6 Bq·kg^{-1} d. w. for ^{226}Ra; 443.7 to 725.6 Bq·kg^{-1} d. w. for ^{40}K; and < 2 to 20 Bq·kg^{-1} d. w. for ^{137}Cs. While ^{226}Ra values remained within normal limits, ^{40}K and ^{232}Th values were above the world mean limits defined by the United Nations Scientific Committee on the Effects of Atomic Radiation [2000]: for ^{226}Ra, it is 35 Bq·kg^{-1} d. w.; for ^{40}K, 400 Bq·kg^{-1} d. w.; and for ^{232}Th, 30 Bq·kg^{-1} d. w.

The Balıkesir province situated in the northwest of Türkiye was investigated in terms of activity levels of radionuclides in the soil. ^{238}U, ^{232}Th, ^{40}K, and ^{137}Cs activities were within the ranges of 7.7–71.9, 10.1–94.9, 96.3–1,831.9, and 0.59–27.80 Bq·kg^{-1} d. w., respectively [Kapdan et al., 2012b].

Environmental radioactivity has been studied by different researchers in various points of the Black Sea coastal area. In 1997–1998, the activity levels of ^{238}U, ^{232}Th, ^{40}K, and ^{137}Cs radionuclides were investigated in sediments sampled from different points along the Turkish Black Sea coast. The activities of ^{238}U, ^{232}Th, ^{40}K, and ^{137}Cs in the sediment samples were within the ranges of < 13 to 56; 17 to 37; 301 to 833; and 11 to 138 Bq·kg^{-1} d. w., respectively. It was reported that ^{137}Cs activity in the sediment sample is an indication that the eastern shore of the Black Sea was more affected by Chernobyl NPP accident than the western shore [Topcuoglu et al., 2001].

Zonguldak city, which has the richest hard coal mines in Türkiye, is located on the Black Sea coast and occupies an important place in the maritime trade between Türkiye and the Black Sea countries, especially with those having ports. In order to determine the radiological status of spring waters in Zonguldak city, 49 different water samples were analyzed, and gross alpha and beta levels were found to be 0.003–0.171 and 0.015–0.244 Bq·L^{-1}, respectively. The measured gross alpha and beta activity concentrations were lower than the limit values suggested by WHO [Aytekin, Bayraktaroğlu, 2017].

Kastamonu is in the northern part of Türkiye, and it is in the Black Sea region. Natural and artificial radionuclide activities were measured in water and soil, which were sampled from Kastamonu province. The gross alpha and beta activity concentrations recorded in water samples were 0.001–0.026 and 0.016–2.241 Bq·L^{-1}, respectively. The radioactivity levels of soil samples were assessed as well (on d. w.); the mean concentrations were found as 32.9 Bq·kg^{-1} for ^{238}U; 27.2 Bq·kg^{-1} for ^{232}Th; 431.4 Bq·kg^{-1} for ^{40}K; and 8.0 Bq·kg^{-1} for ^{137}Cs [Kam, Bozkurt, 2007].

The gross alpha and beta levels of tap water samples were determined in a study conducted in the Eastern region of Türkiye. The activity values ranged 0.004 to 0.01 Bq·L^{-1} for alpha and 0.032–0.191 Bq·L^{-1} for beta in the province of Trabzon. In Giresun, the gross alpha and beta levels ranged 0.003 to 0.011 Bq·L^{-1} and 0.04 to 0.264 Bq·L^{-1}, respectively. The values ranged 0.0002 to 0.015 Bq·L^{-1} for alpha and 0.025 to 0.238 Bq·L^{-1} for beta in the province of Rize. These results indicated that the lowest gross alpha and beta values were obtained in tap water samples from Trabzon. Rize showed the highest gross alpha activity, while the Giresun had the highest gross beta activity. This analysis provided evidence that the gross alpha and beta activity levels in tap waters in Eastern region of Türkiye were in good condition and below the limit values given by WHO [2004] and Turkish regulations [Ministry of Health, 2005] for drinking water [Damla et al., 2006]. A recent study determined the gross alpha and beta concentrations in water samples collected from different areas of Rize Province with the values ranging 0.012 to 0.042 Bq·L^{-1} for gross alpha and 0.027 to 0.211 Bq·L^{-1} for gross beta [Islam, 2016]. The radionuclides values were measured in the drinking water samples of Trabzon region and found as 0.008–0.654 Bq·L^{-1} for ^{238}U; 0.007–0.067 Bq·L^{-1} for ^{232}Th; 0.010–0.337 Bq·L^{-1} for ^{40}K; and 0.0002–0.056 Bq·L^{-1} for ^{137}Cs [Küçükömeroğlu et al., 2021].

The gross alpha and beta radioactivity and annual effective doses were investigated in various waters of Samsun city situated in the central part of the Black Sea coastline, between the deltas of the Yesilırmak and the Kızılırmak rivers. Activity concentrations of gross alpha and beta in tap water samples were detected as 0.024–0.1156 and 0.0408–0.1905 Bq·L^{-1}, respectively. The radioactivity concentrations measured for the Yesilırmak and the Kızılırmak rivers were 0.128 and 0.1556 Bq·L^{-1} for gross alpha and 0.170 and 0.191 Bq·L^{-1} for gross beta, respectively. The calculated annual effective doses of alpha- and beta-emitters were found to be below the reference value recommended

by WHO (0.1 mSv·year^{-1}) for all water samples [Görür et al., 2011]. The radionuclides status in soil and sediment of the Kızılırmak River delta was measured in another study. The following mean values were determined: 28.59 Bq·kg^{-1} d. w. for ^{238}U; 17.48 Bq·kg^{-1} d. w. for ^{232}Th; 150.59 Bq·kg^{-1} d. w. for ^{40}K; and 5.32 Bq·kg^{-1} d. w. for ^{137}Cs; those are below the worldwide mean values given by UNSCEAR. It is stated that ^{137}Cs could result from the Chernobyl NPP accident and nuclear weapon tests conducted by several countries until 1980 [Arıman, Gümüş, 2018; UNSCEAR, 2000].

The Fırtına River, one of the important rivers in the eastern Black Sea region, arises from the slopes of the Kackar Mountains and is connected to the eastern Black Sea near 2 km to Ardesen town in the west of Rize. The natural radioactivity concentrations of water, sediment, and soil samples were investigated in several expeditions. The mean concentration levels (on d. w.) for ^{238}U, ^{232}Th, ^{40}K, and ^{137}Cs in soils and bottom sediment samples were as follows: 50, 42, 643, and 85 Bq·kg^{-1} and 39, 38, 573, and 6 Bq·kg^{-1}, respectively. The presence of ^{137}Cs in soil and sediment samples was related to the Chernobyl NPP accident, as well as to atmospheric nuclear weapon tests carried out by several countries [Kurnaz et al., 2007].

Other radioactivity studies on water and sediment samples of the Fırtına River stated that the natural gross alpha and beta levels in water samples were between 0.012–0.066 and 0.028–0.133 Bq·L^{-1}, respectively. The mean specific activities of gamma-emitting radionuclides in bottom sediments (on d. w.) were as follows: 47.41 Bq·kg^{-1} for ^{226}Ra; 39.93 Bq·kg^{-1} for ^{238}U; 38.55 Bq·kg^{-1} for ^{232}Th; 573.34 Bq·kg^{-1} for ^{40}K; and 6.15 Bq·kg^{-1} for ^{137}Cs. The existence of ^{137}Cs was also related to the Chernobyl NPP accident, the same as in the previous investigation [Küçükömeroğlu et al., 2008]. The radioactivity concentrations of seawater and bottom sediments sampled from five different locations in the Rize province of the Eastern Black Sea were measured in recent study. The concentrations of ^{226}Ra, ^{232}Th, ^{40}K, and ^{137}Cs in bottom sediment samples (on d. w.) and water samples (data presented in parentheses) varied in the following ranges: 9–23 Bq·kg^{-1} (0.16–0.63 Bq·L^{-1}); 6–34 Bq·kg^{-1} (0.07–0.17 Bq·L^{-1}); 223–765 Bq·kg^{-1} (3.44–6.20 Bq·L^{-1}); and 5–12 Bq·kg^{-1} (no values for seawater), respectively [Baltas et al., 2017].

Studies carried out in 2015 and 2019 were focused on the radioactivity status of the Coruh River in Artvin. In 2015, sediments were sampled from 3 different dam reservoirs on the Coruh River. The mean concentrations (on d. w.) of ^{238}U, ^{232}Th, ^{40}K, and ^{137}Cs were determined: in Deriner Dam Lake, 15.8, 13.9, 551.5, and 18.1 Bq·kg^{-1}; in Borcka Dam Lake, 3.7, 12.5, 473.8, and 6.8 Bq·kg^{-1}; and in Muratlı Dam Lake, 14.4, 30.0, 491.7, and 18.2 Bq·kg^{-1}, respectively. It was reported that activity levels of radionuclides decreased from the upper parts of Çoruh River to coastal area [Kobya et al., 2015]. In 2019, the concentrations of radionuclides in sediment samples (on d. w.) collected from the Borcka Dam Lake were determined. The mean activity concentrations were found to be below worldwide mean values given by UNSCEAR [2000]: 12.19 Bq·kg^{-1} for ^{226}Ra; 14.05 Bq·kg^{-1} for ^{232}Th; 396.41 Bq·kg^{-1} for ^{40}K; and 4.20 Bq·kg^{-1} for ^{137}Cs [Şirin, 2019].

Izmir, which is located in the western part of Türkiye, was investigated in terms of gross alpha and beta and uranium levels in surface water of lakes. The mean gross alpha and beta activity levels were determined as 0.03 and 2.62 Bq·L^{-1} for Karagol Lake; 0.75 and 2.35 Bq·L^{-1} for Golcuk Lake; and 0.03 and 1.77 Bq·L^{-1} for Cakalbogaz Lake, respectively. It was also found that the uranium concentration ranged 0.05 to 900 μg·L^{-1} for Karagol Lake; 0.05 to 0.95 μg·L^{-1} for Golcuk Lake; and 3.33 to 10 μg·L^{-1} for Cakalbogaz Lake [Akyil et al., 2009]. In another study aimed at detecting radionuclides in beach sand samples, the following results were obtained: 5.70–38.83 Bq·kg^{-1} d. w. for ^{226}Ra; 3.870–292.7 Bq·kg^{-1} d. w. for ^{232}Th; and 120.4–377.6 Bq·kg^{-1} d. w. for ^{40}K [Gür, Tarakçı, 2018].

The specific activity levels of ^{226}Ra, ^{232}Th, ^{40}K, and ^{137}Cs were determined very recently to evaluate the radiological status of the fisheries ground sediments in the Antalya Bay situated on the Mediterranean Sea coastline. The activity values ranged 10.65 to 23.76 Bq·kg^{-1} for ^{226}Ra; 11.63 to 24.15 Bq·kg^{-1} for ^{232}Th; 316.35 to 414.83 Bq·kg^{-1} for ^{40}K; and 1.48 to 8.58 Bq·kg^{-1} for ^{137}Cs in the sediment samples (on d. w.) where the values were below the world mean activity levels defined by UNSCEAR [Özmen, Güven, 2021; UNSCEAR, 2000].

The natural radioactivity status in different surface waters of Adana, which is located in the southern part of Türkiye, was investigated in 2010. The mean gross alpha and beta levels in drinking water samples were detected as 0.0096 and 0.086 Bq·L^{-1}, respectively. During the studies on sea samples, gross alpha and beta levels were measured as 0.8463 and 3.7395 Bq·L^{-1} in the Karatas Sea and 0.703 and 6.81 Bq·L^{-1} in the Incirli Sea, respectively. The gross alpha and beta levels in other sampling points, Seyhan Dam Lake and the Seyhan River, were found to be below WHO limit values [Degerlier, Karahan, 2010].

The radioactivity level in water samples of Hatay city located in the southeastern region of Türkiye was investigated in 2015. While the mean alpha activity was obtained as 0.037 Bq·L^{-1}, the mean beta activity was assessed as 0.116 Bq·L^{-1}. The annual effective doses were calculated as 7.50 and 58.61 μSv from alpha- and beta-emitting radionuclides, respectively, which were lower than 0.1 mSv·year^{-1} suggested by [Turgay et al., 2016; WHO, 2004].

The gross alpha and beta radioactivity values were investigated in various water samples at 11 different coastal regions of Türkiye. According to the results obtained, the gross alpha radioactivity concentrations ranged between 0.008 Bq·L^{-1} (Antalya) and 0.302 Bq·L^{-1} (Bursa), while the gross beta ranged between 0.01 Bq·L^{-1} (Edirne and Kastamonu) and 0.46 Bq·L^{-1} (İzmir). They were below WHO values [2004]. As observed, the gross beta radiation results were higher than the gross alpha radiation ones, which was related to the difference in geological formation of studied areas [Dogan, 2017].

The summary of the activity concentration of radionuclides in bottom sediment and soil samples at different locations in Türkiye is presented in Table 2.

Table 2. Activity concentration of radionuclides in bottom sediment and soil samples (Bq·kg^{-1} dry weight) at different locations in Türkiye

Area	^{238}U	^{226}Ra	^{232}Th	^{40}K	^{137}Cs	References
Trabzon (soil)	11.5–115	–	8.5–49	153–548	1–201	Küçükömeroğlu et al., 2021
Fırtına River (bottom sediments)	16.10–113.25	15.20–116.55	17.26–87.45	51.41–1,605.26	0.87–41.72	Küçükömeroğlu et al., 2008
Fırtına Valley (soil)	11–188	15–188	10–105	105–1,235	19–232	Kurnaz et al., 2007
Rize (soil)	52.44–240.71	58.4–193.7	14.29–83.83	118.43–520.37	0–219.19	Islam, 2016
Rize (bottom sediments)	–	9–23	6–34	223–765	5–12	Baltas et al., 2017
Borçka Dam Lake (bottom sediments)	–	4.79–21.46	9.36–20.65	238.01–721.26	0.79–6.81	Şirin, 2019
Kızılırmak delta (bottom sediments)	7.00–52.14	–	11.55–34.83	149.24–287.36	12.90–21.39	Arıman, Gümüş, 2018
Kızılırmak delta (soil)	19.64–42.88	–	13.67–33.83	204.91–633.72	1.11–4.11	
Balıkesir (soil)	7.70–71.90	–	10.10–94.90	96.30–1,831.90	0.59–27.80	Kapdan et al., 2012b

Continued on the next page…

Area	^{238}U	^{226}Ra	^{232}Th	^{40}K	^{137}Cs	References
Istanbul (soil)	3–59	–	8–91	117–1,204	2–81	Karahan et al., 2000
Kocaeli (soil)	11–49	10–58	11–65	161–964	2–25	Karakelle et al., 2002
Çanakkale (soil)	82–167	–	152–275	1,015–1,484	0.37–36.03	Kurnaz et al., 2007; Merdanoğlu, Altınsoy, 2006
Çanakkale (bottom sediments)	–	16.90–48.60	17.50–58.30	443.70–725.60	< 2 to 20	Yümün, Kam, 2017
Deriner Dam Lake (bottom sediments)	15.8	–	13.9	551.5	18.1	Kobya et al., 2015
Borcka Dam Lake (bottom sediments)	3.7	–	12.5	473.8	6.8	
Muratlı Dam Lake (bottom sediments)	14.4	–	30.0	491.7	18.2	
Kulakcayırı Lake (bottom sediments)	–	26–29	38–43	325–367	–	Kam et al., 2018
Antalya Bay (bottom sediments)	–	10.65–23.76	11.63–24.15	316.35–414.83	1.48–8.58	Özmen, Güven, 2021
The Golden Horn and the Bosphorus (bottom sediments)	7.18–20.16	–	6.41–27.25	281.9–683	1.12–67.92	Kılıç, Çotuk, 2011
The Marmara Sea (bottom sediments)	6.40–25.90	13.80–34.20	6.30–31.10	378.80–693.60	4.8–16.3	Otansev et al., 2016
The Izmit Bay (bottom sediments)	–	18	–	568	21	Ergül et al., 2013
Yalova Altınova (bottom sediments)	–	19.70	32.70	589.20	4.17	Bayrak, 2018
Kastamonu (soil)	32.93	37.40	27.17	431.43	8.02	Kam, Bozkurt, 2007
Igneada (bottom sediments)	41	–	17	316	11	Topcuoglu et al., 2001
Kilyos (bottom sediments)	26	–	19	350	23	
Amasra (bottom sediments)	17	–	27	301	50	
Sinop (bottom sediments)	40	–	34	501	94	
Persembe (bottom sediments)	< 13	–	36	833	138	
Rize (bottom sediments)	56	–	37	358	104	
Izmir (beach sand)	–	5.70–38.83	3.87–292.7	120.4–377.6	–	Gür, Tarakçı, 2018
Worldwide mean values	35	35	30	400	–	UNSCEAR, 2000

Health assessment. Ionizing radiation can cause physical, chemical, and biological changes in living things at molecular and cellular levels [Varol, 2011]. These changes may be temporary or permanent depending on the type, intensity, amount of ionizing radiation, duration of the exposure, and also the area of the body exposed [Gökoğlan et al., 2020]. Since alpha particles are heavier than beta particles, they can be absorbed by the skin of the body. When taken into the body by inhalation or ingestion,

it can cause serious damage to tissues of lung or stomach walls. Beta particles are faster than alpha particles and can penetrate more into tissue or materials. Skin burns can be seen in cases of excessive exposure to high-energy beta radiation. The major concern with ionizing radiation is its cancer effect and the transmission of defects, called delayed effects, to future generations by genetic means [Varol, 2011]. Therefore, the effect of radiation on human health is still being investigated. In recent years, many analyses have been made on vital water resources. The obtained results are compared with the permissible limit values given by WHO: 0.5 $Bq \cdot L^{-1}$ for gross alpha and 1 $Bq \cdot L^{-1}$ for gross beta. If the measured values are lower than the limits, the sample is considered suitable for drinking water. In case of exceeding the given limits, it is necessary to determine the radionuclide species in the samples. The determined dose amounts of these radionuclides are compared with the effective dose amount (0.1 $mSv \cdot year^{-1}$) that can be taken in a year determined by WHO [2004]. If the dose amounts do not exceed the limit value, the sample complies with the drinking water criteria in terms of radioactivity. Regarding soil samples, the worldwide mean values reported by UNSCEAR are used for comparison: 35 $Bq \cdot kg^{-1}$ d. w. for ^{238}U; 30 $Bq \cdot kg^{-1}$ d. w. for ^{232}Th; and 400 $Bq \cdot kg^{-1}$ d. w. for ^{40}K. If the worldwide mean values are exceeded, the annual mean effective dose is calculated and compared with the value of 70 μSv determined by UNSCEAR [2000].

Conclusions. Türkiye has a geopolitical location between Europe and Asia and is surrounded by sea on three sides. As several European countries, Türkiye, especially Thrace, Istanbul, the western Black Sea region, and the eastern Black Sea region, have experienced the effects of radioactivity shortly after the occurrence of the Chernobyl NPP accident. The presence of the artificial radionuclide cesium-137 in natural samples taken from these regions confirms this. Not only the Chernobyl NPP accident, but also technological developments can cause radioactive pollution from industrial and nuclear wastes, and all living things are exposed to both natural and artificial radiation. Therefore, sustainable monitoring system should be developed in order to assess the radioactivity status in the environment. Studies conducted throughout Türkiye show that the recorded gross alpha and beta levels in coastal waters are generally below the limit values suggested by World Health Organization. However, higher values of gross beta were observed in seawater samples from the Marmara region, the Straits, and Adana. This may be due to the high salinity of seawater and a dissolved form of the radioactive isotope ^{40}K, which causes high beta radioactivity in seawater. Natural radionuclides, such as ^{238}U series, ^{232}Th series, and ^{40}K, were found at various levels in soil and sediment samples. In general, the values remained below the world mean values stated by the United Nations Scientific Committee on the Effects of Atomic Radiation. However, the presence of ^{137}Cs at some points of Türkiye was related to the Chernobyl NPP accident and nuclear weapon tests conducted by several countries. Any radioactive pollution in the environment requires careful monitoring in terms of human health and taking the necessary precautions.

This work is a review study which includes an assessment of the quality of coastal ecosystems along the Turkish coast of the Black Sea in relation to natural and artificial radionuclides. The authors declare no conflict of interest.

REFERENCES

1. Abdel Hady E. E., El-Sayed A. M. A., Ahmed A. A., Hussein A. Z. Natural radioactivity of basement younger granite rocks from the eastern desert. *Radiation Physics and Chemistry*, 1994, vol. 44, iss. 1–2, pp. 223–224. https://doi.org/10.1016/0969-806X(94)90136-8
2. Akengin H., Dölek İ., Özdemir Y. Turkey's seas and coasts. In: *Physical Geography of Turkey* =

Türkiye Fiziki Coğrafyası / H. Akengin, İ. Dölek (Eds). Ankara : Pegem Akademi Yayıncılık, 2016, pp. 287–310. (in Tur.)

3. Akyil S., Aytaş S., Turkozu D. A., Aslani M. A. A., Yusan S. D., Eral M. Radioactivity levels in surface water of lakes around Izmir/Turkey. *Radiation Measurements*, 2009, vol. 44, iss. 4, pp. 390–395. https://doi.org/10.1016/j.radmeas.2009.04.013
4. Arıman S., Gümüş H. Radioactivity levels and health risks due to radionuclides in the soil and sediment of mid-Black Sea: Kızılırmak Deltas-Turkey. *Radiochimica Acta*, 2018, vol. 106, iss. 11, pp. 927–937. https://doi.org/10.1515/ract-2017-2896
5. Aytekin H., Bayraktaroğlu N. An investigation on the quality of natural spring waters in Zonguldak Province (Turkey). *Karaelmas Fen ve Mühendislik Dergisi*, 2017, vol. 7, iss. 2, pp. 485–490.
6. Baltas H., Kiris E., Şirin M. Determination of radioactivity levels and heavy metal concentrations in seawater, sediment and anchovy (*Engraulis encrasicolus*) from the Black Sea in Rize, Turkey. *Marine Pollution Bulletin*, 2017, vol. 116, iss. 1–2, pp. 528–533. https://doi.org/10.1016/j.marpolbul.2017.01.016
7. Bayrak K. *Investigation of Heavy Metal and Environmental Radioactivity in Izmit Gulf of Marmara Sea Altinova Shipyard Region.* MSc thesis. Istanbul, Türkiye : Yıldız Teknik University, 2018, 102 p.
8. Damla N., Çevik U., Karahan G., Kobya A. İ. Gross α and β activities in tap waters in Eastern Black Sea region of Turkey. *Chemosphere*, 2006, vol. 62, iss. 6, pp. 957–960. https://doi.org/10.1016/j.chemosphere.2005.05.051
9. Degerlier M., Karahan G. Natural radioactivity in various surface waters in Adana, Turkey. *Desalination*, 2010, vol. 261, iss. 1–2, pp. 126–130. https://doi.org/10.1016/j.desal.2010.05.020
10. Dogan N. *Investigation of the Radioactivity Content of Water Resources in Turkey.* Ankara : Devlet Su İşleri, 2017, 106 p. (in Tur.)
11. EPA Method 900.0: Gross alpha and gross beta radioactivity in drinking water. EPA/600/4/80/032. In: *United States Environmental Protection Agency / Environmental Sampling and Analytical Methods (ESAM) Program* : [site]. 1980. [Last update: 14 May, 2025]. URL: https://www.epa.gov/esam/epa-method-9000-gross-alpha-and-gross-beta-radioactivity-drinking-water [accessed: 02.06.2025].
12. Ergül H. A., Belivermiş M., Kılıç Ö., Topcuoğlu S., Çotuk Y. Natural and artificial radionuclide activity concentrations in surface sediments of Izmit Bay, Turkey. *Journal of Environmental Radioactivity*, 2013, vol. 126, pp. 125–132. https://doi.org/10.1016/j.jenvrad.2013.07.015
13. *Environmental Radioactivity in Turkish Environment* / T. Bayram, Y. Zayachuk, D. K. Gupta (Eds). Sivas : Sivas Cumhuriyet University Press, 2020, 282 p.
14. Gokmen I. G., Birgül O., Kence A., Gökmen A. Chernobyl radioactivity in Turkish tea and its possible health consequences. *Journal of Radioanalytical and Nuclear Chemistry Articles*, 1995, vol. 198, iss. 2, pp. 487–497. https://doi.org/10.1007/bf02036565
15. Gökoğlan E., Ekinci M., Özgenç E., İlemözdemir D., Aşıkoğlu M. Radyasyon ve İnsan Sağlığı Üzerindeki Etkileri = Radiation and its effects on human health. *Anadolu Kliniği Tıp Bilimleri Dergisi*, 2020, vol. 25, no. 3, pp. 289–294. https://doi.org/10.21673/anadoluklin.709434
16. Görür K. F., Keser R., Dizman S., Okumuşoğlu N. T. Annual effective dose and concentration levels of gross α and β in various waters from Samsun, Turkey. *Desalination*, 2011, vol. 279, iss. 1–3, pp. 135–139. https://doi.org/10.1016/j.desal.2011.05.071
17. Gür F., Tarakçı M. Natural radioactivity of the coastline of Çeşme-Izmir. *MCBÜ Sosyal Bilimler Dergisi*, 2018, vol. 16, no. 1/2, pp. 167–186.
18. IAEA. *Radioactive Particles in the Environment: Sources, Particle Characterization and Analytical Techniques.* Vienna, Austria : International Atomic Energy Agency, 2011, 77 p. (IAEA-TECDOC-1663).
19. Islam I. S. *Total Alpha, Total Beta Activities of Drinking Water in Rize Province and Dose Values.* MSc thesis. Rize, Türkiye : Karadeniz

Technical University, 2016, 74 p.
20. Kam E., Bozkurt A. Environmental radioactivity measurements in Kastamonu region of northern Turkey. *Applied Radiation and Isotopes*, 2007, vol. 65, iss. 4, pp. 440–444. https://doi.org/10.1016/j.apradiso.2006.11.005
21. Kam E., Once M., Yumun S. The origin of the total alpha and beta radiation values of the waters of Çanakkale Strait (Çanakkale/Turkey). *Journal of the Turkish Chemical Society, Section A: Chemistry*, 2017, vol. 4, iss. 3, pp. 729–738. https://doi.org/10.18596/jotcsa.292895
22. Kam E., Yümün Z. Ü., Açıkgöz G., Bayrak K. Concentrations of environmental radioactivity in sediment cores from Kulakcayiri Lake. *Journal of the Turkish Chemical Society. Section A: Chemistry*, 2018, vol. 5, iss. 3, pp. 1371–1374. https://doi.org/10.18596/jotcsa.401086
23. Kapdan E., Taskin H., Kam E., Osmanlioğlu A. E., Karahan G., Bozkurt A. A study of environmental radioactivity measurements for Cankiri, Turkey. *Radiation Protection Dosimetry*, 2012a, vol. 150, iss. 3, pp. 398–404. https://doi.org/10.1093/rpd/ncr416
24. Kapdan E., Varinlioglu A., Karahan G. Outdoor radioactivity and health risks in Balikesir, northwestern Turkey. *Radiation Protection Dosimetry*, 2012b, vol. 148, iss. 3, pp. 301–309. https://doi.org/10.1093/rpd/ncr038
25. Karahan G., Öztürk N., Bayülken A. Natural radioactivity in various surface waters in İstanbul, Turkey. *Water Research*, 2000, vol. 34, iss. 18, pp. 4367–4370. https://doi.org/10.1016/S0043-1354(00)00219-0
26. Karakelle B., Öztürk N., Köse A., Varinlioğbrevelu A., Erkol A. Y., Yılmaz F. Natural radioactivity in soil samples of Kocaeli basin, Turkey. *Journal of Radioanalytical and Nuclear Chemistry*, 2002, vol. 254, iss. 3, pp. 649–651. https://doi.org/10.1023/A:1021635415222
27. Kobya Y., Taşkın H., Yeşilkanat C. M., Varinlioğlu A., Korcak S. Natural and artificial radioactivity assessment of dam lakes sediments in Çoruh River, Turkey. *Journal of Radioanalytical and Nuclear Chemistry*, 2015, vol. 303, iss. 1, pp. 287–295. https://doi.org/10.1007/s10967-014-3420-7
28. Küçükömeroğlu B., Kurnaz A., Keser R., Korkmaz F., Okumusoglu N. T., Karahan G., Sen C., Cevik U. Radioactivity in sediments and gross alpha–beta activities in surface water of Fırtına River, Turkey. *Environmental Geology*, 2008, vol. 55, iss. 7, pp. 1483–1491. https://doi.org/10.1007/s00254-007-1098-7
29. Küçükömeroğlu B., Şen A., Duran S. U., Çiriş A., Taskin H., Ersoy H. Determination of radioactivity level of water supply network in Trabzon province, Turkey. *Isotopes in Environmental and Health Studies*, 2021, vol. 57, iss. 6, pp. 610–622. https://doi.org/10.1080/10256016.2021.1972996
30. Kulahci F., Doğru M. Physical and chemical investigation of water and sediment of the Keban Dam Lake, Turkey. *Journal of Radioanalytical and Nuclear Chemistry*, 2006, vol. 268, iss. 3, pp. 517–528. https://doi.org/10.1556/jrnc.268.2006.3.13
31. Kurnaz A., Küçükömeroğlu B., Keser R., Okumusoglu N. T., Korkmaz F., Karahan G., Çevik U. Determination of radioactivity levels and hazards of soil and sediment samples in Fırtına Valley (Rize, Turkey). *Applied Radiation and Isotopes*, 2007, vol. 65, iss. 11, pp. 1281–1289. https://doi.org/10.1016/j.apradiso.2007.06.001
32. Kılıç Ö., Çotuk Y. Radioactivity concentrations in sediment and mussel of Bosphorus and Golden Horn. *Journal of Radioanalytical and Nuclear Chemistry*, 2011, vol. 289, iss. 2, pp. 627–635. https://doi.org/10.1007/s10967-011-1140-9
33. Merdanoğlu B., Altınsoy N. Radioactivity concentrations and dose assessment for soil samples from Kestanbol granite area, Turkey. *Radiation Protection Dosimetry*, 2006, vol. 121, iss. 4, pp. 399–405. https://doi.org/10.1093/rpd/ncl055
34. Ministry of Health. *Regulation on Water Intended for Human Consumption.* Ankara : Turkish Ministry of Health, 2005.
35. Otansev P., Taşkın H., Başsarı A., Varinlioğlu A. Distribution and environmental impacts of heavy metals and radioactivity in sediment and seawater samples of the Marmara Sea. *Chemosphere*, 2016, vol. 154, pp. 266–275. https://doi.org/10.1016/j.chemosphere.2016.03.122

36. Özmen S. F., Güven O. Sediment radioactivity levels of deep-water fishery grounds in Antalya Bay. *Aquatic Sciences and Engineering*, 2021, vol. 36, iss. 1, pp. 29–33. https://doi.org/10.26650/ASE2020714512
37. Şirin M. Evaluation of radioactive pollution in sediment samples of Borçka Dam Lake, Turkey. *Cumhuriyet Science Journal*, 2019, vol. 40, iss. 3, pp. 624–639. https://doi.org/10.17776/csj.526652
38. TAEK. *Post-Chernobyl Radiation and Radioactivity Measurements in Turkey*. Ankara, Türkiye : Turkish Atomic Energy Authority, 1988.
39. TAEK. *Turkey Environmental Radioactivity Atlas*. Ankara, Türkiye : Turkish Atomic Energy Authority, 2013.
40. Topcuoglu S., Kut D., Esen N., Gungor N., Olmez (Egilli) E., Kirbasoglu C. ^{137}Cs in biota and sediment samples from Turkish coast of the Black Sea, 1997–1998. *Journal of Radioanalytical and Nuclear Chemistry*, 2001, vol. 250, iss. 2, pp. 381–384. https://doi.org/10.1023/A:1017932604374
41. Turgay M. E., Yazici A. N., Taskin H., Kam E., Karahan G. Assessment of gross α and β radioactivity for drinking water in Hatay province, Turkey. *Desalination and Water Treatment*, 2016, vol. 57, iss. 11, pp. 4960–4965. https://doi.org/10.1080/19443994.2014.1000384
42. UNSCEAR. *Sources and Effects of Ionizing Radiation* / United Nations Scientific Committee on the Effects of Atomic Radiation ; UNSCEAR 2000 Report to the National Agency, with Scientific Annexes. New York : United Nations, 2000, 654 p.
43. Varol S. Yeraltı sularında toplam alfa ve beta radyoaktivitesi. *Journal of Engineering Science and Design*, 2011, vol. 1, iss. 3, pp. 101–106.
44. WHO. *Guidelines for Drinking-Water Quality*. Vol. 1. Recommendations. 3rd edition. Geneva, Switzerland : World Health Organization, 2004, 515 p.
45. Yümün Z. Ü., Kam E. Effects of radionuclides on the recent foraminifera from the clastic sediments of the Çanakkale Strait–Turkey. *Journal of African Earth Sciences*, 2017, vol. 131, pp. 179–182. https://doi.org/10.1016/j.jafrearsci.2017.04.018

ОЦЕНКА УРОВНЯ РАДИОАКТИВНОСТИ В ПРИБРЕЖНЫХ ВОДАХ ТУРЦИИ

Н. Доган[1], О. Тунк Деде[2]

[1]Государственное управление гидротехнических сооружений,
департамент технических исследований и контроля качества, Анкара, Турция
[2]Университет Гиресуна, факультет инженерной экологии, Гиресун, Турция
E-mail: *ozlem@tuncdede.com*

Анатолия занимает геополитическое положение между Европой и Азией. С трёх сторон она окружена морями. Чёрное море омывает северное побережье Турции на протяжении 1700 км, от пригородов Стамбула до городка Хопа. После аварии на Чернобыльской атомной электростанции пылевое облако, содержащее радиоактивные элементы (прежде всего, искусственный радионуклид ^{137}Cs), в мае 1986 г. достигло западной Турции и затронуло Фракию, Стамбул и западную часть Черноморского региона. В связи с увеличением радиоактивных выпадений в этих районах Турецкое агентство по атомной энергии инициировало общенациональную программу радиационного мониторинга для определения ядерного и радиологического статуса опасности и для анализа географического распределения радионуклидов. Большое количество исследований было сосредоточено на измерении радиоактивности окружающей среды в воздухе, воде, почве, горных породах и осадках с целью выявления возможного влияния их радиоактивного загрязнения на здоровье местного населения после аварии на Чернобыльской АЭС.

Ключевые слова: Турция, воды Чёрного моря, авария на Чернобыльской АЭС, природные и искусственные радионуклиды

1871
ИнБЮМ – IBSS

Морской биологический журнал
Marine Biological Journal
2025, vol. 10, no. 4, pp. 51–59
https://marine-biology.ru/mbj/article/view/504

UDC [595.371.13:57.06]:575.1/.2

VARIABILITY OF NUCLEOTIDE SEQUENCES IN TWO GENE MARKERS (*COI* AND *H3*) OF *LITOROGAMMARUS KARADAGIENSIS* (GRINTSOV, 2009) (AMPHIPODA, GAMMARIDAE) AND THE SYSTEMATICS OF THE GENUS *LITOROGAMMARUS*

© 2025 **A. Zolotova[1], V. Grintsov[2], V. Ryabushko[2], and Yu. Kartavtsev[1]**

[1]A. V. Zhirmunsky National Scientific Center of Marine Biology FEB RAS, Vladivostok, Russian Federation

[2]A. O. Kovalevsky Institute of Biology of the Southern Seas of RAS, Sevastopol, Russian Federation

E-mail: *anna.o.zolotova@gmail.com*

Received 19.03.2025; revised 20.06.2025;
accepted 12.08.2025.

We investigated intra- and interspecific variability of mitochondrial DNA cytochrome *c* oxidase subunit I gene (*COI*) and nuclear DNA histone *H3* gene in *Litorogammarus* representatives. Our results indicate that histone *H3* molecular marker is not suitable for species identification in this genus due to its insufficient sequence variability. The taxonomy of the studied species was refined based on the analysis of *COI* gene marker. Comprehensive analysis of genetic distances (*p*-distances) performed involving ABGD and ASAP algorithms suggested that *COI* gene fragment is a diagnostic marker for species identification in *Litorogammarus*. Phylogenetic reconstruction based on four methods and analysis of the resulting gene trees for *COI* revealed close genetic relationship between *Litorogammarus karadagiensis* and *L. glareophilus*. For these two species, we found several common morphological features: the presence of plumose setae on the mandibles, first maxillae, maxillipeds, and on the articles of the first and second gnathopods. The combined use of molecular and morphological data proved to be highly valuable for species identification and for resolving taxonomic issues within this group of amphipods.

Keywords: mtDNA, nDNA, *COI*, histone *H3*, *p*-distances, *Litorogammarus karadagiensis*, *Litorogammarus*, Gammaridae, Amphipoda

Litorogammarus karadagiensis (Grintsov, 2009) inhabits the splash zone of pebble-sand beaches. It was first described from the beaches off the Karadag (the Eastern Crimea), Batiliman, and the Laspi Bay (southern coast of the Crimea, the Black Sea) [Grintsov, 2009]. *L. karadagiensis* is the gammarid life form and the kryvophile ecological form (from Greek words 'kryvo' meaning 'to hide' and 'phileo' meaning 'to love') [Grintsov, 2023]. These animals form dense aggregations, up to 1,000 ind. *per* 1 m^2 in beach habitats with a substrate particle size of at least 5–6 mm. This species occurs year-round and is frequently found along with representatives of the genera *Chaetogammarus* Martynov, 1924 and *Pectenogammarus* Reid, 1940. In the paper [Grintsov, 2009], the members of these genera were mentioned as *Echinogammarus ischnus behningi* (Stebbing, 1899), *Echinogammarus foxi* (Schellenberg, 1928), and *Echinogammarus olivii* (H. Milne Edwards, 1830). To date, *E. ischnus behningi* is classified under the genus *Chaetogammarus*, while *E. foxi* and *E. olivii* are attributed to *Pectenogammarus* (https://www.marinespecies.org/). Molecular phylogenetic analyses [Copilaș-Ciocianu et al., 2025; Marin & Palatov, 2021; Marin et al., 2023] indicate that *Litorogammarus karadagiensis* is a close

relative to several recently described species: *Litorogammarus mazestiensis* (Marin & Palatov, 2021), *Litorogammarus dursi* Marin, Palatov & Copilaș-Ciocianu, 2023, *Litorogammarus samuricus* Palatov, Copilaș-Ciocianu & Marin, 2025, and *Litorogammarus glareophilus* Marin, Palatov & Copilaș-Ciocianu, 2025. Its range covers the entire Ponto-Caspian region where adaptive radiation of gammaroids has occurred [Grintsov, 2023]. This evolutionary radiation exhibits remarkable morphological and ecological diversity, comparable to unique amphipod radiations reported for the Lake Baikal [Copilaș-Ciocianu, Sidorov, 2022].

L. karadagiensis (the species originally described as *Echinogammarus karadagiensis* [Grintsov, 2009]), is now classified within the genus *Litorogammarus* [Marin et al., 2023], the family Gammaridae Latreille, 1802, and the superfamily Gammaroidea Latreille, 1802. Molecular markers have prompted a reassessment of the systematic position of the family Gammaridae [Copilaș-Ciocianu, Sidorov, 2022]. The phylogenetic analysis of four molecular markers (*COI*, *28S* rRNA, *18S* rRNA, and histone *H3*) revealed a new position for the monophyletic superfamily Gammaroidea *Echinogammarus* s. l. among the Ponto-Caspian gammarids [Copilaș-Ciocianu et al., 2020]. This arrangement contrasted with the results obtained in previous morphology-based phylogenetic analysis [Lowry, Myers, 2013]. The conducted molecular genetic analysis provided strong evidence for establishing the genus *Litorogammarus* [Marin et al., 2023].

The aim of this study was to test the hypothesis about the species affiliation of a gammarid sample to a previously described *Litorogammarus karadagiensis* based on analysis of nucleotide sequence variation in the mitochondrial DNA (mtDNA) cytochrome *c* oxidase subunit I (*COI*) genetic marker and the nuclear DNA (nDNA) histone *H3* genetic marker. Histone *H3* marker, which was informative for distinguishing *L. mazestiensis* and *L. karadagiensis* [Copilaș-Ciocianu et al., 2023], and the *COI* marker, known for its diagnostic significance in amphipod identification [Copilaș-Ciocianu et al., 2022], were selected to achieve the aim of this work.

MATERIAL AND METHODS

We studied six *L. karadagiensis* specimens [Grintsov, 2009] sampled in Batiliman (southern coast of the Crimea, N44°25′12″, E33°41′48″) on 05.06.2022. The material was sampled in the splash zone of a pebble-sand beach. Sequences from the genetic database GenBank NCBI (https://www.ncbi.nlm.nih.gov/) were additionally used for the analysis.

DNA was extracted from all the samples using the DNA-Extran kit (DNA-Extran-2, Syntol, Moscow, Russia) according to the manufacturer's protocol and stored at −20 °C. Amplification for the mtDNA *COI* marker and the nDNA histone *H3* marker was performed using universal primers (Table 1) according to the protocol as follows: the initial denaturation at +94 °C (5 min); 35 cycles including denaturation at +94 °C (30 s), primer annealing at +45 °C (30 s), and elongation at +72 °C (60 s); and a final cycle at +72 °C (10 min). Sequencing was performed using the BigDye Terminator v3.1 Cycle Sequencing Kit (Applied Biosystems, the USA) in accordance with the manufacturer's protocol. Nucleotide sequencing was carried out on an ABI 3500 Genetic Analyzer (Applied Biosystems).

The obtained sequences were deposited in BOLD Systems (https://boldsystems.org/) and then in GenBank NCBI (Table 2). All available sequences of *Litorogammarus* representatives [Copilaș-Ciocianu et al., 2025] from GenBank NCBI were included in the analysis, with *Chaetogammarus ischnus* [Marin et al., 2023] selected as the outgroup. Following alignment, the sequence lengths were 638 base pairs (bp) for *COI* and 354 bp for histone *H3*.

Table 1. Primers used for amplification and sequencing of the genetic markers studied

Primer	DNA fragment	Sequence	Primer authors
LCO1490-JJ	*COI*	CHACWAAYCATAAAGATATYGG	Astrin, Stüben, 2008
HCO2198-JJ	*COI*	AWACTTCVGGRTGVCCAAARAATCA	Astrin, Stüben, 2008
H3F	Histone *H3*	ATGGCTCGTACCAAGCAGACVGC	Colgan et al., 2000
H3R	Histone *H3*	ATATCCTTRGGCATRATRGTGAC	Colgan et al., 2000

Table 2. List of *Litorogammarus karadagiensis* samples and accession numbers of DNA sequences deposited in BOLD Systems and GenBank NCBI databases

Litorogammarus karadagiensis	BIN number in BOLD Systems	Sequence for *COI* gene in GenBank NCBI	Sequence for histone *H3* gene in GenBank NCBI
01	BOLD:AGE7470	PV053540	PV053546
02	BOLD:AGE7470	PV053541	PV053547
03	BOLD:AGE7470	PV053542	PV053548
04	BOLD:AGE7470	PV053543	PV053549
05	BOLD:AGE7470	PV053544	PV053550
06	BOLD:AGE7470	PV053545	PV053551

Note: BIN stands for Barcoding Index Number, a unique identifier of a DNA barcode in BOLD Systems.

Sequences were analyzed for each genetic marker separately. Phylogenetic (gene) trees were reconstructed by the following methods: neighbor joining (NJ), maximum likelihood (ML), maximum parsimony (MP), and Bayesian analysis (BA). MEGA11 [Tamura et al., 2021] and MrBayes 3.2 [Ronquist, Huelsenbeck, 2003] software was used. Phylogenetic trees were constructed for each gene separately. For tree reconstruction, the most appropriate evolutionary models were calculated (jModelTest) [Posada, 2008]. Based on the Akaike information criterion, the optimal evolutionary models were the Tamura–Nei ones [Tamura, Nei, 1993]: TrN + G for *COI* and TrN for histone *H3*. For BA reconstruction, runs were considered to have converged when the standard deviation of split frequencies was below 0.01 [Ronquist, Huelsenbeck, 2003]. The number of generations was set to 2,000,000, with the first 25% discarded as "burn in." Samples were taken for every 100th generation.

For species identification based on molecular sequences, the automatic barcode gap discovery procedure was applied in software packages ABGD (Automatic Barcode Gap Discovery, https://bioinfo.mnhn.fr/abi/public/abgd/abgdweb.html) [Puillandre et al., 2012] and ASAP (Assemble Species by Automatic Partitioning, https://bioinfo.mnhn.fr/abi/public/asap/asapweb.html) [Puillandre et al., 2021].

RESULTS

Analysis of genetic distances (*p*-distances) ([Nei, Kumar, 2000], p. 33) confirmed the presence of specimens representing five species within the studied sample: *L. dursi*, *L. glareophilus*, *L. mazestiensis*, *L. samuricus*, and *L. karadagiensis*. Interspecific *p*-distances ranged within 13–19.5% (*COI*) (with the exception for *L. mazestiensis* and *L. samuricus*, $p = 4.3\%$). Between our specimens and *L. karadagiensis* from GenBank NCBI, *p*-distance was 1.5% (*COI*) (Table 3), which falls within a range of intraspecific *p*-distances. No differences were detected for histone *H3* gene.

Based on *COI* sequences, both software packages, ABGD and ASAP, allowed revealing four species-level clusters for all the analysis settings: 1) *L. dursi*; 2) *L. glareophilus*; 3) *L. karadagiensis*; 4) *L. mazestiensis* + *L. samuricus*. Histone *H3* gene sequences available for analysis, those for *L. karadagiensis* and *L. mazestiensis*, were grouped into a cluster.

Table 3. Inter- and intraspecies *p*-distances for *COI* genetic markers studied

	LD	*LG*	*LK*	*LK* (our specimens)	*LM*	*LS*	*CI*
LD	**0.0063**	0.0153	0.0153	0.0153	0.0148	0.0147	0.0160
LG	0.1951	**0.0026**	0.0135	0.0134	0.0147	0.0146	0.0165
LK	0.1803	0.1348	**0.0000**	0.0046	0.0143	0.0144	0.0159
LK (our specimens)	0.1787	0.1301	0.0141	**0.0000**	0.0144	0.0144	0.0159
LM	0.1839	0.1708	0.1765	0.1718	**0.0147**	0.0070	0.0158
LS	0.1740	0.1661	0.1689	0.1665	0.0428	**0.0104**	0.0162
CI	0.2241	0.2124	0.2038	0.2053	0.2044	0.2038	**n/c**

Note: below the bold-highlighted diagonal, there are the values of interspecific *p*-distances for *COI*; along the diagonal, there are the values of intraspecific *p*-distances; above the diagonal, there are the values of standard errors for *COI*. *LD*, *Litorogammarus dursi*; *LG*, *Litorogammarus glareophilus*; *LK*, *Litorogammarus karadagiensis*; *LM*, *Litorogammarus mazestiensis*; *LS*, *Litorogammarus samuricus*; *CI*, *Chaetogammarus ischnus*. N/c, not computable.

Phylogenetic reconstructions (BA, ML, NJ, and MP) showed identical topologies for *COI* gene. In the resulting dendrograms, the studied specimens formed five clades with high node support values. These values were 100% for four species. The exception was the *L. samuricus* clade (BA = 63%; ML = 66%; NJ = 97%; and MP = 70%). The clades *L. mazestiensis* + *L. samuricus* and *L. glareophilus* + *L. karadagiensis* formed sister groups, with *L. dursi* as an external clade (Fig. 1).

None of the phylogenetic methods allowed distinguishing the species *L. karadagiensis* and *L. mazestiensis* using histone *H3* gene sequences. The dendrograms showed a random distribution of the studied specimens, with no discernible clade formation.

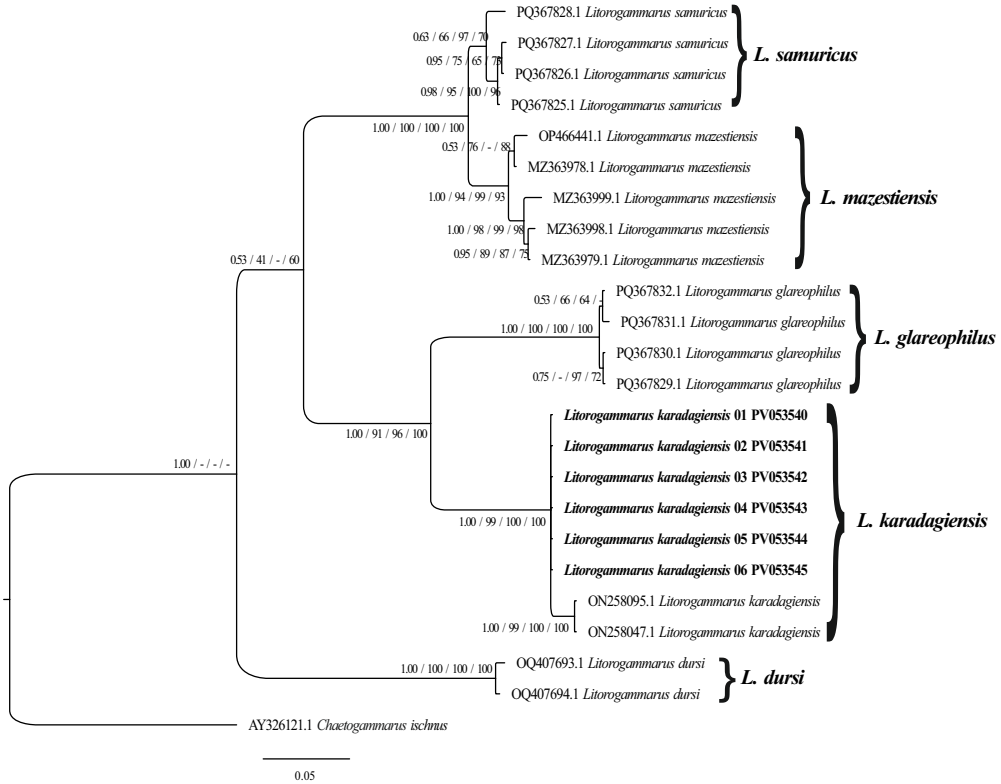


Fig. 1. Phylogenetic relationships among representatives of the genus *Litorogammarus* reconstructed based on *COI* gene sequences. Nodal support values (BA, Bayesian posterior probabilities; ML, maximum likelihood bootstrap; NJ, neighbor-joining bootstrap; MP, maximum parsimony bootstrap) are indicated in the following order: BA / ML / NJ / MP. Our six sequences are highlighted in bold

DISCUSSION

Based on the results of phylogram analysis, calculation of *p*-distances, and analysis involving ABGD and ASAP software packages, no differences were revealed between the histone *H3* gene sequences of the studied samples. Consequently, this nDNA region lacks sufficient resolution for species identification within the genus *Litorogammarus*.

The results of phylogenetic analysis based on the mtDNA *COI* gene nucleotide sequences confirmed the differentiation of *Litorogammarus* species into several clades identified earlier [Copilaș-Ciocianu et al., 2025]. Furthermore, the gene trees show distinct clusters for *L. mazestiensis* and *L. samuricus* representatives supported by topological differentiation. The tree topologies suggest that these species are evolutionarily young, as their clades diverged more recently than clades of *L. glareophilus* and *L. karadagiensis*. *L. mazestiensis* and *L. samuricus* may be young species. However, despite the high support values for tree topologies in both this study (see Fig. 1) and the paper [Copilaș-Ciocianu et al., 2025], the data on *p*-distance analysis and ABGD and ASAP analyses do not support *L. samuricus* identification as a separate species. This conclusion follows from the low interspecific variability between *L. mazestiensis* and *L. samuricus* (4.3%). Interspecific values for other *Litorogammarus* representatives are 10% higher. It may be more appropriate to consider *L. samuricus* as a subspecies of *L. mazestiensis*. Such a conclusion would require a thorough morphological analysis of a sufficiently large sample (meeting statistical requirements), focusing on trait variability to clarify taxonomic status. Currently, the suggested diagnosis [Copilaș-Ciocianu et al., 2025] is the only one distinguishing *L. samuricus* and *L. mazestiensis*. All the differences concern the armament of appendages or body parts and certain proportions. Research on the closely related genus *Pectenogammarus* Reid, 1940 [Grintsov, 2009] has shown that the armament of appendages and body parts (spines, setae, and denticles) are subject to individual variability. This may also apply to body proportions that are known to be variable [Guryanova, 1951].

L. karadagiensis specimens sampled from the species type locality form the closest clades on the phylograms (Fig. 1). Those have minimal *p*-distances (Table 3), and are assigned to a single cluster by both ABGD and ASAP analyses. The sequences of these specimens are close to *COI* sequences of *L. karadagiensis* in GenBank NCBI: ON258095 and ON258047. All these evidences confirm their assignment to the same species-level taxon, which is supported by comparative data for the hierarchy of various taxa (see the concluding paragraph below). Our results reinforce that *L. karadagiensis* is a sister species to *L. glareophilus*.

The morphology of the two *Litorogammarus* species, *L. karadagiensis* and *L. glareophilus*, is pretty similar. Comprehensive morphological descriptions of *L. karadagiensis* are provided in [Grintsov, 2009, 2022], and of *L. glareophilus*, in [Copilaș-Ciocianu et al., 2025]. Unlike other representatives of the genus (*L. dursi*, *L. mazestiensis*, and *L. samuricus*), both *L. karadagiensis* and *L. glareophilus* possess long, plumose setae on the following mouthparts and pereopods: mandibles, first maxillae, maxillipeds, and the articles of the first and second gnathopods. The molecular genetic analysis corroborates the morphological similarity of *L. karadagiensis* and *L. glareophilus* thus suggesting these are sister species (Fig. 1).

According to [Copilaș-Ciocianu et al., 2025], there are few distinguishing morphological traits between these species. *L. karadagiensis* is described as having a small sub-marginal spine on the first epimeral plate, whereas *L. glareophilus* lacks this spine. On the second epimeral plate, *L. karadagiensis* is reported to possess one sub-marginal spine, while *L. glareophilus* possesses two. However, the study [Grintsov, 2024] emphasizes that the armament of epimeral plates with spines

and setae exhibits significant individual variability, rendering these traits unreliable for distinguishing the two species. As noted in [Copilaș-Ciocianu et al., 2025], *L. karadagiensis* has a nearly rounded basipodite on the fifth pereopod, whereas in *L. glareophilus*, the basipodite is narrower and more elongated. This distinction is corroborated by *L. karadagiensis* analysis. Differences in the armament of urosomite 2 are also mentioned [Copilaș-Ciocianu et al., 2025]. Thus, *L. karadagiensis* is reported to have two marginal spines and one lateral spine, while *L. glareophilus* has two marginal spines and two lateral spines. However, research on the armament of two *Pectenogammarus* representatives [Grintsov, 2024] showed that the armament of all urosomal segments is also subject to individual variation and cannot serve as a reliable species marker. Consequently, only one trait remains consistently diagnostic: the shape of the basipodite of the fifth pereopod.

In a summary of genetic distances for more than 20,000 species of vertebrates and invertebrates, *p*-distances for the mtDNA *COI* and *Cyt-b* genes were determined for five hierarchical groups: populations within a species (1); taxa of various ranks, including subspecies and semispecies (2); congeneric species (3); confamilial species (4); and species from different families within the same order (5). The mean unweighted *p*-distances for these five groups are:

- *Cyt-b* for (1), 1.46 ± 0.34; for (2), 5.35 ± 0.95; for (3), 10.46 ± 0.96; for (4), 17.99 ± 1.33; for (5), 26.36 ± 3.88;
- *COI* for (1), 0.72 ± 0.16; for (2), 3.78 ± 1.18; for (3), 10.87 ± 0.66; for (4), 15.00 ± 0.90; for (5), 19.97 ± 0.80.

Notably, the values for subspecies and semispecies are 5.35 ± 0.95 (*Cyt-b*) and 3.78 ± 1.18 (*COI*), while the values for species are 10.46 ± 0.96 (*Cyt-b*) and 10.87 ± 0.66 (*COI*) [Kartavtsev, 2009a]. This is consistent with our findings regarding the taxonomic status of *L. samuricus*. The results of our nucleotide divergence analysis are in line with other data on genetic divergence across taxonomic hierarchies, including non-protein coding genetic markers and complete mitochondrial genomes [Kartavtsev, 2021; Kartavtsev, Masalkova, 2024; Redin, Kartavtsev, 2022], thereby supporting the taxonomic inferences presented in this article. Moreover, the data leads to the general conclusion that at the molecular level, phyletic evolution predominates in the animal world, where speciation primarily follows geographic speciation model [Kartavtsev, 2009a, b, 2011a, b, 2013, 2021].

This work was carried out within the framework of NSCMB FEB RAS state research assignment "Biodiversity of the World Ocean: Taxonomy and evolution, reproductive biology, biogeography, and bioinvasions" (No. 24021900011-9) and IBSS state research assignment "Comprehensive study of the functioning mechanisms of marine biotechnological complexes with the aim of obtaining bioactive substances from hydrobionts" (No. 124022400152-1).

REFERENCES

1. Grintsov V. A. *Amphipods of the Black Sea* : an illustrated guide atlas / A. O. Kovalevsky Institute of Biology of the Southern Seas of RAS. Sevastopol : IBSS, 2022, 476 p. (in Russ.). https://repository.marine-research.ru/handle/299011/12021
2. Grintsov V. A. Ecological groups, ecomorphs and life forms of amphipods (Crustacea, Amphipoda) of the Black Sea and the Sea of Azov. *Ekosistemy*, 2023, no. 33, pp. 38–63. (in Russ.). https://elibrary.ru/lwrmaa
3. Grintsov V. A. Clarification of morphology and ecology of two species of the genus *Pectenogammarus* Reid, 1940 (Gammaridae, Amphipoda) from the Black and Azov seas (Crimea). *Ekosistemy*, 2024, no. 38,

pp. 124–139. (in Russ.). https://doi.org/10.29039/2413-1733-2024-38-124-139
4. Guryanova E. F. *Bokoplavy morei SSSR i sopredel'nykh vod (Amphipoda – Gammaridea).* Moscow ; Leningrad: Izd-vo AN SSSR, 1951, 1029 p. (Opredeliteli po faune SSSR, izdavaemye Zoologicheskim institutom Akademii nauk ; iss. 41). (in Russ.)
5. Astrin J. J., Stüben P. E. Phylogeny in cryptic weevils: Molecules, morphology and new genera of western Palaearctic Cryptorhynchinae (Coleoptera: Curculionidae). *Invertebrate Systematics*, 2008, vol. 22, no. 5, pp. 503–522. https://doi.org/10.1071/is07057
6. Colgan D. J., Ponder W. F., Eggler P. E. Gastropod evolutionary rates and phylogenetic relationships assessed using partial 28S rDNA and histone *H3* sequences. *Zoologica Scripta*, 2000, vol. 29, iss. 1, pp. 29–63. https://doi.org/10.1046/j.1463-6409.2000.00021.x
7. Copilaș-Ciocianu D., Borko Š., Fišer C. The late blooming amphipods: Global change promoted post-Jurassic ecological radiation despite Palaeozoic origin. *Molecular Phylogenetics and Evolution*, 2020, vol. 143, art. no. 106664 (12 p.). https://doi.org/10.1016/j.ympev.2019.106664
8. Copilaș-Ciocianu D., Marin I., Palatov D. Evolution and biogeography of *Litorogammarus* Marin, Palatov & Copilaș-Ciocianu, 2023 (Amphipoda: Gammaridae) with description of two new Caspian endemic species. *Systematics and Biodiversity*, 2025, vol. 23, iss. 1, art. no. 2454025 (27 p.). https://doi.org/10.1080/14772000.2025.2454025
9. Copilaș-Ciocianu D., Palatov D., Rewicz T., Sands A. F., Arbačiauskas K., van Haaren T., Hebert P. D. N., Grabowski M., Marin I. A widespread Ponto-Caspian invader with a mistaken identity: Integrative taxonomy elucidates the confusing taxonomy of *Trichogammarus trichiatus* (= *Echinogammarus*) (Crustacea: Amphipoda). *Zoological Journal of the Linnean Society*, 2023, vol. 198, no. 3, pp. 821–846. https://doi.org/10.1093/zoolinnean/zlad010
10. Copilaş-Ciocianu D., Rewicz T., Sands A. F., Palatov D., Marin I., Arbačiauskas K., Hebert P. D. N., Grabowski M., Audzijonyte A. A DNA barcode reference library for endemic Ponto-Caspian amphipods. *Scientific Reports*, 2022, vol. 12, art. no. 11332 (14 p.). https://doi.org/10.1038/s41598-022-15442-w
11. Copilaș-Ciocianu D., Sidorov D. Taxonomic, ecological and morphological diversity of Ponto-Caspian gammaroidean amphipods: A review. *Organisms Diversity & Evolution*, 2022, vol. 22, iss. 2, pp. 285–315. https://doi.org/10.1007/s13127-021-00536-6
12. Grintsov V. A new amphipod species *Echinogammarus karadagiensis* sp. n. (Amphipoda, Gammaridae) from Crimean coasts (Black Sea, Ukraine). *Vestnik zoologii*, 2009, vol. 43, no. 2, pp. 23–26. https://elibrary.ru/xkirkl
13. Kartavtsev Y. P. Sequence diversity at *Cyt-b* and *Co-1* mtDNA genes in animal taxa proved Neo-Darwinism. *Journal of Phylogenetics and Evolutionary Biology*, 2013, vol. 1, iss. 4, art. no. 1000120 (5 p.). https://doi.org/10.4172/2329-9002.1000120
14. Kartavtsev Y. P., Masalkova N. A. Structure, evolution, and mitochondrial genome analysis of mussel species (Bivalvia, Mytilidae). *International Journal of Molecular Sciences*, 2024, vol. 25, iss. 13, art. no. 6902 (31 p.). https://doi.org/10.3390/ijms25136902
15. Kartavtsev Y. Ph. Analysis of sequence diversity at mitochondrial genes on different taxonomic levels. Applicability of DNA based distance data in genetics of speciation and phylogenetics. In: *Genetic Diversity* / C. L. Mahoney, D. A. Springer (Eds). New York : Nova Science Publishers, 2009a, chap. 1, pp. 1–50.

16. Kartavtsev Y. Ph. Divergence at *Cyt-b* and *Co-1* mtDNA genes on different taxonomic levels and genetics of speciation in animals. *Mitochondrial DNA*, 2011a, vol. 22, iss. 3, pp. 55–65. https://doi.org/10.3109/19401736.2011.588215
17. Kartavtsev Y. Ph. *Molecular Evolution and Population Genetics*. Vladivostok : Far Eastern State University, 2009b, 280 p. (in Russ.; content, table and figure captions are in Eng.)
18. Kartavtsev Y. Ph. Sequence divergence at mitochondrial genes in animals: Applicability of DNA data in genetics of speciation and molecular phylogenetics. *Marine Genomics*, 2011b, vol. 4, iss. 2, pp. 71–81. https://doi.org/10.1016/j.margen.2011.02.002
19. Kartavtsev Yu. Ph. Some examples of the use of molecular markers for needs of basic biology and modern society. *Animals*, 2021, vol. 11, iss. 5, art. no. 1473 (24 p.). https://doi.org/10.3390/ani11051473
20. Lowry J. K., Myers A. A. A phylogeny and classification of the Senticaudata subord. nov. (Crustacea: Amphipoda). *Zootaxa*, 2013, vol. 3610, no. 1, pp. 1–80. https://doi.org/10.11646/zootaxa.3610.1.1
21. Marin I., Palatov D. New and non-alien: *Echinogammarus mazestiensis* sp. n. from the southwestern Caucasus (Amphipoda: Gammaridae). *Zoology in the Middle East*, 2021, vol. 67, iss. 4, pp. 309–320. https://doi.org/10.1080/09397140.2021.1949139
22. Marin I., Palatov D., Copilaș-Ciocianu D. The remarkable Ponto-Caspian amphipod diversity of the lower Durso River (SW Caucasus) with the description of *Litorogammarus dursi* gen. et sp. nov. *Zootaxa*, 2023, vol. 5297, no. 4, pp. 483–517. https://doi.org/10.11646/zootaxa.5297.4.2
23. Nei M., Kumar S. *Molecular Evolution and Phylogenetics*. New York : Oxford University Press, 2000, 333 p.
24. Posada D. jModelTest: Phylogenetic model averaging. *Molecular Biology and Evolution*, 2008, vol. 25, iss. 7, pp. 1253–1256. https://doi.org/10.1093/molbev/msn083
25. Puillandre N., Brouillet S., Achaz G. ASAP: Assemble species by automatic partitioning. *Molecular Ecology Resources*, 2021, vol. 21, iss. 2, pp. 609–620. https://doi.org/10.1111/1755-0998.13281
26. Puillandre N., Lambert A., Brouillet S., Achaz G. ABGD, Automatic Barcode Gap Discovery for primary species delimitation. *Molecular Ecology*, 2012, vol. 21, iss. 8, pp. 1864–1877. https://doi.org/10.1111/j.1365-294X.2011.05239.x
27. Redin A. D., Kartavtsev Y. P. The mitogenome structure of righteye flounders (Pleuronectidae): Molecular phylogeny and systematics of the family in East Asia. *Diversity*, 2022, vol. 14, iss. 10, art. no. 805 (27 p.). https://doi.org/10.3390/d14100805
28. Ronquist F., Huelsenbeck J. P. MrBayes 3: Bayesian phylogenetic inference under mixed models. *Bioinformatics*, 2003, vol. 19, iss. 12, pp. 1572–1574. https://doi.org/10.1093/bioinformatics/btg180
29. Tamura K., Nei M. Estimation of the number of nucleotide substitutions in the control region of mitochondrial DNA in humans and chimpanzees. *Molecular Biology and Evolution*, 1993, vol. 10, iss. 3, pp. 512–526. https://doi.org/10.1093/oxfordjournals.molbev.a040023
30. Tamura K., Stecher G., Kumar S. MEGA11: Molecular Evolutionary Genetics Analysis Version 11. *Molecular Biology and Evolution*, 2021, vol. 38, iss. 7, pp. 3022–3027. https://doi.org/10.1093/molbev/msab120

ИЗМЕНЧИВОСТЬ НУКЛЕОТИДНЫХ ПОСЛЕДОВАТЕЛЬНОСТЕЙ МАРКЕРОВ ДВУХ ГЕНОВ (*CO-1* И *H3*) *LITOROGAMMARUS KARADAGIENSIS* (GRINTSOV, 2009) (AMPHIPODA, GAMMARIDAE) И СИСТЕМАТИКА РОДА *LITOROGAMMARUS*

А. О. Золотова[1], В. А. Гринцов[2], В. И. Рябушко[2], Ю. Ф. Картавцев[1]

[1]Национальный научный центр морской биологии имени А. В. Жирмунского ДВО РАН, Владивосток, Российская Федерация

[2]ФГБУН ФИЦ «Институт биологии южных морей имени А. О. Ковалевского РАН», Севастополь, Российская Федерация

E-mail: *anna.o.zolotova@gmail.com*

Исследована внутри- и межвидовая изменчивость гена субъединицы I цитохромоксидазы *c* митохондриальной ДНК (*Co-1*) и гена гистона *H3* ядерной ДНК представителей рода *Litorogammarus*. Показано, что молекулярный маркер гена гистона *H3* не подходит для видовой идентификации *Litorogammarus* ввиду своей недостаточной изменчивости. Таксономия изученных видов рода уточнена на основании анализа молекулярного маркера гена *Co-1*. Результаты комплексного анализа генетических расстояний (*p*-расстояний), выполненного с помощью ABGD и ASAP, подтверждают значимость участка гена *Co-1* как маркера для идентификации видов рода *Litorogammarus*. На основе информации для четырёх филогенетических реконструкций и анализа топологии соответствующих генных деревьев для *Co-1* выяснена генетическая близость видов *L. karadagiensis* и *L. glareophilus*. Для этих двух видов выявлены общие морфологические признаки — перистые щетинки на мандибулах, максиллах первой пары, максиллипедах и члениках гнатопод первой и второй пар. Использование молекулярных и морфологических данных в интегративном подходе представляется перспективным для идентификации видов и для решения таксономических вопросов в пределах анализируемой группы амфипод.

Ключевые слова: мтДНК, яДНК, *Co-1*, гистон *H3*, *p*-расстояния, *Litorogammarus karadagiensis*, *Litorogammarus*, Gammaridae, Amphipoda

1871
ИнБЮМ – IBSS

Морской биологический журнал
Marine Biological Journal
2025, vol. 10, no. 4, pp. 60–69
https://marine-biology.ru/mbj/article/view/496

UDC 582.261.1:577.1.044

THE EFFECT OF NITROGEN AND PHOSPHORUS ON THE ACCUMULATION OF EXTRACELLULAR MARENNINE-LIKE PIGMENT IN THE CULTURE OF *HASLEA KARADAGENSIS* (BACILLARIOPHYTA)

© 2025 **E. Kirienko and N. Davidovich**

T. I. Vyazemsky Karadag Scientific Station – Nature Reserve of RAS – Branch of IBSS,
Feodosiya, Russian Federation
E-mail: *esk-00@bk.ru*

Received 15.01.2025; revised 15.01.2025;
accepted 12.08.2025.

Currently, five diatom species from the genus *Haslea* are known to produce marennine pigments which slightly differ in their physicochemical characteristics. The available data on these pigments primarily relate to *H. ostrearia*, but given the biodiversity noted, it is important to analyze the pigments in other representatives of the genus, specifically *H. karadagensis*, endemic to the Black Sea. The aim of this study was to investigate the effect of nitrogen and phosphorus on the accumulation of marennine-like pigments in *H. karadagensis* cultures. Literature data on the effects of these essential biogenic elements on pigment accumulation in the cultures are conflicting. For the clones analyzed, the absence of a significant correlation was established between the specific productivity in relation to the release of extracellular marennine and levels of nitrogen and phosphorus in a medium. Growth rates and dynamics of extracellular marennine accumulation in *H. karadagensis* cultures are determined.

Keywords: diatoms, *Haslea karadagensis*, marennine, biogenic elements, pigment accumulation, specific productivity, cell abundance

Marennine is a water-soluble pigment produced by some diatoms from the genus *Haslea*. Pigments of the marennine group are blue, blue-green, or grey-green in color, depending on the producer species, and have antibacterial, antiviral, antiproliferative [Bergé et al., 1999; Carbonnelle et al., 1999; Gastineau et al., 2012b, c], and antioxidant activity [Pouvreau et al., 2008]. Also, they exhibit allelopathy towards bacteria, some microalgae, and invertebrates [Pouvreau et al., 2007; Prasetiya et al., 2016, 2020].

Despite practical interest in using marennine in oyster aquaculture on the Atlantic coast of France [Gastineau et al., 2012c, 2018] and more than a century of its study, the functional purpose, molecular structure, and diversity of pigments of this group remain unclear. It is believed that the pigment is capable of screening excess photosynthetically active radiation, thus acting as a photoprotector [Schubert et al., 1995]. Marennine is known to have 2 forms, differing in chemical composition and spectral characteristics [Pouvreau et al., 2006]. The intracellular form of this pigment is accumulated in the apical parts of cells. The extracellular form of marennine released from a cell into the environment has slightly different physicochemical properties and a lower molecular weight. It has long been believed that the only species capable of producing marennine

is *Haslea ostrearia* (Gaillon) Simonsen. The description in 2012 of a second marennine producer, *H. karadagensis* Davidovich, Gastineau & Mouget [Gastineau et al., 2012a], recorded in the coastal Black Sea area, initiated the study of the marennine diversity [Gastineau et al., 2014].

According to D. Neuville and P. Daste [1972; 1978], the release of marennine by *H. ostrearia* is driven by unfavorable environmental conditions, especially nitrate starvation in the presence of light. T. Lebeau [Lebeau et al., 2000] shares this opinion, claiming that insufficient nitrogen stresses cells thus causing elevated pigment synthesis. R. Nghiem Xuan [Nghiem Xuan et al., 2021] confirms that it is the limitation of silicon and nitrogen, rather than deficiency, that is responsible for a high concentration of extracellular marennine revealed in *H. ostrearia* cultures. Some authors explain a gain in the content of extracellular marennine in a culture by cell lysis when a significant cell density and deficiency of nutrients are reached [Nghiem Xuan et al., 2020], ignoring the fact of the existence of two different pigment forms. Other authors take a different view, claiming that the key factor of the marennine release is the amount and spectral composition of light [Mouget et al., 1999, 2004, 2005; Prasetiya et al., 2016]. A rise in the marennine production was recorded with a decrease in the cell size of *H. ostrearia* throughout its life cycle [Pedron et al., 2023]. Currently, five species capable of producing marennine-like pigments are known. In addition to above-mentioned, those include *H. provincialis* Gastineau, Hansen & Mouget [Gastineau et al., 2016], *H. nusantara* Mouget, Gastineau & Syakti [Prasetiya et al., 2019], and *H. silbo* Gastineau, Hansen & Mouget [Gastineau et al., 2021]. Marennine-like pigments (hereinafter marennine) exhibit some differences in their physicochemical characteristics [Gastineau et al., 2014; Pouvreau et al., 2006]. The diversity of pigments determined the aim of the present work: to reveal the effect of nitrogen and phosphorus concentrations on the efficiency of the marennine production and changes in the cell density in a culture of the diatom *Haslea karadagensis* which had not been previously studied in this regard.

MATERIAL AND METHODS

In an experiment with the addition of biogenic elements, three clones of the marine diatom *H. karadagensis* were used: 23.1113-KS, 23.1129-KE, and 23.1227-KC. Those are descendants of the parental pairs 22.1128-KC + 23.1129-KU, 22.1129-KA + 22.1129-KB, and 22.1228-KE + 22.1128-KH, respectively, from the Collection of Diatoms of the World Ocean (Karadag Scientific Station, IBSS, https://ibss-ras.ru/about-ibss/structure-ibss/tsentry-kollektivnogo-polzovaniya/collection-of-diatoms-of-world-ocean/). Clones 23.1129-KE and 23.1113-KS were characterized by higher concentration of extracellular marennine and cell density, while 23.1227-KC was less productive. On average, cell sizes for clones 23.1129-KE, 23.1113-KS, and 23.1227-KC were (15.3 ± 0.28), (48.5 ± 0.32), and (56.1 ± 0.28) μm, respectively.

Pure cultures were maintained under non-axenic conditions in 50-mL glass Erlenmeyer flasks. A modified artificial ESAW medium (Enriched Seawater, Artificial Water) [Polyakova et al., 2018] was used as a medium, with a salinity level of 20‰ taken as standard cultivation conditions. Cultures were grown at a temperature of +20 °C at two levels of illuminance, 3.3 and 7.2 klx, with the aid of LED lamps LLED-05-T5-FITO-14W-W [ATL Business (Shenzhen) Co., Ltd., China]. The photoperiod was 14 h / 10 h (light / dark). Illuminance was measured with a lux meter Yu-116 (USSR). To the flasks, 0.5 mL of inoculum with a cell density of 100 cells·mL^{-1} was added.

In six clones of *H. karadagensis*, for 20 days, the concentration of pigment released into the medium was measured every 2 days. The cell concentration was estimated in a Fuchs–Rosenthal chamber. The rate of cell division for the first 5 days was determined by a change in the cell density according to the exponential growth model [Wood et al., 2005]. The rate of the marennine accumulation in cultures for the same clones was calculated in a similar manner.

During the study, 24 different nitrogen concentration options and 29 phosphorus concentration options in 154 combinations were tested. For two clones, 12 combinations involving nitrogen and phosphorus were tested at a higher illuminance (7.2 klx).

The main biogenic elements (nitrogen and phosphorus) were preliminarily excluded from the composition of the completely artificial ESAW medium; then, their required amount was added in the form of $NaNO_3$ and NaH_2PO_4 compounds. Concentrations in the medium were within ranges of 0.136–43.2 mg·L^{-1} for nitrogen and 0.014–4.481 mg·L^{-1} for phosphorus. The modified ESAW medium served as a control.

The duration of the culture growth in the experiments was 10 days, during which they were in the exponential growth phase, not reaching the stationary one. In this case, the release of extracellular marennine by cells into the culture medium was intravital as evidenced by the absence of dead cells (empty frustules). In a 10-day period, extracellular marennine was accumulated in the cultures in a concentration sufficient for spectrophotometric analysis.

Non-specific absorption was extremely low, and this allowed the use of unfiltered medium containing dissolved extracellular marennine for spectral analysis. Optical density was measured in a cuvette with an optical path length of 2 cm. Absorption spectra were recorded with a PromEcoLab PE-5400UF spectrophotometer (Shanghai Mapada Instruments Co., Ltd., China) and supplied Scan54 software.

To calculate the concentration of extracellular marennine in *H. karadagensis* according to the Bouguer–Lambert–Beer law, we used the only currently known values of the molar extinction coefficient [ε677 = 120,000 L·mol^{-1}·cm^{-1} for a wavelength of 677 nm] and the molar mass [M = (9,893 ± 1) Da] obtained for extracellular marennine in *H. ostrearia* [Pouvreau et al., 2006]. The wavelength of 677 nm corresponds to the maximum optical density in the red region of the spectrum for extracellular forms of marennine of both species. The cell concentration in the cultures was calculated on the 10th day of the experiment.

The mean values of extracellular marennine content, cell density, and specific cell productivity in terms of extracellular marennine (hereinafter specific productivity) are given in the text and figures taking into account the error of the mean.

RESULTS AND DISCUSSION

Under our standard culture conditions, exponential growth of *H. karadagensis* cells was recorded for at least 5–6 days (Fig. 1A). This is consistent with the data of authors who reported, at different nutrient concentrations, a late exponential phase on the 8th day of cultivation [Pedron et al., 2023]. Subsequently, growth was declining, and cells formed clusters making it impossible to accurately count them in the following days.

During the first week, the marennine concentration in the culture also increased exponentially, and during the following month, linearly (Fig. 1B). The graph of the accumulation rate of extracellular marennine shows as follows: 5–8 days are required to obtain a pigment concentration sufficient for spectrophotometric analysis. During this period, the *H. karadagensis* culture is in the exponential growth

phase, cells do not die, and only the extracellular form of the pigment is accumulated in the medium. By the end of the month, clonal variability in terms of both cell density and extracellular marennine concentration became evident.

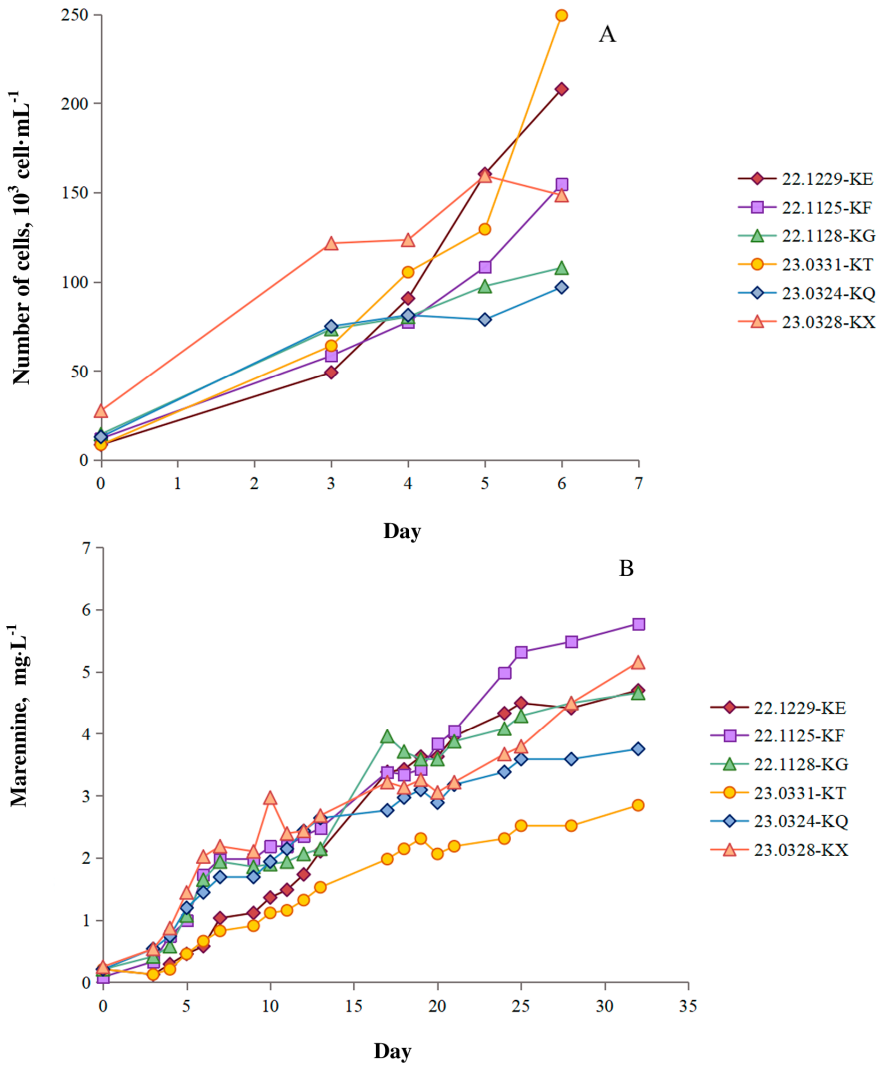


Fig. 1. The cell density growth (A) and extracellular marennine accumulation (B) in *Haslea karadagensis* cultures under standard cultivation conditions. The legend indicates the names of the clones used

With a gain in nitrogen and phosphorus content, we recorded a drop in the concentration of extracellular marennine accumulated in the medium. This dependence was approximated by an exponential function with a high correlation (Fig. 2A, B). Furthermore, the cell density in the cultures significantly decreased with an increase in nitrogen concentration (Fig. 2C), while a rise in phosphorus concentration in the medium within the studied range did not result in a decline in the cell density (Fig. 2D). Our data are quite consistent with the results of other authors for *H. ostrearia* cultures [Lebeau et al., 2000; Neuville, Daste, 1972, 1978; Nghiem Xuan et al., 2021].

In the cultures of the more productive clones, 23.1129-KE and 23.1113-KS, a mean of 1.8 mg·L^{-1} of marennine was accumulated at a nitrogen concentration of 0.177–43.200 mg·L^{-1}, phosphorus concentration of 0.018–4.784 mg·L^{-1}, and illuminance of 3.3 klx. The mean cell density and specific productivity were 77,197 cells·mL^{-1} and 30 pg·cells^{-1}, respectively.

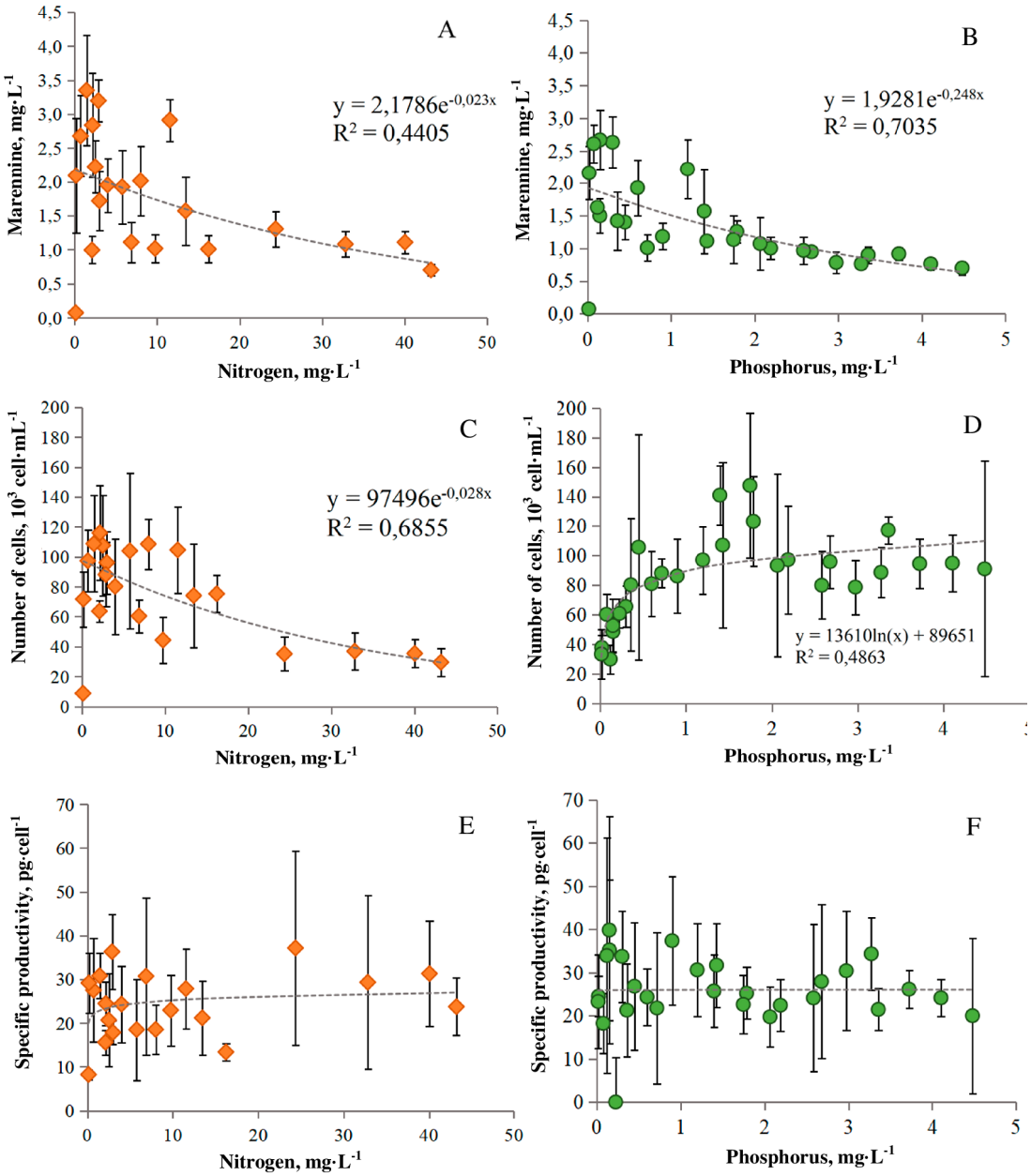


Fig. 2. The mean values of extracellular marennine content (A, B), cell density (C, D), and specific extracellular marennine productivity (E, F) in *Haslea karadagensis* culture for different concentration of nitrogen and phosphorus in the medium at the illuminance level of 3.3 klx. When approximating the data, concentrations of biogenic elements close to zero were excluded (0.136 μg·L^{-1} for nitrogen and 0.014 μg·L^{-1} for phosphorus)

The less productive clone, 23.1227-KC, was characterized by the mean marennine concentration of 1.25 mg·L^{-1}. In the experiments with this clone, the maximum nitrogen content (128.5 mg·L^{-1}) was tested; however, it did not lead to a significant shift in the marennine concentration. No cell death due to nitrogen poisoning was revealed.

For the illuminance level of 7.2 klx, the mean value of extracellular marennine concentration was 3.14 mg·L^{-1}. The cell density was 58,177 cells·mL^{-1}, and the specific productivity was 60 pg·cells^{-1}, *i. e.*, twice as high as at lower illuminance.

At close-to-zero concentrations of biogenic elements, 0.136 mg·L^{-1} of nitrogen and 0.014 mg·L^{-1} of phosphorus, the marennine production was minimal and averaged 0.51 mg·L^{-1}. However, even a slight increase in their content, nitrogen to 0.177 mg·L^{-1} and phosphorus to 0.018 mg·L^{-1}, led to the same concentration of cells and marennine in the medium as with a higher supply of biogenic elements (Fig. 3).

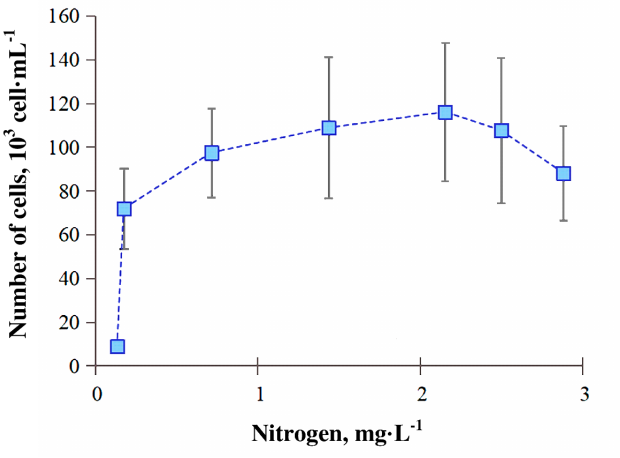


Fig. 3. The cell density in the *Haslea karadagensis* culture after 10 days of cultivation under low nitrogen concentration

According to the data obtained, the specific cell productivity of the *H. karadagensis* culture for marennine (its extracellular form) did not depend on the concentration of the main biogenic elements in a fairly wide range, except for minimal values, and averaged about 30 pg·cells^{-1} (Fig. 2E, F). As assumed, the key factor limiting pigment production is illuminance, since marennine is believed to perform a photoprotective function by shielding chloroplasts from ultraviolet radiation [Schubert et al., 1995]. As noted above, the spectral composition of light is also important: the marennine production significantly increased when *H. ostrearia* cultures were illuminated with blue light compared to illumination with the control white light [Mouget et al., 2005].

The density of diatom cells, according to some authors, is determined chiefly by the availability of silicon [Nghiem Xuan et al., 2021]. The second crucial element affecting the cell density growth is phosphorus [Turpin et al., 1999]. In the ESAW medium we used, the silicon concentration was 3 mg·L^{-1}, and it was quite sufficient for the consumption by cells during 10 days of cultivation.

The marennine accumulation in a medium was shown to depend on its composition [Nghiem Xuan et al., 2020]. It was also noted as follows: if the medium contains both organic and inorganic sources of nitrogen and phosphorus, the marennine production is low. Importantly, the same as in our experiments, an increase in nitrogen content to certain values initially favored the marennine synthesis, and subsequently inhibited the cell density growth and the pigment accumulation in the medium. The composition of the ASW medium (Artificial Seawater) is most similar to that of ESAW. According to the data provided [Nghiem Xuan et al., 2020], a medium developed on the basis of the ES1/3 medium turned out to be optimal for the marennine accumulation. Moreover, in the marennine synthesis, the role of both the composition and the concentration of biogenic elements was significant.

In addition to their general theoretical value, the results obtained have practical significance for biotechnology, in particular for the aquaculture of filter-feeding molluscs, such as oysters. Marennine not only improves their organoleptic properties and increases their commercial value,

but, being a biologically active substance, has a preventive effect: it protects against diseases [Gastineau et al., 2012c, 2018]. Currently, biotechnology for the marennine production involving cultures of *Haslea* representatives is not used; oyster farmers rely on natural and poorly predictable outbreaks of algae development in ponds where these molluscs are kept. Notably, under natural conditions, it is impossible to achieve such a high concentration of marennine as in laboratory cultures. Thus, in a field experiment, when water supplied to oyster ponds was enriched with nitrogen, phosphorus, and silicon, the maximum observed content of extracellular marennine was 2.7 mg·L^{-1} [Turpin et al., 1999]. In a non-laboratory experiment, the marennine concentration reached 3.4 mg·L^{-1} [Turpin et al., 2001]. In *H. ostrearia* culture in a photobioreactor, the marennine content was an order of magnitude higher: 20–30 mg·L^{-1} [Rossignol et al., 2000].

Another noteworthy factor is clonal variability. In our study, three *H. karadagensis* clones were used, and two of them exhibited higher productivity in terms of extracellular marennine synthesis. A similar pattern of variation was recorded in experiments with *H. ostearia* [Mouget et al., 2005; Pedron et al., 2023]. As found, the clones differed in cell size, and this indicates they were at different stages of the life cycle. The highest productivity in terms of pigment accumulation was demonstrated by medium-sized cells. The exact reasons for the variability are unknown, and this may become a topic for new research.

Conclusions. For the marennine-producing diatom *Haslea karadagensis*, we revealed no significant correlation between nitrogen and phosphorus concentration in a medium and the specific productivity in terms of extracellular marennine synthesis. Relatively low content of these biogenic elements, 0.177 mg·L^{-1} of nitrogen and 0.018 mg·L^{-1} of phosphorus, was sufficient for optimal growth of *H. karadagensis* cultures and accumulation of extracellular pigment in the medium. An increase in their concentration negatively affected the cell density growth and accumulation of extracellular marennine in the culture.

The key drivers of the productivity of marennine accumulation were illuminance and, likely, clonal variability. An increase in illuminance from 3.3 to 7.2 klx stimulated a nearly twofold boost in both extracellular pigment concentration and specific productivity. The effect of intraclonal differences requires further study.

The study was carried out with the financial support of the Russian Science Foundation (project No. 24-24-00054).

The work used the materials of the IBSS core facility “Collection of Diatoms of the World Ocean.”

REFERENCES

1. Polyakova S. L., Davidovich O. I., Podunay Yu. A., Davidovich N. A. Modification of the ESAW culture medium used for cultivation of marine diatoms. *Marine Biological Journal*, 2018, vol. 3, no. 2, pp. 73–80. (in Russ.). https://doi.org/10.21072/mbj.2018.03.2.06
2. Bergé J.-P., Bourgougnon N., Alban S., Pojer F., Billaudel S., Chermann J.-C., Robert J.-M., Franz G. Antiviral and anticoagulant activities of a water-soluble fraction of the marine diatom *Haslea ostrearia*. *Planta Medica*, 1999, vol. 65, iss. 7, pp. 604–609. https://doi.org/10.1055/s-1999-14032
3. Carbonnelle D., Pondaven P., Morançais M., Massé G., Bosch S., Jacquot C., Briand G., Robert J.-M., Roussakis C. Antitumor and antiproliferative effects of an aqueous extract from the marine diatom *Haslea ostrearia* (Gaillon) Simonsen against solid tumors: Lung carcinoma (NSCLC-N6), kidney carcinoma (E39) and melanoma (M96) cell lines. *Anticancer Research*, 1999, vol. 19, iss. 1A, pp. 621–624.

4. Gastineau R., Davidovich N. A., Bardeau J.-F., Caruso A., Leignel V., Hardivillier Y., Jacquette B., Davidovich O. I., Rincé Y., Gaudin P., Cox E. J., Mouget J.-L. *Haslea karadagensis* (Bacillariophyta): A second blue diatom, recorded from the Black Sea and producing a novel blue pigment. *European Journal of Phycology*, 2012a, vol. 47, iss. 4, pp. 469–479. https://doi.org/10.1080/09670262.2012.741713
5. Gastineau R., Davidovich N., Hansen G., Rines J., Wulff A., Kaczmarska I., Ehrman J., Hermann D., Maumus F., Hardivillier Y., Leignel V., Jacquette B., Méléder V., Hallegraeff G., Yallop M., Perkins R., Cadoret J.-P., Saint-Jean B., Carrier G., Mouget J.-L. *Haslea ostrearia*-like diatoms: Biodiversity out of the blue. In: *Advances in Botanical Research*. Vol. 71. *Sea Plants* / N. Bourgougnon (Ed.). UK : Academic Press, 2014, pp. 441–465. https://doi.org/10.1016/B978-0-12-408062-1.00015-9
6. Gastineau R., Hansen G., Davidovich N. A., Davidovich O. I., Bardeau J.-F., Kaczmarska I., Ehrman J. M., Leignel V., Hardivillier Y., Jacquette B., Poulin M., Morançais M., Fleurence J., Mouget J.-L. A new blue-pigmented hasleoid diatom, *Haslea provincialis*, from the Mediterranean Sea. *European Journal of Phycology*, 2016, vol. 51, iss. 2, pp. 156–170. https://doi.org/10.1080/09670262.2015.1110861
7. Gastineau R., Hansen G., Poulin M., Lemieux C., Turmel M., Bardeau J.-F., Leignel V., Hardivillier Y., Morançais M., Fleurence J., Gaudin P., Méléder V., Cox E. J., Davidovich N. A., Davidovich O. I., Witkowski A., Kaczmarska I., Ehrman J. M., Onís E. S., Quintana A. M., Mucko M., Mordret S., Sarno D., Jacquette B., Falaise C., Séveno J., Lindquist N. L., Kemp P. S. Jr., Eker-Develi E., Konucu M., Mouget J.-L. *Haslea silbo*, a novel cosmopolitan species of blue diatoms. *Biology*, 2021, vol. 10, iss. 4, art. no. 328 (27 p.). https://doi.org/10.3390/biology10040328
8. Gastineau R., Hardivillier Y., Leignel V., Tekaya N., Morançais M., Fleurence J., Davidovich N. A., Jacquette B., Gaudin P., Hellio C., Bourgougnon N., Mouget J.-L. Greening effect on oysters and biological activities of the blue pigments produced by the diatom *Haslea karadagensis* (Naviculaceae). *Aquaculture*, 2012b, vol. 368–369, pp. 61–67. https://doi.org/10.1016/j.aquaculture.2012.09.016
9. Gastineau R., Pouvreau J.-B., Hellio C., Morançais M., Fleurence J., Gaudin P., Bourgougnon N., Mouget J.-L. Biological activities of purified marennine, the blue pigment produced by the diatom *Haslea ostrearia* and responsible for the greening of oysters. *Journal of Agricultural and Food Chemistry*, 2012c, vol. 60, iss. 14, pp. 3599–3605. https://doi.org/10.1021/jf205004x
10. Gastineau R., Prasetiya F. S., Falaise C., Cognie B., Decottignies P., Morançais M., Méléder V., Davidovich N. A., Turcotte F., Tremblay R., Pasetto P., Dittmer J., Bardeau J.-F., Pouvreau J.-B., Mouget J.-L. Marennine-like pigments: Blue diatom or green oyster cult? In: *Blue Biotechnology: Production and Use of Marine Molecules* : in 2 vols / S. La Barre, S. S. Bates (Eds). Weinheim : Wiley-VCH Verlag GmbH & Co. KGaA, 2018, vol. 2, pp. 529–551. https://doi.org/10.1002/9783527801718.ch16
11. Lebeau T., Gaudin P., Junter G.-A., Mignot L., Robert J.-M. Continuous marennin production by agar-entrapped *Haslea ostrearia* using a tubular photobioreactor with internal illumination. *Applied Microbiology and Biotechnology*, 2000, vol. 54, iss. 5, pp. 634–640. https://doi.org/10.1007/s002530000380
12. Mouget J.-L., Rosa P., Tremblin G. Acclimation of *Haslea ostrearia* to light of different spectral qualities – confirmation of 'chromatic adaptation' in diatoms. *Journal of Photochemistry and Photobiology B: Biology*, 2004, vol. 75, iss. 1–2, pp. 1–11. https://doi.org/10.1016/j.jphotobiol.2004.04.002
13. Mouget J.-L., Rosa P., Vachoux C., Tremblin G. Enhancement of marennine production by blue light in the diatom *Haslea ostrearia*. *Journal of Applied Phycology*, 2005, vol. 17, iss. 5, pp. 437–445. https://doi.org/10.1007/s10811-005-0561-7
14. Mouget J.-L., Tremblin G., Morant-Marceau A., Morançais M., Robert J.-M. Long-term photoacclimation of *Haslea ostrearia* (Bacillariophyta): Effect of irradiance on growth rates, pigment

content and photosynthesis. *European Journal of Phycology*, 1999, vol. 34, iss. 2, pp. 109–115. https://doi.org/10.1080/09670269910001736162

15. Neuville D., Daste P. H. Production du pigment bleu par la diatomée *Navicula ostrearia* (Gaillon) Bory, maintenue en culture uni-algue sur milieu synthétique carencé en azote. *Comptes rendus de l'Académie des Sciences. Sér. D Sciences Naturelles*, 1972, vol. 274, pp. 2030–2033.
16. Neuville D., Daste P. H. Recherches sur le déterminisme de la production de marennine par la diatomée marine *Navicula ostrearia* (Gaillon) Bory en culture *in vitro*. *Revue générale de botanique*, 1978, vol. 85, pp. 255–303.
17. Nghiem Xuan R., Mouget J.-L., Turpin V., Jaouen P., Pruvost J. Optimization of the growth and marennine production by the diatom *Haslea ostrearia* in photobioreactor. *Algal Research*, 2021, vol. 55, art. no. 102251 (17 p.). https://doi.org/10.1016/j.algal.2021.102251
18. Nghiem Xuan R., Safitri I., Mouget J.-L., Pruvost J., Turpin V., Jaouen P. Design of an artificial culture medium to optimize *Haslea ostrearia* biomass and marennine production. *Algal Research*, 2020, vol. 45, art. no. 101653 (11 p.). https://doi.org/10.1016/j.algal.2019.101653
19. Pedron E., Gargouch N., Mouget J.-L., Tremblay R., Deschênes J.-S., Massé A., Gonçalves O. Hybrid photobioreactor operation for the intensified production of *Haslea ostrearia* and marennine in function of strain variability. *Algal Research*, 2023, vol. 75, art. no. 103285 (9 p.). https://doi.org/10.1016/j.algal.2023.103285
20. Pouvreau J.-B., Housson E., Le Tallec L., Morançais M., Rincé Y., Fleurence J., Pondaven P. Growth inhibition of several marine diatom species induced by the shading effect and allelopathic activity of marennine, a blue-green polyphenolic pigment of the diatom *Haslea ostrearia* (Gaillon/Bory) Simonsen. *Journal of Experimental Marine Biology and Ecology*, 2007, vol. 352, iss. 1, pp. 212–225. https://doi.org/10.1016/j.jembe.2007.07.011
21. Pouvreau J.-B., Morançais M., Fleury F., Rosa F., Thion L., Cahingt B., Zal F., Fleurence J., Pondaven P. Preliminary characterization of the blue-green pigment "marennine" from the marine tychopelagic diatom *Haslea ostrearia* (Gaillon/Bory) Simonsen. *Journal of Applied Phycology*, 2006, vol. 18, iss. 6, pp. 757–767. https://doi.org/10.1007/s10811-006-9087-x
22. Pouvreau J.-B., Morançais M., Taran F., Rosa P., Dufossé L., Guérard F., Pin S., Fleurence J., Pondaven P. Antioxidant and free radical scavenging properties of marennine, a blue-green polyphenolic pigment from the diatom *Haslea ostrearia* (Gaillon/Bory) Simonsen responsible for the natural greening of cultured oysters. *Journal of Agricultural and Food Chemistry*, 2008, vol. 56, iss. 15, pp. 6278–6286. https://doi.org/10.1021/jf073187n
23. Prasetiya F. S., Decottignies P., Tremblay R., Mouget J.-L., Sunarto S., Iskandar I., Dhahiyat Y., Cognie B. Not only greening: The effects of marennine produced by *Haslea ostrearia* on physiological traits of three bivalve species. *Aquaculture Reports*, 2020, vol. 18, art. no. 100546 (8 p.). https://doi.org/10.1016/j.aqrep.2020.100546
24. Prasetiya F. S., Gastineau R., Poulin M., Lemieux C., Turmel M., Syakti A. D., Hardivillier Y., Widowati I., Risjani Y., Iskandar I., Subroto T., Falaise C., Arsad S., Safitri I., Mouget J.-L., Leignel V. *Haslea nusantara* (Bacillariophyceae), a new blue diatom from the Java Sea, Indonesia: Morphology, biometry and molecular characterization. *Plant Ecology and Evolution*, 2019, iss. 152, no. 2, pp. 188–202. https://doi.org/10.5091/plecevo.2019.1623
25. Prasetiya F. S., Safitri I., Widowati I., Cognie B., Decottignies P., Gastineau R., Morançais M., Windarto E., Tremblay R., Mouget J.-L. Does allelopathy affect co-culturing *Haslea ostrearia* with other microalgae relevant to aquaculture? *Journal of Applied Phycology*, 2016, vol. 28, iss. 4, pp. 2241–2254. https://doi.org/10.1007/s10811-015-0779-y
26. Rossignol N., Jaouen P., Robert J.-M., Quéméneur F. Production of exocellular pigment by the marine diatom *Haslea ostrearia* Simonsen in a photobioreactor equipped with immersed ultrafiltration membranes. *Bioresource Technology*, 2000, vol. 73, iss. 2,

pp. 197–200. https://doi.org/10.1016/S0960-8524(99)00171-6
27. Schubert H., Tremblin G., Robert J.-M., Sagert S., Rincé Y. *In-vivo* fluorescence measurement of photosynthesis of *Haslea ostrearia* Simonsen in relation to marennine content. *Diatom Research*, 1995, vol. 10, iss. 2, pp. 341–349. https://doi.org/10.1080/0269249X.1995.9705354
28. Turpin V., Robert J.-M., Goulletquer P. Limiting nutrients of oyster pond seawaters in the Marennes-Oléron region for *Haslea ostrearia*: Applications to the mass production of the diatom in mesocosm experiments. *Aquatic Living Resources*, 1999, vol. 12, iss. 5, pp. 335–342. https://doi.org/10.1016/S0990-7440(99)00114-X
29. Turpin V., Robert J.-M., Goulletquer P., Massé G., Rosa P. Oyster greening by outdoor mass culture of the diatom *Haslea ostrearia* Simonsen in enriched seawater. *Aquaculture Research*, 2001, vol. 32, iss. 10, pp. 801–809. https://doi.org/10.1046/j.1365-2109.2001.00615.x
30. Wood A. M., Everroad R. C., Wingard L. M. Measuring growth rates in microalgal cultures. In: *Algal Culturing Techniques* / R. A. Andersen (Ed.). New York : Elsevier Academic Press, 2005, pp. 269–286. https://doi.org/10.1016/B978-012088426-1/50019-6

ВЛИЯНИЕ АЗОТА И ФОСФОРА НА НАКОПЛЕНИЕ ВНЕКЛЕТОЧНОГО МАРЕННИН-ПОДОБНОГО ПИГМЕНТА В КУЛЬТУРЕ *HASLEA KARADAGENSIS* (BACILLARIOPHYTA)

Е. С. Кириенко, Н. А. Давидович

Карадагская научная станция имени Т. И. Вяземского — природный заповедник РАН — филиал ФИЦ ИнБЮМ, Феодосия, Российская Федерация
E-mail: *esk-00@bk.ru*

В настоящее время известно пять видов диатомовых водорослей из рода *Haslea*, которые способны продуцировать пигменты маренниры, слегка различающиеся по своим физико-химическим характеристикам. Имеющиеся сведения относятся главным образом к маренниру *H. ostrearia*. Это делает актуальным изучение маренниры-подобных пигментов у других представителей рода, в частности у *H. karadagensis* — эндемика Чёрного моря. Цель исследования заключалась в анализе влияния азота и фосфора на накопление внеклеточного маренниры-подобного пигмента в клоновых культурах *H. karadagensis*. Следует отметить противоречивость литературных данных о влиянии этих основных биогенных элементов на накопление маренниры в культурах. Для изученных клонов *H. karadagensis* установлено отсутствие значимой корреляции между удельной продуктивностью клеток в отношении выделения внеклеточного маренниры-подобного пигмента и уровнями азота и фосфора в среде. Определены темпы роста численности клеток и динамика накопления внеклеточного пигмента в культурах *H. karadagensis*.

Ключевые слова: диатомовые водоросли, *Haslea karadagensis*, маренниры, биогенные элементы, накопление пигмента, удельная продуктивность, численность клеток

1871
ИнБЮМ – IBSS

Морской биологический журнал
Marine Biological Journal
2025, vol. 10, no. 4, pp. 70–87
https://marine-biology.ru/mbj/article/view/505

UDC [502.175:551.35](265.54.04)

PRELIMINARY RESULTS OF THE COMPREHENSIVE ASSESSMENT OF CONTAMINATION AND TOXIC EFFECTS OF BOTTOM SEDIMENTS IN SHALLOW BIGHTS OF AMUR BAY (SEA OF JAPAN)

© 2025 **A. Ryumina[1], M. Mazur[2], P. Tishchenko[1], and E. Shkirnikova[1]**

[1]V. I. Il'ichev Pacific Oceanological Institute FEB RAS, Vladivostok, Russian Federation

[2]A. V. Zhirmunsky National Scientific Center of Marine Biology FEB RAS, Vladivostok, Russian Federation

E-mail: *ryumina.aa@poi.dvo.ru*

Received 07.05.2024; revised 11.09.2024;
accepted 12.08.2025.

In August 2023, surface bottom sediments (top 5-cm layer) were sampled in three bights of Amur Bay: Melkovodnaya Bight (V1), Kruglaya Bight (V2) (both within Voevoda Bight), and Uglovoy Bight (U1). Despite being neighboring bays, V1 and V2 differ significantly in granulometric composition and distribution of both heavy metal concentration and organic carbon content. Elevated levels of heavy metals and organic carbon were revealed in Kruglaya Bight (at station V2). In its bottom sediments, values of the enrichment factor (EF) for each analyzed metal, except for Co, exceeded levels attributable to natural weathering processes. A high level of enrichment was registered for Cd (EF = 24.08); a moderately high one, for Cu (EF = 6.15) and Pb (EF = 5.51); and a moderate one, for Ni, Zn, and Cr (EF accounted for 4.5, 4.3, and 3.21, respectively). The calculation of the modified degree of contamination index (mCd) showed a moderate degree of contamination at sta. V2 (mCd = 4.38). In bottom sediments from sta. V1, most metals were characterized by a low level of enrichment, except for Cd, with its moderate level (EF = 4.07). EF values for bottom sediments from sta. U1 were significantly below 1.5 providing evidence for the natural-origin input of heavy metals from weathering processes. In the studied bays, biotesting was carried out for the first time, with larvae of the sea urchin *Scaphechinus mirabilis* serving as a test object. During bioassays, the highest abundance of abnormally developed larvae was found at sta. V2. In aqueous extracts of bottom sediments from sta. V2, none of larvae reached the gastrula stage, and the value of the integral toxicity index (ITI) was 9.84 points. In aqueous extracts from sta. V1 and U1, normally developed larvae at the late gastrula stage predominated 18 h after the start of the experiment. In extracts of bottom sediments from Melkovodnaya Bight (sta. V1), the overwhelming majority of larvae developed with severe morphological abnormalities. Larvae at the prism and early pluteus stages were characterized by poorly developed skeletal rods or their lack. Moreover, we found exoforms of larvae with no intestine in their body cavity (it was protruded outward). ITI for bottom sediments from sta. V1 (7.72 points) was twice as high as for samples from sta. U1 (3.5 points). The obtained data indicate that the accumulation of heavy metals in Kruglaya Bight is driven by a combination of factors. In their turn, high concentrations of heavy metals and organic carbon may mediate the formation of unfavorable conditions for benthic organisms.

Keywords: Amur Bay, biotesting, bottom sediments, organic carbon, heavy metals, *Scaphechinus mirabilis*

Sediments play a significant role in marine ecosystem functioning, as those serve as a habitat for benthos. Moreover, in sediments, accumulation and transformation of nutrients occur, as well as of a wide range of pollutants delivered to marine systems *via* terrestrial runoff and precipitation [Roberts, 2012]. Monitoring surveys and research on environmental pollution often target heavy metals currently defined

as metals with an atomic mass exceeding 50 atomic units: V, Cr, Mn, Fe, Co, Ni, Cu, Zn, Mo, Cd, Sn, Hg, Pb, Bi, *etc.* [Naleta et al., 2015]. These contaminants have significant toxic and cumulative effects [Rouchon, Phillips, 2017]. Consequently, an analysis of heavy metal concentrations in marine ecosystems remains an integral component of environmental quality assessments[Marine Water Pollution, 2022; Wilbers et al., 2014].

The toxicity of sediments can be evaluated by comparing concentrations of certain heavy metals and international regulatory values (sediment quality guidelines, SQGs [MacDonald et al., 2004]), and by calculating various individual and comprehensive indices. These approaches only provide information about potential toxic risks to hydrobionts. To fully assess risks associated with pollutant exposure, biological methods are additionally applied. One of them is bioassays on marine sediment extracts involving different test organisms. In this context, echinoderms are widely used as model organisms in ecotoxicological studies, as their responses to environmental stressors can be observed at various levels of biological organization: from the molecular genetic level to the ecosystem one [Canty, 2009]. The use of sea urchin larvae allows for the estimation of teratogenic effect of heavy metals [Chiarelli et al., 2019; Mazur et al., 2020; Rouchon, Phillips, 2017]. Furthermore, these test organisms are listed in numerous regulatory documents as the ones recommended for assessing the toxicity of marine sediments [ABNT-NBR 15350 DE 03/2023, 2025; ASTM, 2012].

Kruglaya and Melkovodnaya bights, located on the western side of Russky Island, are adjacent areas exhibiting pronounced differences in grain size distribution, and also in distribution of heavy metals and organic carbon [Ryumina et al., 2023]. Kruglaya Bight hosts extensive meadows of a seagrass *Zostera marina* Linnaeus, 1753. Moreover, there is an aquaculture farm, where the Yesso scallop *Mizuhopecten yessoensis* (Jay, 1857) and the Pacific blue mussel *Mytilus trossulus* A. Gould, 1850 are cultured [Gavrilova, Kucheryavenko, 2011]. The “Bely Lebed” sanatorium renowned for its therapeutic muds is located on Melkovodnaya Bight shores. Hydrological and hydrochemical studies in Voevoda Bight have shown that its offshore and middle sites (excluding Kruglaya Bight) are the areas that freely exchange waters with Amur Bay [Barabanshchikov et al., 2015]. In Voevoda Bight, the nature of biogeochemical processes is determined by the intensity of the production and decomposition of organic matter derived from three sources: phytoplankton, benthic macrophytes, and periphyton. In Melkovodnaya Bight, its specific coastal morphology, when combined with the effect of river runoff peaking in summer, results in closed cyclonic circulation. Consequently, water exchange between Melkovodnaya Bight and Amur Bay is weakened. Hydrochemical parameters in the bight have local features. Its circulation pattern can facilitate summer phytoplankton blooms that are primarily driven by an increased supply of nutrients from the Russkaya River runoff [Barabanshchikov et al., 2015]. The resulting excess of phytoplankton biomass, not eaten by zooplankton, is decomposed consuming oxygen and releasing carbon dioxide. Along with this, dead fragments of *Z. marina* are decomposed.

The above-described mechanism cannot be applied to Kruglaya Bight, as its waters are not affected by river runoff. There, the oxygen deficiency and elevated partial pressure of carbon dioxide are driven by the decomposition of organic matter produced mainly by a seagrass *Z. marina*.

Hydrochemical studies of Uglovoy Bight have revealed its ongoing ecosystem degradation [Tishchenko et al., 2021]. Its visible manifestations include the disappearance of *Z. marina* meadows, the occurrence of hypoxic events, and the fact that bight waters became a source of carbon dioxide for the atmosphere. Pollution of sediments with heavy metals occurs constantly as a result of economic activity on the bight shores. Pollutants mostly come with river runoff, due to sheet erosion

from the urbanized landscape, and because of the operation of a low-water bridge [Petukhov et al., 2023]. The construction of this bridge (De Frieze–Sedanka) in 2009–2012 also noticeably affected sediments in the bay (now De Frieze Peninsula and Muravyov-Amursky Peninsula are connected by a four-lane highway). Hydraulic engineering construction in the coastal zone is typically accompanied by a significant rise in water turbidity and pollutant concentrations. The volume of suspended matter entering the sea can be comparable to the discharge and annual runoff of large rivers [Mishukov et al., 2009].

The input of heavy metals into sediments of Voevoda Bight is poorly studied. Bioindication research on pollution in coastal waters of Russky Island revealed elevated concentrations of heavy metals in brown algae of the genus *Sargassum*, *S. miyabei* Yendo, 1907 and *S. pallidum* (Turner) C. Agardh, 1820, at stations on the Amur Bay side [Khristoforova et al., 2018]. These toxicants usually enter the aquatic environment through precipitation, chemical weathering of rocks, leaching of sorbed forms from soils, surface runoff, and wastewater (industrial, agricultural, and domestic). Crude oil tankers, product tankers, and other vessels can also contribute to pollution [Khristoforova et al., 2015]. According to previous geochemical surveys, the highest content of zinc and copper was registered in sediment samples from Kruglaya Bight, while the highest concentrations of chromium, nickel, and cobalt were recorded at stations in Uglovoy Bight [Ryumina et al., 2023].

The aim of this study was to carry out a preliminary comprehensive assessment of heavy metal contamination and toxic effects on hydrobionts in surface sediments (top 5-cm layer) from several sites in Amur Bay. The assessment integrates chemical analysis with biotesting involving embryos and larvae of the sand dollar *Scaphechinus mirabilis* (Agassiz, 1864). This test organism is used for bioassay in Amur Bay areas for the first time.

MATERIAL AND METHODS

Uglovoy Bight and Voevoda Bight are shallow second-order basins of Amur Bay (Peter the Great Bay, Sea of Japan) (Fig. 1). The area of Uglovoy Bight is 42 km^2. Numerous small streams and rivers flow into its eastern and northeastern shores; the largest rivers are Chernaya, Bogataya, Vesennyaya, Pyaty Klyuch, Peschanka, Saperka, Gryaznukha, and Aerodromnaya [Losev, 2019]. Voevoda Bight consists of two shallow basins: Kruglaya Bight and Melkovodnaya Bight. The water area of Voevoda Bight is approximately 4.0 km^2 (Melkovodnaya is about 2.4 km^2, and Kruglaya is about 1.6 km^2). The only river on the island, Russkaya (a small one), flows into the bight from the east. Detailed hydrological descriptions of these basins are provided in [Barabanshchikov et al., 2015; Rakov, 2008]. Voevoda Bight is partially covered with *Z. marina* meadows. In Uglovoy Bight, *Z. marina* formed meadows in the 1980s [Rakov, 2008]; by now, they have disappeared [Tishchenko et al., 2021].

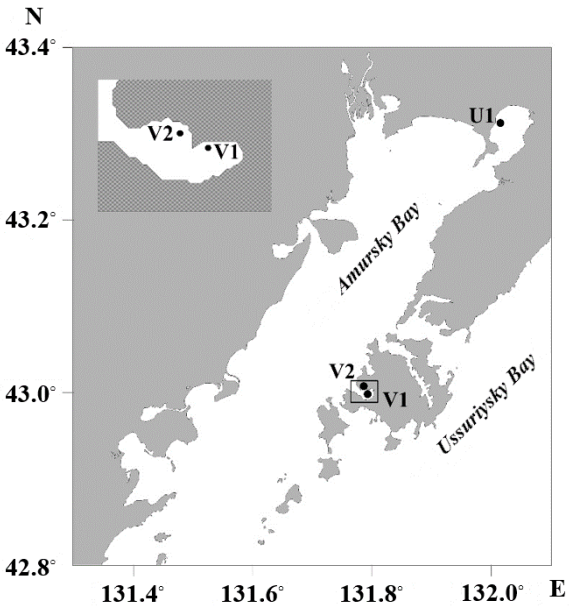


Fig. 1. Geographical location of the study area and sampling stations (hereinafter, V1, Melkovodnaya Bight; V2, Kruglaya Bight; U1, Uglovoy Bight)

In August 2023, three samples of surface sediments (top 5-cm layer) were taken by scuba diving. The sampling covered an area of 1 m^2 and depths of 1.5–3.5 m. A plastic container was used. Three sites within Amur Bay were surveyed: Melkovodnaya Bight (V1), Kruglaya Bight (V2), and Uglovoy Bight (U1). Location of stations is shown in Fig. 1. At sta. V2, sediments were covered with *Z. marina* meadows. The sampled material was delivered to a laboratory for subsequent analysis. The portion of sediments used for bioassay was sorted, frozen, and stored at −18 °C.

Concentrations of heavy metals (Fe, Mn, Zn, Cu, Pb, Cr, Ni, Co, and Cd) in the samples were determined by flame atomic absorption spectrometry on a Shimadzu AA-3600 spectrophotometer (Japan). The samples were prepared in accordance with the methodology for the quantitative chemical analysis of soils, sediments, sewage sludge, and waste (federal environmental regulation PND F 16.1:2.2:2.3:3.36-2002) involving acid digestion. Considering the cumulative errors at all stages of sample preparation and the measurement error inherent to the flame atomic absorption method, the total relative error was estimated to be 5%.

The concentration of organic carbon (C_{org}) in the solid phase of sediments was determined on a TOC-VCPH analyzer coupled with a Shimadzu SSM-5000A solid sample combustion unit (Japan). The analyzer was calibrated with certified reference material: sediment standard "Limestone Silt" (state standard sample GSO 1758-80). Analytical precision was based on parallel measurements, and it was ±3% of the determined value. The result is given as the percentage of C_{org} in dry sediments.

Grain size distribution was assessed on an ANALYSETTE 22 NanoTec laser particle analyzer (Fritsch, Germany). Natural moisture samples were homogenized. To create a dispersion medium, a surfactant 901 (Fritsch) was used. The analyzer was calibrated using a certified standard F-500 (Fritsch).

Pollution and environmental risk indices. Heavy metal concentrations determined in this study were compared with background levels for Peter the Great Bay [Kovekovdova, Simokon, 2004], permissible values [Marine Water Pollution, 2022], and threshold ones [MacDonald et al., 2004] for marine sediments. Also, individual pollution and environmental risk indices were calculated [enrichment factor (EF) and modified hazard quotient (mHQ)], as well as comprehensive ones [modified contamination degree (mCd) and toxic risk index (TRI)].

Individual indices. Enrichment factor (EF) is an effective tool for quantifying the contribution of each analyzed toxicant to the overall sediment pollution load. Its calculation involves the comparison of obtained heavy metal concentrations to those of conservative elements (Al or Fe), less susceptible to anthropogenic load [Li et al., 2015]. In this study, Fe was selected as a reference element. EF value higher than 1.5 indicates an anthropogenic source of heavy metals, whereas a value lower than 1.5 suggests a predominantly natural origin from weathering processes [Li et al., 2015]. Obtained factor values are classified into seven enrichment categories, as detailed in Table 1. EF was calculated by the formula as follows:

$$EF = \frac{(C_n/C_{Fe})_{sample}}{(B_n/B_{Fe})_{background}},$$

where $(C_n/CF_e)_{sample}$ is the ratio of a heavy metal content to Fe concentration in an analyzed sediment sample;

$(B_n/BF_e)_{background}$ is the natural background ratio of heavy metal content to Fe concentration in bottom sediment samples at a reference site (Table 2).

Table 1. Classification of indices

Class	Enrichment factor, EF		Modified hazard quotient, mHQ		Modified contamination degree, mCd		Toxic risk index, TRI	
	Value	Degree of enrichment	Value	Contamination severity	Value	Contamination degree	Value	Risk level
1	EF ≤ 1	depletion	mHQ ≤ 0.5	nil to very low	mCd ≤ 1.5	very low	TRI ≤ 5	no toxic risk
2	1 < EF ≤ 3	minor	0.5 < mHQ ≤ 1.0	very low	1.5 < mCd ≤ 2	low	5 < TRI ≤ 10	low
3	3 < EF ≤ 5	moderate	1.0 < mHQ ≤ 1.5	low	2 < mCd ≤ 4	moderate	10 < TRI ≤ 15	moderate
4	5 < EF ≤ 10	significant	1.5 < mHQ ≤ 2.0	moderate	4 < mCd ≤ 8	high	15 < TRI ≤ 20	considerable
5	10 < EF ≤ 25	high	2.0 < mHQ ≤ 2.5	significant	8 < mCd ≤ 16	very high	TRI > 20	very high
6	25 < EF ≤ 50	very high	2.5 < mHQ ≤ 3.0	high	16 < mCd ≤ 32	extremely high		
7	EF > 50	extremely high	3.0 < mHQ ≤ 3.5	very high	mCd > 32	ultra-high		
8			mHQ > 3.5	extreme				

Table 2. Content of heavy metals (mg·kg^{-1}) and organic carbon (%) in the surface layer of bottom sediments of Melkovodnaya Bight (V1), Kruglaya Bight (V2), and Uglovoy Bight (U1); values of background (BC) and permissible (PC) concentrations; and values of threshold exposure levels (TEL), probabilistic exposure levels (PEL), and severe exposure levels (SEL) for heavy metals analyzed

Element	Bights (n = 3)			BC[1]	PC[2]	TEL[3]	PEL[3]	SEL[3]
	V1	V2	U3					
Fe	14,800	34,500	15,500	–	–	–	–	–
Mn	147	207	170	–	–	–	–	–
Zn	44.4	134	43.3	50	140	124	271	820
Cu	13.3	38.8	5.9	10	35	18.7	108	110
Pb	13	34.3	13.3	10	85	30	112	250
Cr	17	40	24	20	100	52.3	160	110
Ni	9	28	18	10	35	15.9	42.8	75
Co	4.3	7.3	7.5	8	20	–	–	–
Cd	0.3	1.5	0.3	0.1	0.8	0.68	4.21	10
C_{org}	0.83	4.83	1.03					

Note: n, number of samples; [1], [Kovekovdova, Simokon, 2004]; [2], [Warmer, van Dokkum, 2002]; [3], [MacDonald et al., 2004].

Modified hazard quotient (mHQ) characterizes the degree of risk of toxic effect from each studied heavy metal on marine hydrobionts [MacDonald et al., 2004]. The calculation is based on the ratio of the pollutant concentration in sediments to SQGs values for this toxicant: threshold effect level (TEL), probable effect level (PEL), and severe effect level (SEL) (Table 2). To determine mHQ, the following formula is used:

$$mHQ = \sqrt{\frac{C_i}{TEL_i} + \frac{C_i}{PEL_i} + \frac{C_i}{SEL_i}},$$

where C_i is the concentration of the toxicant *i*;

TEL_i, PEL_i, and SEL_i are values of TEL, PEL, and SEL for the toxicant *i*.

The obtained values are ranked according to eight hazard levels (Table 1).

Comprehensive indices. Modified contamination degree (mCd) characterizes the sediment contamination degree and is defined as the sum of all contamination factors (Cf) [Brady et al., 2014]. To calculate mCd, the following formula is applied:

$$mC_d = \frac{\sum_{i=1}^{n} Cf^i}{n},$$

where Cf^i is the contamination factor;

n is the total number of analyzed heavy metals.

The classification of contamination degrees is given in Table 1.

Toxic risk index (TRI) allows for the comprehensive assess of the toxicity for the sediments with TEL and PEL taken into account. The criterion is used to normalize the toxicity of various pollutants. Also, it is applied for further comparison of effects on biological systems [Li et al., 2015]. TRI is calculated as follows:

$$TRI_i = \sqrt{\frac{\left(\frac{C_i}{TEL_i}\right)^2 + \left(\frac{C_i}{PEL_i}\right)^2}{2}}; \quad TRI = \sum_{i=1}^{n} TRI_i,$$

where C_i is the concentration of the analyzed pollutant *i*;

n is the total number of pollutants;

TEL_i and PEL_i are values of TEL and PEL for the toxicant *i* (Table 2).

The results of TRI calculation are ranked according to five risk levels (see Table 1).

Ecotoxicological assessment. Bioassays with the sand dollar *S. mirabilis* were carried out at the "Vostok" marine biological station (NSCMB FEB RAS). For the experiment, we used seawater sampled in Vostok Bay from a 6-m depth *via* a supply system. Seawater was filtered through a three-stage gravel filter and subsequently treated with ultraviolet light.

Aqueous extracts from sediments were prepared following a standard technique [Beiras et al., 2003]. Pre-thawed sediment samples (100 g) were placed in conical flasks and filled with 400 mL of sterile seawater. The mixtures were agitated on an orbital shaker Biosan PSU-20i (Latvia) for 2 h. Subsequently, the samples were allowed to settle, and then filtered through a membrane filter (pore size of 2–3 μm).

Adult mature *S. mirabilis* were sampled along the western coast of Vostok Bay (Peter the Great Bay, Sea of Japan) at a depth of 4–4.5 m. The sand dollars were placed in containers with ice packs to ensure their safe transport to the laboratory. *Prior* to the experiment, sea urchins were acclimated in aquariums with flow-through seawater for 48 h. The temperature was +18…+19 °C.

Spawning of the animals was induced by injecting 0.2 mL of 0.5 M potassium chloride solution into perivisceral cavity. Gametes were collected and prepared following a standard method [Beiras et al., 2003]. For a control fertilization series, 1 mL of egg suspension was placed in beakers filled with 50 mL of sterile seawater. After eggs had settled to bottom, 200 µL of diluted sperm suspension was added. Fertilization success was assessed in 20 min under an Axio Imager A1 microscope (Carl Zeiss, Germany). Batches with a fertilization rate lower than 95% were excluded from the assay.

Throughout the experiment, the temperature was maintained at +18…+19 °C. Bioassays were performed in four replicates using gametes from three parental pairs (N = 3). Fertilization was carried out in filtered sterile seawater. Then, zygotes were transferred to test extracts for further embryonic and larval development [Beiras et al., 2003].

The toxicity of the studied samples was determined by evaluating the developmental status of larvae at the gastrula (18 h) and pluteus (48 h) stages; integrated toxicity index (ITI) was applied [Morroni et al., 2016]. For each parental pair, 400 larvae were examined at each controlled developmental stage. To calculate ITI, the toxic effect was quantified by analyzing the frequency of developmental delays and/or morphological abnormalities; those were ranked on a scale from 0 to 10 points according to the severity of their implications for subsequent larval development. Lower scores were assigned to larvae exhibiting developmental delays without malformations, whereas higher ones, to those with delays accompanied with non-specific morphological changes.

ITI is calculated using the following formula:

$$ITI = \sum_{i=10}^{n} \frac{S_i \times F_I}{100},$$

where S_i is the score assigned to each category of anomalies;

F_i the number of anomalies;

100 the number of larvae counted.

RESULTS

Grain size distribution. According to the results of the analysis of grain size distribution (Fig. 2), at sta. V1 (Melkovodnaya Bight), sediments consisted chiefly of fine-grained material. Thus, the psammitic fraction amounted to 70%, while the aleuritic and pelitic fractions constituted 20% and 7.5%, respectively. The proportion of the gravel fraction did not exceed 2.5%. At sta. V2 (Kruglaya Bight), fine-grained fractions also predominated: the proportion of the psammitic one was 43%; the aleuritic, 44.1%; and the pelitic, 12.5%. The gravel fraction amounted to 0.4% only. At sta. U1 (Uglovoy Bight), sediments were characterized by a predominance of the psammitic fraction: its proportion was 49.9%. The aleuritic and pelitic fractions constituted 37 and 13%, respectively. The proportion of the gravel fraction was 0.1%.

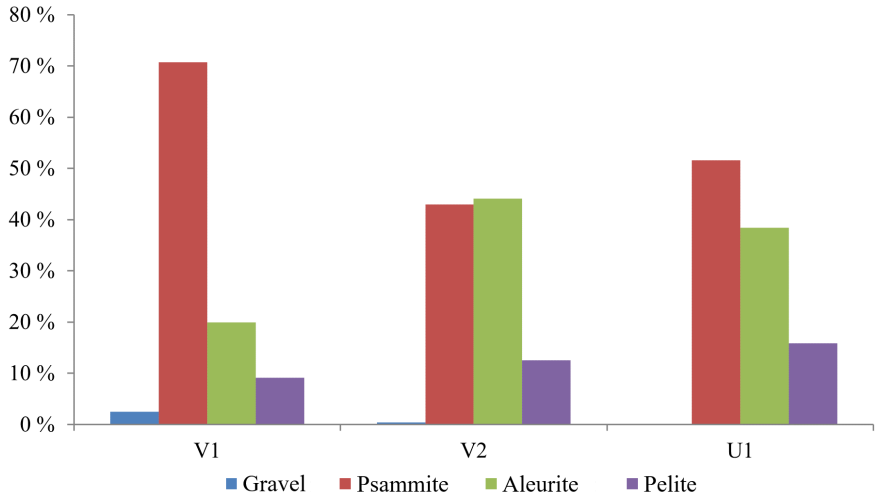


Fig. 2. Grain size distribution of the surface layer of bottom sediments from Melkovodnaya Bight, Kruglaya Bight, and Uglovoy Bight

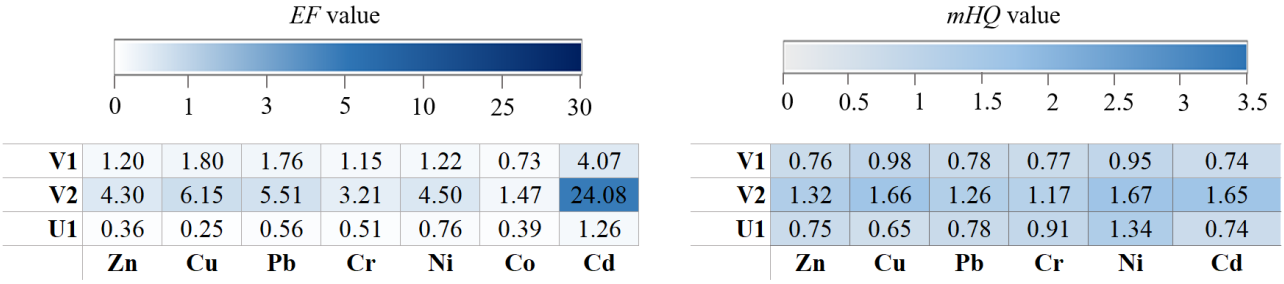
Content of heavy metals and organic carbon in sediments. According to the data presented in Table 2, the surface layer of sediments at sta. V2 featured elevated concentrations of all measured elements, including organic carbon, compared to content at other stations. At this site, the background levels were exceeded for all analyzed elements, except for Co. Concentrations of Cu, Pb, and Cd at sta. V1 were higher than the background level, the same as content of Pb, Cr, Ni, and Cd at sta. U1.

The level of heavy metal pollution in sediments in the study water areas was compared with foreign regulatory levels for heavy metal content listed in the so-called Dutch Lists [Warmer, van Dokkum, 2002]. Importantly, these concentrations are not referenced in regulatory legal acts of any foreign country, and also have no legal force in the Russian Federation. Despite this fact, the levels given in Dutch Lists are used in works assessing the ecological state of sediments [Petukhov et al., 2023]. Moreover, those are used in the compiled reviews and annual reports on the quality of Russian marine waters [Marine Water Pollution, 2022]. In sediments of Kruglaya Bight (sta. V2), permissible concentrations were exceeded for Cu and Cd.

The potential toxic effects of heavy metals were analyzed by comparing their concentrations with SQGs values recommended in the Canadian guidelines for the protection of aquatic life [MacDonald et al., 2004]. Two criteria were used: the threshold effect level and the probable one (TEL and PEL). Their values are based on ecotoxicological studies on representatives of freshwater, marine, and estuarine fauna. TEL describes the permissible concentration of a contaminant for hydrobionts that is considered statistically safe. In contrast, PEL defines the level above which organisms can undergo toxicological effects [MacDonald et al., 2004]. As revealed, TEL was exceeded for Zn, Cu, Pb, Ni, and Cd in sediments at sta. V2, and for Ni at sta. U1.

The calculation of the enrichment factor, EF, allowed revealing similar accumulation patterns for toxic elements in sediments of Melkovodnaya Bight (V1) and Kruglaya Bight (V2): Cd > Cu > Pb > Ni > Cr > Zn > Co for sta. V1 and Cd > Cu > Pb > Ni > Zn > Cr > Co for sta. V2. In Uglovoy Bight (U1), the following pattern was observed: Cd > Ni > Pb > Cr > Co > Zn > Cu. The value of EF higher than 1.5 indicates an anthropogenic source of contaminants. At sta. V2, EF values for all analyzed metals, except for Co, exceeded this threshold (Fig. 3). High degree of enrichment was recorded for Cd (EF = 24.08); significant one, for Cu (EF = 6.15) and Pb (EF = 5.51); and moderate one,

for Ni, Zn, and Cr (EF values were 4.5, 4.3, and 3.21, respectively). At sta. V1, most heavy metals featured minimum degree of enrichment; the exception was Cd, with its moderate degree (EF = 4.07). At sta. U1, all values for sediments were significantly lower than 1.5; this indicates a natural origin of heavy metals: from weathering processes.



	Zn	Cu	Pb	Cr	Ni	Co	Cd
V1	1.20	1.80	1.76	1.15	1.22	0.73	4.07
V2	4.30	6.15	5.51	3.21	4.50	1.47	24.08
U1	0.36	0.25	0.56	0.51	0.76	0.39	1.26

	Zn	Cu	Pb	Cr	Ni	Cd
V1	0.76	0.98	0.78	0.77	0.95	0.74
V2	1.32	1.66	1.26	1.17	1.67	1.65
U1	0.75	0.65	0.78	0.91	1.34	0.74

Fig. 3. Values of enrichment factor (EF) and modified hazard quotient (mHQ) for analyzed bottom sediments

The calculation of mCd showed as follows: sediments from sta. V1 and U1 were characterized by a very low contamination degree (mCd ≤ 1.5), while sediments from sta. V2 (Kruglaya Bight), by a moderate one (mCd = 4.38) (Fig. 4).

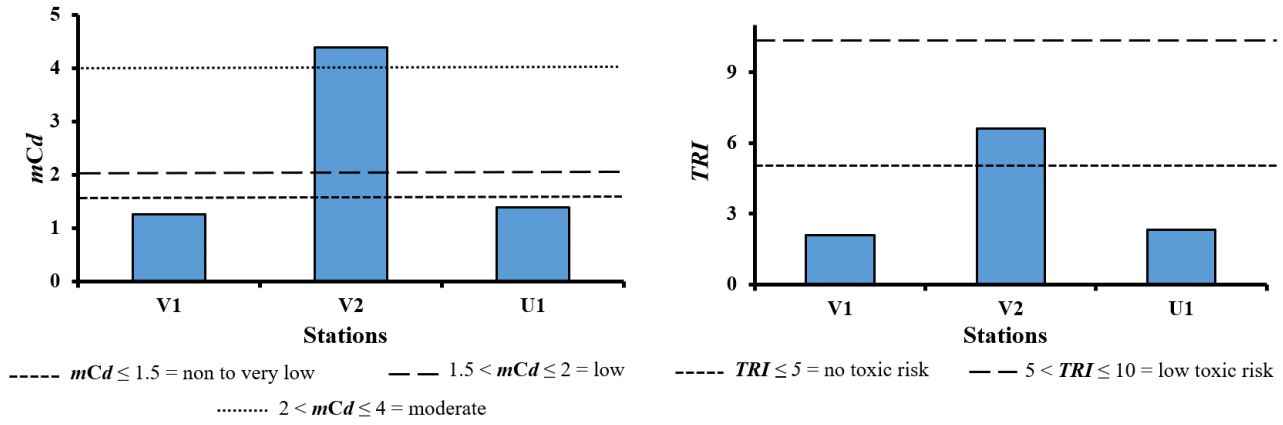


Fig. 4. Values of modified contamination degree (mCd) and toxic risk index (TRI) for analyzed bottom sediments

To assess the contribution of each heavy metal to the total potential toxic effect on hydrobionts, mHQ was calculated (see Fig. 3). In sediments from sta. V2, mHQ values for Ni, Cu, and Cd (1.67, 1.66, and 1.65, respectively) indicated moderate contamination severity, while values for Zn, Pb, and Cr (1.32, 1.26, and 1.17), low one. The values of mHQ for toxic elements in sediments from sta. V1 and U1 allowed to characterize contamination severity as very low. The exception was Ni at sta. U1 (mHQ = 1.34).

To determine the level of integrated effect of heavy metals on benthic hydrobionts, TRI was calculated (Fig. 4). Sediments from sta. V1 and U1 showed no potential toxic risks. The highest value (TRI = 6.62) was obtained for sediments at sta. V2; it corresponded to a low risk level. Importantly, although mHQ calculated for Ni, Cu, and Cd at this station indicated an individual moderate risk level, the value of the integrated index was low.

Ecotoxicological assessment. Aqueous extracts from sediments were biotested on larvae of the sand dollar *S. mirabilis*. The subsequent calculation of ITI yielded the following results. In 18 h after fertilization, the maximum abundance of abnormally developed larvae was observed at sta. V2 (Fig. 5). Specifically, in sediment extracts from this station, the overwhelming majority of embryos stopped their development at the abnormal morula stage, having an uneven surface and larger cells than those of normally developed embryos. A small number of larvae was classified as abnormal blastulae, whose blastocoel exhibited uneven cellular filling. Thus, in aqueous extracts of sediments from sta. V2, not a single larva developed to the gastrula stage, and ITI value was 9.84 points.

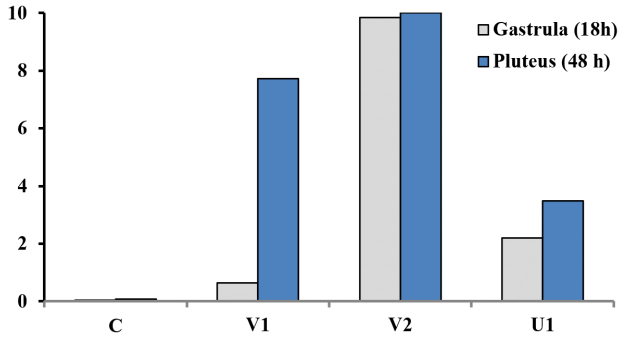


Fig. 5. Values of the integrated toxicity index (ITI) for analyzed bottom sediments 18 and 48 h after the start of the experiment

In 18 h after the start of the experiment, normally developed larvae at the late gastrula stage predominated in aqueous extracts from sta. V1 and U1. Interestingly, extracts from sta. U1 also contained normally formed but developmentally delayed larvae at the early gastrula and mesenchymal blastula stages, as well as abnormally developed blastulae. Accordingly, ITI values at this stage of the bioassay were higher for sediments from sta. U1 (2.2 points), while the value for sta. V1 was minimum (0.64 points).

In 48 h after fertilization, the maximum value of ITI (10 points) was also obtained for extracts from sediments of sta. V2 (Fig. 5). In blastulae developing in these extracts, the morphological abnormalities were noted, and the latter ones prevented larvae from reaching the mid-pluteus stage. Importantly, ITI values at this stage of the experiment for sta. V1 were significantly higher than those for sta. U1. In sediment extracts from Melkovodnaya Bight (V1), the vast majority of larvae developed with severe morphological impairments. Larvae at the prism and early pluteus stages were characterized by the presence of poorly developed skeletal rods or their absence. Furthermore, we found exoforms of larvae with no intestine in their body cavity (it was protruded outward). Although such an intestine has all three anatomical constrictions corresponding to gut subdivisions in normally developed larvae, it is non-functional [Mazur et al., 2020]. For sediments from sta. V1, ITI value (7.72 points) was twice as high as for samples from sta. U1 (3.5 points).

DISCUSSION

At sta. V1 and V2, background concentrations for copper, lead, and cadmium were exceeded. At sta. V2, background values for zinc, chromium, and nickel were exceeded as well. Zn and Cu input to water bodies is typically associated with mining, ore processing, metal smelting, with operation of electroplating shops, or with communal and household effects (both elements are common components of domestic wastewater). At the same time, Cd, Ni, and Pb serve as indicators of anthropogenic load on the environment [Khristoforova et al., 2018].

The enrichment of sediments with heavy metals is a complex and multifactorial process. Their concentrations can result from sorption by mineral and organic matter, complexation, coagulation, formation and sedimentation of poorly soluble compounds, *etc.* The intensity of these processes is governed by the morphometric and hydrological characteristics, and also by the hydrochemical regime of a water body. Post-sedimentation reactions can lead to an increase in content of elements in pore waters, establishing a concentration gradient between pore waters and the overlying bottom ones. If physicochemical conditions (pH, Eh, mineralization, and so on) change, heavy metals can be remobilized from sediments and diffuse from pore waters into the bottom layers; this is a potential threat of secondary pollution of the water area by these chemical elements [Dauvalter, 2012].

The distribution of heavy metals in sediments is also mediated by forms of their compounds with the organic and inorganic matrix. One group of elements closely associated with the organic matrix (Zn, Cu, Pb, and Cd) is characterized by high bioaccumulation coefficients in hydrobionts, and they enter sediments primarily with detritus. Another group includes metals that enter aquatic ecosystems bound within highly dispersed mineral particles, which are carried by allochthonous surface runoff (Cr, Ni, and Co). Also, this group includes typomorphic elements (Fe and Mn) [Ivanov et al., 2020]. In sediments, Fe and Mn commonly occur as hydroxides and oxides. The same as organic matter, those are very effective at accumulating and concentrating heavy metals [Bazilevskaya, Skolotnev, 2019].

In the present study, overall background pollution levels are similar for Kruglaya and Melkovodnaya bights; however, the extent of heavy metal accumulation in their sediments is different. In Kruglaya Bight, an analysis of the vertical distribution of organic carbon and heavy metals in a sediment core revealed a linear correlation between content of C_{org} and concentrations of zinc, lead, copper, and nickel [Ryumina et al., 2023]. The same study examined sediment cores from Melkovodnaya and Uglovoy bights as well, but found no correlation between organic carbon and heavy metals. These facts suggest that the concentration of heavy metals in sediments is more efficient at sites covered with *Z. marina* meadows.

Based on data on grain size distribution, the highest C_{org} content in sediments would be expected at stations where the pelitic fraction prevails [Romankevich, Vetrov, 2021]. Conversely, decline in organic carbon concentration is characteristic of sediments dominated by the psammitic fraction. This pattern is attributed to the mechanical sorting of different-sized particles. In the present study, C_{org} content at sta. V2 was 4.83% (see Table 2), which is almost 5 times higher than the value at sta. U1, 1.03%. C_{org} concentration was 0.83% at sta. V1, where the psammitic fraction clearly predominated; the value was close to that at sta. U1. At sta. V2 and U1, proportions of the pelitic fraction were 12.5 and 13%, respectively; proportions of the aleuritic fraction were 44.1 and 37%. It can be concluded that the distribution of organic carbon is not governed by the mechanical sorting of different-sized particles.

In the absence of allochthonous inputs, the primary source of organic matter for sediments of Kruglaya Bight is suspended matter derived from a seagrass *Z. marina*. A key component can be zosterates: salts of a polysaccharide zosterin, which also acts as a natural ligand for heavy metals [Khozhaenko et al., 2015]. Upon plant senescence, these organic complexes enrich sediments with both organic carbon and heavy metals [Hart, 1982]. The total content of carbohydrates produced by *Z. marina* can be over 35% of seagrass dry mass, with zosterin comprising approximately 20% [Tishchenko et al., 2020].

As already mentioned, sta. V2 area, where sediments were sampled, hosts *Z. marina* meadows. There, a very high degree of enrichment was noted for cadmium (EF = 24.08); a significant, for copper (EF = 6.15) and lead (EF = 5.51); and a moderate, for nickel (EF = 4.5), zinc (EF = 4.3), and chromium (EF = 3.21).

At sta. V2, Fe content (34,500 mg·kg^{-1}) was twice as high as at sta. V1 (14,800 mg·kg^{-1}) and U1 (15,500 mg·kg^{-1}). This also indicates the possible concentration of heavy metals by iron hydroxides, and not just by organic matter.

The calculation of mCd showed that contamination degree at sta. V2 can be characterized as moderate (mCd = 4.38). The determination of mHQ allowed for assessing the contribution of each analyzed heavy metal to the total potential toxic effect on hydrobionts. Thus, in sediments from sta. V2, mHQ values for nickel, copper, and cadmium (1.67, 1.66, and 1.65, respectively) indicated moderate contamination severity, and for zinc, lead, and chromium (1.32, 1.26, and 1.17), low one. The highest TRI value (6.62) was recorded at sta. V2; this corresponds to a low risk level (see Table 1). Interestingly, at this station, mHQ for nickel, copper, and cadmium indicated an individual moderate risk level, but the value of the integrated index was low.

Judging by values of the enrichment factor, in sediments of sta. V1, most heavy metals were characterized by insignificant levels; the exception was Cd which showed a moderate degree of enrichment (EF = 4.07). EF values for sediments from sta. U1 were significantly lower than 1.5 indicating that the input of heavy metals is associated with natural weathering processes.

The calculation of mCd showed that sediments from sta. V1 and U1 are characterized by a very low contamination degree (mCd ≤ 1.5). The values of mHQ for toxic elements in sediments from sta. V1 and U1 reflected very low contamination severity, except for Ni at sta. U1 (mHQ = 1.34). Sediments of these two stations were characterized by the lack of potential toxic risk.

In the water areas studied, the toxic effect of exposure to extracts from sediments can result from either high content of certain pollutants/compounds or the combined action of several contaminants [Gorbacheva, 2018]. In our survey, the highest abundance of abnormally developed larvae was observed in extracts from sta. V2; importantly, it is in sediments from this site that the highest Cu and Cd concentrations (exceeding the permissible ones) were found. According to [Rouchon, Phillips, 2017], exposure to ionic copper at concentrations of 5 and 10 mg·L^{-1} caused growth and developmental delays in larvae of a sea urchin *Evechinus chloroticus* (Valenciennes, 1846), while increasing content to 20 mg·L^{-1} led to a complete cessation of larval development at the gastrula stage. The effective concentration (EC_{50}) of cadmium ions in an experiment with larvae of *Paracentrotus lividus* (Lamarck, 1816) was 1.003 mg·L^{-1}, with developmental defects being primarily skeletal abnormalities and impaired gut differentiation [Manzo et al., 2010]. Notably, the percentage of abnormally developed larvae was high in extracts from sediments of Melkovodnaya Bight (sta. V1). Despite low level of heavy metal pollution and the absence of potential toxic risk to hydrobionts, these extracts had a noticeable effect on sea urchin larval development. As known, sediments accumulate not only the pollutants we analyzed, but also a wide range of contaminants. Those can have potential inhibitory, additive, and synergistic effects on each other, thereby regulating the toxic effect on larvae.

Organic matter accumulated in sediments serves as a primary food source for most benthic organisms. However, its excessive concentrations can lead to community degradation, manifesting in both qualitative changes (decreased species richness) and quantitative ones (reduction in abundance and biomass). When C_{org} content exceeds 2.5%, a drop in abundance and biomass of the benthic community is observed, as well as the restructuring of its species composition [Orekhova et al., 2019]. In a study on the response of macrobenthos to organic matter enrichment in sediments, A. Petrov [2000] proposed a classification covering five threshold levels of C_{org} values. Based on this system, sediments at sta. V1 and U1 have a medium level of eutrophication (II class), whereas those at sta. V2 feature a very high level (V class). The organic matter concentration recorded in Kruglaya Bight is 4.83%. Following the above-mentioned classification, this value is expected to result in the near-complete degradation of benthic communities, with a predominance of opportunistic species. Such a high degree of sediment eutrophication is considered incompatible with favorable habitat conditions for most macrobenthic organisms; moreover, it is likely to facilitate the enhanced accumulation of various organic and inorganic pollutants [Petrov, 2000].

The results of this study, along with the ongoing extensive industrial development of the water areas, indicate the need for continued comprehensive assessments of heavy metal pollution in sediments and its potential toxicity to hydrobionts.

Conclusion. Analysis of heavy metal content in the surface layer of sediments from Melkovodnaya Bight (sta. V1), Kruglaya Bight (sta. V2), and Uglovoy Bight (sta. U1) revealed the highest values for sta. V2. The bottom of this site is extensively covered by *Zostera marina* meadows. Our results indicate that this seagrass contributes much to enriching sediments with both organic matter (4.83%) and heavy metals.

This enrichment has led to a lower overall ecological status for Kruglaya Bight compared to other two shallow basins. Values of individual and comprehensive pollution indices, and also ecological risk indices were the highest for sediments sampled at sta. V2.

Bioassay revealed the highest frequency of abnormally developed larvae of a sea urchin *Scaphechinus mirabilis* at sta. V2. In aqueous extracts of sediments from this station, no larvae developed to the gastrula stage, and the value of the integrated toxicity index (ITI) was 9.84 points. In contrast, aqueous extracts from sta. V1 and U1 supported normal development, with larvae at the late gastrula stage predominating 18 h after fertilization. Within 48 h after fertilization, the vast majority of larvae in extracts from sta. V1 featured severe morphological impairments. ITI value for sediments from sta. V1 (7.72 points) was more than twofold higher than that for samples from sta. U1 (3.5 points).

The results of the bioassay of sediments sampled in Kruglaya Bight were consistent with the calculation of indices of pollution and potential ecological risk for this site. Sediments from Melkovodnaya Bight featured a different pattern. Despite low levels of heavy metal pollution and the absence of any potential toxic risk to hydrobionts, sediment extracts significantly affected the development of the sand dollar larvae. This discrepancy suggests that sediments are contaminated with other pollutants that contribute to the cumulative toxic effect.

This work was carried out with financial support of state programs of POI FEB RAS (registration No. 124022100077-0).

REFERENCES

1. Bazilevskaya E. S., Skolotnev S. G. New data concerning the ferromanganese crusts of the Mendeleev Rise (Arctic Ocean). *Doklady Akademii nauk*, 2019, vol. 486, no. 5, pp. 562–566. (in Russ.). https://doi.org/10.31857/S0869-56524865562-566
2. Barabanshchikov Yu. A., Tishchenko P. Ya., Semkin P. Yu., Volkova T. I., Zvalinsky V. I., Mikhailik T. A., Sagalaev S. G., Sergeev A. F., Tishchenko P. P., Shvetsova M. G., Shkirnikova E. M. Seasonal hydrological and hydrochemical surveys in the Voevoda Bay (Amur Bay, Japan Sea). *Izvestiya TINRO*, 2015, vol. 180, pp. 161–178. (in Russ.). https://elibrary.ru/tuesbh
3. Gavrilova G. S., Kucheryavenko A. V. *Produktivnost' plantatsii dvustvorchatykh mollyuskov v Primor'e.* Vladivostok : TINRO-tsentr, 2011, 112 p. (in Russ.). https://elibrary.ru/qldhvb
4. Gorbacheva E. A. Bioassay for sediment pollution estimation in the southern areas of the Barents Sea. *Uchenye zapiski Petrozavodskogo gosudarstvennogo universiteta*, 2018, no. 8 (177), pp. 67–73. (in Russ.). https://doi.org/10.15393/uchz.art.2018.253
5. Dauvalter V. A. *Geoekologiya donnykh otlozhenii ozer.* Murmansk : Izd-vo MGTU, 2012, 242 p. (in Russ.). https://elibrary.ru/qklcnr
6. Ivanov D. V., Valiev V. S., Ziganshin I. I., Shamaev D. E., Paimikina E. E., Marasov A. A., Malanin V. V., Khasanov R. R., Unkovskaya M. A. Structural relationship of granulometric composition, content of organic matter and heavy metals in sediments. *Gidroekologiya*, 2020, no. 2 (22), pp. 23–30. (in Russ.). https://elibrary.ru/ycqnwh
7. *Marine Water Pollution. Annual Report 2022* / A. Korshenko (Ed). Moscow : Nauka, 2024, 283 p. (in Russ.)
8. Kovekovdova L. T., Simokon M. V. Tendencies in change of chemoecological situation in the coastal area of Primorye. Toxic elements in bottom sediments and aquatic organisms. *Izvestiya TINRO*, 2004, vol. 137, pp. 310–320. (in Russ.). https://elibrary.ru/hpmucn
9. Losev O. V. Analysis of pollution sources of the Uglovoy Bay (Peter the Great Bay) and its pollution factors. *Vestnik Dal'nevostochnogo otdeleniya Rossiiskoi akademii nauk*, 2019, no. 2 (204), pp. 95–103. (in Russ.). https://elibrary.ru/coogca
10. Mazur A. A., Zhuravel E. V., Slobodskova V. V., Mazur M. A. Assessment of the toxic effect of zinc ions and nano-sized zinc oxide on the early development of the sand dollar *Scaphechinus mirabilis* (Agassiz, 1864) (Echinodermata: Echinoidea). *Biologiya morya*, 2020, vol. 46, no. 1, pp. 53–59. (in Russ.). https://doi.org/10.31857/S0134347520010064
11. Mishukov V. F., Kalinchuk V. V., Plotnikov V. V., Voytsytskiy A. V. Effects of polluted grounds dumping on ecological conditions in coastal waters near Vladivostok. *Izvestiya TINRO*, 2009, vol. 159, pp. 243–256. (in Russ.). https://elibrary.ru/mnjqxl
12. Naleta E. V., Kolesnikov S. I., Kazeev K. Sh. *Vliyanie zagryazneniya tyazhelymi metallami na biologicheskie svoistva pochv gorodov Rostovskoi oblasti.* Rostov-on-Don : Izd-vo Yuzhnogo federal'nogo universiteta, 2015, 108 p. (in Russ.). https://elibrary.ru/vwlsah
13. Orekhova N. A., Ovsyany E. I., Tikhonova E. A. Organic carbon and redox

conditions in bottom sediments of the Balaklava Bay. *Uchenye zapiski Krymskogo federal'nogo universiteta imeni V. I. Vernadskogo. Biologiya. Khimiya*, 2019, vol. 5 (71), no. 3, pp. 49–64. (in Russ.). https://elibrary.ru/hvtrpq

14. Petrov A. N. Responses of the Black Sea macrobenthic communities upon organic enrichment impact of bottom sediments. *Ekologiya morya*, 2000, iss. 51, pp. 45–51. (in Russ.). https://repository.marine-research.ru/handle/299011/4297
15. Rakov V. A. Distribution and ecology of oyster reefs in the northern part of the Amur Bay. In: *Current Environmental Condition and Tendencies of Its Change in the Peter the Great Bay, Sea of Japan* / A. S. Astakhov, V. B. Lobanov (Eds). Moscow : GEOS, 2008, pp. 278–291. (in Russ.). https://elibrary.ru/twvleb
16. Romankevich E. A., Vetrov A. A. *Carbon in the World Ocean.* Moscow : GEOS, 2021, 352 p. (in Russ.). https://doi.org/10.34756/GEOS.2021.16.37857
17. Ryumina A. A., Tishchenko P. Y., Shkirnikova E. M. Heavy metals and organic carbon in the bottom sediments of shallow bights of the Peter the Great Bay. *Geokhimiya*, 2023, vol. 68, no. 7, pp. 709–719. (in Russ.). https://doi.org/10.31857/S0016752523060080
18. Tishchenko P. Ya., Barabanshchikov Yu. A., Pavlova G. Yu., Ryumina A. A., Sagalaev S. G., Semkin P. Yu., Tishchenko P. P., Ulanova O. A., Shvetsova M. G., Shkirnikova E. M., Tibenko E. Yu. Hydrochemical state of the Uglovoy Bight (Amur Bay) in different seasons. *Izvestiya TINRO*, 2021, vol. 201, no. 1, pp. 138–157. (in Russ.). https://doi.org/10.26428/1606-9919-2021-201-138-157
19. Tishchenko P. Y., Medvedev E. V., Barabanshchikov Y. A., Pavlova G. Y., Sagalaev S. G., Tishchenko P. P., Shvetsova M. G., Shkirnikova E. M., Ulanova O. A., Tibenko E. Y., Orekhova N. A. Organic carbon and carbonate system in the bottom sediments of shallow bights of the Peter the Great Bay (Sea of Japan). *Geokhimiya*, 2020, vol. 65, no. 6, pp. 583–598. (in Russ.). https://doi.org/10.31857/S001675252005012X
20. Khristoforova N. K., Gamayunova O. A., Afanasyev A. P. State of the Kozmin and Wrangel bays (Peter the Great Bay, Japan Sea): Dynamics of pollution with heavy metals. *Izvestiya TINRO*, 2015, vol. 180, pp. 179–186. (in Russ.). https://elibrary.ru/tuescb
21. Khristoforova N. K., Emelyanov A. A., Efimoff A. V. Bioindication of pollution in the coastal marine waters at Russky Island (Peter the Great Bay, Japan Sea) by heavy metals. *Izvestiya TINRO*, 2018, vol. 192, pp. 157–166. (in Russ.). https://doi.org/10.26428/1606-9919-2018-192-157-166
22. ABNT-NBR 15350 DE 03/2023. *Ecotoxicologia aquática – Toxicida decrônica de curta-duração – Método de ensaio com ouriço-do-mar (Echinodermata: Echinoidea)* : [Standard] ; Quanta ediçãlo. ABNT, Brasil, 2025, 31 p. (Norma Brasileira). URL: https://www.normas.com.br/autorizar/visualizacao-nbr/25082/identificar/visitante [accessed: 05.01.2025].
23. *ASTM. Standard Guide for Conducting Static Acute Toxicity Tests with Echinoid Embryos.* West Conshohocken (PA) : ASTM International, 2012, 22 p. https://doi.org/10.1520/E1563-98R12
24. Beiras R., Fernández N., Bellas J., Besada V., González-Quijano A., Nunes T. Integrative assessment of marine pollution in Galician estuaries using sediment chemistry, mussel

bioaccumulation, and embryo-larval toxicity bioassays. *Chemosphere*, 2003, vol. 52, iss. 7, pp. 1209–1224. https://doi.org/10.1016/s0045-6535(03)00364-3

25. Brady J. P., Ayoko G. A., Martens W. N., Goonetilleke A. Enrichment, distribution and sources of heavy metals in the sediments of Deception Bay, Queensland, Australia. *Marine Pollution Bulletin*, 2014, vol. 81, iss. 1, pp. 248–255. https://doi.org/10.1016/j.marpolbul.2014.01.031
26. Canty M. N. *Marine Pollution and Echinoderms: A Biomarker Study Integrating Different Levels of Biological Organization.* PhD thesis. Plymouth, United Kingdom : University of Plymouth, 2009, 237 p. https://doi.org/10.24382/3680
27. Chiarelli R., Martino C., Roccheri M. C. Cadmium stress effects indicating marine pollution in different species of sea urchin employed as environmental bioindicators. *Cell Stress and Chaperones*, 2019, vol. 24, iss. 4, pp. 675–687. https://doi.org/10.1007/s12192-019-01010-1
28. Hart B. T. Uptake of trace metals by sediments and suspended particulates: A review. *Hydrobiologia*, 1982, vol. 91, iss. 1, pp. 299–313. https://doi.org/10.1007/bf00940121
29. Khozhaenko E. V., Khotimchenko R. Y., Kovalev V. V., Khotimchenko M. Y., Podkorytova E. A. Metal binding activity of pectin isolated from seagrass *Zostera marina* and its derivatives. *Russian Journal of Marine Biology*, 2015, vol. 41, iss. 6, pp. 485–489. https://doi.org/10.1134/S1063074015060073
30. Li Y., Duan Z., Liu G., Kalla P., Scheidt D., Cai Y. Evaluation of the possible sources and controlling factors of toxic metals/metalloids in the Florida Everglades and their potential risk of exposure. *Environmental Science & Technology*, 2015, vol. 49, iss. 16, pp. 9714–9723. https://doi.org/10.1021/acs.est.5b01638
31. MacDonald D. D., Carr R. S., Eckenrod D., Greening H., Grabe S., Ingersoll C. G., Janicki S., Janicki T., Lindskoog R. A., Long E. R., Pribble R., Sloane G., Smorong D. E. Development, evaluation, and application of sediment quality targets for assessing and managing contaminated sediments in Tampa Bay, Florida. *Archives of Environmental Contamination and Toxicology*, 2004, vol. 46, iss. 2, pp. 147–161. https://doi.org/10.1007/s00244-003-2270-z
32. Manzo S., Buono S., Cremisini C. Cadmium, lead and their mixtures with copper: *Paracentrotus lividus* embryotoxicity assessment, prediction, and offspring quality evaluation. *Ecotoxicology*, 2010, vol. 19, iss. 7, pp. 1209–1223. https://doi.org/10.1007/s10646-010-0506-z
33. Morroni L., Pinsino A., Pellegrini D., Regoli F., Matranga V. Development of a new integrative toxicity index based on an improvement of the sea urchin embryo toxicity test. *Ecotoxicology and Environmental Safety*, 2016, vol. 123, pp. 2–7. https://doi.org/10.1016/j.ecoenv.2015.09.026
34. Petukhov V., Petrova E., Kiryanov A., Zheldak E., Kholodov A. Assessment of contamination of marine sediments and their potential toxicity in the Uglovoy Bay, Peter the Great Gulf, Sea of Japan/East Sea. *Environmental Science and Pollution Research*, 2023, vol. 30, iss. 31, pp. 77798–77806. https://doi.org/10.1007/s11356-023-28021-x
35. Roberts D. A. Causes and ecological effects of resuspended contaminated sediments (RCS) in marine environments. *Environment International*, 2012, vol. 40, pp. 230–243. https://doi.org/10.1016/j.envint.2011.11.013

36. Rouchon A. M., Phillips N. E. Acute toxicity of copper, lead, zinc and their mixtures on the sea urchin *Evechinus chloroticus*. *New Zealand Journal of Marine and Freshwater Research*, 2017, vol. 51, no. 3, pp. 333–355. https://doi.org/10.1080/00288330.2016.1239643
37. Warmer H., van Dokkum R. *Water Pollution Control in the Netherlands: Policy and Practice 2021* / [Institute for Inland Water Management and Waste Water Treatment. RIZA]. The Netherlands : RIZA, 2002, 76 p. (RIZA report 2002.009).
38. Wilbers G.-J., Becker M., Thi Nga L., Sebesvari Z., Renaud F. G. Spatial and temporal variability of surface water pollution in the Mekong Delta, Vietnam. *Science of The Total Environment*, 2014, vol. 485–486, pp. 653–665. https://doi.org/10.1016/j.scitotenv.2014.03.049

ПРЕДВАРИТЕЛЬНЫЕ РЕЗУЛЬТАТЫ КОМПЛЕКСНОЙ ОЦЕНКИ ЗАГРЯЗНЕНИЯ И ТОКСИЧЕСКОГО ВОЗДЕЙСТВИЯ ДОННЫХ ОСАДКОВ МЕЛКОВОДНЫХ БУХТ АМУРСКОГО ЗАЛИВА (ЯПОНСКОЕ МОРЕ)

А. А. Рюмина[1], М. А. Мазур[2], П. Я. Тищенко[1], Е. М. Шкирникова[1]

[1]Тихоокеанский океанологический институт имени В. И. Ильичёва ДВО РАН, Владивосток, Российская Федерация
[2]Национальный научный центр морской биологии имени А. В. Жирмунского ДВО РАН, Владивосток, Российская Федерация
E-mail: *ryumina.aa@poi.dvo.ru*

В августе 2023 г. были отобраны образцы поверхностных донных осадков (верхние 5 см грунта) в трёх бухтах Амурского залива — в бухтах Мелководной (V1) и Круглой (V2), которые располагаются в бухте Воевода, а также в заливе Угловой (U1). V1 и V2, являясь соседними бухтами, имеют большие отличия в гранулометрическом составе и в распределении содержания тяжёлых металлов и органического углерода. Выявлено повышенное содержание тяжёлых металлов и органического углерода в бухте Круглой (на станции V2). В донных осадках на ст. V2 значения коэффициента обогащения (EF) для каждого из проанализированных металлов, за исключением Co, превышали уровень естественного выветривания тяжёлых металлов. Сильный уровень обогащения отмечен для Cd (EF = 24,08), умеренно сильный — для Cu (EF = 6,15) и Pb (EF = 5,51), умеренный — для Ni, Zn и Cr (значения EF составили 4,5, 4,3 и 3,21 соответственно). Расчёт модифицированного индекса степени загрязнения (mCd) показал, что на ст. V2 она является умеренной (mCd = 4,38). В донных осадках со ст. V1 большинство металлов характеризовались незначительным уровнем обогащения; исключение — Cd с умеренным уровнем (EF = 4,07). Величи́ны EF для донных осадков со ст. U1 были существенно ниже 1,5; это свидетельствует о поступлении тяжёлых металлов в результате естественных процессов выветривания. В исследуемых бухтах впервые проведено биотестирование с использованием личинок морского ежа *Scaphechinus mirabilis* в качестве тест-объекта. В ходе этого анализа максимальное число аномально развитых личинок выявлено на ст. V2. В водных вытяжках осадков со ст. V2 до стадии гаструлы не развилась ни одна из личинок, а значение интегрального индекса токсичности (ITI) составило 9,84 балла. В водных вытяжках со ст. V1 и U1 спустя 18 ч с начала эксперимента преобладали нормально развитые личинки на стадии поздней гаструлы. В экстрактах осадков из бухты Мелководной (ст. V1) подавляющее большинство личинок развивались с грубыми морфологическими нарушениями. Личинки на стадиях призмы и раннего плутеуса характеризовались наличием слаборазвитых скелетных стержней или их отсутствием. Кроме того, отмечены экзоформы личинок без кишечника в полости тела (он выпячен наружу). Выявленное значение ITI

для донных осадков со ст. V1 (7,72 балла) оказалось вдвое выше, чем для проб со ст. U1 (3,5 балла). Полученные данные указывают на то, что к концентрированию тяжёлых металлов в бухте Круглой приводит совокупность факторов. В свою очередь, высокое содержание тяжёлых металлов и органического углерода может обуславливать формирование неблагоприятных условий жизни для бентосных организмов.

Ключевые слова: Амурский залив, биотестирование, донные осадки, органический углерод, тяжёлые металлы, *Scaphechinus mirabilis*

1871
ИнБЮМ – IBSS

Морской биологический журнал
Marine Biological Journal
2025, vol. 10, no. 4, pp. 88–101
https://marine-biology.ru/mbj/article/view/506

UDC 579.24/.26

THE ROLE OF QUORUM SENSING AND INFOCHEMICALS IN THE INTERACTION BETWEEN PRO- AND MICROEUKARYOTES IN AQUATIC ECOSYSTEMS

© 2025 **E. Sudakova**

Limnological Institute SB RAS, Irkutsk, Russian Federation
E-mail: *bairamovaelvira@gmail.com*

Received 29.07.2024; revised 08.10.2024;
accepted 12.08.2025.

This review presents key insights into the molecular interactions of unicellular organisms. Bacteria are characterized by quorum sensing (QS): an ability to modulate gene expression by microorganisms depending on cell population density. This can, in particular, lead to changes in behavior and the activation of virulence factors. Phytoplankton possesses an analogous system: cells produce infochemicals that can either increase the resistance of recipients to stress factors or trigger programmed cell death in them. While bacterial quorum sensing molecules (QSMs) can activate/inhibit phytoplankton cell growth, the infochemicals produced by the latter can affect the composition of the microbial community and suppress consumer development. Moreover, phytoplankton cells can affect bacterial QS by disrupting the activity of signaling molecules or by imitating them.

Keywords: quorum sensing, autoinducers, phytoplankton, bacteria, infochemicals

In multicellular organisms, cells establish close physical and chemical contacts. These interactions determine their differentiation, metabolism, and function [Brodskii, 2009]. Intercellular interactions are also important for the vital activities of unicellular organisms. This was first demonstrated in studies of autoluminescence in *Vibrio fischeri* [Kempner, Hanson, 1968]. Research showed that luminescence in these bacteria is activated in response to the appearance of extracellular secreted molecules, the synthesis of which is induced at high cell density in the mid-logarithmic phase [Nealson et al., 1970]. It took more than a decade to confirm that this process is transcriptionally regulated. Thus, genes involved in luminescence were discovered (*lux* operon) [Engebrecht, Silverman, 1984]. It was established that *luxCDABEG* genes are required for visible light emission, while *luxI* and *luxR* genes are involved in regulating the operon, controlling activation/inhibition of luminescence genes. The extracellular secreted molecule that activates luminescence at high cell density was identified as *N*-3-oxohexanoyl-L-homoserine lactone (3OC6-HSL) [Eberhard et al., 1981]. Its production requires *luxI* gene, which encodes autoinducer synthase. In turn, *luxR* recognizes 3OC6-HSL and, acting as a transcription factor, activates *lux* operon [Engebrecht, Silverman, 1984].

Gradually, similar gene systems began to be identified in other bacterial species, thereby expanding our understanding of their physiology. It became evident that bacteria produce signaling molecules that are recognized by cell–surface receptors. These molecules enter the cell and affect the transcription

of specific genes: a phenomenon termed quorum sensing (hereinafter QS) [Fuqua et al., 1994]. Studies of intercellular interactions have demonstrated that communication among phytoplankton cells is mediated by infochemicals [Pohnert et al., 2007]. Given that algae and bacteria coexist closely in aquatic environments and have coevolved, a system of interactions has developed between them.

Currently, bacterial QS is a field of active research, as it offers novel strategies for combating pathogenic bacteria. Still, studies on intercellular interactions in phytoplankton remain comparatively scarce. However, this field is important: it provides insight into the mechanisms regulating blooms of unicellular algae, which are an essential link in the trophic chains of water bodies and biogeochemical cycles, affect climate change, and also contribute to half of the Earth's oxygen production [Field et al., 1998]. Bacteria coexisting with phytoplankton in aquatic environments can regulate its abundance: enhance stress tolerance and promote cell division. On the other hand, such bacteria can induce algal death, and this is crucial to consider when developing strategies to mitigate toxic algal blooms, which pose a danger to animals and humans. Given the fragmented and limited nature of conducted studies, the aim of this review was to synthesize key concepts regarding bacterial QS, phytoplankton infochemicals, and the mechanisms of cross-domain interactions mediated by these systems, as well as to identify current knowledge gaps and research perspectives.

Bacterial quorum sensing system. QS enables the differential regulation of gene expression depending on bacterial population density, leading to biofilm formation, biosynthesis of essential enzymes and antibiotics, and shifts in motility and attachment. QS-controlled biofilm formation regulates bacterial virulence by hindering antibiotic access to cells [Preda, Săndulescu, 2019]. Consequently, identifying molecules that inhibit QS is a pressing issue.

QS molecules are referred to as autoinducers (AIs). Those are divided into five main groups (Fig. 1).

1. **AI-1.** Acyl homoserine lactones (AHLs) characteristic of gram-negative bacteria [Papenfort, Bassler, 2016]. AHL molecule consists of a lactone ring and an acyl side chain. Variations in the number of carbon atoms in the acyl chain (from C_4 to C_{18}) and in the substituent groups (oxo and hydroxy) determine the vast diversity and specificity of AHLs. Their molecules are transported into cells and recognized by LuxR-type and CepR-type receptor proteins [Papenfort, Bassler, 2016; Slinger et al., 2019]. AHLs are produced by many genera of gram-negative bacteria; accordingly, various AHL synthases exist, encoded by *luxI* [Engebrecht, Silverman, 1984], *ainS* [Gilson et al., 1995], *hdtS* [Laue et al., 2000], and *CepI* [Slinger et al., 2019] genes.
2. **PQS.** *Pseudomonas* quinolone signal (PQS), 2-heptyl-3-hydroxy-4(1H)-quinolone, characteristic of gram-negative pseudomonads. Proteins involved in its synthesis constitute *PqsABCDEH* gene cluster [Lin et al., 2018]. Upon entering the cell, PQS binds to the transcription factor PqsR, resulting in the activation of virulence genes, particularly those required for biofilm formation [Lin et al., 2018].
3. **DSF.** Diffusible signal factors (DSFs), a family of cis-2-unsaturated fatty acids characteristic of gram-negative bacteria [He et al., 2023]. The mechanism of their action is governed by *rpf* (regulation of pathogenicity factor) gene cluster. In DSF synthesis, rpfF and rpfB proteins are involved. DSF is detected by rpfC, which subsequently activates rpfG [Feng et al., 2023]. DSF signals have emerged as important regulators of virulence and biofilm formation in a wide range of bacterial pathogens [Deng et al., 2010]. DSFs have been shown to mediate not only intra- and interspecies communication but also cross-domain one, particularly with fungi, plants, and insects [He et al., 2023; Ryan et al., 2015]. However, no effect on phytoplankton has been demonstrated to date.

4. **AI-2.** QS signal characteristic of both gram-negative and gram-positive bacteria; a group of interconverting furanones derived from dihydroxy-2,3-pentanedione (DPD), which undergoes a series of spontaneous rearrangements. In DPD synthesis, luxS enzyme is involved, conserved in many bacteria [Surette et al., 1999]. Two types of DPD-derived AI-2 have been described: boron-containing S-2-methyl-2,3,3,4-tetrahydroxytetrahydrofuran-borate (S-THMF-borate) and nonborated R-2-methyl-2,3,3,4-tetrahydroxytetrahydrofuran (R-THMF). These compounds are specific to various bacteria, are recognized by different receptors, but are interconvertible, enabling to facilitate interspecies bacterial communication. S-THMF-borate is recognized by LuxP (*Vibrio* spp.), whereas R-THMF targets LsrB (*Escherichia coli*, *Salmonella typhimurium*, *Bacillus anthracis* str. *ames*, and *Sinorhizobium meliloti*), RbsB (*Aggregatibacter actinomycetemcomitans*), and dCACHE domain of PctA and TlpQ chemoreceptors (*Pseudomonas aeruginosa*) [Rodrigues et al., 2023].
5. **AIP.** Autoinducing peptides characteristic of gram-positive bacteria. The mechanism of their action is similar across various species: peptides are synthesized by certain AIP synthases and later undergo post-translational modification, and are secreted *via* ABC transporters with ATP-dependent release. On the surface of recipient cells, AIPs are recognized by histidine kinase; it becomes activated and triggers a signaling cascade, ultimately leading to changes in the expression of genes involved in production of virulence factors [Verbeke et al., 2017].

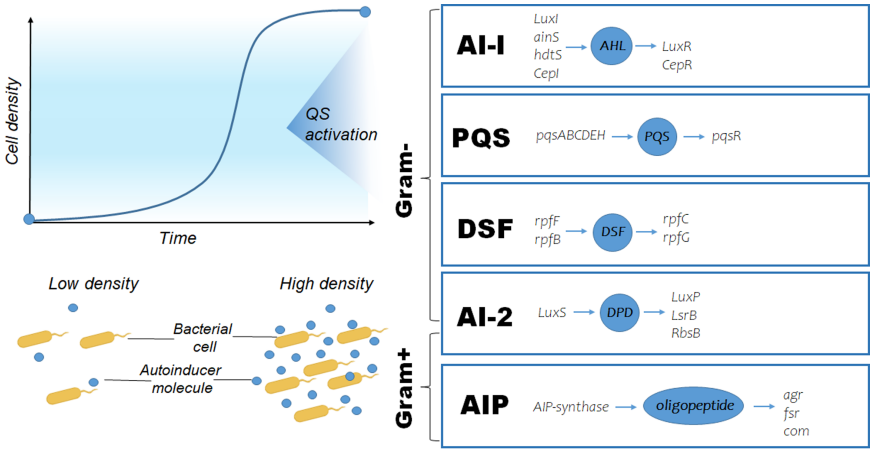


Fig. 1. Quorum sensing regulation. Schematic representation of quorum sensing activation (left) and the main types of autoinducers with key genes involved in their synthesis and perception by cells (right). The autoinducer molecule is represented by a blue circle. AI, autoinducer; AHL, acyl homoserine lactone; PQS, *Pseudomonas* quinolone signal; DSF, diffusible signal factors; DPD, dihydroxy-2,3-pentanedione; AIP, autoinducing peptide

The diversity of quorum sensing molecules enables not only intraspecies but also interspecies communication. AI-2 molecules mediate signal exchange between gram-positive and gram-negative bacteria. Moreover, gram-negative bacteria have been shown to regulate their metabolism using different AIs. Thus, epibionts of *Trichodesmium* use QS to enhance phosphate uptake *via* alkaline phosphatases (a process regulated by AI-1); AI-2 production governs a decrease in phosphate uptake [Van Mooy et al., 2012].

Infochemicals of phytoplankton. The best-studied signaling molecules of phytoplankton are oxylipins: short-chain polyunsaturated aldehydes (PUAs) and other degradation products of oxygenated fatty acids (Fig. 2). To date, PUAs under investigation include decadienal, decatrienal, octadienal, octatrienal, and heptadienal [Cutignano et al., 2006; Wichard et al., 2005]. In addition to diatoms,

haptophytes [Hansen et al., 2004] and chrysophytes [Rashash et al., 1995] are capable of producing these compounds. PUA production increases upon membrane disruption following grazing by consumers, as well as during the stationary growth phase, at high cell density. PUAs serve as a defense against grazers, regulate the bacterial community composition in the phycosphere of microalgae, and participate in their stress responses, either enhancing adaptation or leading to programmed cell death.

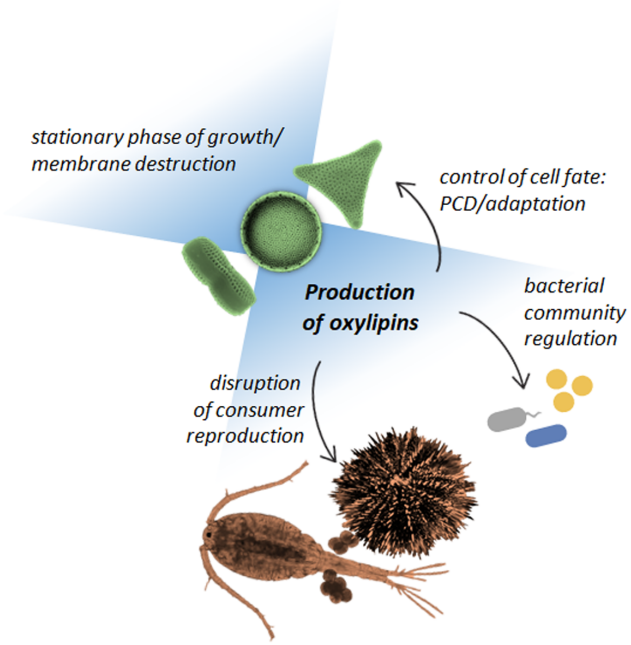


Fig. 2. Effects of oxylipins produced by diatoms on coexisting organisms in the environment

It was found as follows: when copepods feed on diatoms, cell and chloroplast membranes of the latter are damaged, and this results in the release of polyunsaturated fatty acids. Oxidation and enzymatic cleavage of these fatty acids (by phospholipases and glycolipases) mediates the formation of PUAs [Cutignano et al., 2006; Pohnert, 2002], which exert teratogenic effects on copepods [Caldwell et al., 2002; Ianora et al., 2004] and disrupt their embryonic development [Miralto et al., 1999]. Furthermore, PUAs were found to induce embryonic cleavage abnormalities in sea urchins, polychaetes, and ascidians [Lettieri et al., 2015; Ruocco et al., 2019].

Oxylipins were discovered as a defensive response of phytoplankton to grazing by consumers. However, during subsequent research, it was found that their environmental significance is much higher. Oxylipins not only function as intraspecific signals but also affect various phytoplankton taxa and thereby contribute to the structuring of aquatic communities.

It has been demonstrated that PUA production increases with culture age and under nutrient depletion [Ribalet et al., 2007; Vidoudez, Pohnert, 2008]. Mechanical disruption of the cell membrane (as occurs during copepod grazing) is not strictly required for PUA production: during the terminal stages of *Skeletonema marinoi* blooms, PUA production was positively correlated with abundance of cells and the rate of their lysis [Ribalet et al., 2014]. PUAs produced by diatoms have been shown to affect the division of other phytoplankton species: haptophytes, chrysophytes, and dinoflagellates [Pichierri et al., 2016; Ribalet et al., 2007]. Additionally, PUAs participate in regulating abundance and metabolic activity of phytoplankton-associated bacteria [Ribalet et al., 2008].

Under stress conditions, phytoplankton cells produce aldehyde (2E,4E/Z)-decadienal (DD) [Pohnert, 2002]. At high concentrations, DD induces intracellular signaling *via* nitric oxide (NO), culminating in programmed cell death [Vardi et al., 2006]. However, at low concentrations, DD initiates a cascade of reactions that confer resistance to stress, including elevated DD levels [Dolch et al., 2017; Vardi et al., 2006].

Bacteria–phytoplankton interactions. Research into the mechanisms of bacteria–phytoplankton interactions is of great practical importance: its results are useful for wastewater treatment and mitigation of algal blooms [Wu et al., 2022]. Furthermore, scientists continue the search for QS-inhibiting compounds for effective treatment of diseases caused by multidrug-resistant bacterial strains [Pacheco et al., 2021; Ćirić et al., 2019].

The primary site of interaction between microalgae and bacteria is the phycosphere (Fig. 3). This region, that surrounds a phytoplankton cell, contains higher concentrations of nutrients and secondary metabolites as compared to environment [Seymour et al., 2017].

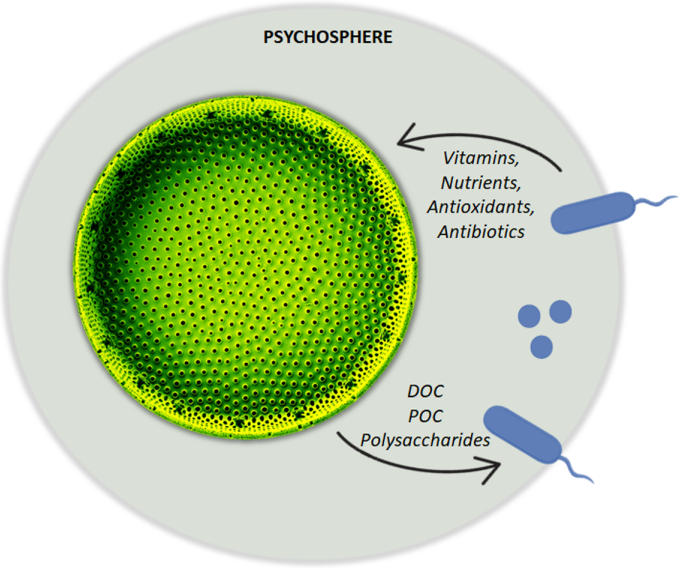


Fig. 3. Scheme of interaction of microalgae and bacteria in the phycosphere (DOC, dissolved organic carbon; POC, particulate organic carbon)

Interactions between bacteria and microalgal cells are remarkably diverse, ranging from mutualism to parasitism [Amin et al., 2012]. In this review, we consider the aspects of bacteria–phytoplankton interactions that are directly related to bacterial QS and phytoplankton-derived infochemicals.

Regulation of algicidal activity in bacteria. The hypothesis that bacteria–microaglae interactions are mediated by QS is supported by metagenomic data, which have revealed bacterial gene sequences involved in the synthesis of autoinducers within actively developing phytoplankton populations in aquatic environments [Huang et al., 2018]. Under such conditions, QS may be directed toward protecting bacteria from antibacterial compounds produced by rapidly dividing phytoplankton cells, as well as toward securing the supply of additional nutrients released from dead algal cells. Moreover, occurrence of compounds released during decomposition of phytoplankton can trigger QS induction in bacteria. For example, cells of *Phaeobacter gallaeciensis*, strain BS107, which coexist with *Emiliania huxleyi*, provide coccolithophores with the phytohormone auxin (a growth promoter) during their exponential growth

phase, while also protecting them from pathogens *via* antibiotic production. In turn, *E. huxleyi* produces dimethylsulfoniopropionate (DMSP), which bacteria utilize as a source of sulfur. During the stationary growth phase, when products of algal decomposition, such as *n*-coumaric acid, are accumulated in the environment, *P. gallaeciensis* metabolism shifts in response to the production of algicidal compounds (in this case, roseobactericides) [Seyedsayamdost et al., 2011]. A flavobacterium *Kordia algicida* also uses QS to control its algicidal activity. Thus, upon reaching high densities, its cells produce an algicidal protease that affects *Skeletonema*, *Thalassiosira*, and *Phaeodactylum* representatives [Paul, Pohnert, 2011]. However, the same study showed that the algicide produced did not affect *Chaetoceros didymus*. Further investigation revealed that *C. didymus* releases its own proteases, which, upon sensing *K. algicida* proteins, may serve as a chemical defense mechanism [Paul, Pohnert, 2013]. The mechanism of QS-mediated activation of algicidal substance production has been demonstrated in *Aeromonas* [Guo et al., 2016], *Ponticoccus* [Chi et al., 2017], and *Bacillus subtilis* [Zhang et al., 2020].

Effects of quorum sensing molecules on phytoplankton cells. Quorum sensing molecules themselves can be a source of stress for phytoplankton, as they lead to lipid accumulation and a slight reduction in biomass, as demonstrated in Chlorophyta [Zhang et al., 2018]. Cultivation of *Chlorella sorokiniana* with bacterial quorum sensing molecules, specifically AHLs, resulted in increased algal biomass, as well as a significant boost in lipid and protein content [Das et al., 2019]. Marine *Roseobacter* isolates have been found to produce AHLs, and some isolates can inhibit cell division of a diatom *Skeletonema costatum* [Ziesche et al., 2015]. Spontaneous rearrangement of AHLs can occur, with formation of tetramic acids (TAs) [Stock et al., 2019]. A high diversity of TAs has been reported. These compounds exhibit antibacterial, antifungal, and antiviral activities [Jiang et al., 2020], and also algicidal effects. Notably, the rearrangement product of oxo-C12-AHL (TA12) suppresses cell division and photosynthesis in *Phaeodactylum tricornutum* [Stock et al., 2019]. Also, the effect of TA14 (oxo-C14-HSL) has been shown on *Seminavis robusta* [Stock et al., 2020]. However, C14-HSL enhanced cell division of this species. Transcriptomic analysis revealed that the mechanism of action of C14-HSL and oxo-C14-HSL involves activation of gene expression related to intracellular signaling, and also alteration of the cell cycle-dependent gene expression in diatoms. Lipid metabolism was altered as well, leading the researchers to suggest that *S. robusta* may utilize AHLs (C14-HSL) as an external energy source [Stock et al., 2020].

Quinolones exert a strong toxic effect on phytoplankton. Pentylquinolone isolated from *Alteromonas* sp. KNS-16 was shown to suppress the growth of *Heterosigma akashiwo*: a bloom-forming toxic microalga [Cho, 2012]. A marine bacterium *Pseudoalteromonas piscicida* produces heptylquinolone, which is toxic to *E. huxleyi* at a low concentration (1 μM) [Harvey et al., 2016]. The mechanism of its action differs slightly among phytoplankton species. When affecting *E. huxleyi*, heptylquinolone disrupted photosynthesis by inhibiting photosystem II and a cytochrome b6f [Harvey et al., 2016], and also suppressed cell cycle and DNA repair [Pollara et al., 2021]. In a green alga *Dunaliella tertiolecta*, photosynthesis was inhibited *via* inactivation of photosystem II, whereas in a diatom *P. tricornutum*, the compound hindered electron transport by blocking the cytochrome b6f complex [Dow et al., 2020]. A positive effect of heptylquinolone on *E. huxleyi* was also observed: the induction of resistance to viral infection [Pollara et al., 2021].

Effects of phytoplankton on bacterial quorum sensing. Certain phytoplankton species are capable of mimicking bacterial signals, thereby suppressing QS (Table 1). This mechanism is termed quorum quenching (QQ) [Sikdar, Elias, 2020].

Table 1. Quorum quenching system in phytoplankton

Producer	Compound	Effect on recipient	Reference
Chlamydomonas reinhardtii	Not identified	Activation of QS in *Sinorhizobium meliloti*	Teplitski et al., 2004
	Not identified, with a lactone ring	Effect on CepR QS receptors in *Aeromonas veronii*: reduction of biofilm formation	Rajamani et al., 2011
	Lumichrome	Activation of QS in *Pseudomonas aeruginosa*	Rajamani et al., 2008
Asterionellopsis glacialis	Rosmarinic acid	Inhibition of motility, and biofilm formation in *Roseobacter*	Fei et al., 2020
Anabaena sp.	Acylase	Degradation of AHL	Romero et al., 2008
Nitzschia cf. *pellucida*	Haloperoxidase	Degradation of AHL	Syrpas et al., 2014

Upon prolonged cultivation, cells of a green alga *Chlamydomonas reinhardtii* produce a number of compounds that mimic AHLs by stimulating QS receptors: LasR or CepR. Exposure of *S. meliloti* cells at low density to such a mimic (partially purified and of unidentified chemical nature) altered the bacterial proteome to an extent similar to that caused by genuine AHLs [Teplitski et al., 2004]. Treatment with lactonase (a metalloenzyme) abolished the effect of the *C. reinhardtii* mimic on *Aeromonas veronii* CepR receptors, suggesting that the QS-mimicking compound produced by this alga contains a lactone ring with an amide bond, the same as bacterial AHLs [Rajamani et al., 2011]. Another study showed that *C. reinhardtii* cells produce riboflavin, that subsequently forms lumichrome; the latter can stimulate LasR receptors in *P. aeruginosa* [Rajamani et al., 2008].

Bacteria of the *Roseobacter* group colonize the phycosphere and are symbionts of a diatom *Asterionellopsis glacialis*. The alga, in turn, can use mimics of quorum sensing molecules to trigger inhibition of bacterial motility and biofilm formation [Fei et al., 2020]. Rosmarinic acid produced by *A. gracialis* may facilitate colonization of the phycosphere by bacteria *via* impairing their motility [Fei et al., 2020].

Filamentous cyanobacteria, *Anabaena* sp., possess AHL-acylase activity and genes encoding acylases (homologous sequences of the acylase-encoding gene have also been found in *Nostoc punctiforme*, *Gloeobacter violaceus*, and *Synechocystis* sp.). Its production probably allows it to avoid interference from external signals in its own signaling system or makes it possible to affect other organisms [Romero et al., 2008].

A diatom *Nitzschia* cf. *pellucida* is capable of degrading AHLs *via* bromine-mediated halogenation of oxo-AHLs, leading to hydrolysis of both the acyl and lactone moieties [Syrpas et al., 2014]. It is hypothesized that this mechanism is available to many diatoms, but further investigation is required. Bioinformatic analysis revealed that the genome of a diatom *Fragilariopsis cylindrus* contains a candidate gene encoding a haloperoxidase, which may inhibit bacterial QS through halogenation of AHL acyl chains [Amin et al., 2012]. Thus, diatoms can degrade AHLs, thereby inhibiting not only algicidal effects but also QS-mediated changes in bacteria.

Effects of phytoplankton oxylipins on bacterial cells. As was shown, the composition of the bacterial community in the phycosphere is dependent on the growth stage of algal cells and may be associated with the release of secondary metabolites. Differential effects of oxylipins have been observed among

bacterial strains isolated during the active growth phase of *S. marinoi* population, with these compounds either stimulating or inhibiting cell division [Ribalet et al., 2008]. However, several studies have failed to detect a correlation between bacterial diversity and the production of PUAs [Eastabrook et al., 2020; Paul et al., 2012]. Apparently, oxylipins, while not the sole determinant, constitute an important factor in algae–bacteria interactions. A recent study has demonstrated that *Cyclotella cryptica* modulates its PUA profile depending on co-cultivated bacteria [Hernanz-Torrijos et al., 2023].

Research perspectives. Chemical interactions between unicellular organisms are mainly explored *in vitro*, that undoubtedly provides the foundation for investigating natural phenomena. This approach certainly allows the detection of various compounds responsible for cellular signaling and the elucidation of basic principles of cell interactions. Under laboratory conditions, we can model specific processes to study cellular responses, examine changes in gene expression induced by various infochemicals, isolate novel compounds from cells, and use genetic engineering approaches to investigate the effects of turning on and off genes involved in the synthesis of target compounds. However, it is impossible to model *in vitro* all environmental factors that affect an organism, and consequently, to capture all possible cellular responses. Numerous questions remain unsolved, including the following ones: how does microbiome of the algal phycosphere affect its response to environmental changes, and what concentrations of infochemicals are sufficient to transmit signals in the water column? To understand the role of bacteria in the mechanisms of phytoplankton population development, interdisciplinary laboratory studies need to be complemented by comprehensive *in vivo* investigations: metagenomic (to identify bacteria associated with various phytoplankton species), metatranscriptomic (to elucidate cellular responses to environmental changes), and metabolomic ones (to detect induced signaling compounds).

Understanding the processes of cellular interactions provides fundamental knowledge about development of phytoplankton population that has several practical applications. First, obtaining stable and high biomass of unicellular algae is a key issue in biotechnology. Elucidating the mechanisms of population regulation will open up relevant opportunities. Second, phytoplankton metabolites are a source of bioactive compounds, particularly for the production of new antibiotics [Pradhan, Ki, 2022]. In turn, bacterial compounds can be used for species-specific control of algal overgrowth in water bodies, which is crucial for mitigating harmful algal blooms [Sun et al., 2018].

Conclusion. Molecular interactions between unicellular organisms in aquatic ecosystems play a key role in shaping both competitive and cooperative dynamics within population. A wide diversity of signaling molecules produced by microorganisms facilitates not only intra- and interspecific communication but also interactions between pro- and microeukaryotes. Bacterial quorum sensing (QS) enables colonization of the microalgal phycosphere and can affect algal physiology. The production of algicidal compounds is known to be a quorum-dependent mechanism capable of regulating phytoplankton population dynamics. In turn, microalgae can modulate bacterial development through their own infochemicals and interfere with bacterial QS by either degrading autoinducers or mimicking them. Nevertheless, the prevalence of quorum quenching across different phytoplankton species, as well as the mechanisms by which oxylipins affect the microbial community of the phycosphere, remain poorly understood. Numerous unresolved questions underscore the need for further research aimed at elucidating the principles of coexistence of organisms in aquatic ecosystems, cellular adaptation to environmental changes, and the search for novel compounds for controlling pathogenic bacteria and mitigating harmful algal blooms.

This work was carried out within the framework of LIN SB RAS state research assignment no. 0279-2021-0008 (no. 121032300186-9).

REFERENCES

1. Amin S. A., Parker M. S., Armbrust E. V. Interactions between diatoms and bacteria. *Microbiology and Molecular Biology Reviews*, 2012, vol. 76, no. 3, pp. 667–684. https://doi.org/10.1128/mmbr.00007-12
2. Brodskii V. Y. The cell theory. Progress in studies on cell-cell communications. *Russian Journal of Developmental Biology*, 2009, vol. 40, iss. 5, pp. 255–263. https://doi.org/10.1134/S1062360409050014
3. Caldwell G. S., Olive P. J. W., Bentley M. G. Inhibition of embryonic development and fertilization in broadcast spawning marine invertebrates by water soluble diatom extracts and the diatom toxin 2-*trans*,4-*trans* decadienal. *Aquatic Toxicology*, 2002, vol. 60, iss. 1–2, pp. 123–137. https://doi.org/10.1016/s0166-445x(01)00277-6
4. Chi W., Zheng L., He C., Han B., Zheng M., Gao W., Sun C., Zhou G., Gao X. Quorum sensing of microalgae associated marine *Ponticoccus* sp. PD-2 and its algicidal function regulation. *AMB Express*, 2017, vol. 7, art. no. 59 (10 p.). https://doi.org/10.1186/s13568-017-0357-6
5. Cho J. Y. Algicidal activity of marine *Alteromonas* sp. KNS-16 and isolation of active compounds. *Bioscience, Biotechnology and Biochemistry*, 2012, vol. 76, iss. 8, pp. 1452–1458. https://doi.org/10.1271/bbb.120102
6. Cutignano A., d'Ippolito G., Romano G., Lamari N., Cimino G., Febbraio F., Nucci R., Fontana A. Chloroplastic glycolipids fuel aldehyde biosynthesis in the marine diatom *Thalassiosira rotula*. *ChemBioChem*, 2006, vol. 7, iss. 3, pp. 450–456. https://doi.org/10.1002/cbic.200500343
7. Das S., Das S., Ghangrekar M. M. Quorum-sensing mediated signals: A promising multi-functional modulators for separately enhancing algal yield and power generation in microbial fuel cell. *Bioresource Technology*, 2019, vol. 294, art. no. 122138 (8 p.). https://doi.org/10.1016/j.biortech.2019.122138
8. Deng Y., Wu J., Eberl L., Zhang L.-H. Structural and functional characterization of diffusible signal factor family quorum-sensing signals produced by members of the *Burkholderia cepacia* complex. *Applied and Environmental Microbiology*, 2010, vol. 76, no. 14, pp. 4675–4683. https://doi.org/10.1128/aem.00480-10
9. Dolch L. J., Lupette J., Tourcier G., Bedhomme M., Collin S., Magneschi L., Conte M., Seddiki K., Richard C., Corre E., Fourage L., Laeuffer F., Richards R., Reith M., Rébeillé F., Jouhet J., McGinn P., Maréchal E. Nitric oxide mediates nitrite-sensing and acclimation and triggers a remodeling of lipids. *Plant Physiology*, 2017, vol. 175, iss. 3, pp. 1407–1423. https://doi.org/10.1104/pp.17.01042
10. Dow L., Stock F., Peltekis A., Szamosvári D., Prothiwa M., Lapointe A., Böttcher T., Bailleul B., Vyverman W., Kroth P. G., Lepetit B. The multifaceted inhibitory effects of an alkylquinolone on the diatom *Phaeodactylum tricornutum*. *ChemBioChem*, 2020, vol. 21, iss. 8, pp. 1206–1216. https://doi.org/10.1002/cbic.201900612
11. Eastabrook C. L., Whitworth P., Robinson G., Caldwell G. S. Diatom-derived polyunsaturated aldehydes are unlikely to influence the microbiota composition of laboratory-cultured diatoms. *Life*, 2020, vol. 10, iss. 3, art. no. 29 (14 p.). https://doi.org/10.3390/life10030029
12. Eberhard A., Burlingame A. L., Eberhard C., Kenyon G. L., Nealson K. H., Oppenheimer N. J. Structural identification of autoinducer of *Photobacterium fischeri* luciferase. *Biochemistry*, 1981, vol. 20, iss. 9, pp. 2444–2449. https://doi.org/10.1021/bi00512a013
13. Engebrecht J., Silverman M. Identification of genes and gene products necessary for bacterial bioluminescence. *The Proceedings of the National Academy of Sciences*, 1984, vol. 81,

no. 13, pp. 4154–4158. https://doi.org/10.1073/pnas.81.13.4154

14. Fei C., Ochsenkühn M. A., Shibl A. A., Isaac A., Wang C., Amin S. A. Quorum sensing regulates 'swim-or-stick' lifestyle in the phycosphere. *Environmental Microbiology*, 2020, vol. 22, iss. 11, pp. 4761–4778. https://doi.org/10.1111/1462-2920.15228
15. Feng Y.-M., Long Z.-Q., Xiang H.-M., Ran J.-N., Zhou X., Yang S. Research on diffusible signal factor-mediated quorum sensing in *Xanthomonas*: A mini-review. *Molecules*, 2023, vol. 28, iss. 2, art. no. 876 (12 p.). https://doi.org/10.3390/molecules28020876
16. Field C. B., Behrenfeld M. J., Randerson J. T., Falkowski P. Primary production of the biosphere: Integrating terrestrial and oceanic components. *Science*, 1998, vol. 281, iss. 5374, pp. 237–240. https://doi.org/10.1126/science.281.5374.237
17. Fuqua W. C., Winans S. C., Greenberg E. P. Quorum sensing in bacteria: The LuxR-LuxI family of cell density-responsive transcriptional regulators. *Journal of Bacteriology*, 1994, vol. 176, no. 2, pp. 269–275. https://doi.org/10.1128/jb.176.2.269-275.1994
18. Gilson L., Kuo A., Dunlap P. V. AinS and a new family of autoinducer synthesis proteins. *Journal of Bacteriology*, 1995, vol. 177, no. 23, pp. 6946–6951. https://doi.org/10.1128/jb.177.23.6946-6951.1995
19. Guo X., Liu X., Wu L., Pan J., Yang H. The algicidal activity of *Aeromonas* sp. strain GLY-2107 against bloom-forming *Microcystis aeruginosa* is regulated by *N*-acyl homoserine lactone-mediated quorum sensing. *Environmental Microbiology*, 2016, vol. 18, pp. 3867–3883. https://doi.org/10.1111/1462-2920.13346
20. Hansen E., Ernstsen A., Eilertsen H. C. Isolation and characterization of a cytotoxic polyunsaturated aldehyde from the marine phytoplankter *Phaeocystis pouchetii* (Hariot) Lagerheim. *Toxicology*, 2004, vol. 199, iss. 2–3, pp. 207–217. https://doi.org/10.1016/j.tox.2004.02.026
21. Harvey E. L., Deering R. W., Rowley D. C., El Gamal A., Schorn M., Moore B. S., Johnson M. D., Mincer T. J., Whalen K. E. A bacterial quorum-sensing precursor induces mortality in the marine coccolithophore, *Emiliania huxleyi*. *Frontiers in Microbiology*, 2016, vol. 7, art. no. 59 (12 p.). https://doi.org/10.3389/fmicb.2016.00059
22. He Y.-W., Deng Y., Miao Y., Chatterjee S., Tran T. M., Tian J., Lindow S. DSF-family quorum sensing signal-mediated intraspecies, interspecies, and inter-kingdom communication. *Trends in Microbiology*, 2023, vol. 31, iss. 1, pp. 36–50. https://doi.org/10.1016/j.tim.2022.07.006
23. Hernanz-Torrijos M., Ortega M. J., Úbeda B., Bartual A. Polyunsaturated aldehydes profile in the diatom *Cyclotella cryptica* is sensitive to changes in its phycosphere bacterial assemblages. *Marine Drugs*, 2023, vol. 21, iss. 11, art. no. 571 (21 p.). https://doi.org/10.3390/md21110571
24. Huang X., Zhu J., Cai Z., Lao Y., Jin H., Yu K., Zhang B., Zhou J. Profiles of quorum sensing (QS)–related sequences in phycospheric microorganisms during a marine dinoflagellate bloom, as determined by a metagenomic approach. *Microbiological Research*, 2018, vol. 217, pp. 1–13. https://doi.org/10.1016/j.micres.2018.08.015
25. Ianora A., Miralto A., Poulet S. A., Carotenuto Y., Buttino I., Romano G., Casotti R., Pohnert G., Wichard T., Colucci-D'Amato L., Terrazzano G., Smetacek V. Aldehyde suppression of copepod recruitment in blooms of a ubiquitous planktonic diatom. *Nature*, 2004, vol. 429, pp. 403–407. https://doi.org/10.1038/nature02526
26. Jiang M., Chen S., Li J., Liu L. The biological and chemical diversity of tetramic acid compounds from marine-derived microorganisms. *Marine Drugs*, 2020, vol. 18, iss. 2, art. no. 114 (43 p.). https://doi.org/10.3390/md18020114
27. Kempner E. S., Hanson F. E. Aspects of light production by *Photobacterium fischeri*. *Journal of Bacteriology*, 1968, vol. 95, no. 3, pp. 975–979. https://doi.org/10.1128/jb.95.3.975-979.1968
28. Laue B. E., Jiang Y., Chhabra S. R., Jacob S., Stewart G. S. A. B., Hardman A., Downie J. A., O'Gara F., Williams P. The biocontrol strain *Pseudomonas fluorescens* F113 produces the *Rhizobium small* bacteriocin, *N*-(3-hydroxy-7-*cis*-tetradecenoyl)homoserine lactone, *via* HdtS, a putative novel

N-acylhomoserine lactone synthase. *Microbiology*, 2000, vol. 146, iss. 10, pp. 2469–2480. https://doi.org/10.1099/00221287-146-10-2469

29. Lettieri A., Esposito R., Ianora A., Spagnuolo A. *Ciona intestinalis* as a marine model system to study some key developmental genes targeted by the diatom-derived aldehyde decadienal. *Marine Drugs*, 2015, vol. 13, iss. 3, pp. 1451–1465. https://doi.org/10.3390/md13031451
30. Lin J., Cheng J., Wang Y., Shen X. The *Pseudomonas* quinolone signal (PQS): Not just for quorum sensing anymore. *Frontiers in Cellular and Infection Microbiology*, 2018, vol. 8, art. no. 230 (9 p.). https://doi.org/10.3389/fcimb.2018.00230
31. Miralto A., Barone G., Romano G., Poulet S. A., Ianora A., Russo G. L., Buttino I., Mazzarella G., Laabir M., Cabrini M., Giacobbe M. G. The insidious effect of diatoms on copepod reproduction. *Nature*, 1999, vol. 402, pp. 173–176. https://doi.org/10.1038/46023
32. Nealson K. H., Platt T., Hastings J. W. Cellular control of the synthesis and activity of the bacterial luminescent system. *Journal of Bacteriology*, 1970, vol. 104, no. 1, pp. 313–322. https://doi.org/10.1128/jb.104.1.313-322.1970
33. Pacheco T., Gomes A. E. I., Siqueira N. M. G., Assoni L., Darrieux M., Venter H., Ferraz L. F. C. SdiA, a quorum-sensing regulator, suppresses fimbriae expression, biofilm formation, and quorum-sensing signaling molecules production in *Klebsiella pneumoniae*. *Frontiers in Microbiology*, 2021, vol. 12, art. no. 597735 (15 p.). https://doi.org/10.3389/fmicb.2021.597735
34. Papenfort K., Bassler B. L. Quorum sensing signal–response systems in gram-negative bacteria. *Nature Reviews Microbiology*, 2016, vol. 14, pp. 576–588. https://doi.org/10.1038/nrmicro.2016.89
35. Paul C., Pohnert G. Induction of protease release of the resistant diatom *Chaetoceros didymus* in response to lytic enzymes from an algicidal bacterium. *PLoS One*, 2013, vol. 8, iss. 3, art. no. e57577 (7 p.). https://doi.org/10.1371/journal.pone.0057577
36. Paul C., Pohnert G. Interactions of the algicidal bacterium *Kordia algicida* with diatoms: Regulated protease excretion for specific algal lysis. *PLoS One*, 2011, vol. 6, iss. 6, art. no. e21032 (8 p.). https://doi.org/10.1371/journal.pone.0021032
37. Paul C., Reunamo A., Lindehoff E., Bergkvist J., Mausz M. A., Larsson H., Richter H., Wängberg S.-Å., Leskinen P., Båmstedt U., Pohnert G. Diatom derived polyunsaturated aldehydes do not structure the planktonic microbial community in a mesocosm study. *Marine Drugs*, 2012, vol. 10, iss. 4, pp. 775–792. https://doi.org/10.3390/md10040775
38. Pichierri S., Pezzolesi L., Vanucci S., Totti C., Pistocchi R. Inhibitory effect of polyunsaturated aldehydes (PUAs) on the growth of the toxic benthic dinoflagellate *Ostreopsis* cf. *ovata*. *Aquatic Toxicology*, 2016, vol. 179, pp. 125–133. https://doi.org/10.1016/j.aquatox.2016.08.018
39. Pohnert G. Phospholipase A_2 activity triggers the wound-activated chemical defense in the diatom *Thalassiosira rotula*. *Plant Physiology*, 2002, vol. 129, iss. 1, pp. 103–111. https://doi.org/10.1104/pp.010974
40. Pohnert G., Steinke M., Tollrian R. Chemical cues, defense metabolites and the shaping of pelagic interspecific interactions. *Trends in Ecology and Evolution*, 2007, vol. 22, iss. 4, pp. 198–204. https://doi.org/10.1016/j.tree.2007.01.005
41. Pollara S. B., Becker J. W., Nunn B. L., Boiteau R., Repeta D., Mudge M. C., Downing G., Chase D., Harvey E. L., Whalen K. E. Bacterial quorum-sensing signal arrests phytoplankton cell division and impacts virus-induced mortality. *mSphere*, 2021, vol. 6, no. 3, art. no. e00009-21 (17 p.). https://doi.org/10.1128/mSphere.00009-21
42. Pradhan B., Ki J.-S. Phytoplankton toxins and their potential therapeutic applications: A journey toward the quest for potent pharmaceuticals. *Marine Drugs*, 2022, vol. 20, iss. 4, art. no. 271 (24 p.). https://doi.org/10.3390/md20040271
43. Preda V. G., Săndulescu O. Communication is the key: Biofilms, quorum sensing, formation and prevention. *Discoveries*, 2019, vol. 7, no. 3, art. no. e100 (11 p.). https://doi.org/10.15190/d.2019.13
44. Rajamani S., Bauer W. D., Robinson J. B., Farrow III J. M., Pesci E. C., Teplitski M., Gao M.,

Sayre R. T., Phillips D. A. The vitamin riboflavin and its derivative lumichrome activate the LasR bacterial quorum-sensing receptor. *Molecular Plant-Microbe Interactions*, 2008, vol. 21, no. 9, pp. 1184–1192. https://doi.org/10.1094/mpmi-21-9-1184

45. Rajamani S., Teplitski M., Kumar A., Krediet C. J., Sayre R. T., Bauer W. D. *N*-acyl homoserine lactone, AiiA, inactivation of quorum-sensing agonists produced by *Chlamydomonas reinhardtii* (Chlorophyta) and characterization of *aiiA* transgenic algae. *Journal of Phycology*, 2011, vol. 47, iss. 5, pp. 1219–1227. https://doi.org/10.1111/j.1529-8817.2011.01049.x
46. Rashash D. M. C., Dietrich A. M., Hoehn R. C., Parker B. C. The influence of growth conditions on odor-compound production by two chrysophytes and two cyanobacteria. *Water Science and Technology*, 1995, vol. 31, iss. 11, pp. 165–172. https://doi.org/10.1016/0273-1223(95)00472-Y
47. Ribalet F., Bastianini M., Vidoudez C., Acri F., Berges J., Ianora A., Miralto A., Pohnert G., Romano G., Wichard T., Casotti R. Phytoplankton cell lysis associated with polyunsaturated aldehyde release in the northern Adriatic Sea. *PLoS One*, 2014, vol. 9, iss. 1, art. no. e85947 (10 p.). https://doi.org/10.1371/journal.pone.0085947
50. Ribalet F., Berges J. A., Ianora A., Casotti R. Growth inhibition of cultured marine phytoplankton by toxic algal-derived polyunsaturated aldehydes. *Aquatic Toxicology*, 2007, vol. 85, iss. 3, pp. 219–227. https://doi.org/10.1016/j.aquatox.2007.09.006
49. Ribalet F., Intertaglia L., Lebaron P., Casotti R. Differential effect of three polyunsaturated aldehydes on marine bacterial isolates. *Aquatic Toxicology*, 2008, vol. 86, iss. 2, pp. 249–255. https://doi.org/10.1016/j.aquatox.2007.11.005
50. Ribalet F., Wichard T., Pohnert G., Ianora A., Miralto A., Casotti R. Age and nutrient limitation enhance polyunsaturated aldehyde production in marine diatoms. *Phytochemistry*, 2007, vol. 68, iss. 15, pp. 2059–2067. https://doi.org/10.1016/j.phytochem.2007.05.012
51. Rodrigues M. V., Kis P., Xavier K. B., Ventura M. R. Synthesis and potential of Autoinducer-2 and analogs to manipulate interspecies quorum sensing. *Israel Journal of Chemistry*, 2023, vol. 63, iss. 5–6, art. no. e202200091 (28 p.). https://doi.org/10.1002/ijch.202200091
52. Romero M., Diggle S. P., Heeb S., Cámara M., Otero A. Quorum quenching activity in *Anabaena* sp. PCC 7120: Identification of AiiC, a novel AHL-acylase. *FEMS Microbiology Letters*, 2008, vol. 280, iss. 1, pp. 73–80. https://doi.org/10.1111/j.1574-6968.2007.01046.x
53. Ruocco N., Annunziata C., Ianora A., Libralato G., Manfra L., Costantini S., Costantini M. Toxicity of diatom-derived polyunsaturated aldehyde mixtures on sea urchin *Paracentrotus lividus* development. *Scientific Reports*, 2019, vol. 9, art. no. 517 (9 p.). https://doi.org/10.1038/s41598-018-37546-y
54. Ryan R. P., An S.-q., Allan J. H., McCarthy Y., Dow J. M. The DSF family of cell–cell signals: An expanding class of bacterial virulence regulators. *PLoS Pathogens*, 2015, vol. 11, iss. 7, art. no. e1004986 (14 p.). https://doi.org/10.1371/journal.ppat.1004986
55. Seyedsayamdost M. R., Case R. J., Kolter R., Clardy J. The Jekyll-and-Hyde chemistry of *Phaeobacter gallaeciensis*. *Nature Chemistry*, 2011, vol. 3, pp. 331–335. https://doi.org/10.1038/nchem.1002
56. Seymour J. R., Amin S. A., Raina J.-B., Stocker R. Zooming in on the phycosphere: The ecological interface for phytoplankton–bacteria relationships. *Nature Microbiology*, 2017, vol. 2, art. no. 17065 (12 p.). https://doi.org/10.1038/nmicrobiol.2017.65
57. Sikdar R., Elias M. Quorum quenching enzymes and their effects on virulence, biofilm, and microbiomes: A review of recent advances. *Expert Review of Anti-infective Therapy*, 2020, vol. 18, iss. 12, pp. 1221–1233. https://doi.org/10.1080/14787210.2020.1794815
58. Slinger B. L., Deay J. J., Chandler J. R., Blackwell H. E. Potent modulation of the CepR quorum sensing receptor and virulence in a *Burkholderia cepacia* complex member

using non-native lactone ligands. *Scientific Reports*, 2019, vol. 9, art. no. 13449 (12 p.). https://doi.org/10.1038/s41598-019-49693-x

59. Stock F., Bilcke G., De Decker S., Osuna-Cruz C. M., Van den Berge K., Vancaester E., De Veylder L., Vandepoele K., Mangelinckx S., Vyverman W. Distinctive growth and transcriptional changes of the diatom *Seminavis robusta* in response to quorum sensing related compounds. *Frontiers in Microbiology*, 2020, vol. 11, art. no. 1240 (14 p.). https://doi.org/10.3389/fmicb.2020.01240
60. Stock F., Syrpas M., Graff van Creveld S., Backx S., Blommaert L., Dow L., Stock W., Ruysbergh E., Lepetit B., Bailleul B., Sabbe K., De Kimpe N., Willems A., Kroth P. G., Vardi A., Vyverman W., Mangelinckx S. *N*-acyl homoserine lactone derived tetramic acids impair photosynthesis in *Phaeodactylum tricornutum*. *ACS Chemical Biology*, 2019, vol. 14, iss. 2, pp. 198–203. https://doi.org/10.1021/acschembio.8b01101
61. Sun R., Sun P., Zhang J., Esquivel-Elizondo S., Wu Y. Microorganisms-based methods for harmful algal blooms control: A review. *Bioresource Technology*, 2018, vol. 248, pt B, pp. 12–20. https://doi.org/10.1016/j.biortech.2017.07.175
62. Surette M. G., Miller M. B., Bassler B. L. Quorum sensing in *Escherichia coli*, *Salmonella typhimurium*, and *Vibrio harveyi*: A new family of genes responsible for autoinducer production. *Proceedings of the National Academy of Sciences*, 1999, vol. 96, no. 4, pp. 1639–1644. https://doi.org/10.1073/pnas.96.4.1639
63. Syrpas M., Ruysbergh E., Blommaert L., Vanelslander B., Sabbe K., Vyverman W., De Kimpe N., Mangelinckx S. Haloperoxidase mediated quorum quenching by *Nitzschia* cf. *pellucida*: Study of the metabolization of *N*-acyl homoserine lactones by a benthic diatom. *Marine Drugs*, 2014, vol. 12, iss. 1, pp. 352–367. https://doi.org/10.3390/md12010352
64. Teplitski M., Chen H., Rajamani S., Gao M., Merighi M., Sayre R. T., Robinson J. B., Rolfe B. G., Bauer W. D. *Chlamydomonas reinhardtii* secretes compounds that mimic bacterial signals and interfere with quorum sensing regulation in bacteria. *Plant Physiology*, 2004, vol. 134, iss. 1, pp. 137–146. https://doi.org/10.1104/pp.103.029918
65. Van Mooy B. A. S., Hmelo L. R., Sofen L. E., Campagna S. R., May A. L., Dyhrman S. T., Heithoff A., Webb E. A., Momper L., Mincer T. J. Quorum sensing control of phosphorus acquisition in *Trichodesmium* consortia. *The ISME Journal*, 2012, vol. 6, iss. 2, pp. 422–429. https://doi.org/10.1038/ismej.2011.115
66. Vardi A., Formiggini F., Casotti R., De Martino A., Ribalet F., Miralto A., Bowler C. A stress surveillance system based on calcium and nitric oxide in marine diatoms. *PLoS Biology*, 2006, vol. 4, iss. 3, art. no. e60 (9 p.). https://doi.org/10.1371/journal.pbio.0040060
67. Verbeke F., De Craemer S., Debunne N., Janssens Y., Wynendaele E., Van de Wiele C., De Spiegeleer B. Peptides as quorum sensing molecules: Measurement techniques and obtained levels *in vitro* and *in vivo*. *Frontiers in Neuroscience*, 2017, vol. 11, art. no. 183 (18 p.). https://doi.org/10.3389/fnins.2017.00183
68. Vidoudez C., Pohnert G. Growth phase-specific release of polyunsaturated aldehydes by the diatom *Skeletonema marinoi*. *Journal of Plankton Research*, 2008, vol. 30, iss. 11, pp. 1305–1313. https://doi.org/10.1093/plankt/fbn085
69. Wichard T., Poulet S. A., Halsband-Lenk C., Albaina A., Harris R., Liu D., Pohnert G. Survey of the chemical defense potential of diatoms: Screening of fifty species for α,β,γ,δ-unsaturated aldehydes. *Journal of Chemical Ecology*, 2005, vol. 31, iss. 4, pp. 949–958. https://doi.org/10.1007/s10886-005-3615-z
70. Wu X., Kong L., Pan J., Feng Y., Liu S. Metagenomic approaches to explore the quorum sensing-mediated interactions between algae and bacteria in sequence membrane photo-bioreactors. *Frontiers in Bioengineering and Biotechnology*, 2022, vol. 10, art. no. 851376 (11 p.). https://doi.org/10.3389/fbioe.2022.851376
71. Zhang C., Li Q., Fu L., Zhou D., Crittenden J. C. Quorum sensing molecules

in activated sludge could trigger microalgae lipid synthesis. *Bioresource Technology*, 2018, vol. 263, pp. 576–582. https://doi.org/10.1016/j.biortech.2018.05.045

72. Zhang S.-J., Du X.-P., Zhu J.-M., Meng C.-X., Zhou J., Zuo P. The complete genome sequence of the algicidal bacterium *Bacillus subtilis* strain JA and the use of quorum sensing to evaluate its antialgal ability. *Biotechnology Reports*, 2020, vol. 25, art. no. e00421 (7 p.). https://doi.org/10.1016/j.btre.2020.e00421
73. Ziesche L., Bruns H., Dogs M., Wolter L., Mann F., Wagner-Döbler I., Brinkhoff T., Schulz S. Homoserine lactones, methyl oligohydroxybutyrates, and other extracellular metabolites of macroalgae-associated bacteria of the *Roseobacter* clade: Identification and functions. *ChemBioChem*, 2015, vol. 16, iss. 14, pp. 2094–2107. https://doi.org/10.1002/cbic.201500189
74. Ćirić A. D., Petrović J. D., Glamočlija J. M., Smiljković M. S., Nikolić M. M., Stojković D. S., Soković M. D. Natural products as biofilm formation antagonists and regulators of quorum sensing functions: A comprehensive review update and future trends. *South African Journal of Botany*, 2019, vol. 120, pp. 65–80. https://doi.org/10.1016/j.sajb.2018.09.010

РОЛЬ ЧУВСТВА КВОРУМА И ИНФОХИМИЧЕСКИХ ВЕЩЕСТВ ВО ВЗАИМОДЕЙСТВИИ ПРО- И МИКРОЭУКАРИОТ В ВОДНЫХ ЭКОСИСТЕМАХ

Э. М. Судакова

Лимнологический институт СО РАН, Иркутск, Российская Федерация
E-mail: *bairamovaelvira@gmail.com*

В обзоре представлены ключевые знания о молекулярных взаимодействиях одноклеточных организмов. Для бактерий характерно чувство кворума (quorum sensing, QS) — способность к регулированию экспрессии генов микроорганизмами в зависимости от плотности клеточной популяции. Это, в частности, может приводить к изменению поведения и к активации факторов вирулентности. У фитопланктона есть аналогичная система: клетки продуцируют инфохимические вещества, которые могут либо повышать устойчивость реципиентов к стрессовым воздействиям, либо запускать в них программируемую гибель. В то время как бактериальные молекулы чувства кворума (quorum sensing molecules, QSM) могут активировать/ингибировать рост клеток фитопланктона, продуцируемые последними инфохимические вещества могут влиять на состав микробного сообщества и подавлять развитие консументов. Кроме того, клетки фитопланктона могут воздействовать на QS бактерий, нарушая активность сигнальных молекул либо имитируя их.

Ключевые слова: чувство кворума, аутоиндукторы, фитопланктон, бактерии, инфохимические вещества

1871
ИнБЮМ – IBSS

Морской биологический журнал
Marine Biological Journal
2025, vol. 10, no. 4, pp. 102–105
https://marine-biology.ru/mbj/article/view/500

UDC 597.31-153(262)

TROPHIC INTERACTIONS BETWEEN THE GIANT DEVIL RAY *MOBULA MOBULAR* AND SHARKS IN SICILIAN WATERS (MEDITERRANEAN SEA)

© 2025 **F. Tiralongo[1,2], G. Torre[2], and A. De Maddalena[3]**

[1]Department of Biological, Geological, and Environmental Sciences, University of Catania, Catania, Italy
[2]Ente Fauna Marina Mediterranea, Avola, Italy
[3]Shark Museum, Simon's Town, Cape Town, South Africa
E-mail: *francesco.tiralongo@unict.it*

Received 24.02.2025; revised 24.02.2025;
accepted 12.08.2025.

We report two cases of trophic interactions between the giant devil ray and sharks in Sicilian waters, Mediterranean Sea. These include a shortfin mako filmed while feeding on a giant devil ray in the Messina Strait in May 2018, and a female giant devil ray stranded in Milazzo in January 2025 showing bite marks likely inflicted by a blue shark.

Keywords: devil fish, giant devil ray, *Mobula mobular*, shortfin mako shark, *Isurus oxyrinchus*, diet, predation, scavenging

The giant devil ray, or devil fish, *Mobula mobular* (Bonnaterre, 1788) belongs to the order Myliobatiformes and the family Mobulidae. Its lozenge-shaped disc is much broader than long, with wide and pointed pectoral fins. The tail is filamentous, with a small dorsal fin and a spine near its base. Prominent fleshy cephalic lobes extend forward on each side of the head [Last, Stevens, 2009]. The mouth is broad and subterminal, with 150–160 rows of minute teeth in each jaw. There are five pairs of gill slits located ventrally. Dorsal surface is brown to bluish-black with a blackish collar across the head; ventral surface is white [Ebert, Dando, 2021]. The giant devil ray is known to inhabit the eastern Atlantic and the Mediterranean Sea, but it may have a circumglobal distribution in temperate and tropical waters [FishBase, 2024]. It is pelagic, coastal, and oceanic, occurring at a depth range from 0 to 700 m [Canese et al., 2011; Weigmann, 2016]. The embryonic development of this species is aplacental viviparous, with a gestation period of up to 25 months and litter size of 1–2 young [Ebert, Dando, 2021]. Its disc width at birth is 90–160 cm, and the disc can attain a maximum size of 320 cm [Ebert, Dando, 2021]. It feeds on planktonic crustaceans and small schooling fishes, filtering water over its gill filter-plates [McEachran, Capapé, 1984].

In the present article, we report two cases of trophic interactions between giant devil rays and sharks in Sicilian waters, Italy, central Mediterranean Sea.

MATERIAL AND METHODS

In May 2018, a video documenting a juvenile shortfin mako shark *Isurus oxyrinchus* Rafinesque, 1809, swimming with a giant devil ray in its mouth, was filmed in the Messina Strait, Italy. The 1 min and 13 s video was filmed by Giuseppe Morabito from the feluca "Felicia II," a traditional fishing boat used to catch swordfish. The shark can be seen holding the head of the giant devil ray in its mouth while swimming calmly at the water surface. The giant devil ray is apparently dead: it is turned upside down, and has the apex of its right pectoral fin removed by an apparent bite of the shark (Fig. 1).



Fig. 1. Juvenile shortfin mako shark *Isurus oxyrinchus* with a giant devil ray *Mobula mobular* in its mouth, observed in the Messina Strait, Italy, in May 2018. Photo from a video by Giuseppe Morabito

On 3 January, 2025, a stranded female giant devil ray was found recently deceased on a beach in Milazzo, approximately 30 km west of the Messina Strait, Italy (N38.23095°, E15.24882°). The estimated width of the disc was 2.6 m. The ray was tied with a rope, probably by some fishermen. The right pectoral fin of the ray bore at least two shark bites. The injury had an overall length of about 30 cm (Figs 2–4). Pictures of the giant devil ray and a tissue sample were taken by the second author.



Fig. 2. Female giant devil ray *Mobula mobular* found dead on a beach in Milazzo, Italy, on 3 January, 2025. Photo by Giancarlo Torre



Fig. 3. Ventral view of the giant devil ray *Mobula mobular* found dead on a beach in Milazzo, Italy, on 3 January, 2025. The right pectoral fin of the ray bears at least two shark bites. Photo by Giancarlo Torre



Fig. 4. Close-up of the shark bites on the giant devil ray *Mobula mobular* found dead on a beach in Milazzo, Italy, on 3 January, 2025. Photo by Giancarlo Torre

RESULTS AND DISCUSSION

Concerning the case of the shortfin mako observed carrying a giant devil ray in its mouth in the Messina Strait, it is unclear if it was a case of predation or scavenging. The shark may have caught and killed the ray, or it may have simply found the ray after it had been caught by fishermen and discarded at sea. It is also possible that the shark found the ray when it was hooked, still alive or already dead.

Concerning the case of the giant devil ray stranded in Milazzo, it seems reasonable to conclude that the ray was first caught on a longline hook or in a net. At that stage, a shark found the ray, still alive or more likely already dead, and bit off part of the ray's pectoral fin. Then, the fishermen found the ray and brought it on board the fishing vessel by tying a rope around its damaged pectoral fin. The fishermen may have brought the ray to the beach, or they may have thrown it back into the sea, at which point the waves would have washed it ashore.

Examination of the shark bites on the giant devil ray reveals that on the ventral surface, the cut is clean and sharp, while on the dorsal surface, it is more irregular, with some clean cuts but also tears and punctures. Therefore, teeth of the upper jaw of the shark must have been different from those of the lower jaw.

The very clean cuts on the ventral surface suggest the upper teeth of a blue shark *Prionace glauca* (Linnaeus, 1758), and the more irregular ones on the dorsal surface could be compatible with the lower teeth of the same species. However, the identification of the shark species responsible cannot be confirmed.

Conclusions. To the best of our knowledge, the two cases reported in this article are the first ones reported in the scientific literature of trophic interactions between the giant devil ray and sharks. Moreover, while it is known that the shortfin mako can feed on rays [De Maddalena et al., 2005], the case recorded in the Messina Strait in May 2018 is the first observation of *Isurus oxyrinchus* feeding on a species of the family Mobulidae.

Acknowledgement. The authors wish to thank Eric Glenn Haenni for taking the time to edit the manuscript. Alessandro De Maddalena thanks Alessandra, Antonio, and Phoebe for their support and love.

REFERENCES

1. Canese S., Cardinali A., Romeo T., Giusti M., Salvati E., Angiolillo M., Greco S. Diving behavior of the giant devil ray in the Mediterranean Sea. *Endangered Species Research*, 2011, vol. 14, pp. 171–176. https://doi.org/10.3354/esr00349
2. De Maddalena A., Preti A., Smith R. *Mako Sharks.* Malabar : Krieger Publishing, 2005, 72 p.
3. Ebert D. A., Dando M. *Field Guide to Sharks, Rays & Chimaeras of Europe and the Mediterranean.* Princeton : Princeton University Press, 2021, 384 p. https://doi.org/10.2307/j.ctv12sdwkk
4. *FishBase.* World Wide Web electronic publication, version 07/2024 / R. Froese, D. Pauly (Eds) : [site], 2024. URL: https://fishbase.org/ [accessed: 01.02.2025].
5. Last P. R., Stevens J. D. *Sharks and Rays of Australia.* 2nd edition. Collingwood : CSIRO, 2009, 644 p.
6. McEachran J. D., Capapé C. Mobulidae. In: *Fishes of the North-eastern Atlantic and the Mediterranean*. Vol. 1 / P. J. P. Whitehead, M. L. Bauchot, J. C. Hureau, J. Nielsen, E. Tortonese (Eds). Paris : UNESCO, 1984, pp. 210–211.
7. Weigmann S. Annotated checklist of the living sharks, batoids and chimaeras (Chondrichthyes) of the world, with a focus on biogeographical diversity. *Journal of Fish Biology*, 2016, vol. 88, iss. 3, pp. 837–1037. https://doi.org/10.1111/jfb.12874

ТРОФИЧЕСКИЕ ВЗАИМОДЕЙСТВИЯ МЕЖДУ СРЕДИЗЕМНОМОРСКИМ РОГАЧОМ *MOBULA MOBULAR* И АКУЛАМИ В ВОДАХ СИЦИЛИИ (СРЕДИЗЕМНОЕ МОРЕ)

Ф. Тиралонго[1,2], Дж. Торре[2], А. Де Маддалена[3]

[1]Катанийский университет, Катания, Италия
[2]Управление морской фауны Средиземноморья, Авола, Италия
[3]Музей акул, Саймонс-Таун, Кейптаун, Южная Африка
E-mail: *francesco.tiralongo@unict.it*

Сообщается о двух случаях трофических взаимодействий между средиземноморским рогачом и акулами в Средиземном море. Приведена фотография акулы-мако во время поедания ею средиземноморского рогача в Мессинском проливе в мае 2018 г. На теле самки средиземноморского рогача, выброшенной на берег в Милаццо в январе 2025 г., видны следы укусов, вероятно нанесённые синей акулой.

Ключевые слова: средиземноморская мобула, средиземноморский рогач, *Mobula mobular*, акула-мако, *Isurus oxyrinchus*, рацион, хищничество, питание падалью

1871
ИнБЮМ – IBSS

Морской биологический журнал
Marine Biological Journal
2025, vol. 10, no. 4, pp. 106–112
https://marine-biology.ru/mbj/article/view/497

UDC 594.124-19

EXPANSION OF THE RANGE OF A NEW INVASIVE SPECIES, *MYTILUS GALLOPROVINCIALIS* (BIVALVIA: MYTILIDAE), IN THE CASPIAN SEA

© 2025 **M. Khlopkova, R. Barkhalov, and E. Lobachev**

Precaspian Institute of Biological Resources of the Dagestan Federal Research Centre of RAS,
Makhachkala, Russian Federation
E-mail: *hlopkovam@mail.ru*

Received 28.01.2025; revised 17.04.2025;
accepted 12.08.2025.

The article reports the finding of an invasive species: a bivalve, atypical for the native fauna of the Dagestan coast of the Middle Caspian. Based on conchiological features, this species was identified as *Mytilus galloprovincialis* (Lamarck, 1819). In the autumn of 2024, single living individuals of this new invasive species were recorded on the Dagestan coast of the Middle Caspian near the Samur River mouth and in the Karaman-7 area. In the winter of 2025, those were registered in the Dagestanskie Ogni beach vicinity. In March 2025, 29 mussel shells were found in storm surges on the coast, near the border of Dagestan and Azerbaijan. Most likely, the invader entered the Caspian Sea from the Sea of Azov–Black Sea basin *via* the Volga–Don Canal with ballast waters. Further monitoring of invasions of new molluscs on the Dagestan coast of the Russian sector of the Caspian Sea is needed.

Keywords: invasive species, mussel, Dagestan coast, Russian sector of the Caspian Sea

To date, the registered Caspian Sea fauna covers 34 bivalve species [Identification Keys, 2013, Wesselingh et al., 2019].

Adaptation and naturalization of invasive hydrobionts often occur against the backdrop of destabilization of local fauna populations. Therefore, forecasting the consequences of unwanted invasions is currently one of the pressing problems for researchers of the Caspian Sea.

In recent decades, cargo transportation from the Sea of Azov–Black Sea basin along the Volga–Don Canal to the Makhachkala commercial port has intensified significantly in the Dagestan region of the Caspian Sea [Rossiya, 2025]. The active exploitation of the northern invasion corridor contributed to a rise in the influx of invaders into the Caspian Sea basin. Thus, within a short period of time (2013 to 2024), phytoplankton representatives [dinophytes *Ceratium tripos* var. *balticum*], bivalves [*Corbicula fluminalis* (O. F. Müller, 1774) and *C. fluminea* (O. F. Müller, 1774)], a crustacean [the oriental river prawn *Macrobrachium nipponense* (De Haan, 1849)], a North American polychaete of the genus *Marenzelleria* (Mesnil, 1896)], and fish [*Pseudorasbora parva* (Temminck et Schlegel, 1846) and *Hemiculter leucisculus* (Basilewsky, 1855)] penetrated the Dagestan region of the Caspian Sea and successfully acclimatized there [Khlopkova et al., 2023].

Mytilus galloprovincialis (Lamarck, 1819) quickly colonizes new water bodies, and this fact is a typical example of a mollusc distribution after an accidental anthropogenic invasion into different areas of the World Ocean and the formation of a range in Asia, North America, South Africa, and Europe. Until recently, this mussel inhabited only the areas of the Black Sea, Sea of Azov, and Sea of Japan. With the development of sea and river transport, the range of this mollusc has expanded significantly [Lutaenko, Kolpakov, 2016; Minakova et al., 2024; Shamionova, 2023].

MATERIAL AND METHODS

During seasonal hydrobiological surveys (September 2024 to March 2025) focused on benthos, large molluscs were found, previously not recorded on the Dagestan coast of the Caspian Sea (Fig. 1).

Laboratory processing was performed by generally accepted methods [Metody izucheniya, 1990]. Molluscs were identified down to the species level based on their main conchiological features. The length (L), height (H), and convexity of two valves (D) were measured with a caliper, with an accuracy of 0.1 mm. To characterize the shape of the shell, the coefficients of elongation (H/L) and convexity (D/H) were calculated.



Fig. 1. Schematic map of the first findings of *Mytilus galloprovincialis* in the Caspian Sea. The red arrows indicate the spots where invasive mussels were registered on the Dagestan coast of the Caspian Sea in September–October 2024 and February–March 2025 (authors' data). The triangles indicate the spots where mussels were recorded in May–August 2023 [Minakova et al., 2024; Shamionova, 2023]

The individual age of mussels was estimated by growth retardation rings (growth marks) on the shell surface and by the corresponding dark concentric areas (those are clearly visible in thin-valved mytilids when a valve is viewed through the light), as well as by marks on muscle imprints – in accordance with common methods [Selin, Lysenko, 2006; Zolotarev, 1989].

RESULTS AND DISCUSSION

The specimens we found in 2024 were identified as *M. galloprovincialis*. The invasive mollusc differs (Fig. 2) in the general shell habitus from a mytilid *Mytilaster lineatus* (Gmelin, 1791) which settled in the Caspian Sea back in the 1920s. Both the mussel and the mytilaster are characterized by a thin-walled (fragile) equal-valve unequal-sided shell with an apex located terminally. The valves are connected at the dorsal part by an external ligament [Metody izucheniya, 1990; Mitilidy Chernogo morya, 1990]. Yearlings of the above-mentioned species, up to 10 mm in size, are poorly distinguishable.

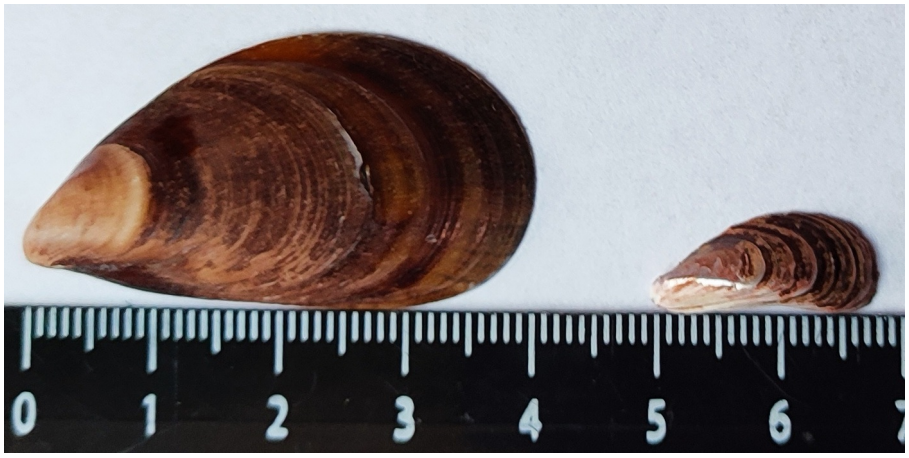


Fig. 2. *Mytilus galloprovincialis* and *Mytilaster lineatus*, invasive species of the Dagestan coast of the Caspian Sea

The differences between these two species are observed primarily when comparing the shell sizes of large specimens. Specifically, the shell length of juveniles we recorded ranged 13 to 42 mm (adult mussels grow up to 100–140 mm). Importantly, in the Caspian Sea, the mytilaster grows only up to 15–20 mm (in the Black Sea, up to 25 mm) [Aligadzhiev, Osmanov, 2023; Mitilidy Chernogo morya, 1990; Zevina, 1972].

The mussel shell is quadrangular-wedge-shaped, while the mytilaster shell is wedge-shaped: triangular to irregularly quadrangular [Mitilidy Chernogo morya, 1990]. *M. galloprovincialis* shell is more flattened and wider (H/L is 0.56–0.67; D/L is 0.46–0.58). *M. lineatus* shell, compared to the mussel one, is strongly elongated (H/L is 0.4–0.55) and more convex (D/L is 0.97–1.0).

In the mussel, the keel is weakly expressed. In the mytilaster, the keel bend is well expressed (see Fig. 2); it separates the wide dorsal area from the narrow ventral one (flat or concave). The mussel periostracum is black-blue (in surf specimens) or reddish-brown (in silt specimens). The mytilaster periostracum is brown-lilac. The nacreous layer of the mussel endostracum is thin, with a blue tint; sometimes, it is undeveloped. The mytilaster has a more developed and durable nacreous layer, with a lilac tint.

The hinge area of *M. galloprovincialis* is significantly reduced. It is represented by several small tooth-like tubercles (up to 7) under the apex on the ventral edge. In *M. lineatus*, the hinge teeth are located on the dorsal edge [Mitilidy Chernogo morya, 1990].

During autumn surveys, the first single specimens of the new invader were recorded in two samples from different coastal areas. In September 2024, on the Samur River coast, not far from the border with Azerbaijan, a single mussel was noted in a sample from a *Dreissena polymorpha andrusovi* (Pallas, 1771) biocenosis. The coordinates of the site of this finding are N41.5524°, E48.2905°. The salinity there is 7‰. The sediment in the sampling area is mostly silted sand. Sizes of the mussel shell were as follows: L = 32 mm; H = 20 mm; and D = 14 mm. The age of the mollusc was about a year. Another specimen was registered in October in the Karaman-7 area (N43.0651°, E47.2818°). The salinity there is 7‰. Sizes of the mussel shell were as follows: L = 38 mm; H = 22 mm; and D = 18 mm. The age of the specimen was two years. The periostracum was reddish-brown.

In February 2025, 2 ind. were found on a beach near the Dagestanskie Ogni village. Sizes of the larger mussel shell were as follows: L = 37 mm; H = 21.5 mm; and D = 15 mm. The periostracum was brown.

During spring surveys (March 2025), near the border with Azerbaijan, in storm-washed mytilaster shells, 29 mussel shells were recorded, with the length ranging 24 to 40 mm and with fresh ligament (Fig. 2).

Previously, in the spring and summer of 2023, this invasive mussel was already noted on the Azerbaijan coast of the Caspian Sea [Shamionova, 2023]. At the same time, a new species was reported from the border of the Northern and Middle Caspian by researchers from the Volga–Caspian branch of the VNIRO (CaspNIRKh). They confirmed the reliability of the morphological identification by molecular genetic methods [Minakova et al., 2024].

M. galloprovincialis is a common inhabitant of the Black Sea; at a salinity of 13–22‰, shells of this mollusc are characterized by noticeable annual growth rates. One of the reasons for the small size of the mussels we found may be the low salinity in the surveyed sites: 7‰ (at the lower end of their tolerant range). At 13‰, in the Kazakh Bay, the largest individuals for the Caspian Sea were registered [Minakova et al., 2024].

The distribution of the Black Sea mussel in the Caspian Sea will be driven primarily by such factors, as the salinity range, features of sediments, and competition with fouling organisms: both native species (*Dreissena*) and invaders (*Mytilaster* and *Balanus* representatives).

Thus, the acclimatization of the mytilaster in the Caspian Sea occurred under conditions of fierce competition with the native species of the genus *Dreissena* (as a result, two ones, *Dreissena caspia* and *D. elata*, were completely displaced and became extinct). At the intersections of their ranges, strained biotic relationships are observed: those include competition for food and substrate. Closer to a shore, the mytilaster predominates, while deeper, *Dreissena* representatives prevail [Aligadzhiev, Osmanov, 2023]. Most likely, a similar pattern of competitive relations should be expected, first of all, with the mytilaster (a representative of the same family).

The mytilaster cannot spread north of Makhachkala (into the zone of silty sediments). Researchers report occurrence of this mollusc on silted sands and its absence on silts [Aligadzhiev, Osmanov, 2023]. Usually, the Black Sea mussels are foulers of hard substrates, but they can inhabit silty sediments as well attaching to empty shells of dead molluscs. This provides some advantage in competitive relations.

High fertility and rapid maturation in the absence of natural enemies can also mediate quick and successful acclimatization of the Black Sea mussels in the Caspian Sea. For the Caspian Sea mytilaster, the fertility value is 0.02–0.14 million eggs *per* year. The fertility of the mussel is higher: 0.2–10 million eggs *per* each clutch. The lifespan of the mytilaster is 2–4 years. The mussel lives longer, 6–9 years, and matures early, in 6–8 months (or when its shell length reaches 18–28 mm). Interestingly, this hydrobiont produces more and more eggs with age [Biologiya, 1989; Mitilidy Chernogo morya, 1990; Zolotarev, 1989].

Under conditions of climate change and due to the absence of natural predators (the rapa whelk, starfish, rays, and cod), the mussel can successfully and quickly acclimatize in new biotopes of the Caspian Sea.

Meanwhile, the consequences of the invasion of this species can also be negative. Fouling molluscs attach to a hard substrate with a byssus and form druses. In the Caspian Sea, a rapid rise in biomass of fouling organisms (along with that of barnacles, the mytilaster, and *Dreissena* species) may result in failures of hydraulic structures of the oil industry [Minakova et al., 2024; Shamionova, 2023].

Conclusions. An expansion of the *Mytilus galloprovincialis* range was established, as indicated by the displacement of sites where this new invader is found. The records of different-aged individuals provide evidence for the beginning of the formation of the mollusc population. Naturalization of this invader may govern the displacement of endemic species (*Didacna* and *Dreissena* representatives) and the ones that invaded earlier (*Abra* and *Mytilaster* ones) in the Caspian Sea while competing for habitat and food. This will result in a simplification of the biocenosis structure and a decrease in its resistance to external factors. To assess the consequences (those can be positive, neutral, or negative), regular monitoring of invasions of new molluscs on the Dagestan coast of the Russian sector of the Caspian Sea is required.

The work was carried out within the framework of the state research assignment of the Precaspian Institute of Biological Resources of the Dagestan Federal Research Centre of RAS "The current state of the structure of commercial fish populations and their food objects under the effect of Sea of Azov–Black Sea invaders on ecosystem formation in the western Caspian basin" (No. 125020501448-8).

REFERENCES

1. Aligadzhiev M. M., Osmanov M. M. Distribution and some ecological and biological characteristics of *Mytilaster lineatus* Gmelin, 1789 of the middle Caspian Sea. *Vestnik Dagestanskogo nauchnogo tsentra RAN*, 2023, no. 88, pp. 6–11. (in Russ.). https://elibrary.ru/qhuiin
2. *Biologiya kul'tiviruemykh midii* / V. V. Murina (Ed.) ; AN USSR, Institut biologii yuzhnykh morei imeni A. O. Kovalevskogo. Kyiv : Naukova dumka, 1989, 100 p. (in Russ.). https://repository.marine-research.ru/handle/299011/1398
3. Zevina G. B. *Obrastaniya v moryakh SSSR* / G. M. Belyaev (Ed.). Moscow : Izd-vo Mosk. un-ta, 1972, 214 p. (in Russ.)
4. Zolotarev V. N. *Sklerokhronologiya morskikh dvustvorchatykh mollyuskov* / AN USSR, Institut biologii yuzhnykh morei imeni A. O. Kovalevskogo. Kyiv : Naukova dumka, 1989, 112 p. (in Russ.)
5. Lutaenko K. A., Kolpakov E. V. The extension

of the distributional range of an invasive mussel, *Mytilus galloprovincialis* (Bivalvia: Mytilidae) in the Sea of Japan. *Byulleten' Dal'nevostochnogo malakologicheskogo obshchestva*, 2016, vol. 20, no. 1, pp. 57–76. (in Russ.). https://elibrary.ru/whgoyb

6. *Metody izucheniya dvustvorchatykh mollyuskov* / G. L. Shkorbatov, Ya. I. Starobogatov (Eds). Leningrad : Zoologicheskii institut, 1990, 208 p. (Trudy Zoologicheskogo instituta AN SSSR ; vol. 219). (in Russ.)
7. Minakova E. V., Zhatkina O. V., Kashin R. D., Mikhailova A. V., Kozlova N. V., Tikhonova E. Yu. On introduction of Black Sea mussel *Mytilus galloprovincialis* (Lamarck, 1819) to the Caspian Sea basin. *Izvestiya TINRO*, 2024, vol. 204, no. 3, pp. 602–608. (in Russ.). https://doi.org/10.26428/1606-9919-2024-204-602-608
8. *Mitilidy Chernogo morya* / V. E. Zaika (Ed.) ; AN USSR, Institut biologii yuzhnykh morei imeni A. O. Kovalevskogo. Kyiv : Naukova dumka, 1990, 208 p. (in Russ.). https://repository.marine-research.ru/handle/299011/1459
9. *Identification Keys for Fish and Invertebrates.* Vol. 1. *Fish and Molluscs* / N. G. Bogutskaya, P. V. Kijashko, A. M. Naseka, M. I. Orlova. Saint Petersburg ; Moscow : KMK Scientific Press Ltd., 2013, 543 p. (in Russ.). https://elibrary.ru/uaeplj
10. Rossiya vplotnuyu zanyalas' transportnym koridorom "Sever – Yug". In: *Nezavisimaya gazeta* : [site]. (in Russ.). URL: https://www.ng.ru/economics/2024-11-11/1_9132_sanctions.html [accessed: 11.04.2025].
11. Selin N. I., Lysenko V. N. Size and age composition of populations and growth of *Mytilus trossulus* (Bivalvia: Mytilidae) in the subtidal area of Western Kamchatka. *Biologiya morya*, 2006, vol. 32, no. 6, pp. 421–427. (in Russ.). https://elibrary.ru/hzjksf
12. Khlopkova M. V., Barkhalov R. M., Guseynov K. M., Gasanova A. Sh., Zurkhaeva U. D. Invasions of new morphotypes of *Corbicula fluminalis* and *Corbicula fluminea* (Bivalvia: Corbiculidae) to the basin of the Dagestan region of the Caspian Sea. *Rossiiskii zhurnal biologicheskikh invazii*, 2023, vol. 16, no. 1, pp. 166–179. (in Russ.). https://doi.org/10.35885/1996-1499-16-1-166-179
13. Shamionova N. S. Ozhidaemye posledstviya vseleniya midii *Mytilus galloprovincialis* Lamarck, 1819 (Bivalvia: Mytilida) v Kaspiiskoe more. *Vestnik nauki i tvorchestva*, 2023, no. 6 (88), pp. 34–38. (in Russ.). https://elibrary.ru/ebmokn
14. Wesselingh F. P., Neubauer T. A., Anistratenko V. V., Vinarski M. V., Yanina T., ter Poorten J. J., Kijashko P., Albrecht C., Anistratenko O. Yu., D'Hont A., Frolov P., Gándara A. M., Gittenberger A., Gogaladze A., Karpinsky M., Lattuada M, Popa L., Sands A. F., van de Velde S., Vandendorpe J., Wilke T. Mollusc species from the Pontocaspian region – an expert opinion list. *ZooKeys*, 2019, iss. 827, pp. 31–124. https://doi.org/10.3897/zookeys.827.31365

РАСШИРЕНИЕ АРЕАЛА НОВОГО ВСЕЛЕНЦА, *MYTILUS GALLOPROVINCIALIS* (BIVALVIA: MYTILIDAE), В КАСПИЙСКОМ МОРЕ

М. В. Хлопкова, Р. М. Бархалов, Е. Н. Лобачев

Прикаспийский институт биологических ресурсов
Дагестанского федерального исследовательского центра РАН, Махачкала, Российская Федерация
E-mail: *hlopkovam@mail.ru*

В статье сообщается об обнаружении нетипичного для нативной фауны дагестанского побережья Среднего Каспия вида — двустворчатого моллюска, идентифицированного на основе конхиологических признаков как *Mytilus galloprovincialis* (Lamarck, 1819). На дагестанском побережье Среднего Каспия единичные живые особи нового инвазивного вида зарегистрированы осенью 2024 г. вблизи устья реки Самур и в районе Карамана-7, а также зимой 2025 г. в районе пляжа Дагестанские Огни. В марте 2025 г. обнаружено 29 раковин мидий в штормовых выбросах на побережье, вблизи границы Дагестана и Азербайджана. Вероятнее всего, вселенец проник в Каспийское море из Азово-Черноморского бассейна через Волго-Донской канал с балластными водами. Необходим дальнейший мониторинг инвазий новых моллюсков на дагестанском побережье российского сектора Каспийского моря.

Ключевые слова: инвазивный вид, мидия, дагестанское побережье, российский сектор Каспийского моря

1871
ИнБЮМ – IBSS

Морской биологический журнал
Marine Biological Journal
2025, vol. 10, no. 4, pp. 113–122
https://marine-biology.ru/mbj/article/view/507

UDC 582.261.1-152.644(262.54)

ANNOTATED LIST OF EPIPHYTIC DIATOMS FROM MACROPHYTES OF THE AQUATIC-ROCK COMPLEX KAZANTIP CAPE (THE CRIMEA, SEA OF AZOV)

© 2025 **A. Shiroyan, A. Bondarenko, and L. Ryabushko**

A. O. Kovalevsky Institute of Biology of the Southern Seas of RAS, Sevastopol, Russian Federation
E-mail: *arminka_shir@mail.ru*

Received 19.11.2024; revised 23.01.2025;
accepted 12.08.2025.

The paper is the first one to summarize original data on the diatom species composition for 129 samples of 14 macrophyte species from the upper sublittoral of the aquatic-rock complex Kazantip Cape (the Sea of Azov). The sampling was carried out in 2022–2023 at depths of 0.1–1.0 m at a temperature of +3.7…+29.0 °C and water salinity of 13.6–15.6 g·L^{-1}. The annotated list covers 98 Bacillariophyta species and intraspecific taxa from 3 classes, 21 orders, 27 families, and 45 genera. Data on their sizes, occurrence, ecological and phytogeographic characteristics, abundance, and biomass are provided. High species diversity of diatoms was noted for the class Bacillariophyceae (72 taxa) and for three genera: *Nitzschia* (12 species), *Navicula* (11), and *Licmophora* (6). The highest number of diatom species was recorded on thalli of a green alga *Ulva linza* (61 species), red alga *Carradoriella denudata* (45), and brown alga *Ericaria crinita* (40), as well as in epiphyton of the seagrass *Zostera marina* (37) and its association with *Zannichellia palustris* subsp. *major* (35). The lowest number of species was revealed for epiphyton of a red alga *Pyropia leucosticta* (9). A benthic diatom *Berkeleya scopulorum* was found in the Sea of Azov for the first time. In epiphytic communities, benthic (83%), marine (51%), and cosmopolitan species (35%) predominate. In total, 30 colonial species were identified. Out of them, the following diatoms occur year-round: *Achnanthes brevipes*, *Berkelya rutilans*, *Grammatophora marina*, *Melosira moniliformis*, *Navicula ramosissima*, *Rhoicosphenia marina*, and *Tabularia tabulata*. Cosmopolitan species *Cocconeis scutellum*, *Gr. marina*, *Licmophora abbreviata*, *Rh. marina*, and *T. tabulata* dominate in abundance. We recorded 11 species capable of causing water blooms and 45 serving as indicators of saprobity of water organic pollution.

Keywords: diatoms, macrophytes, epiphyton, aquatic-rock complex Kazantip Cape, Sea of Azov

The coastal zone of the Kazantip Cape has long attracted the attention of algologists as an area with high biodiversity and minimum anthropogenic impact. Since the mid-20th century, aquatic macroflora has been periodically studied there, and annotated lists of macroalgae, aquatic flowering plants, and benthic cyanobacteria have been compiled and updated [Belich et al., 2019; Gromov, 1999; Maslov, 2004; Sadogurskaya, 2001; Sadogurskaya et al., 2006]. The surveys of this zone are important given the conservation status of terrestrial sites and coastal waters within the aquatic-rock complex Kazantip Cape [Litvinyuk, 2016].

In 2005–2010, the species composition and quantitative characteristics of benthic microalgae from various ecotopes of the Crimean coast of the Sea of Azov, including the Kazantip Nature Reserve and the cape water area, were studied [Bondarenko, 2017; Bondarenko, Ryabushko, 2010; Bondarenko et al., 2018; Ryabushko, Bondarenko, 2016]. In the shallow Sea of Azov, the interaction between benthic and pelagic zones is especially noticeable; planktonic and benthic microalgae represent a single ecological and floristic species complex there. At the initial stage of the survey, in order to clarify the species list, a search of literature sources was carried out (summaries, species guidelines, reference books, serials, abstracts, algal database, and also our own data) for the inventory and revision of the taxonomic composition of planktonic and benthic microalgae of the Sea of Azov as a whole [Ryabushko, Bondarenko, 2011]. As a result, a checklist of 1,060 taxa comprising 9 divisions was compiled, with a predominance of Bacillariophyta (538 taxa). In plankton, 621 taxa were revealed, and in benthos, 370; 69 taxa were common to the two biotopes. From the presented data, a lag in the study of microphytobenthos is evident.

Diatoms are known to be the key group of marine microphytobenthos in terms of their diversity and abundance. These microalgae feature high primary productivity and make a significant contribution to the formation of biodiversity in the benthic community. Along with other benthic organisms, diatoms are sensitive to environmental changes: fluctuations in water temperature, its salinity, and pollution with toxicants. These microalgae can be used as indicators of the quality of their habitat when assessing the environmental situation, *inter alia* in protected areas [Barinova et al., 2019b; Ryabushko, 2013].

In seas, diatoms inhabit all natural and artificial substrates. However, according to many authors, macrophytes are a preferred substrate for colonization by microalgae [Bondarenko, 2017; Korotkevich, 1960; Lee et al., 1975; Nikolaev, 1970; Ryabushko, 2013; Shiroyan, 2022; Siqueiros-Beltrones, Hernández-Almeida, 2006]. Therefore, in 2022–2023, we expanded our research on diatoms in the epiphyton of aquatic vegetation in the coastal waters of the Kazantip Cape. The study of the epiphyton of 11 macroalgal species allowed revealing 97 taxa of Bacillariophyta; out of those, 51 species were recorded in the area for the first time. Moreover, dominant species were identified, the qualitative and quantitative composition was analyzed, and also the structure of diatom communities depending on the season and the species of colonized macroalgae was surveyed [Bondarenko et al., 2024].

When we finished processing the material from the one-year studies, information on diatoms of the epiphyton of other macrophytes was added to the previously published results [Bondarenko et al., 2024]. Also, comprehensive data on the ecological, phytogeographic, and quantitative characteristics of diatoms were accumulated. Generalized information of this kind is valuable for understanding the ecology of species and the environmental effects on the formation of microphytobenthic communities. Moreover, such material is helpful when compiling databases covering information on microalgal habitats, ranges, morphological traits, *etc.* In addition, revealing the trends in the qualitative and quantitative distribution of diatoms in benthic macrophyte communities, especially in coastal ecosystems, is required to establish general patterns of interaction between diatoms, macrophytes, and their habitat.

The aim of this work is to summarize the original results of studying the species composition and autecology of diatoms of macrophyte epiphyton of the coastal waters of Kazantip Cape in order to compile an annotated list covering data on diatom dimensions, their occurrence, ecological and phytogeographic characteristics, abundance, and biomass.

MATERIAL AND METHODS

The material for the summarization was 129 samples of epiphyton of 12 macroalgal species:

- brown algae – *Ericaria crinita* (Duby) Molinari et Guiry, 2020, *Gongolaria barbata* (Stackhouse) Kuntze, 1891, and *Cladosiphon mediterraneus* Kützing, 1843;
- red algae – *Callithamnion corymbosum* (Smith) Lyngbye, 1819, *Ceramium arborescens* J. Agardh, 1894, *Pyropia leucosticta* (Thuret) Neefus et J. Brodie, 2011, and *Carradoriella denudata* (Dillwyn) Savoie et G. W. Saunders, 2018;
- green algae – *Bryopsis hypnoides* J. V. Lamouroux, 1809, *Cladophora liniformis* Kützing, 1849, *Cl. sericea* (Hudson) Kützing, 1843, *Ulva intestinalis* Linnaeus, 1753, and *U. linza* Linnaeus, 1753;

and also, the seagrass *Zostera marina* Linnaeus, 1753 alone and in its association with another flowering plant, *Zannichellia palustris* subsp. *major* (Hartman) Ooststroom et Reichgelt, 1964.

Sampling was carried out from October 2022 to September 2023 in the upper sublittoral zone of four bays of the Kazantip Cape (the Sea of Azov): the Shirokaya and Kunushkay (both within the Kazantip Nature Reserve area), Russkaya, and Tatarskaya (Fig. 1).

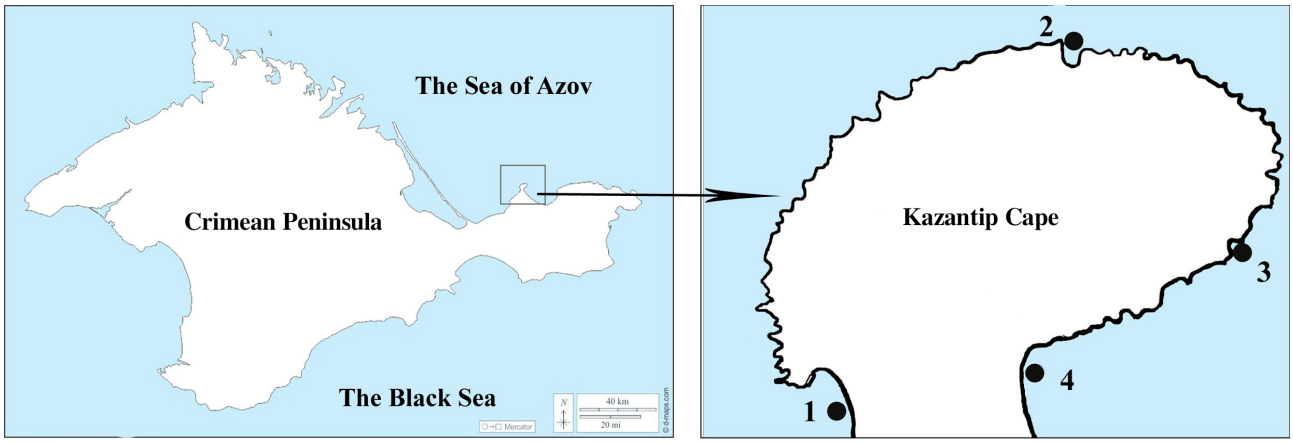


Fig. 1. Sites of the algological sampling in the Kazantip Cape area: 1, the Russkaya Bay; 2, the Shirokaya Bay; 3, the Kunushkay Bay; 4, the Tatarskaya Bay

Sampling was carried out at depths of 0.1–1.0 m and at temperatures from +3.7 to +29.0 °C. Water salinity varied from 13.6 to 15.6 g·L^{-1} (Table 1).

Table 1. Hydrological conditions of epiphyton sampling in various months of 2022–2023 in the Kazantip Cape bays (the Sea of Azov)

Parameter	2022		2023								
	13.10	29.11	31.01	28.02	29.03	25.04	31.05	22.06	27.07	29.08	25.09
Depth, m	0.5	0.2	0.5	0.2	0.5	0.2	0.5	0.1–1	0.1–1	0.1	0.1–0.5
Temperature, °C	+17.0	+10.0	+3.7	+4.9	+8.1	+14.0	+19.2	+26.2	+27.3	+29.0	+23.9
Salinity, g·L^{-1}	15.0	15.6	15.0	15.6	15.1	15.0	14.9	14.9	13.6	13.6	15.0

In the study area, samples occasionally contained various macroalgal species floating freely at the water's surface; their thalli were tightly intertwined. These samples were used only for qualitative analysis of the diatom composition.

For taxonomic identification, aqueous and permanent preparations were used. Diatom valves were cleaned by a standard acid-based technique [The Diatoms of the USSR, 1974]. After washing, frustules were embedded in Naphrax LTD resin (refractive index was 1.74). Living cells and frustules were studied under an Axioskop 40 light microscope (Carl Zeiss, Germany) at magnifications of 10 × 20 and 10 × 40, with a ×100 objective, and with immersion oil added (Carl Zeiss) (refractive index n_e = 1.518). Also, frustules were examined under a Hitachi SU3500 scanning electron microscope (Japan).

When analyzing the taxonomic structure of diatoms, we mostly used the system developed by F. Round *et al.* [1990], with amendments and additions of new data [AlgaeBase, 2025; Ryabushko, 2013; Ryabushko, Begun, 2015, 2016]. The taxonomic affiliation was determined based on literature sources [Diatomovyi analiz, 1950; Guslyakov et al., 1992; Kuylenstierna, 1989, 1990; Ryabushko, 2013; Ryabushko, Begun, 2015, 2016; Smith, 1853; Witkowski et al., 2000]. The ecological and phytogeographic characteristics of diatoms were analyzed using a number of publications [AlgaeBase, 2025; Barinova et al., 2019a, b; Bondarenko et al., 2024; Guslyakov et al., 1992; Ryabushko, 2013; Ryabushko, Begun, 2016; Sládeček, 1986]. Quantitative characteristics of diatoms (abundance and biomass) were determined according to the method [Ryabushko, 2013].

RESULTS AND DISCUSSION

As a result of the study of the diatom biodiversity in the epiphyton of coastal macrophyte thickets in the Kazantip Cape water area in 2022–2023, an annotated list was compiled; it includes 98 species and intraspecific taxa from 3 classes, 21 orders, 27 families, and 45 genera and provides the description of their taxonomic affiliation. For the first time, autecology data are presented for each taxon, including phytogeographic and quantitative characteristics (see Supplement: https://marine-biology.ru/mbj/article/view/507).

Two genera, *Nitzschia* and *Navicula*, are characterized by high taxonomic diversity (12 and 11 species accordingly). *Licmophora* is less represented (6 species). This genus is followed by *Amphora*, *Diploneis*, *Lyrella*, and *Melosira* (4 species each). Frequently encountered species were identified: *Achnanthes brevipes*, *Berkeleya rutilans*, *Cocconeis scutellum*, *Cylindrotheca closterium*, *Grammatophora marina*, *Licmophora abbreviata*, *Navicula cancellata*, *N. ramosissima*, *Nitzschia sigma*, *N. sigmoidea*, *Rhoicosphenia marina*, *Tabularia tabulata*, and *Trachyneis aspera*. Several species were found singly: *Amphora laevis*, *Grammatophora angulosa*, *Licmophora rostrata*, *Lyrella lyra*, *L. lyroides*, *Navicula cancellata* var. *gregoryi*, *Navicula dumontiae*, *Nitzschia dissipata*, *N. inconspicua*, *Planothidium delicatulum*, and *Petroneis humerosa*.

For the first time, *Berkeleya scopulorum* (Fig. 2F) was recorded in the Sea of Azov. It was registered in the Russkaya Bay of the Kazantip Cape in August, in epiphyton of *Z. marina*.

In epiphyton communities, 30 colonial species were noted. Out of those, 7 occurred year-round: *A. brevipes*, *B. rutilans*, *Gr. marina*, *Melosira moniliformis*, *N. ramosissima*, *Rh. marina*, and *T. tabulata*. In various months, 5 cosmopolitan species dominated: *C. scutellum*, *Gr. marina*, *L. abbreviata*, *Rh. marina*, and *T. tabulata* (Fig. 2A–E).

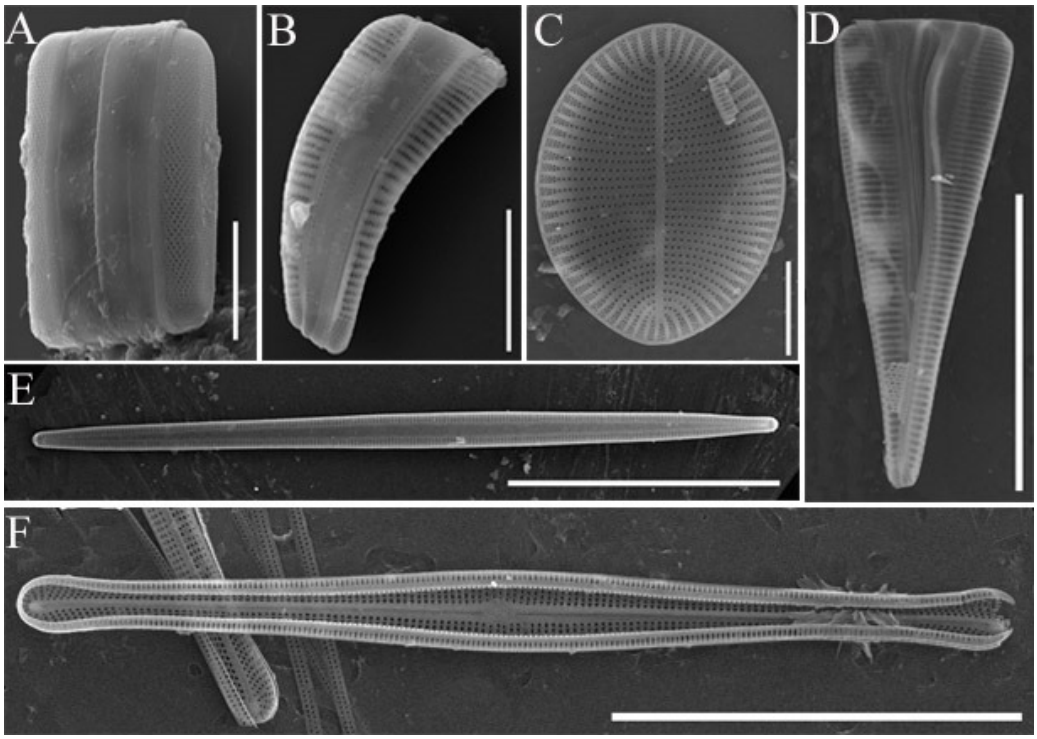


Fig. 2. Benthic diatom species in epiphyton of macrophytes (a scanning electron microscope). A, *Grammatophora marina*; B, *Rhoicosphenia marina*; C, *Cocconeis scutellum*; D, *Licmophora abbreviata*; E, *Tabularia tabulata*; F, *Berkeleya scopulorum*. Scale bars are 10 μm (A–C), 20 μm (F), 30 μm (D), and 50 μm (E)

In coastal mycrophyte thickets, 11 bloom-forming species were recorded: *B. rutilans*, *C. closterium*, *Gr. marina*, *L. abbreviata*, *Licmophora flabellata*, *Parlibellus delognei*, *Striatella unipunctata*, *Tabularia fasciculata*, and *T. tabulata*, as well as planktonic ones *Skeletonema costatum* and *Sk. subsalsum*. Also, *Halamphora coffeiformis* was registered: a potentially toxic species. As a rule, it occurs in epiphyton communities throughout the year; however, its abundance does not reach high values.

The highest number of diatom species was recorded on thalli of macroalgae: *U. linza* (61), *C. denudata* (45), and *E. crinita* (40), and also in the epiphyton of the seagrass *Z. marina* alone (37) and in its association with *Zannichellia palustris* subsp. *major* (35). The lowest number of taxa was noted in the epiphyton of a red alga *P. leucosticta* (9). Interestingly, the epiphyton of *U. linza* featured a high diatom species richness in August and September only (in other months, thalli of *Ulva* were colonized much less frequently). The minimum values of diatom abundance and biomass were often registered in its epiphyton (see Supplement: https://marine-biology.ru/mbj/article/view/507). Apparently, thalli of *U. linza*, which grew by the end of summer, served as a kind of “nets” on which diatoms settled, reaching the peak of their development by the end of summer.

Ecological analysis of the qualitative composition of the epiphyton community of diatoms showed the predominance of benthic forms (83%), marine ones (51%) and, to a lesser extent, brackish-marine ones (36%). Proportions of brackish, freshwater-brackish, and freshwater forms were small (5, 5, and 3%, respectively).

Saprobic indices were established for 45 diatom species. According to the system [Barinova et al., 2019a; Sládeček, 1986] and to our data [Barinova et al., 2019b; Bondarenko et al., 2024], 32 species out of these 45 are indicators of moderate organic water pollution (water quality class 3), and the leading role is played by a group of beta-mesosaprobes. We revealed 10 species inhabiting oligotrophic water

bodies, and 6 species typical of eutrophic waters. The occurrence of oligosaprobes in communities, despite the constant influx of organic matter, including anthropogenic one, is likely to indicate the ability of coastal ecosystems to neutralize excess organic matter *via* self-purification processes, in which microalgae also participate.

In benthic communities, the proportion of marine species increased, and the proportion of freshwater species significantly decreased. Shifts in species composition and size structure were also reported for diatoms from upper sediments sampled in 1998 and 2019 at 32 stations in various areas of the Sea of Azov [Kovaleva, Gavrilova, 2021]. The authors highlight a noticeable drop in the number of frustules of the size fraction 5–10 μm and an elevated number of large-celled species. Those were related to the taxonomic restructuring of the complex of dominant diatoms, among which medium- and large-sized taxa, chiefly marine and brackish-marine forms, began to prevail in terms of their frequency of occurrence and abundance.

Taking into account our and literature data, it can be concluded that the revealed restructuring of the algal flora reflects a trend of increasing salinity of the Sea of Azov in recent decades [Berdnikov, 2023; Kovaleva, Gavrilova, 2021].

As established, by the end of the biological summer (August and September), in the coastal area of the Kazantip Cape, there is a noticeable rise in the quantitative characteristics of some algal bloom-forming species [Bondarenko et al., 2024]. One of the risk factors for the occurrence of this phenomenon is the summer-associated elevated recreational load on the Sea of Azov coast in the Crimea and, as a consequence, the influx of organic matter with untreated sewage and household wastewater into the coastal zone [Ryabushko, 2003]. On the one hand, various organic matter, being mineralized, becomes a source of biogenic elements available for microalgae and stimulating a boost in their abundance. On the other hand, organic matter causes an outbreak of heterotrophs, which include some diatoms (representatives of *Amphora*, *Cocconeis*, *Licmophora*, *Navicula*, *Striatella*, and *Tabularia*). Notably, algal bloom is a regular problem of the Sea of Azov, since humus and dissolved organic matter constantly enter this initially eutrophic water body along with the runoff of the Don, Kuban and numerous small rivers, and the concentration of biogenic elements does not reach analytical zero [Aleksandrova et al., 1998; Gidrometeorologiya i gidrokhimiya morei SSSR, 1991]. In shallow water, algal bloom is caused by the mass development of both planktonic and benthic microalgae. Therefore, information on the species composition and quantitative characteristics of diatoms of macrophyte epiphyton is an important component in a comprehensive assessment of the state of coastal ecosystems.

Conclusion. The original data on the study of epiphytic diatom biodiversity from macrophytes of the upper sublittoral zone of the aquatic-rock complex Kazantip Cape in 2022–2023 are summarized; information on diatom ecology (relation of species to habitat, water salinity, and saprobity), phytogeography, abundance, and biomass is given. An annotated list was compiled. It includes 98 Bacillariophyta species and intraspecific taxa from 3 classes, 21 orders, 27 families, and 45 genera, and provides the description of their taxonomic affiliation. For the first time, autecology data for each taxon are presented, including phytogeographic and quantitative characteristics. In the surveyed algal flora, a benthic diatom *Berkeleya scopulorum* was registered, new for the Sea of Azov; its scanning electron micrograph is presented. The highest taxonomic diversity was recorded for three genera: *Nitzschia* (12 species), *Navicula* (11), and *Licmophora* (6). In epiphyton communities, 30 colonial species were found; out of those, 7 occur year-round: *Achnanthes brevipes*, *Berkeleya rutilans*, *Grammatophora marina*, *Melosira moniliformis*, *Navicula ramosissima*, *Rhoicosphenia marina*, and *Tabularia tabulata*. In terms of abundance,

the cosmopolitan species are dominant ones: *Cocconeis scutellum*, *Gr. marina*, *Licmophora abbreviata*, *Rh. marina*, and *T. tabulata*. The bioindicator properties of the identified saprobic diatoms can be used in further monitoring of the dynamics of anthropogenic load in the Sea of Azov.

This work was carried out within the framework of IBSS state research assignment "Comprehensive study of the functioning mechanisms of marine biotechnological complexes with the aim of obtaining bioactive substances from hydrobionts" (No. 124022400152-1).

Acknowledgments. We express our gratitude to N. A. Litvinyuk, senior researcher of the Federal State Budgetary Institution "Zapovedny Krym" of the Kazantip State Nature Reserve, for her assistance in sampling.

REFERENCES

1. Aleksandrova Z. V., Semenov A. D., Romova M. G., Baskakova T. E. The oxygen regime and the content of biogenic compounds in the Azov Sea over the period of 1957–1997. In: *The Main Problems of Fisheries and Protection of Waterbodies with Fisheries in the Azov Sea Basin* : collected articles (1996–1997) / Research Institute of the Azov Sea fishery problems (AzNIIRKh). Rostov-on-Don : AzNIIRKh, 1998, pp. 34–48. (in Russ.). https://elibrary.ru/jjtyrb
2. Barinova S. S., Bilous O. P., Tsarenko P. M. *Algal Indication of Water Bodies in Ukraine: Methods and Perspectives.* Haifa ; Kyiv : University of Haifa Publisher, 2019a, 367 p. (in Russ.)
3. Belich T. V., Sadogurskiy S. Ye., Sadogurskaya S. A. Revision flora of macrophytes of the aquatory of the Kazantip nature reserve. *Nauchnye zapiski prirodnogo zapovednika "Mys Mart'yan"*, 2019, no. 10, pp. 61–72. (in Russ.). https://doi.org/10.36305/2413-3019-2019-10-61-72
4. Bondarenko A. V. *Mikrovodorosli bentosa krymskogo pribrezh'ya Azovskogo morya.* [dissertation]. Sevastopol, 2017, 237 p. (in Russ.). https://elibrary.ru/hfszxc
5. Bondarenko A. V., Ryabushko L. I. Vidovoi sostav i sezonnaya dinamika kolichestvennykh kharakteristik diatomovykh vodoroslei bentosa pribrezhnoi chasti Kazantipskogo zapovednika (Azovskoe more). In: *Sistemy kontrolya okruzhayushchei sredy* : sbornik nauchnykh trudov / NAN Ukrainy ; Morskoi gidrofizicheskii institut. Sevastopol : [EKOSI-Gidrofizika], 2010, iss. 13, pp. 231–237. (in Russ.). https://elibrary.ru/gmxjcz
6. Bondarenko A. V., Ryabushko L. I., Sadogurskaya S. A. Microalgae of benthos and plankton in the coastal waters of the nature reserve (zapovednik) "Kazantipskiy" (the Sea of Azov, Crimea). *Biota i sreda zapovednykh territorii*, 2018, no. 4, pp. 25–48. (in Russ.). https://elibrary.ru/yyocjf
7. Volkov L. I. Materialy k flore Azovskogo morya. *Trudy Rostovskogo oblastnogo biologicheskogo obshchestva*, 1940, iss. 4, pp. 114–137. (in Russ.)]
8. *Gidrometeorologiya i gidrokhimiya morei SSSR.* Vol. 5. *Azovskoe more.* Saint Petersburg : Gidrometeoizdat, 1991, 235 p. (in Russ.)
9. Gromov V. V. Donnaya morskaya i pribrezhnovodnaya rastitel'nost'. In: *Sovremennoe razvitie estuarnykh ekosistem na primere Azovskogo morya* / G. G. Matishov (Ed.). Apatity : KNTs RAN, 1999, pp. 130–166. (in Russ.). https://elibrary.ru/vzndyd
10. Guslyakov N. E., Zakordonets O. A., Gerasimyuk V. P. *Atlas diatomovykh vodoroslei bentosa severo-zapadnoi chasti Chernogo morya i prilegayushchikh vodoemov* / AN USSR, Institut botaniki imeni N. G. Kholodnogo. Kyiv : Naukova dumka, 1992, 112 p., 140 p. ill. (in Russ.)
11. *Diatomovyi analiz.* Book 3. *Opredelitel' iskopaemykh i sovremennykh diatomovykh vodoroslei. Poryadok Pennales* / A. N. Krishtofovich, A. I. Proshkina-Lavrenko (Eds). Leningrad : Gosizdat, 1950, 398 p. (in Russ.)
12. *The Diatoms of the USSR. Fossil and Recent.* Vol. 1 / A. I. Proshkina-Lavrenko (Ed.). Leningrad : Nauka, Leningr. otd-nie, 1974, 403 p. (in Russ.)
13. Kovaleva G. V., Gavrilova I. Yu. Changes

in the dominant species and size structure of diatoms from the surface bottom sediments of the Sea of Azov over the past 20 years. *Ekologiya. Ekonomika. Informatika. Seriya: Sistemnyi analiz i modelirovanie ekonomicheskikh i ekologicheskikh sistem*, 2021, vol. 1, no. 6, pp. 96–103. (in Russ.). https://doi.org/10.23885/2500-395X-2021-1-6-96-103

14. Korotkevich O. S. Diatomovaya flora litorali Barentseva morya. *Trudy Murmanskogo morskogo biologicheskogo instituta*, 1960, iss. 1 (5), pp. 68–338. (in Russ.)
15. Litvinyuk N. A. Cadastral documentation of the state budgetary establishment of the Republic of Crimea "Kazantip Nature Reserve". *Nauchnye zapiski prirodnogo zapovednika "Mys Mart'yan"*, 2016, iss. 7, pp. 27–55. (in Russ.). https://elibrary.ru/xcbzoj
16. Maslov I. I. Fitobentos nekotorykh zapovednykh i estestvennykh akval'nykh kompleksov Azovskogo morya. *Sbornik nauchnykh trudov Gosudarstvennogo Nikitskogo botanicheskogo sada*, 2004, vol. 123, pp. 68–75. (in Russ.). https://elibrary.ru/yofwsv
17. Nikolaev V. A. *Diatomovye vodorosli bentosa zaliva Pos'et Yaponskogo morya.* [dissertation]. Leningrad, 1970, 227 p. (in Russ.)
18. Ryabushko L. I. *Microphytobenthos of the Black Sea.* Sevastopol : EKOSI-Gidrofizika, 2013, 416 p. (in Russ.). https://repository.marine-research.ru/handle/299011/8301
19. Ryabushko L. I. *Potentially Harmful Microalgae of the Azov and Black Sea Basin* / V. I. Ryabushko (Ed.). Sevastopol : EKOSI-Gidrofizika, 2003, 288 p. (in Russ.). https://repository.marine-research.ru/handle/299011/8904
20. Ryabushko L. I., Begun A. A. *Diatoms of Microphytobenthos of the Sea of Japan.* Sevastopol ; Simferopol : N.Orianda, 2015, vol. 1, 288 p. (in Russ.). https://repository.marine-research.ru/handle/299011/7924
21. Ryabushko L. I., Begun A. A. *Diatoms of Microphytobenthos of the Sea of Japan (Synopsis and Atlas)* : in 2 vols. Sevastopol : KIA, 2016, vol. 2, 324 p. (in Russ.). https://repository.marine-research.ru/handle/299011/7925
22. Ryabushko L. I., Bondarenko A. V. *Microalgae of the Plankton and Benthos of the Sea of Azov (Check-list, Synonyms, Comment).* Sevastopol : EKOSI-Gidrofizika, 2011, 211 p. (in Russ.). https://repository.marine-research.ru/handle/299011/9273
23. Sadogurskaya S. A. Flora Cyanophyta supralitorali Kazantipskogo prirodnogo zapovednika (Azovskoe more). *Sbornik nauchnykh trudov Gosudarstvennogo Nikitskogo botanicheskogo sada*, 2001, vol. 120, pp. 124–131. (in Russ.). https://elibrary.ru/yluqiz
24. Sadogurskaya S. A., Sadogursky S. E., Belich T. V. Annotated list of phytobenthos of the Kazantip nature reserve. *Sbornik nauchnykh trudov Gosudarstvennogo Nikitskogo botanicheskogo sada*, 2006, vol. 126, pp. 190–208. (in Russ.). https://elibrary.ru/smkdhb
25. Shiroyan A. G. *Diatomovye vodorosli epifitona makrofitov krymskogo pribrezh'ya Chernogo morya.* [dissertation]. Sevastopol, 2022, 167 p. (in Russ.). https://elibrary.ru/nttgmy
26. *AlgaeBase.* World-wide electronic publication, National University of Ireland, Galway / M. D. Guiry, G. M. Guiry (Eds) : [site], 2025. URL: http://www.algaebase.org [accessed: 03.01.2025].
27. Barinova S., Bondarenko A., Ryabushko L., Kapranov S. Microphytobenthos as an indicator of water quality and organic pollution in the western coastal zone of the Sea of Azov. *Oceanological and Hydrobiological Studies*, 2019b, vol. 48, iss. 2, pp. 125–139. https://doi.org/10.1515/ohs-2019-0013
28. Berdnikov S. V., Kulygin V. V., Dashkevich L. V. Reasons for rapid increase of water salinity in the Sea of Azov in the 21st century. *Physical Oceanography*, 2023, vol. 30, no. 6, pp. 714–730. https://elibrary.ru/drnrju
29. Bondarenko A., Shiroyan A., Ryabushko L., Barinova S. Diatoms of the macroalgae epiphyton and bioindication of the protected coastal waters of the Kazantip Cape (Crimea, the Sea of Azov). *Journal of Marine Science and Engineering*, 2024, vol. 12, iss. 7, art. no. 1211 (22 p.). https://doi.org/10.3390/jmse12071211

30. Kuylenstierna M. *Benthic Algal Vegetation in the Nordre Älv Estuary (Swedish West Coast).* PhD thesis. Göteborg, Sweden : University of Göteborg–Sweden, 1989, vol. 1, 244 p.
31. Kuylenstierna M. *Benthic Algal Vegetation in the Nordre Älv Estuary (Swedish West Coast).* PhD thesis. Göteborg, Sweden : University of Göteborg–Sweden, 1990, vol. 2 [plates], 76 p.
32. Lee J. J., McEnery M. E., Kennedy E. M., Rubin H. A nutritional analysis of a sublittoral diatom assemblage epiphytic on *Enteromorpha* from a Long Island salt marsh. *Journal of Phycology*, 1975, vol. 11, iss. 1, pp. 14–49. https://doi.org/10.1111/j.1529-8817.1975.tb02746.x
33. Round F. E., Crawford R. M., Mann D. G. *The Diatoms. Biology and Morphology of the Genera.* Cambridge, UK : Cambridge University Press, 1990, 747 p.
34. Ryabushko L. I., Bondarenko A. V. The qualitative and quantitative characteristics of the benthic diatoms near Kazantip Cape of the Sea of Azov. *Journal of the Black Sea / Mediterranean Environment*, 2016, vol. 22, no. 3, pp. 237–249. https://elibrary.ru/izzvxm
35. Siqueiros-Beltrones D. A., Hernández-Almeida O. U. Florística de diatomeas epifitas en un manchón de macroalgas subtropicales. *CICIMAR Oceánides*, 2006, vol. 21, no. 1–2, pp. 11–61.
36. Sládeček V. Diatoms as indicators of organic pollution. *Acta Hydrochimica et Hydrobiologica*, 1986, vol. 14, iss. 5, pp. 555–566. https://doi.org/10.1002/aheh.19860140519
37. Smith W. F. *A Synopsis of the British Diatomaceae* : with remarks on their structure, functions and distribution; and instructions for collecting and preserving specimens. In 2 vols. Vol. 1. London : Printed for Smith and Beck, publ. by J. Van Voorst, 1853, 89 p. https://doi.org/10.5962/bhl.title.10706
38. Witkowski A., Lange-Bertalot H., Metzeltin D. *Diatom Flora of Marine Coasts.* 1. Ruggell ; Königstein : Gantner Verlag : Koeltz Scientific Books, 2000, 925 p. (Iconographia Diatomologica : Annotated Diatom Micrographs ; vol. 7: Diversity – Taxonomy – Identification / H. Lange-Bertalot (Ed.))

АННОТИРОВАННЫЙ СПИСОК ДИАТОМОВЫХ ВОДОРОСЛЕЙ ЭПИФИТОНА МАКРОФИТОВ АКВАЛЬНО-СКАЛЬНОГО КОМПЛЕКСА «МЫС КАЗАНТИП» (КРЫМ, АЗОВСКОЕ МОРЕ)

А. Г. Широян, А. В. Бондаренко, Л. И. Рябушко

ФГБУН ФИЦ «Институт биологии южных морей имени А. О. Ковалевского РАН»,
Севастополь, Российская Федерация
E-mail: *arminka_shir@mail.ru*

Впервые представлены обобщённые оригинальные данные о видовом составе диатомовых водорослей в 129 пробах эпифитона 14 видов макрофитов из верхней сублиторали аквально-скального комплекса «Мыс Казантип» Азовского моря. Пробы отобраны в 2022–2023 гг. на глубинах 0,1–1,0 м при температуре от +3,7 до +29,0 °С и солёности воды от 13,6 до 15,6 г·л$^{-1}$. Аннотированный список включает 98 видов и внутривидовых таксонов отдела Bacillariophyta из 3 классов, 21 порядка, 27 семейств и 45 родов; указаны их размеры, встречаемость, экологические и фитогеографические характеристики, численность и биомасса. Высокое видовое разнообразие диатомовых водорослей отмечено для класса Bacillariophyceae (72 таксона) и родов *Nitzschia* (12 видов), *Navicula* (11) и *Licmophora* (6). В эпифитоне зелёной водоросли *Ulva linza* обнаружен 61 вид, красной *Carradoriella denudata* — 45, бурой *Ericaria crinita* — 40,

морской травы *Zostera marina* — 37, её ассоциации с *Zannichellia palustris* subsp. *major* — 35. Наименьшее число видов найдено в эпифитоне красной водоросли *Pyropia leucosticta* — 9. Обнаружен новый для Азовского моря бентосный вид *Berkeleya scopulorum*. В сообществах эпифитона преобладают бентосные (83 %), морские (51 %) и космополитные виды (35 %) диатомовых водорослей. Выявлено 30 колониальных видов, из них круглогодично присутствуют *Achnanthes brevipes*, *Berkeleya rutilans*, *Grammatophora marina*, *Melosira moniliformis*, *Navicula ramosissima*, *Rhoicosphenia marina* и *Tabularia tabulata*. По численности доминируют космополиты *Cocconeis scutellum*, *Gr. marina*, *Licmophora abbreviata*, *Rh. marina* и *T. tabulata*. Выявлено 11 видов, вызывающих «цветение» воды, и 45 видов — индикаторов сапробности органического загрязнения вод.

Ключевые слова: диатомовые водоросли, макрофиты, эпифитон, аквально-скальный комплекс «Мыс Казантип», Азовское море

1871
ИнБЮМ – IBSS

Морской биологический журнал
Marine Biological Journal
2025, vol. 10, no. 4, pp. 123–124
https://marine-biology.ru/mbj/article/view/520

CHRONICLE AND INFORMATION

ON THE ANNIVERSARY OF SERGEY FESENKO



On 17 September, 2025, Sergey Fesenko celebrated his 70th birthday. He is a leading radioecologist respected in the scientific community both in our country and abroad, D. Sc. (1997), Professor (1999), and laureate of the Russian Federation National Award (2002). He has made a significant contribution to the development of agricultural, forest, aquatic, and general radioecology, as well as environmental radiation protection and dosimetry.

S. Fesenko was born in 1955 in Simferopol and graduated from secondary school No. 14 in 1972 there. In 1978, he graduated with honors from the Moscow Engineering Physics Institute (MEPhI) (specializing in dosimetry and protection), and in 1982, from the Lomonosov Moscow State University, the Faculty of Mechanics and Mathematics (specializing in applied mathematics). In 1983, he completed the full-time postgraduate course at MEPhI.

Sergey Fesenko began his scientific career in 1981 as a junior researcher. Then, he worked as a senior and leading researcher, head of a laboratory, and deputy director for scientific affairs. Currently, he is the chief researcher at the Russian Institute of Radiology and Agroecology of the National Research Centre “Kurchatov Institute” (until 1991, the All-Union Research Institute of Agricultural Radiology). In 2004–2017, he worked at the International Atomic Energy Agency (IAEA) coordinating research and practical assessment of the environmental hazards of nuclear energy use and the rehabilitation of contaminated sites. During this period, he prepared over 15 international guidelines and recommendations on determining the effect of ionizing radiation on the environment and people, and on the rehabilitation of radioactively contaminated areas. S. Fesenko participated in the cleanup efforts following the Chernobyl and Fukushima Daiichi nuclear power plant accidents.

In 1985, Sergey Fesenko defended his PhD thesis *Assessment of the Effect of the Accident at the ‘Mayak’ Chemical Plant on Freshwater Ecosystems*, in physics and mathematics. In 1997, he defended his D. Sc. thesis *Agricultural and Forest Ecosystems: Radioecological Consequences and Effectiveness of Protective Measures in Case of Radioactive Contamination*, in radiobiology.

He has studied the fundamental mechanisms of behavior of natural and artificial radionuclides in natural and agricultural ecosystems. A set of migration and dosimetric models has been developed which allowed for reconstructing the radiation doses of hydrobionts in Lake Uruskul (the Urals) and providing a long-term assessment of the radiation effect on ecosystems at different levels of biological organization.

S. Fesenko has determined quantitative parameters and developed a set of models to assess the contribution of agricultural products to the exposure of the local population in radioactively contaminated sites.

He has established fundamental patterns of change in the biological availability of ^{137}Cs in agricultural ecosystems and identified the key factors causing this change. He presented a theoretical description of mechanisms governing changes in ^{137}Cs mobility in agroecosystems and a long-term forecast of the dynamics of its content in soils and vegetation of various ecosystems.

Sergey Fesenko has carried out the research to assess the consequences of radioactive contamination of agricultural land for various radiation exposure scenarios: in the context of nuclear war, normal operation of radiation-hazardous facilities, and emergency situations. He has developed a set of models describing environmental protection measures in agriculture in radioactively contaminated areas and carried out a comparative analysis of countermeasure strategies in agriculture after the Chernobyl nuclear accident.

He has carried out a comprehensive radioecological assessment of the effect of normalized and emergency emissions from nuclear power plants on forest and agricultural ecosystems. The materials of his research and the methods he developed were used for environmental expertise in the construction and expansion of several Russian nuclear power plants.

For the long-term period after the Chernobyl nuclear accident, he proposed a fundamentally new, targeted approach to the rehabilitation of agricultural land.

S. Fesenko has authored and co-authored 12 monographs and more than 400 articles in leading Russian and foreign scientific journals. He has supervised 2 D. Sc. and 15 PhDs. He serves on editorial boards of *Marine Biological Journal*, *Radiation Biology. Radioecology*, and *Civil Security Technology*.

The significance of his scientific work is confirmed by his receipt of a number of national and international awards. He is a laureate of the Russian Federation National Award in science and technology (2002), for establishing the scientific foundations of agro-industrial production and implementing a system of protective and rehabilitation measures within the zone of the Chernobyl nuclear accident, and also the Nobel Peace Prize laureate (jointly with IAEA, 2005). Sergey Fesenko was presented with the prestigious IAEA Superior Achievement Award (2017) and the V. Klechkovsky Gold Medal of the Russian Academy of Sciences (2021) for outstanding achievements in radioecology. He has been awarded certificates of honor from the Ministry of Agriculture of the Russian Federation (2001), the Russian Academy of Agricultural Sciences (2000), the Obninsk administration (2007 and 2011), the Governor of the Kaluga Oblast (2003), the Minister for Emergency Situations of the Republic of Belarus (2016), and the Russian Academy of Sciences (2020).

Colleagues from IBSS Department of Radiation and Chemical Biology sincerely congratulate Sergey Fesenko on his anniversary and wish him good health, active creative longevity, happiness, new scientific achievements, and family well-being!

With deep respect,
the team of IBSS Department of Radiation and Chemical Biology

К ЮБИЛЕЮ СЕРГЕЯ ВИКТОРОВИЧА ФЕСЕНКО

17 сентября 2025 г. отметил своё 70-летие д. б. н., проф. Сергей Викторович Фесенко — выдающийся специалист, чей вклад в развитие сельскохозяйственной, водной и общей радиоэкологии трудно переоценить. С. В. Фесенко исследовал фундаментальные механизмы поведения естественных и искусственных радионуклидов в природных и аграрных экосистемах, занимался оценкой последствий радиоактивного загрязнения сельскохозяйственных земель и их реабилитацией при различных сценариях радиационного воздействия, а также анализировал влияние нормализованных и аварийных выбросов АЭС на лесные и аграрные экосистемы.

ISSN 2499-9768 25004
9 772499 976005 >

Вниманию читателей!

Зоологический институт РАН,
Институт биологии южных морей
имени А. О. Ковалевского РАН

издают
научный журнал

Морской биологический журнал
Marine Biological Journal

- МБЖ — периодическое издание открытого доступа. Подаваемые материалы проходят независимое двойное слепое рецензирование. Журнал публикует обзорные и оригинальные научные статьи, краткие сообщения и заметки, содержащие новые данные теоретических и экспериментальных исследований в области морской биологии, материалы по разнообразию морских организмов, их популяций и сообществ, закономерностям распределения живых организмов в Мировом океане, результаты комплексного изучения морских и океанических экосистем, антропогенного воздействия на морские организмы и экосистемы.
- Целевая аудитория: биологи, экологи, биофизики, гидро- и радиобиологи, океанологи, географы, учёные других смежных специальностей, аспиранты и студенты соответствующих научных и отраслевых профилей.
- Статьи публикуются на русском и английском языках.
- Периодичность — четыре раза в год.
- Подписной индекс в каталоге «Пресса России» — Е38872. Цена свободная.

Заказать журнал

можно в научно-информационном отделе ИнБЮМ.
Адрес: ФГБУН ФИЦ «Институт биологии южных морей имени А. О. Ковалевского РАН», пр-т Нахимова, 2, г. Севастополь, 299011, Российская Федерация.
Тел.: +7 8692 54-06-49.
E-mail: *mbj@imbr-ras.ru*.

Zoological Institute of RAS,
A. O. Kovalevsky Institute of Biology
of the Southern Seas of RAS

publish
scientific journal

Морской биологический журнал
Marine Biological Journal

- MBJ is an open access, peer reviewed (double-blind) journal. The journal publishes original articles as well as reviews and brief reports and notes focused on new data of theoretical and experimental research in the fields of marine biology, diversity of marine organisms and their populations and communities, patterns of distribution of animals and plants in the World Ocean, the results of a comprehensive studies of marine and oceanic ecosystems, anthropogenic impact on marine organisms and on the ecosystems.
- Intended audience: biologists, ecologists, biophysicists, hydrobiologists, radiobiologists, oceanologists, geographers, scientists of other related specialties, graduate students, and students of relevant scientific profiles.
- The articles are published in Russian and English.
- The journal is published four times a year.
- The subscription index in the “Russian Press” catalogue is E38872. The price is free.

You may order the journal

in the scientific information department of IBSS.
Address: A. O. Kovalevsky Institute of Biology of the Southern Seas of RAS, 2 Nakhimov avenue, Sevastopol, 299011, Russian Federation.
Tel.: +7 8692 54-06-49.
E-mail: *mbj@imbr-ras.ru*.